



HAL
open science

Supersymmetric phenomenology: polarized collisions and precision calculations

Josselin Proudom

► **To cite this version:**

Josselin Proudom. Supersymmetric phenomenology: polarized collisions and precision calculations. High Energy Physics - Phenomenology [hep-ph]. LPSC - Laboratoire de Physique Subatomique et de Cosmologie 2015. English. NNT: . tel-01378813

HAL Id: tel-01378813

<https://hal.science/tel-01378813>

Submitted on 10 Oct 2016

HAL is a multi-disciplinary open access archive for the deposit and dissemination of scientific research documents, whether they are published or not. The documents may come from teaching and research institutions in France or abroad, or from public or private research centers.

L'archive ouverte pluridisciplinaire **HAL**, est destinée au dépôt et à la diffusion de documents scientifiques de niveau recherche, publiés ou non, émanant des établissements d'enseignement et de recherche français ou étrangers, des laboratoires publics ou privés.

Public Domain

THÈSE

Pour obtenir le grade de

DOCTEUR DE L'UNIVERSITÉ DE GRENOBLE

Spécialité : **Physique Subatomique et Astroparticules**

Arrêté ministériel : 7 août 2006

Présentée par

Josselin Proudom

Thèse dirigée par **Ingo Schienbein et Benjamin Fuks**

préparée au sein **du LPSC**
et de **l'École doctorale de physique de Grenoble**

Supersymmetric phenomenology: polarized collisions and precision calculations

Thèse soutenue publiquement le **19 Octobre 2015**,
devant le jury composé de :

Dr. Roberto Bonciani

Doctor researcher, Università degli Studi di Roma "La Sapienza", Rapporteur

Prof. Johann Collot

Professeur, LPSC Grenoble, Université de Grenoble, Président

Prof. Aldo Deandrea

Professeur, Université Claude Bernard Lyon 1, Examineur

Prof. Benjamin Fuks

Professeur, Université Pierre et Marie Curie, Co-Directeur de thèse

Dr. Ingo Schienbein

MCF, Université Joseph Fourier de Grenoble, Directeur de thèse

Prof. Dominik Stöckinger

Professor, Institut für Kern- und Teilchenphysik, TU Dresden University,
Rapporteur



Remerciements

La thèse est une expérience intense, et unique en son genre. Au-delà des pures connaissances académiques, et de la méthodologie scientifique qu'elle permet d'acquérir et de mettre en oeuvre, elle revêt également un caractère instructif sur un plan plus personnel, et permet d'en apprendre énormément sur soi-même, et sur autrui. Une thèse est une expérience grisante et passionnante, durant laquelle les moments de doute, de stress, et d'allégresse se suivent, et se succèdent inlassablement. Cependant, même dans les moments difficiles, pas un seul instant je n'ai regretté ce choix qui m'a conduit à Grenoble. Alors que ma présence en ces lieux touche à sa fin, je souhaiterais remercier toutes les personnes ayant contribué à faire de cette thèse une expérience unique, et inoubliable.

En premier lieu, Ingo et Benjamin, mes deux co-directeurs de thèse, qui m'ont apporté leur soutien, et leur conseils avisés à de multiples occasions au cours de ces trois dernières années. Merci tout d'abord à Ingo d'avoir été un directeur de thèse à l'écoute, toujours bienveillant, et avec lequel discuter est aussi instructif que plaisant. J'ai beaucoup apprécié travailler avec toi, et j'espère pouvoir continuer à collaborer avec toi même après mon départ du LPSC. Merci à toi aussi Benjamin pour m'avoir initié, avec ferveur et enthousiasme, à la physique des particules durant mes stages de M1, et de M2 à Strasbourg, c'est toi qui m'a donné goût à cette discipline. Je tenais en outre à te remercier pour la patience dont tu as fait preuve à mon encontre, pour m'avoir fait confiance pour le stage de M2, et pour m'avoir permis de participer à tous ces projets passionnants. J'ai énormément appris à tes côtés, et grâce à ta présence au CERN pendant deux ans, j'ai eu la chance de pouvoir bénéficier d'un environnement de travail extrêmement stimulant.

Je tiens ensuite à remercier mes deux rapporteurs, Dominik Stöckinger et Roberto Bonciani, pour avoir accepté de lire mon manuscrit en un temps record, et avoir contribué à son amélioration par leur remarques et commentaires. Je souhaiterais ensuite remercier mes examinateurs, Aldo Deandrea et Johann Collot, pour avoir accepté de faire partie de mon jury de thèse, malgré leur multiples responsabilités, et leur emploi du temps chargé. De la même manière, je souhaiterais remercier tous mes collaborateurs pour les échanges que nous avons eu, et qui ont contribué à faire de moi un meilleur physicien.

Mon infinie gratitude va aussi au comité de sélection du Labex Enigmass, qui m'a soutenu financièrement durant ces trois années de thèse, et à qui je dois donc évidemment beaucoup, ainsi qu'aux membres (et ex-membres) du groupe de théorie, sans lesquels cette thèse n'aurait pas eu la même saveur. Merci donc à Sabine, Christopher, Mariane, Guillaume (pour sa bonne humeur, et pour m'avoir permis de participer au cours de renormalisation en QED), Dipan, Olek (pour nos discussions, et les randonnées en montagne), Akin (pour nos discussions dans le bus le soir, et pour m'avoir fait découvrir le Bombay), Suchita (pour m'avoir permis de prendre en charge l'organisation des séminaires du groupe de théorie), Quentin, Zhao-ting (pour sa gentillesse, et ses repas dignes des plus grands chefs), Jérémy, Ursula, Béranger, Gabin, et Savvas bien évidemment. Mes plus sincères remerciements vont à Florian et Tomáš, pour m'avoir aidé à mon arrivée au sein du groupe, pour toutes nos discussions, qu'elles soient liées ou non à la physique, et enfin pour leur aide durant la rédaction du présent manuscrit. Merci infiniment à

vous deux, cette thèse n'aurait pas été la même sans vos conseils.

Enfin, je souhaiterais remercier ceux qui m'ont accompagné et soutenu sur un plan plus personnel durant ces trois années, à savoir les amis et la famille. Un grand merci en particulier à Gromick (pour son Courage!), Louis, Marie-Anne, Gabriel, Juliana, Pauline, Sébastien, Clément, et Samuel. Merci ensuite à ma famille, et à Alice, Catherine et Gilles pour leur soutien, et pour tous les bons moments. Merci évidemment à celle qui partage ma vie, Mathilde, pour sa patience, son soutien sans faille, et sa capacité à toujours trouver les mots pour me faire sourire, même dans les moments difficiles. Merci enfin, et par-dessus tout, à mon père et ma mère (à qui cette thèse est entièrement dédiée), pour m'avoir soutenu et encouragé tout au long de mes études. Je vous dois beaucoup à tous les deux.

Résumé :

Les théories supersymétriques, telles que le Modèle Standard Supersymétrique Minimal, constituent des extensions très populaires du Modèle Standard de physique des particules, et sont activement recherchées au Large Hadron Collider (LHC). Dans cette thèse, nous nous concentrons sur deux aspects de la phénoménologie des théories supersymétriques aux collisionneurs hadroniques de haute-énergie, à savoir les collisions polarisées, et les calculs de précision. Dans un premier temps, nous réalisons une étude au Leading Order (LO), dans laquelle nous montrons comment la présence de faisceaux polarisés (longitudinalement) pourrait nous aider à différencier des modèles de Nouvelle Physique présentant la même signature à l'état final. A titre d'exemple, nous considérons le cas d'une classe particulière de scénarios, menant à la production de monotops, qui correspondent à la production d'un quark top en association avec de l'énergie transverse manquante. Nous présentons nos résultats pour un LHC polarisé à 14 TeV, et pour le récemment proposé Futur Collisionneur Circulaire (FCC), supposé opérer à 100 TeV. Par la suite, nous nous concentrons sur la réalisation de prédictions de précisions pour la production de paires squark-antisquark, de sgluons, et de gluinos au next-to-leading order (NLO) en QCD supersymétrique, avec ou sans violation non-minimale de saveur, et avec ou sans Parton Shower (PS). Plus particulièrement, nous fournissons les premiers résultats (préliminaires) pour la production de squark-antisquark au NLO en SUSY-QCD avec violation non-minimale de saveur, dans le cas d'un calcul à ordre perturbatif fixe, et considérons dans le contexte de modèles simplifiés la production par paires de particules colorées de type scalaire (stops et sgluons), et Majorana (gluinos) au NLO avec PS via l'environnement de travail automatisé MADGRAPH5_aMC@NLO.

Abstract :

Supersymmetric theories, such as the Minimal Supersymmetric Standard Model (MSSM), constitute very popular extensions of the Standard Model of particle physics, and are extensively searched for at the Large Hadron Collider (LHC). In this thesis, we focus on two specific aspects of the phenomenology of supersymmetric theories at high-energy hadron colliders, namely polarized collisions and precision calculations. First, we perform a Leading Order (LO) study, in which we show how the availability of (longitudinally) polarized proton beams could help us to disentangle various Beyond the Standard Model (BSM) scenarios exhibiting the same final-state signature. For the sake of illustration, we focus on the case of one particular class of scenarios leading to monotop production, which corresponds to the production of a top quark in association with missing transverse energy. We present our results for a polarized LHC at 14 TeV, and for the recently proposed Future Circular Collider (FCC), supposed to operate at 100 TeV. Then, we concentrate on predictions for squark-antisquark, sgluon, and gluino pair production at next-to-leading order (NLO) in supersymmetric QCD, with or without Non-Minimal Flavour Violations (NMFV), and with or without matching those predictions with Parton Showers (PS). More specifically, we provide the first preliminary results for squark-antisquark hadroproduction at NLO in SUSY-QCD with NMFV, in the context of a fixed order calculation, and consider, in the context of simplified models, the pair production of coloured scalar (stops and sgluons) and coloured Majorana (gluinos) particles at NLO matched with PS within the automated MADGRAPH5_aMC@NLO framework.

Contents

1	Introduction	1
1.1	Conceptual and æsthetical flaws of the Standard Model	1
1.2	Observational problems with the Standard Model	7
1.3	Organization of the thesis	10
2	Supersymmetry	13
2.1	Motivations	13
2.2	Supersymmetric algebra	14
2.3	Superspace formalism and superfields	16
2.4	Supersymmetric transformations	16
2.5	Supersymmetric chiral Lagrangians	18
2.6	Supersymmetric gauge theories	20
2.7	The Minimal Supersymmetric Standard Model	26
2.8	Supersymmetry breaking	28
2.9	Higgs sector	29
2.10	Gaugino and Higgsino sector	32
2.11	Sfermion sector	35
3	Leading Order phenomenology at polarized hadron colliders	37
3.1	Motivations	37
3.2	Spin asymmetries at polarized hadron colliders	38
3.3	Physics case: monotop production	44
3.3.1	Monotop production in the RPV MSSM	45
3.3.2	Other scenarios for monotop production	48
3.3.3	Impact of monotop charge tagging	50
3.3.4	Summary	51
3.4	Conclusions	52
4	Regularization and Renormalization	55
4.1	Regularization scheme	56
4.2	Dimensional Reduction	60
4.3	Evaluation of scalar one-loop integrals	62
4.4	Passarino-Veltman reduction	67
4.5	Renormalization	77
5	Squark-antisquark production at NLO with NMFV	83
5.1	Theoretical set-up	84
5.2	Tree-level matrix element	85
5.3	Renormalization set-up	87

5.4	Self-energies	88
5.5	Vertex corrections	96
5.6	Box contributions	110
5.7	Status report on the calculation	111
6	Matching NLO predictions with parton showers	113
6.1	Coloured scalar pair production	113
6.2	Gluino pair production	120
7	Conclusions and outlook	127
A	Conventions	129
B	Basic facts on $\mathfrak{su}(N)$	131
C	Parton distributions C++ interface	135
D	Euler-Gamma and Beta functions	139
E	γ^5 in D-dimensions	141
F	NMFV SUSY-QCD Feynman rules	143

Chapter 1

Introduction

The Standard Model (SM) of particle physics [1] is a theory that describes fundamental interactions between elementary particles. More precisely, it is a renormalizable local quantum field theory (QFT) invariant under the non-abelian gauge group $SU(3)_C \times SU(2)_L \times U(1)_Y$, which provides a microscopic description of the electroweak and strong interactions between quarks and leptons, and accounts for the dynamics of the gauge fields. This theory is made out of two pieces. The first one, based on the gauge group $SU(3)_C$, is called Quantum ChromoDynamics (QCD) [2–15], and describes the dynamics of the strong interactions (responsible *e.g.* for binding protons and neutrons together into atomic nuclei). The second one, built on $SU(2)_L \times U(1)_Y$, is called the electroweak Standard Model [16–18], and describes within a unified framework, electromagnetic as well as weak interactions (responsible for nuclear β -decays).

For more than forty years, this refined theoretical edifice has withstood all attempts at falsification. Tested with an ever increasing degree of precision, the Standard Model has revealed itself fully compatible and consistent with a wide class of experiments. It has successfully predicted the existence and the form of the electroweak interactions, the mass of the W and Z boson [17, 18], the existence of the charm quark as required by the Glashow-Iliopoulos-Maiani (GIM) mechanism [19], and the top quark mass with a $\mathcal{O}(10)$ GeV accuracy [20], even before it was discovered at Fermilab in 1995 [21, 22]. However, the greatest achievement of the Standard Model most certainly remains the Brout-Englert-Higgs-Guralnik-Hagen-Kibble mechanism [23–28], which describes the spontaneous breaking of the electroweak symmetry thanks to which it is possible for all the elementary particles to acquire a mass. This mechanism, theorized fifty years ago, was experimentally confirmed in 2012 by the ATLAS [29] and CMS [30] collaborations at the Large Hadron Collider (LHC), after the observation of a particle whose properties are consistent with a 125 GeV Standard Model-like Higgs boson [31–33].

In addition to all the aforementioned virtues, the Standard Model (supplemented with massive neutrinos) can also account for neutrino oscillations [34, 35], a phenomenon for which we now have strong experimental evidences [1], and therefore seems to provide a particularly consistent and relevant description of Nature, so far in perfect agreement with (almost) all data collected at collider-based experiments. Nevertheless, despite its really impressive phenomenological successes, the SM still exhibits conceptual and experimental shortcomings that leave many fundamental questions unanswered.

1.1 Conceptual and æsthetical flaws of the Standard Model

From a theoretical point of view, the first, and certainly the most severe design flaw of the SM is that it does not include gravity, which is described at the classical level by the theory of general relativity (GR). The Standard Model of particle physics and general relativity are two pillars

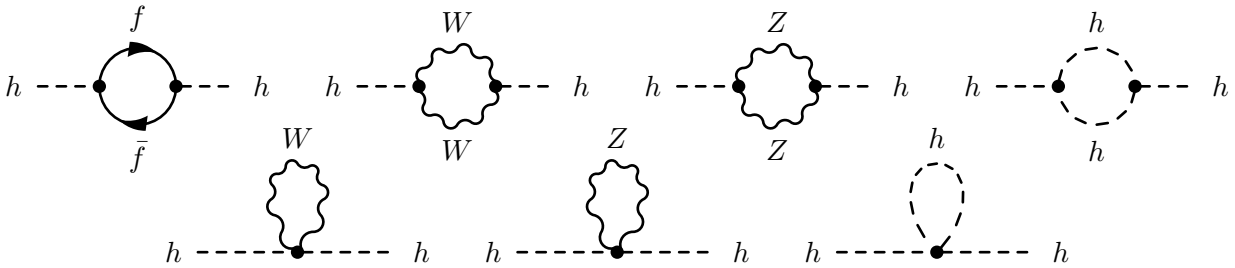


Figure 1.1: Physical contributions to the Higgs mass corrections at one-loop, in the Feynman gauge, with loops containing in order, Dirac fermions, W bosons, Z bosons, Higgs bosons, a quartic h/W coupling, a quartic h/Z coupling, and a Higgs quartic coupling.

of modern physics, yet those two pillars cannot be consistently merged into a unified picture of interactions due to their vastly different nature¹. One possibility to merge gravity with the other forces at high energies would be to formulate a quantum theory of gravity. No satisfactory answer to this problem has however been found so far. Building a quantum field theory of gravity is indeed far from being trivial, especially because such a theory is perturbatively non-renormalizable, *i.e.* loop corrections containing gravitons diverge faster and faster as the order of the perturbative series expansion increases. At TeV colliders like the LHC, quantum effects of gravity should stay out of reach², seeing that at such energy scales the strength of the gravitational interaction is much weaker than all the other ones. Yet, at energies of the order of the Planck scale $M_p \sim 10^{19}$ GeV, the strength of the gravitational force is expected to become comparable to the other ones, and thus quantum effects of gravity should become non-negligible. Due to its intrinsic inability to describe quantum effects of gravity, the Standard Model is therefore expected to break down (at least) at energies of the order of the Planck scale.

There are however other reasons to think that the Standard Model could cease to be valid even before the Planck scale. The first one is connected to the Higgs sector. In the SM, mass parameters originate from a non-vanishing vacuum expectation value (vev) of the Higgs field spontaneously breaking the electroweak symmetry $SU(2)_L \times U(1)_Y$ down to the gauge group of electromagnetism $U(1)_Q$. Experimentally, this vev is known to be approximately³ $v = 246$ GeV [37–39]. Understanding why this vev is so small compared to the Planck scale M_p of $\mathcal{O}(10^{19})$ GeV, is usually referred to as the *naturalness/hierarchy problem* in the literature [40–44].

Hierarchy problem

The hierarchy problem is widely believed to be one of the most severe conceptual issue of the Standard Model, and essentially arises when assuming that the SM is not the final theory of Nature, but rather a low-energy Effective Field Theory (EFT) of a more fundamental one emerging in between the electroweak and the Planck scale. The reason why we have a hierarchy problem in the Standard Model is deeply connected to the scalar nature of the Higgs boson. More specifically, unlike fermions and gauge bosons whose masses are respectively protected by means of chiral, and gauge symmetry, the Higgs mass is not protected from large radiative corrections by any symmetry in the SM. This lack of symmetry affecting the mass of the Higgs boson reflects itself in the fact that the latter receives radiative corrections which quadratically

¹The SM is a quantum field theory, while GR is a classical field theory.

²Assuming that known laws of gravity are valid at all scales and that the space-time remains four-dimensional. Otherwise effects of extra-dimensions could lower the scale at which quantum effects of gravity would kick in [36].

³According to our normalization conventions for the vev.

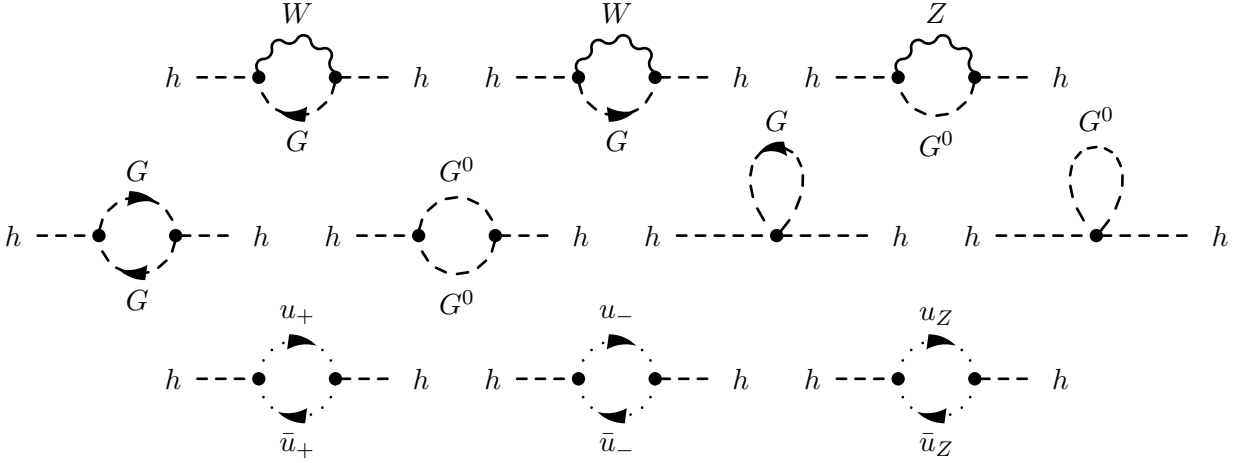


Figure 1.2: Unphysical contributions to the Higgs mass corrections at one-loop, in the Feynman gauge, with loops containing in order, W /charged Goldstone bosons, Z /neutral Goldstone bosons, charged Goldstone bosons, neutral Goldstone bosons, a quartic h/G coupling, a quartic h/G^0 coupling, charged ghosts u_{\pm} , and neutral ghosts u_Z .

depend on the cut-off/New Physics scale⁴ Λ , and thus are *naturally* of $\mathcal{O}(\Lambda^2)$. If we explicitly calculate in the broken phase the full one-loop corrections to the Higgs mass in the SM (*cf.* Fig. 1.1 and Fig. 1.2), we obtain the following expression for its quadratically divergent part⁵

$$\delta m_h^2 = \frac{3\Lambda^2}{16\pi^2 v^2} \left[2m_W^2 + m_Z^2 + m_h^2 - \sum_{f,i} \frac{4n_c^f}{3} m_{f,i}^2 \right], \quad (1.1)$$

where m_W , m_Z , m_h , $m_{f,i}$, n_c^f , v and Λ are respectively, the W boson mass, the Z boson mass, the Higgs boson mass, the fermion masses, the number of colours, the vev of the Higgs field, and the new physics scale/cut-off regulating loop-integrals in the Ultra-Violet (UV) limit. This expression matches with results already available in the literature [46,47].

The problem with (1.1) is that if Λ is significantly higher than the electroweak scale, *i.e.* if the SM remains valid up to very high scales, the $\mathcal{O}(\Lambda^2)$ corrections of δm_h^2 become particularly large, and *naturally* drive the Higgs mass to the New Physics scale Λ . This is in clear contradiction with *i)* our expectations of a $\mathcal{O}(100)$ GeV Higgs boson which stems from both theoretical reasons (such as unitarity of WW scattering), and precision measurements in the electroweak sector, *ii)* the direct observation of a 125 GeV Standard Model-like Higgs boson at the LHC. There are in principle several options at hand to stabilize the hierarchy between the electroweak and the Planck scale, and to keep the physical mass of the Higgs boson at the electroweak scale.

The first one is to enforce the cancellation of the $\mathcal{O}(\Lambda^2)$ corrections by performing a fine adjustment between the bare Higgs mass and its quadratic one-loop corrections δm_h^2 (at the level of one part in 10^{32} if $\Lambda = M_p$), so that it is *in fine* possible to recover a physical Higgs mass of $\mathcal{O}(100)$ GeV. The main problem with this first option is that there is probably too much arbitrariness in adjusting very precisely the parameters of a theory so that its predictions can match with observations. In other words, such a fortuitous and spectacular cancellation, although not logically excluded, seems highly contrived [48]. This problem is closely connected to the hierarchy problem, and usually referred to as the *fine-tuning* problem [49,50]. It should be noted for completeness that accepting the enormous amount of *fine-tuning* in the Higgs sector

⁴If we use the momentum cut-off regularization technique.

⁵Assuming a common cut-off Λ regulating both fermion and boson loops [45].

still remains a possible option. This option has been studied especially in the context of the multiverse framework (like the string theory landscape) where one assumes the existence of a vast landscape of vacua, among which one is selected according to an *anthropic principle*.

The second option at hand consists in imposing a specific relationship between masses (or dimensionless parameters) of the Standard Model in order to enforce the exact cancellation of the quadratic divergences, whatever the value of the New Physics scale Λ is. This strictly amounts to enforcing the following condition at the one-loop level in the broken phase:

$$2m_W^2 + m_Z^2 + m_h^2 - \sum_{f,i} \frac{4n_c^f}{3} m_{f,i}^2 = 0. \quad (1.2)$$

The first problem with this so-called Veltman condition [43] is that it requires at the one-loop level a ~ 315 GeV Higgs boson, which is in clear conflict with experimental data. The second problem with the Veltman condition is that it is not an all-order result, and therefore even if the Veltman condition were satisfied at the one-loop level, this would not automatically imply that the Standard Model would be two-loop natural⁶. More precisely, at all orders, the quadratically divergent Higgs mass loop corrections would take the following generic form

$$\delta m_h^2 = \Lambda^2 \sum_{n=0}^{+\infty} c_n(\lambda_i) \ln^n(\Lambda/m_h), \quad (1.3)$$

and would *de facto* require an infinite number of Veltman-like constraints of the type $c_n(\lambda_i) = 0$ to ensure the absence of quadratic divergences at all orders in perturbation theory [51]. This set of independent conditions would however vastly over constrain the value of the input parameters λ_i seeing that there would be infinitely many independent constraint equations for only a finite number of input parameters. The system of equations would hence have no solution [47], thus making the exact cancellation of quadratic divergences impossible. For complementary discussions on the Veltman condition, the reader is referred to [47, 52].

The third (and next-to-last⁷) option to stabilize the hierarchy between the electroweak and the Planck scale consists in assuming that a new symmetry would protect the Higgs mass from receiving too large radiative corrections, order by order in perturbation theory [54, 55]. Supersymmetric theories, extra-dimensions, and Little Higgs models, are precisely implementations of this very simple idea. For most of them, such theories invoke New Physics at a rather low-scale, typically $\Lambda \sim \mathcal{O}(1)$ TeV, in order to achieve the cancellation of quadratic divergences between the bare Higgs mass and the one-loop corrections with a "reasonable" amount of fine-tuning⁸. In this thesis we will exclusively focus on supersymmetric extensions of the Standard Model.

Since its original formulation in the early eighties by Susskind [41], 't Hooft [42] and Veltman [43], the *naturalness/hierarchy problem* has been one of the major guiding principles for physics Beyond the Standard Model (BSM), and most certainly remains one of the strongest motivation for New Physics at the TeV scale. It should however be kept in mind that this problem first and foremost remains a problem of æsthetical nature, and whether the *naturalness* criterion should be considered as a guiding principle for particle physics is *stricto sensu* a matter of taste. As such, it is indeed perfectly acceptable to give-up on the hierarchy problem⁹, yet it should be emphasized that choosing this option would directly imply (putting aside cosmological constraints coming

⁶Natural in the sense of Veltman, meaning that radiative corrections to a given physical observable are supposed to be of the same order (or much smaller) than the actually observed values [43].

⁷A fourth solution called cosmological relaxation which involves a QCD axion, and an inflation sector has been developed during the redaction of this manuscript, for more details see [53].

⁸A reasonable amount of fine-tuning remains a highly subjective notion though.

⁹The hierarchy problem could even be solved at the Planck scale by the same (yet unknown) mechanism in charge of solving the cosmological constant problem (which is also a fine-tuning problem).

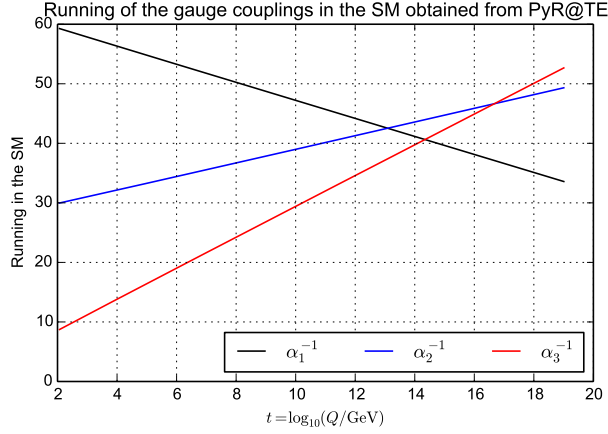


Figure 1.3: Running of gauge coupling constants α_i in the Standard Model at two-loops in PyR@TE [56], with the energy Q , and $\alpha_i^{-1} = (g_i^2/4\pi)^{-1}$. The normalization of g_1 is set to $\sqrt{5/3}$.

from dark matter relic density discussed later in this chapter) that we would have no clue on what could be the scale where New Physics would take over. As a final remark, let us just note that if the extreme sensitivity of the Higgs mass to high scales is made manifest by the cut-off regularization technique (which breaks translational and gauge invariance by the way), an equivalent result can be obtained using dimensional regularization. As a matter of fact, if we assume the existence of new heavy particles of mass M coupling to the Higgs field, the Higgs mass automatically receives from them one-loop corrections of $\mathcal{O}(M^2 \ln(M^2/\mu_R^2))$ even after having subtracted the poles at the renormalization scale μ_R . If M is then taken significantly higher than the electroweak scale, the $\mathcal{O}(M^2 \ln(M^2/\mu_R^2))$ corrections of δm_h^2 become particularly large, and once again *naturally* drive the Higgs mass to the typical scale of New Physics, namely M . So, no matter what regularization scheme we choose, the hierarchy problem still remains. Moreover, even if those new heavy particles were not directly coupling to the Higgs field, but only to SM fermions, or gauge bosons, they would most likely re-introduce the same problem at the two-loop level (and beyond).

Gauge group of the Standard Model and gauge couplings unification

Another series of reasons why the Standard Model could cease to be valid before the Planck scale actually originate from the intricate structure of the SM gauge group. The SM gauge group $SU(3)_C \times SU(2)_L \times U(1)_Y$ is a complicated and quite unnatural direct product of three different gauge groups¹⁰, where the gauge factors $SU(3)_C$ and $SU(2)_L \times U(1)_Y$ (respectively describing the strong and the electroweak interactions) are completely decoupled one from another, and quite inelegantly remain un-unified. Two comments are in order at this stage. First, if the Standard Model seems to provide an accurate description of data collected at collider-based experiments, it still does not tell us why the symmetry of the theory has to be the complicated direct product $SU(3)_C \times SU(2)_L \times U(1)_Y$, and not something simpler.

Second, if we take the values of the SM gauge couplings at low-energy, *i.e.* $\mathcal{O}(100)$ GeV, and evolve them to high energies by means of the Renormalization Group Equations (RGEs), we notice that they nearly meet at scales of $\mathcal{O}(10^{14} - 10^{16})$ GeV, as depicted in Fig. 1.3. The running of the gauge couplings may hence suggest a possible unification at high energies of the SM gauge groups into a larger symmetry group (with only one coupling constant). This apparent

¹⁰Each coming with its own energy-dependent gauge coupling.

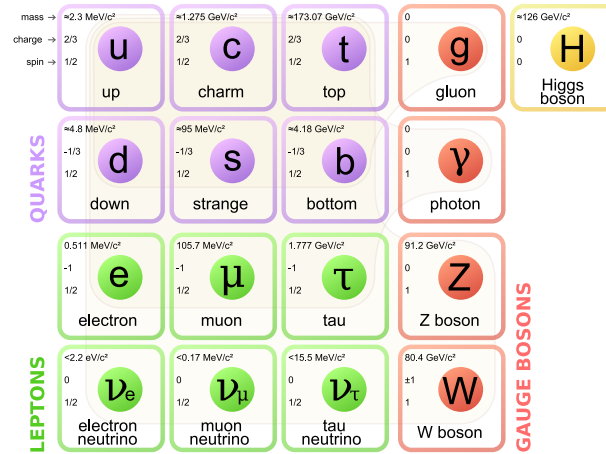


Figure 1.4: The particle content of the Standard Model re-organized in terms of the properties of its fundamental building blocks.

convergence of the SM gauge couplings at high scales might still be purely accidental, but just like the electromagnetic and weak interactions (partially) unify in the Standard Model, it is tempting to think that all gauge interactions could unify into a larger symmetry group at high energies. Such a framework is usually referred to as a Grand Unified Theory (GUT) [57–60]. Just like for the hierarchy problem, those issues related to the gauge group of the Standard Model are of æsthetical nature, and whether unification of the gauge groups should be deemed a guiding principle for New Physics is once again a matter of taste.

Flavour puzzle and mixing pattern

Besides unification and the hierarchy problem, there are also other æsthetical reasons to consider the Standard Model unsatisfactory from a conceptual point of view, especially in the fermion sector. First of all, almost all matter on Earth is made out of fermions of the first family (ν_e , e , u and d), yet laboratory experiments show that there are two additional heavier replicas of the first chiral generation, namely (ν_μ , μ , c and s) and (ν_τ , τ , t and b) [61]. The Standard Model neither accounts for the number of fermion generations, nor for the role of the heavier families. In addition, unlike gauge bosons masses which are entirely fixed by the value of the gauge couplings and the vev of the Higgs field, there are no direct predictions for the fermion masses in the Yukawa sector.

This sector actually introduces a substantial number of free parameters in the Standard Model. More specifically, out of the 26 free parameters of the SM, 12 of them are Yukawa couplings. Even worse, the SM cannot account for the large hierarchy between the Yukawa couplings which intriguingly span over six orders of magnitude (the top Yukawa coupling y_t is of $\mathcal{O}(1)$ ¹¹, while the one of the electron, y_e , is of $\mathcal{O}(10^{-6})$). Naively, we would expect all the Yukawas to be of $\mathcal{O}(1)$, experimentally this is not the case. Things are getting even worse when the SM is supplemented with massive neutrinos, inasmuch as neutrino masses are found to be extremely tiny. This peculiarity often referred to as the flavour puzzle might well stem from some new flavour dynamics coming into play at high energy scales.

In addition to the previous points, the Standard Model gives no hint on the origin of the observed mixing pattern in the Cabibbo-Kobayashi-Maskawa (CKM) [62, 63], and Pontecorvo-Maki-Nakagawa-Sakata (PMNS) matrices [34, 35]. The structure of those mixing matrices is not

¹¹It is the only *natural* Yukawa coupling of the theory.

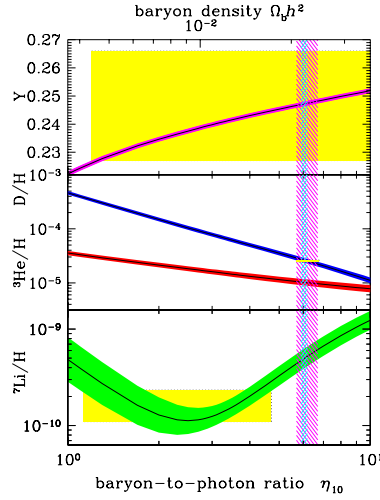


Figure 1.5: The abundances of ${}^4\text{He}$, D , ${}^3\text{He}$, and ${}^7\text{Li}$ as predicted by the Standard Model of Big-Bang nucleosynthesis. The bands show the 95% CL range. Yellow boxes indicate the observed light element abundances. The narrow vertical band indicates the Cosmic Microwave Background (CMB) measure of the cosmic baryon density (multiplied by 10^{10}), while the wider band indicates the BBN concordance range (both at 95% CL). Taken from [1].

predicted by the SM, but has to be derived from experiments, and introduces as well a substantial number of free parameters in the theory. As a matter of fact, out of the 26 free parameters of the Standard Model, 8 of them are related to the CKM and PMNS mixing matrices, $2 \times (3 \text{ angles} + 1 \text{ CP-violating phase}^{12})$. In summary, this means that out of the 26 parameters of the SM, 20 of them are related to the fermion sector, while there are only 3 free parameters in the gauge sector, namely the gauge couplings g_s , g and g' , and 2 free parameters in the Higgs sector, namely the vev v of the Higgs field, and the quartic coupling λ of the Higgs potential. The Standard Model does not explain at all why there is so much arbitrariness and so many free parameters in the Yukawa sector, and this is particularly intriguing.

1.2 Observational problems with the Standard Model

If the Standard Model of particle physics exhibits so far no statistically significant deviation from data collected at collider-based experiments, there are still facts at the astrophysical and cosmological level that the SM cannot explain in its current form, like for instance the observed imbalance between matter and anti-matter in the Universe, which is usually referred to as Baryon Asymmetry in the Universe (BAU).

Baryon Asymmetry in the Universe

Experimentally, it is observed that we are living in a matter-antimatter asymmetric world. The latest measurements performed by the Planck collaboration [64, 65] are consistent with the ones obtained from WMAP [66], and Big Bang Nucleosynthesis (BBN) (*cf.* Fig.1.5), and confirm the existence of a tiny excess of matter over antimatter. The most up-to-date value for the baryon-to-photon ratio η obtained from [65] reads as follows

$$\eta = \frac{n_B - n_{\bar{B}}}{n_\gamma} = (6.0965 \pm 0.0439) \times 10^{-10}, \quad (1.4)$$

¹²One CP-violating phase if neutrinos are Dirac fermions, three if they are Majorana fermions.

where n_B , $n_{\bar{B}}$, and n_γ are the number densities of baryons, antibaryons, and CMB photons respectively. It is thus widely accepted that at least the observable part of our Universe must have developed an excess of particles over anti-particles at some point in the cosmological history [67]. One possible mechanism for generating this BAU is called ElectroWeak Baryogenesis (EWBG) [68, 69]. This mechanism aims at dynamically generating a net baryon asymmetry during the Electroweak Phase Transition (EWPT), starting out from a baryon symmetric universe¹³.

A successful baryogenesis requires three necessary ingredients often referred to as the Sakharov conditions [70]. These conditions are *i*) baryon number violation (BNV) *ii*) C and CP violation *iii*) departure from thermal equilibrium. All three ingredients are (in principle) already present in the Standard Model.

The first criterion is possibly fulfilled thanks to non-perturbative processes called sphalerons [71–73]. Sphalerons are static saddle-points solutions to the classical $SU(2)_L$ field equations, sitting at the top of the configuration ridge between degenerate electroweak vacua. Those processes allow for transition between topologically different $SU(2)_L$ vacua [74], violate $B + L$, and conserve $B - L$. More specifically, sphalerons violate baryon and lepton number by 3 units,

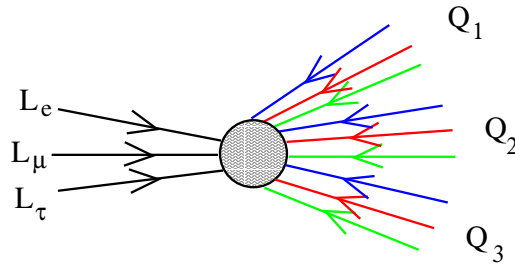


Figure 1.6: Sphaleron process. The quantum numbers of the initial state are $L = 3$ and $B = 0$. The quantum numbers of the final state are $L = 0$, $B = -3$. Taken from [68].

and amount to converting three left-handed leptons (one from each generation), into nine left-handed antiquarks (one from each generation, each of them coming in three different colours) as depicted in Fig. 1.6. These processes have so far never been observed experimentally, because at zero temperature their rates are expected to be exponentially suppressed. However at higher temperatures, sphalerons could play a significant role [75], inasmuch as the thermal energy available could potentially ease transitions between degenerate vacua by allowing the system to overcome the associated energy barriers instead of just proceeding through quantum tunnelling (see [76, 77] and references therein).

The second criterion could be fulfilled thanks to the CP-violating phase of the CKM matrix, which is usually considered as the only source of CP violation in the Standard Model (without massive neutrinos). The amount of CP violation of a given theory is usually quantized in a phase-convention-independent way by means of the following invariant

$$J_{CP} = \prod_{q_u \in \{u, c, t\} > q'_u} (m_{q_u}^2 - m_{q'_u}^2) \prod_{q_d \in \{d, s, b\} > q'_d} (m_{q_d}^2 - m_{q'_d}^2) \text{Im}(V_{ii}V_{jj}V_{ij}^*V_{ji}^*) \quad \text{with } i \neq j, \quad (1.5)$$

where $\text{Im}(V_{ii}V_{jj}V_{ij}^*V_{ji}^*)$ is the Jarlskog invariant, also noted J [78], which is defined such that

$$J = c_{12}c_{23}c_{13}^2 s_{12}s_{23}s_{13} \sin \delta_{KM} \quad \text{with} \quad \text{Im}(V_{ij}V_{kl}V_{ik}^*V_{jl}^*) = J \sum_{m,n} \epsilon_{ikm} \epsilon_{jln}. \quad (1.6)$$

Normalizing J_{CP} over the typical critical temperature of the EWPT, namely $T_c = 100$ GeV, one

¹³Any pre-existing baryon asymmetry would be erased in a scenario including an inflationary epoch.

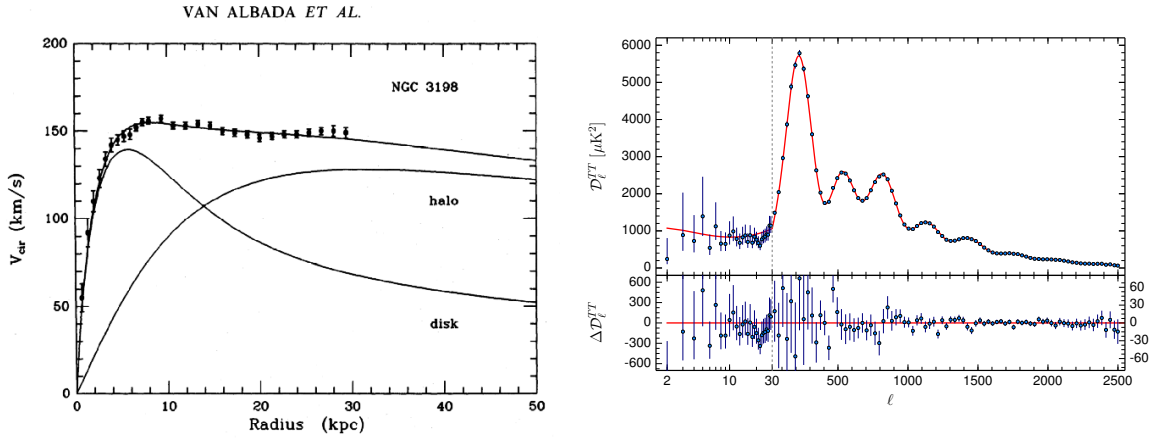


Figure 1.7: Left: Rotation curve of NGC 3198. The line marked “disk” shows the expected rotation curve if the only mass in the galaxy were that in the visible stars. The line marked “halo” corresponds to the rotation curve of the extra dark matter halo only (the two curves are not additive). Taken from [82]. Right: The Planck 2015 temperature power spectrum of the CMB. Taken from [65].

obtains the following dimensionless quantity d_{CP}

$$d_{CP} = \frac{J_{CP}}{T_c^{12}} \sim 10^{-19}, \quad (1.7)$$

which gives a rough estimate of the amount of CP-violation induced by the CKM complex phase, and has to be compared with the measured baryon-to-photon ratio η of (1.4). Comparing (1.4) to (1.7), it appears that CP-violation in the Standard Model is too weak (by nine orders of magnitude) to explain the measured baryon-to-photon ratio. New sources of CP-violation hence seem to be required to correctly describe data.

The third and last criterion, namely departure from thermal equilibrium, is possibly provided by a strongly first-order Electroweak Phase Transition. Lattice calculations however show that a strongly first order phase transition requires a Higgs mass below 75 GeV [79–81], which is at odds with present observations. For a 125 GeV Standard Model-like Higgs boson, only a cross-over between the broken and the unbroken phase is possible. Consequently bubbles of broken phase cannot nucleate within the symmetric phase, no loss of thermal equilibrium is possible, and hence no net baryon asymmetry can ever be transmitted to the broken phase. So either New Physics has to increase the value of the Higgs mass up to which a strongly first-order phase transition is still allowed, or some alternative mechanism has to generate BAU.

Dark matter

More data supporting the idea that the Standard Model is not the ultimate theory of Nature comes from astrophysics, with the so-called Dark Matter problem. The first experimental hint pointing toward the existence of Dark Matter (DM) goes back to a study of Fritz Zwicky in 1933 related to dispersion velocities of galaxies within the Coma cluster [83]. In this study, Zwicky pointed out the fact that the outer members of the Coma clusters were moving significantly faster than expected from predictions of classical Newtonian dynamics, by showing that the gravitational mass of the cluster¹⁴ was $\mathcal{O}(100)$ times larger than its luminous mass. One

¹⁴Zwicky assumed pure gravitational interactions described by Newton’s theory, and then employed the Virial theorem to infer the gravitational mass of the Coma cluster from dispersion velocities of the various galaxies.

interpretation of this "missing mass" (without which the cluster would be torn apart) made by Zwicky was that there could exist some kind of non-luminous matter (hence its name Dark Matter), interacting only gravitationally, which would constitute the main component of the mass of the cluster, and would ensure its integrity. More than forty years later, a similar behaviour was also observed at galactic scales in a series of studies [82, 84] conducted on rotation curves of stars within isolated galaxies. In those studies, it was shown that stars residing in the outermost regions of the galaxy were also experiencing strong deviations from predictions of Newtonian gravity as can be seen in Fig.1.7 on the left-hand panel. The velocity of stars in those regions indeed seemed to be almost constant, no matter how far they were from the galactic center, which was (and is still) in clear contradiction with the luminous matter disk profile exhibiting a $1/\sqrt{r}$ suppression at large radius r . Once again assuming that standard laws of gravity were valid at galactic scales, Rubin *et al.* suggested in [84] that such a startling feature could be explained by a missing mass taking the form of a dark matter halo. As depicted on Fig.1.7, it indeed seems that adding an hypothetical DM halo component to luminous matter produces a curve whose shape and normalization perfectly fits to experimental data.

At the astrophysical and cosmological scales, there are still several other experimental facts supporting the existence of Dark Matter, such as large scale structure formation, current observations in the Bullet Cluster, as well as CMB fluctuations (see right-panel of Fig. 1.7). The latest results obtained by the Planck collaboration [65], which originate from a combination of various cosmological observations, give the following hypothetical cold dark matter relic density

$$\Omega_c h^2 = 0.1188 \pm 0.0010, \quad (1.8)$$

where h is the reduced Hubble constant. This energy density represents approximately 25% of the energy content of the Universe, and is five times bigger than the contribution of the ordinary baryonic matter $\Omega_b h^2 = 0.02230 \pm 0.00014$. The main problem is that the Standard Model does not provide any Dark Matter candidate with the desired properties, and therefore New Physics seems to be required.

1.3 Organization of the thesis

If the previous arguments are the main motivations for Beyond the Standard Model (BSM) physics, it should however be noted for completeness, that other reasons, such as the strong-CP problem [85], also exist, yet for brevity they are not reviewed in the present manuscript. Among all the possible BSM theories available in the literature, we consider in this thesis (almost) exclusively supersymmetric extensions of the Standard Model, and more specifically concentrate on the phenomenology of $\mathcal{N} = 1$ supersymmetric theories¹⁵, for which we provide theoretical predictions at leading order (LO), and next-to-leading order (NLO) in perturbation theory, at polarized and unpolarized hadron colliders. The manuscript is organized as follows:

In Chapter 2, we provide a short introduction to $\mathcal{N} = 1$ supersymmetry (SUSY), in which we first recall some basic facts about SUSY (history, motivations, superalgebra and properties of the supermultiplets), before introducing the superspace formalism and detailing the various steps inherent to the construction of supersymmetric Lagrangians. In the second part of this chapter, we focus on one particular implementation of $\mathcal{N} = 1$ supersymmetry, namely the Minimal Supersymmetric Standard Model (MSSM), which is repeatedly used in this manuscript, and fix the notations and conventions used in the rest of the thesis.

¹⁵Supersymmetric extensions of the Standard Model with $\mathcal{N} \geq 2$ are not considered here, because in the latter left- and right-handed fermions are part of the same supermultiplet. Left- and right-handed fermions have consequently the same interactions, and therefore parity violation is not allowed in such theories.

Chapter 3 is based on [86], in which we show how the availability of (longitudinally) polarized beams at high-energy proton-proton colliders could help us to disentangle various BSM scenarios with the same final-state signature. In this tree-level phenomenological study, we first discuss in a model-independent way how this discriminating power arises from the differences between polarized and unpolarized parton distribution functions. We then demonstrate how polarized beams allow one not only to disentangle different production mechanisms giving the same final-state signature, but also to obtain information on the parameters of the hypothetical new physics sector of the theory. This is illustrated in the case of a particular class of scenarios leading to monotop production, which corresponds to the production of a top quark in association with missing transverse energy (\cancel{E}_T). We consider three specific models that could produce a monotop signature (one being the MSSM with R -parity violation) in unpolarized proton collisions, and show how they could be distinguished by means of single- and double-spin asymmetries in polarized collisions. Our results are presented for both the Large Hadron Collider operating at a center-of-mass energy of 14 TeV and a recently proposed Future Circular Collider (FCC) assumed to collide protons at a center-of-mass energy of 100 TeV.

Chapter 4 consists of a brief introduction to one-loop calculation techniques. In this chapter, we first recall the various challenges of NLO calculations, before providing a constructive (and mathematically consistent) definition of both Dimensional Regularization (DREG), and Dimensional Reduction (DRED)¹⁶. Then, we detail how to evaluate scalar integrals that are frequently encountered in the context of one-loop calculations, and introduce the Passarino-Veltman reduction scheme designed to decompose vector and tensor loop integrals into linear combinations of simpler scalar integrals multiplied by Lorentz invariants. The last part of chapter 4 is dedicated to the procedure of renormalization, which primarily aims at absorbing UV divergences into the redefinition of all the bare fields and parameters of the original tree-level Lagrangian.

In Chapter 5, we apply the concepts reviewed in the previous chapter to the case of squark-antisquark pair production at next-to-leading order in SUSY-QCD with Non-Minimal Flavour Violation (NMFV), which has never been investigated before. In the first part of this chapter, we detail the field content of the model, give the analytical expression of the tree-level matrix element, and define the set-up employed to renormalize the theory at the one-loop level. In the second part of this chapter, we concentrate on the derivation of the self-energies and vertex corrections, and provide the analytical expression of all the Renormalization Constants (RCs) that are needed for the process of our interest. In the third part of this chapter, we briefly discuss the box contributions, and provide a short report on the status of this on-going calculation [87].

In Chapter 6, which is based on [88] and [89], we present for the first time the full automation of collider predictions matched with parton showers at the next-to-leading accuracy in QCD within non-trivial extensions of the Standard Model. As an application, we explore scenarios beyond the Standard Model, where new coloured scalar (stops and sgluons), and Majorana particles (gluinos) can be pair produced in hadron collisions. Using simplified models to describe the new field interactions with the Standard Model, we present precision predictions for the LHC within the MADGRAPH5_aMC@NLO framework.

Finally, in Chapter 7, we draw our conclusions and provide a short outlook. Note that some technical details are relegated to the appendices.

¹⁶A variant of DREG designed for supersymmetric theories

Chapter 2

Supersymmetry

Supersymmetric theories were not originally designed to solve any of the problems mentioned in the previous chapter. They were constructed out of theoretical and æsthetical considerations in the early seventies [90–96], and initially constituted an attempt to merge external and internal symmetries into a larger symmetry group. It was only found later on that SUSY could address a certain number of the Standard Model shortcomings. More than forty years after the seminal work of Wess and Zumino, supersymmetry is now one of the most studied extensions of the Standard Model, and is extensively searched for at the LHC [97,98]. In this chapter, we provide a short introduction to $\mathcal{N} = 1$ supersymmetry, and focus more specifically on one of its most popular implementations, namely the Minimal Supersymmetric Standard Model (MSSM).

2.1 Motivations

The starting point for supersymmetry goes back to 1967 with the formulation of the Coleman-Mandula "no-go" theorem [99], which demonstrates the impossibility of combining external (space-time) and internal (gauge) symmetries in any but a trivial way, *i.e.* symmetries of the S -matrix must be isomorphic to a direct product of the Poincaré group $ISO(1,3)$ with any compact gauge group G_{int} . The story of supersymmetry would have stopped there if it was not for the fact that the Coleman-Mandula theorem only holds for Lie algebras with the commutator as a bilinear operation. Haag, Lopuzanski and Sohnius found a way to bypass the previous restriction [96] by considering graded Lie algebras, which naturally include fermionic (anticommuting) generators Q that can turn bosons into fermions and the other way around

$$Q |\text{Boson}\rangle = |\text{Fermion}\rangle, \quad Q |\text{Fermion}\rangle = |\text{Boson}\rangle. \quad (2.1)$$

The fact that supersymmetry is the only known non-trivial extension of the Poincaré group in four dimensions is *per se* not a motivation, but still remains one of its major theoretical assets. As we are going to see now however, there exist other reasons to study supersymmetry.

As mentioned in the previous chapter when reviewing the hierarchy problem, a theory with fundamental scalars should at least include a symmetry which protects them from large radiative corrections. One symmetry that can play such a role is supersymmetry. In supersymmetry, each Standard Model Weyl fermion is paired with a complex scalar superpartner coupling to the Higgs with a strength $\lambda_{\tilde{f}}$. The hierarchy problem is solved in this context by exploiting the fact that fermion and boson loop contributions have opposite signs. More specifically, if the couplings of the fermions and the scalars are related by supersymmetry such that $\lambda_{\tilde{f}} = |\lambda_f|^2$, the quadratic UV divergences of Fig. 2.1 then exactly cancel one against the other, leaving only sub-leading logarithmic corrections. If the masses of the scalar superpartners are moreover not

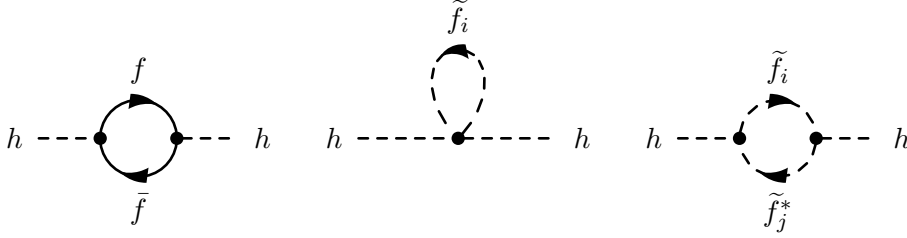


Figure 2.1: Representative Feynman diagrams contributing to δm_h^2 at the one-loop level. The loops contain in order Dirac fermions f , and their supersymmetric partners \tilde{f} .

too large, *i.e.* in the TeV range, the logarithmic corrections also remain small, and it is then possible to keep the physical mass of the Higgs boson at the electroweak scale without too much fine-tuning.

In the previous chapter we have seen that gauge couplings do not unify at high energies in the SM. In the MSSM however this unification seems possible around 10^{16} GeV (*cf.* Fig. 2.2), and is completely natural, meaning here that the model is not tailored to possess this feature, which is genuinely due to the fact that the SUSY particles modify the RGEs of the theory.

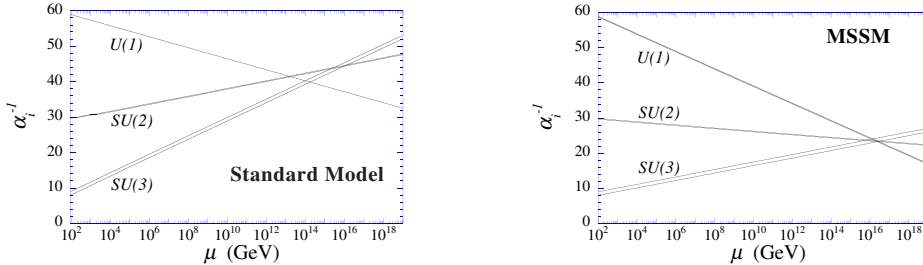


Figure 2.2: Running of gauge coupling constants α_i in the Standard Model and in the MSSM, at the one-loop level, and with $\alpha_i^{-1} = (g_i^2/4\pi)^{-1}$ [100].

At last, but not least, supersymmetric theories with conserved R -parity (which will be introduced in detail in section 2.7 when discussing the MSSM) also provide a good candidate for Dark Matter as the Lightest Supersymmetric Particle (LSP) appears in this case to be completely stable.

2.2 Supersymmetric algebra

An $\mathcal{N} = 1$ supersymmetric algebra consists of a \mathbb{Z}_2 -graded vector space $\mathfrak{g} = \mathfrak{g}_0 \oplus \mathfrak{g}_1$, which is spanned by the generators of the Poincaré and the internal symmetry algebra for its bosonic part $\mathfrak{g}_0 = \mathfrak{iso}(1, 3) \times \mathfrak{g}_{\text{int}}$, and by one Majorana spinor, $\mathfrak{g}_1 = \{Q_\alpha, \alpha = 1, 2\} \oplus \{\bar{Q}_{\dot{\alpha}}, \dot{\alpha} = 1, 2\}$, for its fermionic part. The supercharges Q_α and $\bar{Q}_{\dot{\alpha}}$ are left- and right-handed Weyl spinors, and respectively lie in the $(\mathbf{2}, \mathbf{1})$ and $(\mathbf{1}, \mathbf{2})$ representation of the Lorentz algebra. The $\mathcal{N} = 1$ supersymmetry algebra reads as follows

$$\begin{aligned}
 [M^{\mu\nu}, M^{\rho\sigma}] &= i(-\eta^{\mu\rho}M^{\nu\sigma} + \eta^{\mu\sigma}M^{\nu\rho} + \eta^{\nu\rho}M^{\mu\sigma} - \eta^{\nu\sigma}M^{\mu\rho}) \\
 [M^{\mu\nu}, P^\rho] &= i(\eta^{\nu\rho}P^\mu - \eta^{\mu\rho}P^\nu); \quad [P^\mu, P^\nu] = 0 \\
 [Q_\alpha, M^{\mu\nu}] &= (\sigma^{\mu\nu})_\alpha{}^\beta Q_\beta; \quad [\bar{Q}_{\dot{\alpha}}, M^{\mu\nu}] = (\bar{\sigma}^{\mu\nu})^{\dot{\alpha}}{}_{\dot{\beta}} \bar{Q}^{\dot{\beta}} \\
 [P^\mu, Q_\alpha] &= 0; \quad [P^\mu, \bar{Q}_{\dot{\alpha}}] = 0 \\
 \{Q_\alpha, \bar{Q}_{\dot{\alpha}}\} &= 2\sigma_{\alpha\dot{\alpha}}^\mu P_\mu; \quad \{Q_\alpha, Q_\beta\} = 0; \quad \{\bar{Q}_{\dot{\alpha}}, \bar{Q}_{\dot{\beta}}\} = 0 \\
 [T^a, T^b] &= i f^{abc} T^c; \quad [T^a, P^\mu] = 0; \quad [T^a, M^{\mu\nu}] = 0,
 \end{aligned} \tag{2.2}$$

where T^a , $M^{\mu\nu}$ and P^μ are the generators of the internal, and the Poincaré symmetry group.

Representations of the Poincaré superalgebra

In this section we recall some basic properties of the supermultiplets in $\mathcal{N} = 1$ supersymmetry.

1. All the particles belonging to the same irreducible supermultiplet must have exactly the same mass. This statement is a direct consequence of the fact that $P_\mu P^\mu = m^2$ is a Casimir operator, *i.e.* it commutes with every single generator of the Poincaré superalgebra. Irreducible representations of the Poincaré superalgebra are characterized by the eigenvalues of the Casimir operators. Therefore, all the members of the same supermultiplet must have the same mass.
2. Supermultiplets contain an equal number of bosonic and fermionic degrees of freedom. From (2.2), we can see that irreducible representations in SUSY contain both fermionic and bosonic degrees of freedom (*dofs*). Let us consider a finite dimensional representation of the supersymmetry algebra, and introduce a fermion number operator such that the latter takes eigenvalues $+1$ and -1 for bosons and fermions respectively

$$(-1)^N |B\rangle = |B\rangle, \quad (-1)^N |F\rangle = -|F\rangle. \quad (2.3)$$

From (2.3), we obtain

$$\begin{aligned} Q_\alpha (-1)^N |F\rangle &= -|B\rangle & Q_\alpha (-1)^N |B\rangle &= |F\rangle \\ -(-1)^N Q_\alpha |F\rangle &= -|B\rangle & -(-1)^N Q_\alpha |B\rangle &= |F\rangle, \end{aligned}$$

and thus deduce that

$$Q_\alpha (-1)^N = -(-1)^N Q_\alpha. \quad (2.4)$$

If we now calculate

$$\begin{aligned} \text{Tr} \left((-1)^N \{Q_\alpha, \bar{Q}_{\dot{\alpha}}\} \right) &\stackrel{(2.4)}{=} \text{Tr} \left(-Q_\alpha (-1)^N \bar{Q}_{\dot{\alpha}} + Q_\alpha (-1)^N \bar{Q}_{\dot{\alpha}} \right) = 0 \\ \text{Tr} \left((-1)^N \{Q_\alpha, \bar{Q}_{\dot{\alpha}}\} \right) &= 2\sigma_{\alpha\dot{\alpha}}^\mu P_\mu \text{Tr} \left((-1)^N \right), \end{aligned}$$

we obtain the following equality

$$0 = \text{Tr} \left((-1)^N \right) = \sum_{n_B=0}^{n_B} \langle B | (-1)^N | B \rangle + \sum_{n_F=0}^{n_F} \langle F | (-1)^N | F \rangle = n_B - n_F,$$

which proves that

$$n_B = n_F. \quad (2.5)$$

Supermultiplets must therefore contain an equal number of fermionic and bosonic *dofs*.

3. A particle and its superpartner within a supermultiplet have different spins. The Pauli-Lubanski operator W_μ is defined such that

$$W_\mu = \frac{1}{2} \varepsilon_{\mu\nu\rho\sigma} P^\nu M^{\rho\sigma}. \quad (2.6)$$

This operator commutes with all the generators of the Poincaré superalgebra but the fermionic generators Q_α , and $\bar{Q}^{\dot{\alpha}}$, as can be seen from (2.2) with the non-zero commutators

$$[Q_\alpha, M^{\mu\nu}] = (\sigma^{\mu\nu})_\alpha{}^\beta Q_\beta, \quad \text{and} \quad [\bar{Q}^{\dot{\alpha}}, M^{\mu\nu}] = (\bar{\sigma}^{\mu\nu})^{\dot{\alpha}}{}_{\dot{\beta}} \bar{Q}^{\dot{\beta}}. \quad (2.7)$$

The Pauli-Lubanski operator is therefore not a Casimir operator of the SUSY algebra, and thus all the members of a given supermultiplet are not required to have the same spin.

2.3 Superspace formalism and superfields

In the previous section, we have seen that supersymmetric transformations alter the spin of the fields on which they act, and hence can turn bosons into fermions, and the other way around. For practical purpose (compact notations and easier calculations), it seems particularly desirable to embed all the fields belonging to the same supermultiplet into a single object which manifestly preserves supersymmetry. Such an object is called a superfield. A superfield is a function which lives in a non-trivial extension of the ordinary space-time not only comprising the usual space-time coordinates but also a set of new anticommuting spinor coordinates, called Grassmann variables. Those Grassmann variables transform as two-component Weyl spinors with opposite chirality, and form a Majorana spinor labeled $(\theta, \bar{\theta})$. The standard Minkowski space augmented with fermionic coordinates is called the superspace. A superfield is a function which explicitly depends on the superspace coordinates, and can always be expanded as a Taylor series with respect to θ and $\bar{\theta}$. All terms of this series containing more than two powers of θ and $\bar{\theta}$ vanish. A generic scalar superfield Φ_g thus contains only a finite number of terms, and reads as follows

$$\begin{aligned} \Phi_g(x, \theta, \bar{\theta}) = & \phi(x) + \theta.\psi(x) + \bar{\theta}.\bar{\varphi}(x) + \theta.\theta f(x) + \bar{\theta}.\bar{\theta}g(x) + \theta\sigma^\mu\bar{\theta}v_\mu(x) \\ & + \theta.\theta\bar{\theta}.\bar{\theta}\zeta(x) + \bar{\theta}.\bar{\theta}\theta.\theta\xi(x) + \theta.\theta\bar{\theta}.\bar{\theta}d(x), \end{aligned} \quad (2.8)$$

where ϕ, f, g and d are complex scalar fields, $\psi, \bar{\varphi}, \bar{\zeta}$ and ξ are complex Weyl fermions, and v_μ is a complex vector field. The fields $\phi, f, g, d, \psi, \bar{\varphi}, \bar{\zeta}, \xi$, and v_μ form a supermultiplet and are the so-called component fields of the superfield Φ_g . At this level, two comments are in order. First, in (2.8) we have only considered the case where Φ_g is a scalar superfield. Superfields can however carry a Lorentz, or a spinor index, as we will see later in this chapter. Second, the generic scalar superfield Φ_g of (2.8) gives rise to a large number of degrees of freedom, 32 in total (16 for its bosonic part and 16 for its fermionic part). This number is too large to match with the one expected from an irreducible representation of a $\mathcal{N} = 1$ supersymmetry algebra. Not all the component fields of (2.8) are thus necessary to build an irreducible supermultiplet, and therefore additional constraints are needed to reduce the number of component fields.

2.4 Supersymmetric transformations

Before constraining the superfield of (2.8), it is first necessary to define the action of the SUSY generators in the superspace. The key idea motivating the use of the superspace formalism is to represent supersymmetric transformations as generalized translations. Since P_μ is associated to the usual space-time coordinates x_μ , it seems reasonable to associate the supercharges $(Q_\alpha, \bar{Q}^{\dot{\alpha}})$ to the Grassmanian coordinates $(\theta^\alpha, \bar{\theta}_{\dot{\alpha}})$. Any point of the superspace is then parameterized by

$$G(x, \theta, \bar{\theta}) = e^{i(x^\mu P_\mu + \theta.Q + \bar{Q}.\bar{\theta})}. \quad (2.9)$$

Knowing that

$$\begin{aligned} [\theta.Q + \bar{Q}.\bar{\theta}, \epsilon.Q + \bar{Q}.\bar{\epsilon}] &= [\cancel{\theta.Q, \epsilon.Q}] + [\theta.Q, \bar{Q}.\bar{\epsilon}] + [\bar{Q}.\bar{\theta}, \epsilon.Q] + [\cancel{\bar{Q}.\bar{\theta}, \bar{Q}.\bar{\epsilon}}] \\ &= \theta^\alpha \{Q_\alpha, \bar{Q}_{\dot{\beta}}\} \bar{\epsilon}^{\dot{\beta}} - \epsilon^\beta \{Q_\beta, \bar{Q}_{\dot{\alpha}}\} \bar{\theta}^{\dot{\alpha}} = -2i(\epsilon\sigma^\mu\bar{\theta} - \theta\sigma^\mu\bar{\epsilon})\partial_\mu, \end{aligned}$$

where ϵ^α and $\bar{\epsilon}^{\dot{\alpha}}$ are spinorial parameters, and then using the Campbell-Baker-Hausdorff identity, the most general supersymmetric transformation acting on the right reads as follows

$$\begin{aligned} G(x, \theta, \bar{\theta}) G(0, \epsilon, \bar{\epsilon}) &= e^{i(x^\mu P_\mu + \theta.Q + \bar{Q}.\bar{\theta})} e^{i(\epsilon.Q + \bar{Q}.\bar{\epsilon})} \\ &= e^{i(x^\mu P_\mu + (\theta+\epsilon).Q + \bar{Q}.\bar{(\theta+\bar{\epsilon})}) + \frac{i}{2}[\theta.Q + \bar{Q}.\bar{\theta}, \epsilon.Q + \bar{Q}.\bar{\epsilon}]} \\ &= e^{i(x^\mu - i(\epsilon\sigma^\mu\bar{\theta} - \theta\sigma^\mu\bar{\epsilon}))P_\mu + i(\theta+\epsilon).Q + i\bar{Q}.\bar{(\theta+\bar{\epsilon})}}. \end{aligned}$$

The infinitesimal supersymmetric transformations acting on the right are therefore given by

$$\delta_R x^\mu = -i(\epsilon \sigma^\mu \bar{\theta} - \theta \sigma^\mu \bar{\epsilon}), \quad \delta_R \theta^\alpha = \epsilon^\alpha, \quad \delta_R \bar{\theta}^{\dot{\alpha}} = \bar{\epsilon}^{\dot{\alpha}}. \quad (2.10)$$

In a very similar manner, one can compute the effects of a supersymmetric transformation acting on the left. One eventually obtains

$$\delta_L x^\mu = i(\epsilon \sigma^\mu \bar{\theta} - \theta \sigma^\mu \bar{\epsilon}), \quad \delta_L \theta^\alpha = \epsilon^\alpha, \quad \delta_L \bar{\theta}^{\dot{\alpha}} = \bar{\epsilon}^{\dot{\alpha}}. \quad (2.11)$$

Until now, we have made a heavy use of the operator formalism, yet we still have to project the supercharges $Q_{L,R\alpha}$ and $\bar{Q}_{L,R\dot{\alpha}}$ (mass dimension 1/2) on a suitable basis, so that we can associate to these operators a differential representation. In the previous section, we have seen that any point in the superspace is parameterized by the coordinates $X = (x^\mu, \theta, \bar{\theta})$. A natural choice thus consists in parameterizing the differential representation in terms of the supercoordinates

$$Q_{L,R\alpha} = a_{L,R\alpha}^\mu \partial_\mu + b_{L,R} \frac{\partial}{\partial \theta^\alpha} + c_{L,R\alpha\dot{\alpha}} \frac{\partial}{\partial \bar{\theta}^{\dot{\alpha}}}, \quad (2.12)$$

$$\bar{Q}_{L,R\dot{\alpha}} = \bar{a}_{L,R\dot{\alpha}}^\mu \partial_\mu + \bar{b}_{L,R} \frac{\partial}{\partial \bar{\theta}^{\dot{\alpha}}} + \bar{c}_{L,R\dot{\alpha}\alpha} \frac{\partial}{\partial \theta^\alpha}. \quad (2.13)$$

Note that for convenience, we will now use the abbreviations $\bar{\partial}^{\dot{\alpha}}$ and ∂_α for $\partial/\partial \bar{\theta}^{\dot{\alpha}}$ and $\partial/\partial \theta^\alpha$ respectively. Recalling moreover that ∂_μ has mass-dimension 1, and that ∂_α and $\bar{\partial}_{\dot{\alpha}}$ have mass-dimension 1/2, we conclude that $b_{L,R}$, $\bar{b}_{L,R}$, $c_{L,R\alpha\dot{\alpha}}$ and $\bar{c}_{L,R\dot{\alpha}\alpha}$ must be dimensionless, while $a_{L,R\alpha}^\mu$ and $\bar{a}_{L,R\dot{\alpha}}^\mu$ must have dimension $-1/2$. The latter coefficients take the form

$$a_{L,R\alpha}^\mu = a_{L,R}(\sigma^\mu)_{\alpha\dot{\alpha}} \bar{\theta}^{\dot{\alpha}}, \\ \bar{a}_{L,R\dot{\alpha}}^\mu = \bar{a}_{L,R} \theta^\alpha (\sigma^\mu)_{\alpha\dot{\alpha}}.$$

Using (2.10) to constrain the right-handed supercharges, we have

$$\delta_R x^\mu = i(\epsilon^\alpha Q_{R\alpha} + \bar{Q}_{R\dot{\alpha}} \bar{\epsilon}^{\dot{\alpha}}) x^\mu = i a_{R\alpha} \epsilon^\alpha \sigma_{\alpha\dot{\alpha}}^\mu \bar{\theta}^{\dot{\alpha}} + i \bar{a}_{R\dot{\alpha}} \theta^\alpha \sigma_{\alpha\dot{\alpha}}^\mu \bar{\epsilon}^{\dot{\alpha}} = -i(\epsilon \sigma^\mu \bar{\theta} - \theta \sigma^\mu \bar{\epsilon}), \quad (2.14)$$

$$\delta_R \theta^\alpha = i(b_R \epsilon^\beta \partial_\beta + \bar{c}_{R\dot{\beta}}^\beta \partial_\beta \bar{\epsilon}^{\dot{\beta}}) \theta^\alpha = \epsilon^\alpha, \quad (2.15)$$

$$\delta_R \bar{\theta}^{\dot{\alpha}} = i(\bar{b}_R \bar{\partial}_{\dot{\beta}} \bar{\epsilon}^{\dot{\beta}} + \epsilon^\beta c_{R\beta\dot{\beta}} \bar{\partial}^{\dot{\beta}}) \bar{\theta}^{\dot{\alpha}} = \bar{\epsilon}^{\dot{\alpha}}, \quad (2.16)$$

which gives

$$a_R = -1, \quad b_R = -i, \quad c_{R\dot{\beta}}^{\dot{\beta}} = 0, \quad (2.17)$$

$$\bar{a}_R = 1, \quad \bar{b}_R = i, \quad \bar{c}_{R\dot{\beta}}^{\dot{\beta}} = 0, \quad (2.18)$$

and as a consequence of what we obtain

$$Q_{R\alpha} = -i(\partial_\alpha - i \sigma_{\alpha\dot{\alpha}}^\mu \bar{\theta}^{\dot{\alpha}} \partial_\mu), \quad \bar{Q}_{R\dot{\alpha}} = -i(-\bar{\partial}_{\dot{\alpha}} + i \theta^\alpha \sigma_{\alpha\dot{\alpha}}^\mu \partial_\mu).$$

Analogously, one can compute the left-handed charges using the constraints (2.11). This gives

$$Q_{L\alpha} = -i(\partial_\alpha + i \sigma_{\alpha\dot{\alpha}}^\mu \bar{\theta}^{\dot{\alpha}} \partial_\mu), \quad \bar{Q}_{L\dot{\alpha}} = i(\bar{\partial}_{\dot{\alpha}} + i \theta^\alpha \sigma_{\alpha\dot{\alpha}}^\mu \partial_\mu).$$

Defining $Q = Q_L$, $\bar{Q} = \bar{Q}_L$, $D = iQ_R$, and $\bar{D} = -i\bar{Q}_R$, where D_α , and $\bar{D}_{\dot{\alpha}}$ are spinorial covariant derivatives (also called superderivatives), one obtains

$$Q_\alpha = -i(\partial_\alpha + i \sigma_{\alpha\dot{\alpha}}^\mu \bar{\theta}^{\dot{\alpha}} \partial_\mu), \quad \bar{Q}_{\dot{\alpha}} = i(\bar{\partial}_{\dot{\alpha}} + i \theta^\alpha \sigma_{\alpha\dot{\alpha}}^\mu \partial_\mu), \quad (2.19)$$

$$D_\alpha = \partial_\alpha - i \sigma_{\alpha\dot{\alpha}}^\mu \bar{\theta}^{\dot{\alpha}} \partial_\mu, \quad \bar{D}_{\dot{\alpha}} = \bar{\partial}_{\dot{\alpha}} - i \theta^\alpha \sigma_{\alpha\dot{\alpha}}^\mu \partial_\mu, \quad (2.20)$$

for which we have

$$\{Q_\alpha, D_\beta\} = \{Q_\alpha, \bar{D}_\beta\} = \{\bar{Q}_\alpha, D_\beta\} = \{\bar{Q}_\alpha, \bar{D}_\beta\} = 0, \quad (2.21)$$

$$\{Q_\alpha, Q_\beta\} = \{D_\alpha, D_\beta\} = \{\bar{Q}_\alpha, \bar{Q}_\beta\} = \{\bar{D}_\alpha, \bar{D}_\beta\} = 0, \quad (2.22)$$

$$\{Q_\alpha, \bar{Q}_\beta\} = 2\sigma^\mu_{\alpha\beta} P_\mu, \quad \{D_\alpha, \bar{D}_\beta\} = -2\sigma^\mu_{\alpha\beta} P_\mu. \quad (2.23)$$

Using (2.19), the infinitesimal supersymmetric transformation δ can finally be rewritten as

$$\begin{aligned} \delta &= i(\epsilon.Q + \bar{\epsilon}.\bar{Q}) = i(-i\epsilon^\alpha[\partial_\alpha + i\sigma^\mu_{\alpha\dot{\alpha}}\bar{\theta}^{\dot{\alpha}}\partial_\mu] - i\bar{\epsilon}^{\dot{\alpha}}[\bar{\partial}_{\dot{\alpha}} + i\theta^\alpha\sigma^\mu_{\alpha\dot{\alpha}}\partial_\mu]) \\ &= \epsilon^\alpha\partial_\alpha - \bar{\epsilon}_{\dot{\alpha}}\bar{\partial}^{\dot{\alpha}} + i(\epsilon^\alpha\sigma^\mu_{\alpha\dot{\alpha}}\bar{\theta}^{\dot{\alpha}}\partial_\mu - \theta^\alpha\sigma^\mu_{\alpha\dot{\alpha}}\bar{\epsilon}^{\dot{\alpha}})\partial_\mu. \end{aligned} \quad (2.24)$$

Applying (2.24) to (2.8) gives the following transformation laws for the various component fields

$$\begin{aligned} \delta\phi &= \epsilon.\psi + \bar{\epsilon}.\bar{\varphi}, & \delta\psi &= 2\epsilon f + \sigma^\mu\bar{\epsilon}(v_\mu - i\partial_\mu\phi), & \delta\bar{\varphi} &= 2g\bar{\epsilon} - \bar{\sigma}^\mu\epsilon(v_\mu + i\partial_\mu\phi), \\ \delta v_\mu &= -\frac{i}{2}\epsilon\partial_\mu\psi - i\epsilon\sigma_{\nu\mu}\partial^\nu\psi + \frac{i}{2}\bar{\epsilon}\partial_\mu\bar{\varphi} - i\bar{\epsilon}\bar{\sigma}_{\nu\mu}\partial^\nu\bar{\varphi} - \bar{\epsilon}\bar{\sigma}_\mu\xi - \bar{\zeta}\bar{\sigma}_\mu\epsilon, \\ \delta\xi &= -i\sigma^\mu\bar{\epsilon}\partial_\mu g + \frac{i}{2}\epsilon\partial^\mu v_\mu - \frac{i}{2}\sigma^{\mu\nu}\epsilon F_{\mu\nu} + 2\epsilon d, \\ \delta\bar{\zeta} &= -i\bar{\sigma}^\mu\bar{\epsilon}\partial_\mu f - \frac{i}{2}\bar{\epsilon}\partial^\mu v_\mu + \frac{i}{2}\bar{\sigma}^{\mu\nu}\bar{\epsilon}F_{\mu\nu} + 2\bar{\epsilon}d, \\ \delta f &= \frac{i}{2}\partial_\mu\psi\sigma^\mu\bar{\epsilon} + \bar{\epsilon}.\bar{\zeta}, & \delta g &= -\frac{i}{2}\epsilon\sigma^\mu\partial_\mu\bar{\varphi} + \epsilon.\xi, & \delta d &= \frac{i}{2}\partial_\mu\xi\sigma^\mu\bar{\epsilon} - \frac{i}{2}\epsilon\sigma^\mu\partial_\mu\bar{\zeta}. \end{aligned} \quad (2.25)$$

One important thing to note here is that the d -term of (2.8) transforms as a total derivative. So, if the residual surface terms are omitted, the associated action is then invariant under supersymmetric transformations. We will repeatedly make use of this property in the coming sections when discussing and constructing supersymmetric Lagrangians.

2.5 Supersymmetric chiral Lagrangians

In section 2.3, we have seen that not all the component fields of Φ_g are necessary to build an irreducible supermultiplet, and that additional constraints on (2.8) are *in fine* needed. The goals of this section are *i*) to introduce a first type of constrained superfields $\Phi(x, \theta, \bar{\theta})$ called chiral superfields which include a component for standard matter *ii*) to construct a kinetic term describing the dynamics of the chiral superfields *iii*) to construct interaction terms between different matter supermultiplets in the context of the Wess-Zumino model.

Chiral superfields

A chiral superfield Φ (respectively anti-chiral superfield Φ^\dagger) satisfies by definition

$$\bar{D}_{\dot{\alpha}}\Phi = 0, \quad D_\alpha\Phi^\dagger = 0, \quad (2.26)$$

where $\bar{D}_{\dot{\alpha}}$, and D_α are the superderivatives of (2.20). The constraint (2.26) is a first order differential equation which can be solved by an appropriate change of space-time coordinates

$$x^\mu \rightarrow y^\mu = x^\mu - i\theta\sigma^\mu\bar{\theta}, \quad (2.27)$$

where y^μ has the following properties

$$D_\alpha y^\mu = (\partial_\alpha - i\sigma^\nu_{\alpha\dot{\alpha}}\bar{\theta}^{\dot{\alpha}}\partial_\nu)(x^\mu - i\theta\sigma^\mu\bar{\theta}) = -2i\sigma^\mu_{\alpha\dot{\alpha}}\bar{\theta}^{\dot{\alpha}}, \quad (2.28)$$

$$\bar{D}_{\dot{\alpha}} y^\mu = (\bar{\partial}_{\dot{\alpha}} - i\theta^\alpha\sigma^\nu_{\alpha\dot{\alpha}}\partial_\nu)(x^\mu - i\theta\sigma^\mu\bar{\theta}) = 0, \quad (2.29)$$

$$D_\alpha y^{\mu\dagger} = (\partial_\alpha - i\sigma^\nu_{\alpha\dot{\alpha}}\bar{\theta}^{\dot{\alpha}}\partial_\nu)(x^\mu + i\theta\sigma^\mu\bar{\theta}) = 0, \quad (2.30)$$

$$\bar{D}_{\dot{\alpha}} y^{\mu\dagger} = (\bar{\partial}_{\dot{\alpha}} - i\theta^\alpha\sigma^\nu_{\alpha\dot{\alpha}}\partial_\nu)(x^\mu + i\theta\sigma^\mu\bar{\theta}) = -2i\theta^\alpha\sigma^\mu_{\alpha\dot{\alpha}}. \quad (2.31)$$

With the new space-time coordinates y^μ , the solution to (2.26) takes the form of

$$\Phi(y, \theta) = \phi(y) + \sqrt{2}\theta.\psi(y) - \theta.\theta F(y), \quad (2.32)$$

which is equivalent in the x^μ set of coordinates to

$$\begin{aligned} \Phi(x, \theta) &= \phi(x) + \sqrt{2}\theta.\psi(x) - \theta.\theta F(x) - i\theta\sigma^\mu\bar{\theta}\partial_\mu\phi(x) \\ &\quad + \frac{i}{\sqrt{2}}\theta.\theta\partial_\mu\psi(x)\sigma^\mu\bar{\theta} - \frac{1}{4}\theta.\theta\bar{\theta}.\bar{\theta}\square\phi(x). \end{aligned} \quad (2.33)$$

Φ describes the association of a complex scalar field ϕ with a Weyl fermion ψ , and an auxiliary complex scalar field F allowing for the SUSY algebra to close off-shell, as can be seen from the transformation laws of ϕ , ψ and F

$$\begin{aligned} \delta\phi &= \sqrt{2}\epsilon.\psi, & \delta\psi_\alpha &= -\sqrt{2}F\epsilon_\alpha - i\sqrt{2}\sigma^\mu_{\alpha\dot{\alpha}}\bar{\epsilon}^{\dot{\alpha}}\partial_\mu\phi, \\ \delta F &= -i\sqrt{2}\partial_\mu(\psi\sigma^\mu\bar{\epsilon}), \end{aligned} \quad (2.34)$$

which are obtained by applying (2.24) to (2.33). Note for completeness that an on-shell SUSY algebra contains a complex scalar field (two *dofs*), and a real two-components Weyl spinor (two *dofs*), while an off-shell SUSY algebra includes a complex scalar field (two *dofs*), and a complex Weyl spinor (four *dofs*). In order to restore equality between bosonic and fermionic *dofs*, an additional auxiliary complex scalar field F is thus required.

At this stage, two observations regarding (2.34) can be made. First, the variation of the field ϕ (resp. ψ) under supersymmetric transformation is proportional to its fermionic counterpart ψ (resp. bosonic counterpart ϕ). Second, the F -term of (2.32) transforms as a total derivative. Its action is therefore completely invariant under supersymmetric transformations (up to residual surface terms). Those F -terms, which are of $\mathcal{O}(\theta^2)$ (resp. $\mathcal{O}(\bar{\theta}^2)$) for anti-chiral superfields) are consequently the terms we need to build Lagrangians invariant under SUSY transformations.

Kinetic terms for chiral superfields

The goal of the present subsection is to construct a kinetic term describing the propagation of the various component fields of a set of chiral superfields $\{\Phi^i\}$. The Φ^i are so far the only building blocks of the theory, and therefore are an essential ingredient for the construction of the kinetic Lagrangian, together with the requirement of invariance under SUSY transformations. Using the fact that the product of two superfields is a superfield, and that d -terms transform as total derivatives, we find that $\Phi_i^\dagger\Phi^i|_{\theta^2\bar{\theta}^2}$ has all the properties required to be a good kinetic term. After simplifications, the kinetic Lagrangian therefore reads as follows

$$\Phi_i^\dagger\Phi^i|_{\theta^2\bar{\theta}^2} = -\frac{1}{4}\left(\phi_i^\dagger\square\phi^i + \square\phi_i^\dagger\phi^i\right) + F_i^\dagger F^i + \frac{i}{2}\left(\psi^i\sigma^\mu\partial_\mu\bar{\psi}_i - \partial_\mu\psi^i\sigma^\mu\bar{\psi}_i\right) + \frac{1}{2}\partial^\mu\phi_i^\dagger\partial_\mu\phi^i.$$

Integrating by parts the first term of the previous expression, and omitting the residual surface terms we obtain

$$\Phi_i^\dagger\Phi^i|_{\theta^2\bar{\theta}^2} = \partial^\mu\phi_i^\dagger\partial_\mu\phi^i + \frac{i}{2}\left(\psi^i\sigma^\mu\partial_\mu\bar{\psi}_i - \partial_\mu\psi^i\sigma^\mu\bar{\psi}_i\right) + F_i^\dagger F^i. \quad (2.35)$$

The first term in (2.35) corresponds to the free Lagrangian of a massless complex scalar field. The second one to the Lagrangian of a massless complex Weyl spinor. The fact that the last term of (2.35) does not contain any space-time derivative ensures that the auxiliary fields do not physically propagate. Their equations of motion give $F^i = 0$, so they must vanish on-shell.

Superpotential

In the Wess-Zumino model, non-gauge interactions are contained in $W(\Phi)|_{\theta^2}$ ($W^*(\Phi^\dagger)|_{\bar{\theta}^2}$), which is a (anti)holomorphic function of the (anti)chiral superfields. The notation $W(\Phi)|_{\theta^2}$ here means that in order to build the most general interaction Lagrangian invariant under SUSY transformations, we only consider terms of $\mathcal{O}(\theta^2)$ in the superpotential (the same way of reasoning applies to $W^*(\Phi^\dagger)|_{\bar{\theta}^2}$). The superpotential can then be re-expressed in terms of the content of the superfield by performing a Taylor expansion with respect to θ , such that

$$\begin{aligned} W(\Phi) &= W(\phi + \sqrt{2}\theta.\psi - \theta.\theta F) \\ &= W(\phi) + (\sqrt{2}\theta.\psi^i - \theta.\theta F^i) \frac{\partial W(\phi)}{\partial \phi^i} + \frac{1}{2}(\sqrt{2}\theta.\psi^i)(\sqrt{2}\theta.\psi^j) \frac{\partial^2 W(\phi)}{\partial \phi^i \partial \phi^j} \\ &= W(\phi) + (\sqrt{2}\theta.\psi^i - \theta.\theta F^i) \frac{\partial W(\phi)}{\partial \phi^i} + \theta.\psi^i \theta.\psi^j \frac{\partial^2 W(\phi)}{\partial \phi^i \partial \phi^j}, \end{aligned}$$

where i and j are the chiral superfield indices. The previous expression can be rewritten as

$$W(\Phi) = W(\phi) + \sqrt{2}\theta.\psi^i \frac{\partial W(\phi)}{\partial \phi^i} - \theta.\theta \left(F^i \frac{\partial W(\phi)}{\partial \phi^i} + \frac{1}{2} \psi^i.\psi^j \frac{\partial^2 W(\phi)}{\partial \phi^i \partial \phi^j} \right).$$

Keeping only the $\theta.\theta$ component of $W(\Phi)$ (resp. the $\bar{\theta}.\bar{\theta}$ component of $W^*(\Phi^\dagger)$), we obtain

$$W(\Phi)|_{\theta^2} = -F^i \frac{\partial W(\phi)}{\partial \phi^i} - \frac{1}{2} \psi^i.\psi^j \frac{\partial^2 W(\phi)}{\partial \phi^i \partial \phi^j} \quad (2.36)$$

$$W^*(\Phi^\dagger)|_{\bar{\theta}^2} = -F_i^\dagger \frac{\partial W^*(\phi^\dagger)}{\partial \phi_i^\dagger} - \frac{1}{2} \bar{\psi}_i.\bar{\psi}_j \frac{\partial^2 W^*(\phi^\dagger)}{\partial \phi_i^\dagger \partial \phi_j^\dagger}. \quad (2.37)$$

Let us just note for completeness that the Wess-Zumino superpotential could in principle include terms of order higher than three in Φ . Yet, those terms would be non-renormalizable, and thus would lead to severe complications at one-loop and beyond. In what follows, we thus consider that the superpotential is at most a (holomorphic) cubic function of the chiral superfields.

Complete Wess-Zumino Lagrangian

After combining (2.35), (2.36), (2.37), and solving the equations of motion of the auxiliary fields F^i , one obtains the following Wess-Zumino Lagrangian for a theory with chiral superfields only

$$\begin{aligned} \mathcal{L} &= \partial^\mu \phi_i^\dagger \partial_\mu \phi^i + \frac{i}{2} \left(\psi^i \sigma^\mu \partial_\mu \bar{\psi}_i - \partial_\mu \psi^i \sigma^\mu \bar{\psi}_i \right) - \frac{\partial W(\phi)}{\partial \phi^i} \frac{\partial W^*(\phi^\dagger)}{\partial \phi_i^\dagger} \\ &\quad - \frac{1}{2} \psi^i.\psi^j \frac{\partial^2 W(\phi)}{\partial \phi^i \partial \phi^j} - \frac{1}{2} \bar{\psi}_i.\bar{\psi}_j \frac{\partial^2 W^*(\phi^\dagger)}{\partial \phi_i^\dagger \partial \phi_j^\dagger}. \end{aligned} \quad (2.38)$$

2.6 Supersymmetric gauge theories

So far, we have considered supersymmetric theories involving only matter supermultiplets. The latter contain exclusively Weyl fermions and scalar bosons, yet we know that fundamental interactions are mediated by spin-1 particles, the gauge fields. The goal of this section are *i*) to introduce a new type of constrained superfields $V(x, \theta, \bar{\theta})$ called vector superfields which include by definition a vector component *ii*) to construct gauge invariant kinetic terms describing the propagation of the vector superfields (and consequently of their respective component fields) *iii*) to construct gauge invariant interaction terms between chiral and vector supermultiplets.

Vector superfield

Gauge bosons being real vector fields, a natural constraint for vector superfields is

$$V = V^\dagger . \quad (2.39)$$

Under this reality condition, the most general vector superfield can be written as follows

$$\begin{aligned} V = & C + i\theta.\chi - i\bar{\theta}.\bar{\chi} + \frac{i}{2}\theta.\theta(M + iN) - \frac{i}{2}\bar{\theta}.\bar{\theta}(M - iN) + \theta\sigma^\mu\bar{\theta}v_\mu \\ & + i\theta.\theta\bar{\theta}.\bar{\lambda} - \frac{i}{2}\bar{\sigma}^\mu\partial_\mu\chi) - i\bar{\theta}.\bar{\theta}\theta.\lambda - \frac{i}{2}\sigma^\mu\partial_\mu\bar{\chi}) + \frac{1}{2}\theta.\theta\bar{\theta}.\bar{\theta}(D - \frac{1}{2}\square C) , \end{aligned} \quad (2.40)$$

where C , D , M and N are real scalar fields, $(\lambda, \bar{\lambda})$ and $(\chi, \bar{\chi})$ are real Majorana spinors, v_μ is a real vector field, and where the x dependence of all the aforementioned fields has been omitted for brevity. In total, V has 16 degrees of freedom (8 for both its bosonic and fermionic part). This number is still too large to match with the one expected from a vector supermultiplet. A suitable supergauge choice can however remove all the unnecessary degrees of freedom as we are going to see now. If Φ is a chiral superfield, then $(\Phi + \Phi^\dagger)$ has to be a real superfield. The following transformation therefore inherently preserves the reality condition of V

$$V \rightarrow V + (\Phi + \Phi^\dagger) . \quad (2.41)$$

This gives in practice

$$\begin{aligned} V + (\Phi + \Phi^\dagger) = & C + i\theta.\chi - i\bar{\theta}.\bar{\chi} + \frac{i}{2}\theta.\theta(M + iN) - \frac{i}{2}\bar{\theta}.\bar{\theta}(M - iN) + \theta\sigma^\mu\bar{\theta}v_\mu \\ & + i\theta.\theta\bar{\theta}.\bar{\lambda} - \frac{i}{2}\bar{\sigma}^\mu\partial_\mu\chi) - i\bar{\theta}.\bar{\theta}\theta.\lambda - \frac{i}{2}\sigma^\mu\partial_\mu\bar{\chi}) + \frac{1}{2}\theta.\theta\bar{\theta}.\bar{\theta}(D - \frac{1}{2}\square C) \\ & + \phi + \sqrt{2}\theta.\psi - \theta.\theta F - i\theta\sigma^\mu\bar{\theta}\partial_\mu\phi + \frac{i}{\sqrt{2}}\theta.\theta\partial_\mu\psi\sigma^\mu\bar{\theta} - \frac{1}{4}\theta.\theta\bar{\theta}.\bar{\theta}\square\phi \\ & + \phi^\dagger + \sqrt{2}\bar{\theta}.\bar{\psi} - \bar{\theta}.\bar{\theta}F^\dagger + i\theta\sigma^\mu\bar{\theta}\partial_\mu\phi^\dagger - \frac{i}{\sqrt{2}}\bar{\theta}.\bar{\theta}\theta\sigma^\mu\partial_\mu\psi^\dagger - \frac{1}{4}\theta.\theta\bar{\theta}.\bar{\theta}\square\phi^\dagger , \end{aligned}$$

and thus the following transformations laws

$$\begin{aligned} C & \rightarrow C + \phi + \phi^\dagger , & \chi & \rightarrow \chi - i\sqrt{2}\psi , & \lambda & \rightarrow \lambda , & D & \rightarrow D , \\ v_\mu & \rightarrow v_\mu - i(\partial_\mu\phi - \partial_\mu\phi^\dagger) , & M + iN & \rightarrow M + iN + 2i F . \end{aligned}$$

The transformation law of the vector field v_μ exactly corresponds to an (abelian) gauge transformation, which is why the transformation $V \rightarrow V + (\Phi + \Phi^\dagger)$ is usually considered as the supersymmetric extension of an (abelian) gauge transformation. The fields C , M , N , χ , and $\bar{\chi}$ can then be removed by means of a suitable gauge choice, the so-called Wess-Zumino gauge, which is defined such that

$$C = -(\phi + \phi^\dagger) , \quad \chi = i\sqrt{2}\psi , \quad M + iN = -2i F . \quad (2.42)$$

In the Wess-Zumino gauge, the vector superfield V can then be rewritten as

$$V = \frac{1}{2}\theta.\theta\bar{\theta}.\bar{\theta}D + i\theta.\theta\bar{\theta}.\bar{\lambda} - i\bar{\theta}.\bar{\theta}\theta.\lambda + \theta\sigma^\mu\bar{\theta}v_\mu , \quad (2.43)$$

where V has the following properties

$$V^2 = \theta\sigma^\mu\bar{\theta}v_\mu\theta\sigma^\nu\bar{\theta}v_\nu = \frac{1}{2}\theta.\theta\bar{\theta}.\bar{\theta}v^\mu v_\mu , \quad V^3 = 0 . \quad (2.44)$$

In the Wess-Zumino gauge, the vector superfield includes (as expected) one real vector field v_μ , one Majorana fermion $(\lambda, \bar{\lambda})$, and one non-propagating auxiliary scalar field D , necessary to recover the equality between bosonic and fermionic *dofs* in the off-shell representation of the SUSY algebra. Analogously to F -fields, D -fields are removed through their equations of motion, and transform as a total derivative under supersymmetric transformations.

Spinor superfield: the abelian case

Now that the vector superfield has been introduced, we would like to construct a kinetic term describing the propagation of its various component fields (including the spin-1 vector field). This requires in practice the generalization of the concept of field strength tensor at the superspace level. Such an object is called a superfield strength tensor. Superfield strength tensors are spinor superfields which are defined as follows in a $U(1)$ supersymmetric gauge theory,

$$W_\alpha = -\frac{1}{4}\bar{D}\cdot\bar{D}D_\alpha V, \quad \bar{W}_{\dot{\alpha}} = -\frac{1}{4}D\cdot D\bar{D}_{\dot{\alpha}}V. \quad (2.45)$$

Note for completeness that *i*) W_α and $\bar{W}_{\dot{\alpha}}$ are respectively chiral and anti-chiral by construction, as $\bar{D}_{\dot{\alpha}}\bar{D}\cdot\bar{D} = 0$ and $D_\alpha D\cdot D = 0$ *ii*) the superfield strength tensor W_α and $\bar{W}_{\dot{\alpha}}$ are invariant under supersymmetric gauge transformations, as can be seen below for W_α

$$\begin{aligned} W_\alpha(V + \Phi + \Phi^\dagger) &= W_\alpha(V) - \frac{1}{4}\bar{D}\cdot\bar{D}D_\alpha\Phi - \frac{1}{4}\bar{D}\cdot\bar{D}D_\alpha\Phi^\dagger = W_\alpha(V) - \frac{1}{4}\bar{D}\cdot\bar{D}D_\alpha\Phi \\ &= W_\alpha(V) + \frac{1}{4}\bar{D}^{\dot{\alpha}}\bar{D}_{\dot{\alpha}}D_\alpha\Phi = W_\alpha(V) + \frac{1}{4}\bar{D}^{\dot{\alpha}}[-D_\alpha\bar{D}_{\dot{\alpha}} + \{D_\alpha, \bar{D}_{\dot{\alpha}}\}]\Phi \\ &= W_\alpha(V) + \frac{1}{4}\bar{D}^{\dot{\alpha}}(-2i\sigma_{\alpha\dot{\alpha}}^\mu\partial_\mu)\Phi = W_\alpha(V). \end{aligned}$$

The goal is now to obtain the analytical expressions of the superfield strength tensors in terms of their component fields. The first step is to re-express the action of the superderivatives D_α and $\bar{D}_{\dot{\alpha}}$ on the vector superfield (in the Wess-Zumino gauge), in the case where V depends on the modified space-time coordinates y^μ . Using the fact that

$$\begin{cases} D_\alpha V(y, \theta, \bar{\theta}) = D_\alpha y^\mu \frac{\partial V}{\partial y^\mu} + D_\alpha \theta^\beta \partial_\beta V + D_\alpha \bar{\theta}^{\dot{\beta}} \bar{\partial}_{\dot{\beta}} V, \\ \bar{D}_{\dot{\alpha}} V(y, \theta, \bar{\theta}) = \bar{D}_{\dot{\alpha}} y^\mu \frac{\partial V}{\partial y^\mu} + \bar{D}_{\dot{\alpha}} \bar{\theta}^{\dot{\beta}} \bar{\partial}_{\dot{\beta}} V + \bar{D}_{\dot{\alpha}} \theta^\beta \partial_\beta V, \end{cases}$$

and recalling (2.28) and (2.29), one obtains

$$\begin{cases} D_\alpha V(y, \theta, \bar{\theta}) = \partial_\alpha V - 2i\sigma_{\alpha\dot{\alpha}}^\mu \bar{\theta}^{\dot{\alpha}} \partial_{y^\mu} V, \\ \bar{D}_{\dot{\alpha}} V(y, \theta, \bar{\theta}) = \bar{\partial}_{\dot{\alpha}} V. \end{cases}$$

With the previous expressions, one finds that

$$\begin{aligned} D_\alpha V(x, \theta, \bar{\theta}) &= D_\alpha V(y + i\theta\sigma\bar{\theta}, \theta, \bar{\theta}) \\ &= (\partial_\alpha - 2i\sigma_{\alpha\dot{\alpha}}^\mu \bar{\theta}^{\dot{\alpha}} \partial_\mu) \left(\frac{1}{2}\theta\cdot\theta\bar{\theta}\cdot\bar{\theta}D + i\theta\cdot\theta\bar{\theta}\cdot\bar{\lambda} - i\bar{\theta}\cdot\bar{\theta}\theta\cdot\lambda + \theta\sigma^\nu\bar{\theta}v_\nu + i\theta\sigma^\rho\bar{\theta}\theta\sigma^\nu\bar{\theta}\partial_\rho v_\nu \right), \end{aligned}$$

which gives after simplifications

$$D_\alpha V(y, \theta, \bar{\theta}) = \sigma_{\alpha\dot{\alpha}}^\mu \bar{\theta}^{\dot{\alpha}} v_\mu - \frac{i}{2}\bar{\theta}\cdot\bar{\theta}(\sigma^\mu\bar{\sigma}^\nu\theta)_\alpha F_{\mu\nu} - i\bar{\theta}\cdot\bar{\theta}\lambda_\alpha + 2i\theta_\alpha\bar{\theta}\cdot\bar{\lambda} - \theta\cdot\theta\bar{\theta}\cdot\bar{\theta}\sigma_{\alpha\dot{\alpha}}^\mu \partial_\mu \bar{\lambda}^{\dot{\alpha}} + \theta_\alpha\bar{\theta}\cdot\bar{\theta}D.$$

As $\bar{D}_{\dot{\alpha}} = \bar{\partial}_{\dot{\alpha}}$, after considering y instead of x , the spinor superfield W_α can be written as

$$W_\alpha = -\frac{1}{4}\bar{\partial}\cdot\bar{\partial}\left[\sigma_{\alpha\dot{\alpha}}^\mu \bar{\theta}^{\dot{\alpha}} v_\mu - \frac{i}{2}\bar{\theta}\cdot\bar{\theta}(\sigma^\mu\bar{\sigma}^\nu\theta)_\alpha F_{\mu\nu} - i\bar{\theta}\cdot\bar{\theta}\lambda_\alpha + 2i\theta_\alpha\bar{\theta}\cdot\bar{\lambda} - \theta\cdot\theta\bar{\theta}\cdot\bar{\theta}\sigma_{\alpha\dot{\alpha}}^\mu \partial_\mu \bar{\lambda}^{\dot{\alpha}} + \theta_\alpha\bar{\theta}\cdot\bar{\theta}D\right].$$

After applying twice the operator $\bar{\partial}$ on the previous expression, only the $\mathcal{O}(\bar{\theta}^2)$ terms remain, such that

$$W_\alpha = -\frac{i}{2}(\sigma^\mu \bar{\sigma}^\nu \theta)_\alpha F_{\mu\nu} - i\lambda_\alpha - \theta.\theta \sigma_{\alpha\dot{\alpha}}^\mu \partial_\mu \bar{\lambda}^{\dot{\alpha}} + \theta_\alpha D. \quad (2.46)$$

Using the fact that $W^\alpha = \varepsilon^{\alpha\beta} W_\beta$, one can deduce the expression of W^α from (2.46), this gives

$$W^\alpha = \frac{i}{2}(\theta\sigma^\mu \bar{\sigma}^\nu)^\alpha F_{\mu\nu} - i\lambda^\alpha + \theta.\theta(\partial_\mu \bar{\lambda} \bar{\sigma}^\mu)^\alpha + \theta^\alpha D.$$

The kinetic term of the vector superfield is given by the product $W^\alpha W_\alpha$, so

$$W^\alpha W_\alpha = [-i\lambda^\alpha + \theta^\alpha D + \theta.\theta(\partial_\mu \bar{\lambda} \bar{\sigma}^\mu)^\alpha + \frac{i}{2}(\theta\sigma^\rho \bar{\sigma}^\sigma)^\alpha F_{\rho\sigma}] [-i\lambda_\alpha + \theta_\alpha D + \theta.\theta \sigma_{\alpha\dot{\alpha}}^\mu \partial_\mu \bar{\lambda}^{\dot{\alpha}} - \frac{i}{2}(\sigma^\mu \bar{\sigma}^\nu \theta)_\alpha F_{\mu\nu}],$$

which finally reduces to

$$W^\alpha W_\alpha = -\lambda.\lambda - 2i\lambda.\theta D + \theta.\theta(D^2 + 2i\lambda\sigma^\mu \partial_\mu \bar{\lambda} - \frac{1}{2}F^{\mu\nu} F_{\mu\nu} - \frac{i}{4}\varepsilon^{\mu\nu\rho\sigma} F_{\mu\nu} F_{\rho\sigma}).$$

The spinor superfields W_α , and $\bar{W}_{\dot{\alpha}}$ being respectively chiral and anti-chiral superfields, only their F -terms can be used to build supersymmetric Lagrangians. For $W^\alpha W_\alpha$, we obtain

$$W^\alpha W_\alpha|_{\theta^2} = D^2 + 2i\lambda\sigma^\mu \partial_\mu \bar{\lambda} - \frac{1}{2}F^{\mu\nu} F_{\mu\nu} - \frac{i}{4}\varepsilon^{\mu\nu\rho\sigma} F_{\mu\nu} F_{\rho\sigma}. \quad (2.47)$$

Note that a similar relationship holds for the hermitian conjugate $\bar{W}_{\dot{\alpha}} \bar{W}^{\dot{\alpha}}|_{\bar{\theta}^2}$. Introducing finally an *ad hoc* normalization factor of 1/4, the free Lagrangian for a vector superfield reads,

$$\mathcal{L}_V = \frac{1}{4}W^\alpha W_\alpha|_{\theta^2} + \frac{1}{4}\bar{W}_{\dot{\alpha}} \bar{W}^{\dot{\alpha}}|_{\bar{\theta}^2},$$

or equivalently in terms of the component fields

$$\mathcal{L}_V = \frac{1}{2}D^2 + \frac{i}{2}(\lambda\sigma^\mu \partial_\mu \bar{\lambda} - \partial_\mu \lambda\sigma^\mu \bar{\lambda}) - \frac{1}{4}F^{\mu\nu} F_{\mu\nu} \quad (2.48)$$

Abelian supersymmetric gauge theory

The last missing part of the theory consists of the interactions between matter and gauge supermultiplets, the goal of the present subsection is precisely to find such a term. For simplicity we first consider the particular case of the abelian gauge symmetry $U(1)_Q$, which describes electromagnetic interactions between electrically charged particles. Needless to say however that this discussion can be extended to any $U(1)$ group. In section 2.5, we have seen that $\Phi_i^\dagger \Phi^i|_{\theta^2 \bar{\theta}^2}$ is a good candidate for the kinetic term of a collection of chiral superfields, yet in the context of a supersymmetric gauge theory this term is not appropriate as it explicitly breaks gauge invariance. This statement can be deduced from the following gauge transformation laws

$$\Phi \longrightarrow e^{-2ieQ\Lambda} \Phi, \quad \Phi^\dagger \longrightarrow \Phi^\dagger e^{2ieQ\Lambda^\dagger}, \quad (2.49)$$

where Q is the electric charge, e is the electromagnetic coupling constant, and where Λ is a chiral superfield with $\Lambda \neq \Lambda^\dagger$ by definition. Gauge invariance can however be restored in the case where $\Phi_i^\dagger \Phi^i|_{\theta^2 \bar{\theta}^2}$ is replaced by $\Phi_i^\dagger e^{-2eQV} \Phi^i|_{\theta^2 \bar{\theta}^2}$, since one can impose that

$$\Phi^\dagger e^{-2eQV} \Phi \longrightarrow \Phi^\dagger e^{2ieQ\Lambda^\dagger} e^{-2eQV'} e^{-2ieQ\Lambda} \Phi = \Phi^\dagger e^{-2eQV} \Phi,$$

such that the vector superfield must transform as

$$e^{-2eQV} \longrightarrow e^{-2eQV'} = e^{-2ieq\Lambda^\dagger} e^{-2eQV} e^{2ieQ\Lambda} , \quad (2.50)$$

where $e^{-2ieQ\Lambda}$ and $e^{-2ieQ\Lambda^\dagger}$ are two unitary operators defined as

$$e^{2ieQ\Lambda} e^{-2ieQ\Lambda} = 1 \quad \text{and} \quad e^{2ieQ\Lambda^\dagger} e^{-2ieQ\Lambda^\dagger} = 1 . \quad (2.51)$$

Using the Campbell-Baker-Hausdorff formula, we obtain the following transformation law for V

$$\delta V = -i(\Lambda - \Lambda^\dagger) . \quad (2.52)$$

Using the properties (2.44) of the Wess-Zumino gauge, it is possible to linearize the exponential factor in $\Phi_i^\dagger e^{-2eQV} \Phi^i|_{\theta^2\bar{\theta}^2}$, by performing a series expansion with respect to V , such that

$$\Phi_i^\dagger e^{-2eQV} \Phi^i|_{\theta^2\bar{\theta}^2} = \Phi_i^\dagger \Phi^i|_{\theta^2\bar{\theta}^2} - 2eQ\Phi_i^\dagger V \Phi^i|_{\theta^2\bar{\theta}^2} + 2e^2Q^2\Phi_i^\dagger V^2 \Phi^i|_{\theta^2\bar{\theta}^2} .$$

The first term on the right hand-side of the previous equation is known from (2.35), so only the second and third terms need to be calculated. Using (2.43) and (2.44), we obtain

$$\begin{aligned} 2eQ\Phi_i^\dagger V \Phi^i|_{\theta^2\bar{\theta}^2} &= eQ\phi_i^\dagger D\phi^i + eQ\psi^i \sigma^\mu \bar{\psi}_i v_\mu + ieQ\partial_\mu \phi_i^\dagger v^\mu \phi^i - ieQv_\mu \phi_i^\dagger \partial^\mu \phi^i \\ &\quad - ieQ\sqrt{2}\bar{\psi}_i \cdot \bar{\lambda} \phi^i + ieQ\sqrt{2}\phi_i^\dagger \psi^i \cdot \lambda , \\ 2e^2Q^2\Phi_i^\dagger V^2 \Phi^i|_{\theta^2\bar{\theta}^2} &= e^2Q^2\phi_i^\dagger v_\mu v^\mu \phi^i , \end{aligned}$$

which gives the following Lagrangian after solving the equation of motion for the auxiliary fields

$$\begin{aligned} \mathcal{L} &= -\frac{1}{4}F_{\mu\nu}F^{\mu\nu} + \frac{i}{2}(\lambda\sigma^\mu\partial_\mu\bar{\lambda} - \partial_\mu\lambda\sigma^\mu\bar{\lambda}) + (D_\mu\phi)_i^\dagger(D^\mu\phi^i) \\ &\quad + ieQ\sqrt{2}\bar{\lambda}\cdot\bar{\psi}_i\phi^i - ieQ\sqrt{2}\phi_i^\dagger\psi^i\cdot\lambda - \frac{i}{2}(D_\mu\bar{\psi}_i\bar{\sigma}^\mu\psi^i - \bar{\psi}_i\bar{\sigma}^\mu D_\mu\psi^i) \\ &\quad - \frac{1}{2}\psi^i\cdot\psi^j\frac{\partial^2 W}{\partial\phi^i\partial\phi^j} - \frac{1}{2}\bar{\psi}_i\cdot\bar{\psi}_j\frac{\partial^2 W^*}{\partial\phi_i^\dagger\partial\phi_j^\dagger} - \left[\frac{1}{2}e^2Q^2(\phi^\dagger\phi)(\phi^\dagger\phi) + \frac{\partial W}{\partial\phi^i}\frac{\partial W^*}{\partial\phi_i^\dagger} \right] , \end{aligned} \quad (2.53)$$

with the covariant derivative $D_\mu = \partial_\mu - ieQv_\mu$. This Lagrangian describes a supersymmetric extension of QED, where the ψ_i and ϕ are respectively the charged fermions, and sfermions, and where v_μ and λ are respectively the photon and its supersymmetric partner, the photino.

Non-abelian supersymmetric gauge theory

The construction of non-abelian supersymmetric gauge theories is slightly more complicated than in the abelian case. For simplicity, we set in what follows $V = V^a T_a$, with V^a a collection of vector superfields, and with T_a the generators of the Lie algebra associated to the non-abelian gauge group. The reality condition (2.39) can thus be generalized, such that

$$V^\dagger = (V^a T_a)^\dagger = T_a^\dagger V^{a\dagger} = T_a V^a = V . \quad (2.54)$$

Generalizing the procedure detailed in the previous section for the abelian case, we find that

$$\delta V^a = -i(\Lambda^a - \Lambda^{a\dagger}) - g f^{abc} V^b (\Lambda^{c\dagger} + \Lambda^c) . \quad (2.55)$$

Non-abelian spinor Superfield

The non-abelian version of the superfield strength tensor introduced in (2.45) is defined as

$$W_\alpha = -\frac{1}{4}\bar{D}\cdot\bar{D}e^{2gV}D_\alpha e^{-2gV} . \quad (2.56)$$

Using (2.44), it is possible to linearize the exponential factors of the previous expression by performing a series expansion with respect to V . This gives

$$\begin{aligned} e^{2gV}D_\alpha e^{-2gV} &= [1 + 2gV + 2g^2V^2]D_\alpha[1 - 2gV + 2g^2V^2] \\ &= -2gD_\alpha V - 2g^2[V, D_\alpha V] , \end{aligned}$$

such that

$$W_\alpha = -\frac{1}{4}\bar{D}\cdot\bar{D}(-2gD_\alpha V - 2g^2[V, D_\alpha V]) , \quad (2.57)$$

where the first term is similar to the abelian case, and where the second one gives

$$[V, D_\alpha V] = -\frac{1}{2}\bar{\theta}\cdot\bar{\theta}(\sigma^\mu\bar{\sigma}^\nu\theta)_\alpha[v_\mu, v_\nu] + i\theta\cdot\theta\bar{\theta}\cdot\bar{\theta}(\sigma^\mu[v_\mu, \bar{\lambda}])_\alpha . \quad (2.58)$$

The complete non-abelian superfield strength tensor therefore reads

$$\begin{aligned} W_\alpha &= \frac{g}{2}\bar{D}\cdot\bar{D}D_\alpha V + \frac{g^2}{2}\bar{D}\cdot\bar{D}(i\theta\cdot\theta\bar{\theta}\cdot\bar{\theta}(\sigma^\mu[v_\mu, \bar{\lambda}])_\alpha - \frac{1}{2}\bar{\theta}\cdot\bar{\theta}(\sigma^\mu\bar{\sigma}^\nu\theta)_\alpha[v_\mu, v_\nu]) \\ &= \frac{g}{2}\bar{D}\cdot\bar{D}(D_\alpha V + \frac{g}{2}\bar{\theta}\cdot\bar{\theta}(\sigma^\mu\bar{\sigma}^\nu\theta)_\alpha[v_\mu, v_\nu] - ig\theta\cdot\theta\bar{\theta}\cdot\bar{\theta}(\sigma^\mu[v_\mu, \bar{\lambda}])_\alpha) . \end{aligned}$$

After having introduced the non-abelian field strength tensor $F_{\mu\nu} = \partial_\mu v_\nu - \partial_\nu v_\mu - ig[v_\mu, v_\nu]$, and the covariant derivative $D_\mu = \partial_\mu - igv_\mu$, the previous expression can be reduced to

$$W_\alpha = -2g(-i\lambda_\alpha - \frac{i}{2}(\sigma^\mu\bar{\sigma}^\nu\theta)_\alpha F_{\mu\nu} + \theta_\alpha D - \theta\cdot\theta(D_\mu\bar{\lambda})_\alpha) , \quad (2.59)$$

$$W^\alpha = -2g(-i\lambda^\alpha + \frac{i}{2}(\theta\sigma^\mu\bar{\sigma}^\nu)^\alpha F_{\mu\nu} + \theta^\alpha D + \theta\cdot\theta(D_\mu\bar{\lambda}\bar{\sigma}^\mu)^\alpha) . \quad (2.60)$$

After some practical manipulations, one can derive the following gauge kinetic terms

$$\text{Tr}(W^\alpha W_\alpha|_{\theta^2}) = 4g^2\text{Tr}(2i\lambda\sigma^\mu D_\mu\bar{\lambda} + D^2 - \frac{1}{2}F^{\mu\nu}F_{\mu\nu} - \frac{i}{4}\varepsilon^{\mu\nu\rho\sigma}F_{\mu\nu}F_{\rho\sigma}) . \quad (2.61)$$

The generic Lagrangian for a renormalizable non-abelian supersymmetric gauge theories is thus

$$\mathcal{L} = \Phi^\dagger e^{-2gV}\Phi|_{\theta^2\bar{\theta}^2} + \frac{1}{16g^2\tau_R}\text{Tr}(W^\alpha W_\alpha|_{\theta^2}) + \frac{1}{16g^2\tau_R}\text{Tr}(\bar{W}_{\dot{\alpha}}\bar{W}^{\dot{\alpha}}|_{\bar{\theta}^2}) + W(\Phi)|_{\theta^2} + W^*(\Phi^\dagger)|_{\bar{\theta}^2} ,$$

where $\tau_R = 1/2$. In the component field formalism, this Lagrangian reads as follows

$$\begin{aligned} \mathcal{L} &= -\frac{1}{4}F_{\mu\nu}^a F_a^{\mu\nu} + \frac{i}{2}(\lambda^a\sigma^\mu D_\mu\bar{\lambda}_a - D_\mu\lambda^a\sigma^\mu\bar{\lambda}_a) + (D_\mu\phi)^\dagger(D^\mu\phi) \\ &\quad + ig\sqrt{2}\bar{\lambda}^a\cdot\bar{\psi}T_a\phi - ig\sqrt{2}\phi^\dagger T_a\psi\cdot\lambda^a + \frac{1}{2}D^a D_a - gD^a\phi^\dagger T_a\phi \\ &\quad + \frac{i}{2}(\psi\sigma^\mu D_\mu\bar{\psi} - D_\mu\psi\sigma^\mu\bar{\psi}) + F_i^\dagger F^i - (F^i\frac{\partial W}{\partial\phi^i} + \frac{1}{2}\psi^i\cdot\psi^j\frac{\partial^2 W}{\partial\phi^i\partial\phi^j} + \text{h.c.}) . \end{aligned} \quad (2.62)$$

When solving the equations of motion for the auxiliary fields, we find that

Chiral superfield		Scalars	Fermions	$SU(3)_C, SU(2)_L, U(1)_Y$
(s)quarks ($\times 3$ generations)	Q_L^i	$\tilde{q}_L^i = (\tilde{u}_L^i \tilde{d}_L^i)$	$q_L^i = (u_L^i d_L^i)$	$(\mathbf{3}, \mathbf{2}, \frac{1}{6})$
	U_R^i	$\tilde{u}_R^{i\dagger}$	$u_R^{i c}$	$(\bar{\mathbf{3}}, \mathbf{1}, -\frac{2}{3})$
	D_R^i	$\tilde{d}_R^{i\dagger}$	$d_R^{i c}$	$(\bar{\mathbf{3}}, \mathbf{1}, \frac{1}{3})$
(s)leptons ($\times 3$ generations)	L_L^i	$\tilde{\ell}_L^i = (\tilde{\nu}_L^i \tilde{e}_L^i)$	$\ell_L^i = (\nu_L^i e_L^i)$	$(\mathbf{1}, \mathbf{2}, -\frac{1}{2})$
	E_R^i	$\tilde{e}_R^{i\dagger}$	$e_R^{i c}$	$(\mathbf{1}, \mathbf{1}, 1)$
Up-type Higgs(ino)	H_U	$H_u = (H_u^+ H_u^0)$	$\tilde{H}_u = (\tilde{H}_u^+ \tilde{H}_u^0)$	$(\mathbf{1}, \mathbf{2}, \frac{1}{2})$
Down-type Higgs(ino)	H_D	$H_d = (H_d^0 H_d^-)$	$\tilde{H}_d = (\tilde{H}_d^0 \tilde{H}_d^-)$	$(\mathbf{1}, \mathbf{2}, -\frac{1}{2})$

Table 2.1: Chiral superfield content of the MSSM. Scalar and fermion components are given together with their representations under the gauge group $SU(3)_c \times SU(2)_L \times U(1)_Y$. The superscripts c and $i = 1, 2, 3$ respectively denote the charge conjugation operation, and the fermion generation index. The name of the SUSY partner of the SM particle is given in brackets.

$$\left\{ \begin{array}{l} \frac{\partial \mathcal{L}}{\partial F^i} = F_i^\dagger - \frac{\partial W}{\partial \phi^i} = 0 \longrightarrow F_i^\dagger = \frac{\partial W}{\partial \phi^i}, \\ \frac{\partial \mathcal{L}}{\partial F^i} = F^i - \frac{\partial W^*}{\partial \phi_i^\dagger} = 0 \longrightarrow F^i = \frac{\partial W^*}{\partial \phi_i^\dagger}, \\ \frac{\partial \mathcal{L}}{\partial D^a} = D_a - g\phi^\dagger T_a \phi = 0 \longrightarrow D_a = g\phi^\dagger T_a \phi, \end{array} \right.$$

and therefore that

$$\begin{aligned} \frac{1}{2} D^a D_a &= \frac{1}{2} g^2 (\phi^\dagger T^a \phi) (\phi^\dagger T_a \phi), & -g D^a \phi^\dagger T_a \phi &= -g^2 (\phi^\dagger T^a \phi) (\phi^\dagger T_a \phi), \\ F_i^\dagger F^i - F^i \frac{\partial W}{\partial \phi^i} - F_i^\dagger \frac{\partial W^*}{\partial \phi_i^\dagger} &= -\frac{\partial W}{\partial \phi^i} \frac{\partial W^*}{\partial \phi_i^\dagger}, \end{aligned}$$

which ultimately gives the following master Lagrangian

$$\begin{aligned} \mathcal{L} &= -\frac{1}{4} F_{\mu\nu}^a F_a^{\mu\nu} + \frac{i}{2} (\lambda^a \sigma^\mu D_\mu \bar{\lambda}_a - D_\mu \lambda^a \sigma^\mu \bar{\lambda}_a) + (D_\mu \phi)^\dagger (D^\mu \phi) \\ &+ ig\sqrt{2} \bar{\lambda}^a \cdot \bar{\psi} T_a \phi - ig\sqrt{2} \phi^\dagger T_a \psi \cdot \lambda^a - \frac{i}{2} (D_\mu \bar{\psi} \bar{\sigma}^\mu \psi - \bar{\psi} \bar{\sigma}^\mu D_\mu \psi) \\ &- \frac{1}{2} \psi^i \cdot \psi^j \frac{\partial^2 W}{\partial \phi^i \partial \phi^j} - \frac{1}{2} \bar{\psi}_i \cdot \bar{\psi}_j \frac{\partial^2 W^*}{\partial \phi_i^\dagger \partial \phi_j^\dagger} - \left[\frac{1}{2} g^2 (\phi^\dagger T^a \phi) (\phi^\dagger T_a \phi) + \frac{\partial W}{\partial \phi^i} \frac{\partial W^*}{\partial \phi_i^\dagger} \right]. \end{aligned} \quad (2.63)$$

2.7 The Minimal Supersymmetric Standard Model

The Minimal Supersymmetric Standard Model (MSSM) results from the direct supersymmetrization of the SM Lagrangian, and is minimal in the sense that it requires the smallest possible number of superfields and new interactions to remain phenomenologically consistent. More specifically, the supersymmetrization procedure of the SM Lagrangian consists in promoting all Higgs and matter fields (Weyl fermions) to chiral superfields identically charged under $SU(3)_C \times SU(2)_L \times U(1)_Y$ (see Tab. 2.1), and all gauge fields to vector superfields with the same quantum numbers (see Tab. 2.2). In practice, each gauge field is then paired with a Majorana fermion (a gaugino), each chiral fermion with a scalar field (a sfermion), and each Higgs field

with a Dirac fermion (a Higgsino). The naming scheme in SUSY works as follows, the name of the fermionic partners of the Higgses and the SM gauge bosons is obtained with the addition of the suffix "-ino", and the name of the scalar partners of the SM chiral fermions is obtained with the addition of the prefix "s-". Although they are just scalar particles, the sfermions also keep track of the chirality of their fermionic counterpart with the addition of the subscript L/R .

Note that the Higgs sector requires in the MSSM the introduction of a second Higgs doublet. This addition is made necessary for two reasons. First of all, Yukawa interactions are derived from the superpotential, which is a holomorphic function of the chiral superfields, *i.e.* it cannot depend on a chiral superfield Φ_i and its complex conjugate Φ_i^* at the same time. Therefore, the trick employed in the SM, which consists in taking the charge conjugate of the Higgs field in order to give mass to both the upper and lower components of $SU(2)_L$ fermion doublets with the same Higgs field, cannot be applied to the MSSM. Two Higgs doublets are hence needed to give mass to both up-type and down-type fermions. The MSSM Higgs sector is, in this respect, completely analogous to a Two-Higgs-Doublet Model (THDM) of type II. The second reason why we need another Higgs supermultiplet in SUSY is that the fermionic superpartners of the Higgs bosons, the Higgsinos, also contribute to chiral anomalies appearing in triangular diagrams with axial current. A single Higgs(ino) doublet leads to non-vanishing gauge anomalies, and makes the theory inconsistent at the quantum level. Adding a second Higgs(ino) doublet with opposite hypercharge allows for the Higgsino contributions to chiral anomalies to cancel each other.

Once the chiral superfield content of the MSSM has been specified (see Tab. 2.1), one can build the MSSM superpotential. Gauge invariance bounds the form of the possible renormalizable interaction terms of the MSSM superpotential. Following the conventions of [101], the most general form of superpotential can be written as,

$$W_{\text{MSSM}} = (Y_u)_{ij} Q_L^i \cdot H_U U_R^j + (Y_d)_{ij} Q_L^i \cdot H_D D_R^j + (Y_e)_{ij} L_L^i \cdot H_D E_R^j - \mu H_D \cdot H_U + W_{\text{RPV}}, \quad (2.64)$$

where Q_L^i , U_R^j , D_R^j , L_L^i , and E_R^j are chiral superfields, H_D and H_U are the Higgs superfields, Y_u , Y_d and Y_e are the 3×3 Yukawa matrices generating the quark and lepton masses after electroweak symmetry breaking, i and j with $i, j = 1, 2, 3$ are the generation indices, μ is a complex quantity of mass-dimension one called the Higgs/Higgsino mass parameter, and the notation "." corresponds to the contraction of $SU(2)_L$ doublets. The last term of (2.64) is the so-called R -Parity Violating (RPV) superpotential and reads as follows

$$W_{\text{RPV}} = \frac{1}{2} \lambda_{ijk} L_L^i \cdot L_L^j E_R^k + \lambda'_{ijk} L_L^i \cdot Q_L^j D_R^k + \frac{1}{2} \lambda''_{ijk} U_R^i U_R^j D_R^k - \kappa_i L_L^i \cdot H_U, \quad (2.65)$$

where $i, j, k = 1, 2, 3$ are the generation indices, λ , λ' , λ'' are respectively $3 \times 3 \times 3$ tensors in the flavour space, and κ is a vector in the flavour space. The RPV superpotential violates explicitly lepton number (L) and baryon number (B). More specifically, the first, the second and the last term of (2.65) violate lepton number, while only the third term violates baryon number. The simultaneous violation of B and L has serious phenomenological implications, *e.g.* fast proton decay, which is why RPV interactions are usually forbidden by the introduction of a discrete \mathbb{Z}_2 -symmetry dubbed R -parity, and defined at the particle level by

$$R = (-1)^{3B+L+2S}, \quad (2.66)$$

where S conventionally denotes the spin. Standard Model particles have $R = +1$, while their supersymmetric counterparts have $R = -1$. R being a multiplicative quantum number, superpartners can only be pair produced (if R -parity is conserved). For the same reason, superpartners can only decay into an odd-number of SUSY particles. The Lightest Supersymmetric Particle is therefore completely stable in this case, and provides *de facto* a good candidate for Dark Matter.

Vector superfield		Gauge bosons	Gauginos	$SU(3)_C, SU(2)_L, U(1)_Y$
B , bino	V_B	B	\tilde{B}	$(\mathbf{1}, \mathbf{1}, 0)$
W , winos	V_W	$W^- \quad W_3 \quad W^+$	$\tilde{W}^- \quad \tilde{W}_3 \quad \tilde{W}^+$	$(\mathbf{1}, \mathbf{3}, 0)$
gluons, gluinos	V_G	g	\tilde{g}	$(\mathbf{8}, \mathbf{1}, 0)$

Table 2.2: Vector superfields content in the MSSM. Gauge bosons and gauginos components are given together with their representations under the $SU(3)_c \times SU(2)_L \times U(1)_Y$ gauge group.

2.8 Supersymmetry breaking

At the beginning of this chapter we have seen that an exact supersymmetry dictates a mass degeneracy between SM particles and their supersymmetric counterparts. Since no light superpartners have been experimentally observed so far, supersymmetry has to be a broken symmetry. The way supersymmetry is broken is currently not known, yet some possible candidate mechanisms are, among others, Gauge-Mediated Supersymmetry Breaking (GMSB), Anomaly-Mediated Supersymmetry Breaking (AMSB), Gravity-Mediated Supersymmetry Breaking (SUGRA).

Most phenomenological analyses, however do not attempt to understand the genuine SUSY-breaking mechanism, they rather parameterize its effects in the visible sector by explicitly adding to the Lagrangian all the possible soft SUSY-breaking terms, *i.e.* the terms that do not spoil the solution to the hierarchy problem by reintroducing quadratic UV divergences in δm_h^2 . All possible soft SUSY-breaking terms have been identified and classified in [102]. These are *i)* the gaugino mass terms *ii)* the scalar mass terms *iii)* the trilinear scalar interactions *iv)* the Higgs bilinear term. The soft SUSY-breaking Lagrangian is chosen accordingly to [103] and reads

$$\begin{aligned}
\mathcal{L}_{soft} = & \frac{1}{2} \left[M_1 \tilde{B} \cdot \tilde{B} + M_2 \tilde{W}^i \cdot \tilde{W}_i + M_3 \tilde{g}^a \cdot \tilde{g}_a + \text{h.c.} \right] - m_{H_d}^2 H_d^\dagger H_d - m_{H_u}^2 H_u^\dagger H_u \\
& - (m_u^2)_{ij} \tilde{u}_R^i \tilde{u}_R^{j\dagger} - (m_d^2)_{ij} \tilde{d}_R^i \tilde{d}_R^{j\dagger} - (m_e^2)_{ij} \tilde{e}_R^i \tilde{e}_R^{j\dagger} - (m_q^2)_{ij} \tilde{q}_L^i \tilde{q}_L^{j\dagger} - (m_\ell^2)_{ij} \tilde{\ell}_L^i \tilde{\ell}_L^{j\dagger} \quad (2.67) \\
& - \left[(T_u)_{ij} \tilde{q}_L^i \cdot H_u \tilde{u}_R^{j\dagger} - (T_d)_{ij} \tilde{q}_L^i \cdot H_d \tilde{d}_R^{j\dagger} - (T_e)_{ij} \tilde{\ell}_L^i \cdot H_d \tilde{e}_R^{j\dagger} + B\mu H_u \cdot H_d + \text{h.c.} \right].
\end{aligned}$$

The first term between brackets corresponds to the gaugino masses, where M_1 , M_2 and M_3 are respectively the mass of the bino, winos and gluinos. The next seven terms are the scalar mass terms, where $m_{H_d}^2$ and $m_{H_u}^2$ are the Higgs masses, and where m_u^2 , m_d^2 , m_e^2 , m_q^2 and m_ℓ^2 are the 3×3 hermitian sfermion mass matrices living in the flavour space with $i, j = 1, 2, 3$. The first three terms of the last line of (2.67) are the trilinear scalar interactions, where T_u , T_d , and T_e are the 3×3 hermitian coupling strength matrices also living in the flavour space. Those trilinear couplings are usually parameterized as $(T_\phi)_{ij} = (Y_\phi)_{ij} A_\phi$, where the $(Y_\phi)_{ij}$ are the entries of the Yukawa matrix for a field of type ϕ , and where A_ϕ consists of its associated soft SUSY-breaking parameter. The last term of (2.67) finally corresponds to the off-diagonal bilinear Higgs term, where B is a parameter responsible for triggering the electroweak symmetry breaking.

At the price of model-independence, the soft SUSY-breaking parameterization introduces in the MSSM a significant number of free parameters that cannot be rotated away by field redefinitions. More specifically, assuming that R -parity is conserved and that the neutrino/sneutrino sector and the CP -violating QCD sector are decoupled from the theory, the MSSM with soft terms exhibits in total 124 free parameters, out of which, 18 correspond to the Standard Model ones, one is the Higgs mass originating from the second Higgs doublet, and 105 are new masses, phases and real mixing angles introduced in the squark, slepton, and gaugino/Higgsino sectors.

2.9 Higgs sector

Analogously to what happens in the Standard Model, we ultimately want to break the electroweak symmetry in order to give mass to both SM fermions and W and Z gauge bosons. As we have seen before, two Higgs doublets are required in the MSSM to enforce the cancellation of chiral anomalies, and to account for both up- and down-type fermion masses. Knowing that the electric charge Q , the hypercharge Y , and the third component of the weak isospin T_3 are linked by the Gell-Mann-Nishijima formula $Q = T_3 + Y$, we obtain the following Higgs doublets

$$H_d = \begin{pmatrix} H_d^0 \\ H_d^- \end{pmatrix}, \quad H_u = \begin{pmatrix} H_u^+ \\ H_u^0 \end{pmatrix}, \quad (2.68)$$

by requiring the hypercharge of H_d and H_u to be respectively $-1/2$ and $+1/2$. Each doublet contains four real degrees of freedom, and consists of one neutral and one charged component, respectively H_d^0 and H_d^- for H_d , and H_u^0 and H_u^+ for H_u . In total, the Higgs sector exhibits eight degrees of freedom. Just like in the Standard Model, three of them, namely the Goldstone bosons G^\pm , and G^0 , are "eaten" by the W^\pm and Z^0 gauge bosons, which thereby become massive, and hence acquire a longitudinal polarization mode. The remaining five degrees of freedom mix together after electroweak symmetry breaking and yield five physical Higgs bosons.

The Higgs potential receives contributions from the F -terms, the D -terms, and the soft-SUSY breaking potential (through the Higgs bilinear and mass terms), and reads as follows

$$\begin{aligned} V_{\text{Higgs}} &= \frac{g^2 + g'^2}{8} \left[H_d^{0\dagger} H_d^0 + H_d^{-\dagger} H_d^- - H_u^{0\dagger} H_u^0 - H_u^{+\dagger} H_u^+ \right]^2 \\ &+ \frac{g^2}{2} \left[\begin{aligned} &\left(H_d^{0\dagger} H_d^0 + H_d^{-\dagger} H_d^- \right) \left(H_u^{0\dagger} H_u^0 + H_u^{+\dagger} H_u^+ \right) \\ &+ \left(H_d^{-\dagger} H_u^{+\dagger} - H_d^{0\dagger} H_u^{0\dagger} \right) \left(H_d^0 H_u^0 - H_d^- H_u^+ \right) \end{aligned} \right] \\ &+ \left(|\mu|^2 + m_{H_d}^2 \right) \left(H_d^{0\dagger} H_d^0 + H_d^{-\dagger} H_d^- \right) + \left(|\mu|^2 + m_{H_u}^2 \right) \\ &\left(H_u^{0\dagger} H_u^0 + H_u^{+\dagger} H_u^+ \right) + \left(B\mu \left(H_u^+ H_d^- - H_u^0 H_d^0 \right) + \text{h.c.} \right). \end{aligned} \quad (2.69)$$

After the two Higgs doublets have acquired a vev, we require the minimum of (2.69) to break the electroweak symmetry $SU(2)_L \times U(1)_Y$ down to the gauge group of electromagnetism $U(1)_Q$. At this minimum, we always have the possibility to rotate away the vev of the charged component of one of the two Higgs doublets by means of a $SU(2)_L$ gauge transformation. The minimization condition associated to this charged component then directly imply that the vev of the charged component of the second doublet also vanishes, which gives

$$\langle H_d \rangle = \frac{1}{\sqrt{2}} \begin{pmatrix} v_d \\ 0 \end{pmatrix}, \quad \langle H_u \rangle = \frac{1}{\sqrt{2}} \begin{pmatrix} 0 \\ v_u \end{pmatrix}, \quad (2.70)$$

such that the $U(1)_Q$ symmetry is preserved¹. Since the charged components of the Higgs doublets do not acquire a vev, only the neutral part of (2.69) has to be minimized. The latter reads

$$\begin{aligned} V_{\text{neutral}} &= \frac{g^2 + g'^2}{8} \left[H_d^{0\dagger} H_d^0 - H_u^{0\dagger} H_u^0 \right]^2 + \left(|\mu|^2 + m_{H_d}^2 \right) H_d^{0\dagger} H_d^0 \\ &+ \left(|\mu|^2 + m_{H_u}^2 \right) H_u^{0\dagger} H_u^0 - B\mu \left(H_u^0 H_d^0 + H_u^{0\dagger} H_d^{0\dagger} \right), \end{aligned} \quad (2.71)$$

where $B\mu$, which is the only factor sensitive to complex phases in (2.71), has been chosen to be real and positive by means of an appropriate phase redefinition of H_u and H_d . The

¹Charged scalars cannot acquire a vev, otherwise electromagnetism is broken.

Higgs potential is in this case CP-conserving at tree level. The generic minimization conditions obtained from the previous equation are

$$\left. \frac{\partial V_{\text{neutral}}}{\partial H_d^0} \right|_{\text{vev}} = 0 = \frac{g^2 + g'^2}{8} (v_d^2 - v_u^2) + |\mu|^2 + m_{H_d}^2 - B\mu \tan \beta \quad (2.72)$$

$$\left. \frac{\partial V_{\text{neutral}}}{\partial H_u^0} \right|_{\text{vev}} = 0 = \frac{g^2 + g'^2}{8} (v_u^2 - v_d^2) + |\mu|^2 + m_{H_u}^2 - B\mu \cotan \beta \quad (2.73)$$

with

$$\tan \beta = \frac{v_u}{v_d}, \quad \cotan \beta = \frac{v_d}{v_u}, \quad \text{and} \quad 0 \leq \beta \leq \frac{\pi}{2}. \quad (2.74)$$

In order to spontaneously break the electroweak symmetry, the Higgs potential must be bounded from below, whatever the values of the vevs are. For largely different vevs v_d and v_u this is always the case, as the quartic term prevails over all the others, and stabilize the Higgs potential. Yet, in the case where the two vevs are equal, the so-called "*D-flat directions*", the potential is bounded from below only if the following condition is satisfied

$$2|\mu|^2 + m_{H_d}^2 + m_{H_u}^2 - 2B\mu > 0. \quad (2.75)$$

Moreover, in order to avoid the configuration where $v_d = v_u = 0$ is a minimum, one also imposes that the determinant of the Hessian matrix M_H^2

$$M_H^2 = \begin{pmatrix} |\mu|^2 + m_{H_d}^2 & -B\mu \\ -B\mu & |\mu|^2 + m_{H_u}^2 \end{pmatrix}, \quad (2.76)$$

is negative such that

$$\left(|\mu|^2 + m_{H_d}^2 \right) \left(|\mu|^2 + m_{H_u}^2 \right) - (B\mu)^2 < 0. \quad (2.77)$$

Note that (2.75), and (2.77) cannot be simultaneously satisfied if $m_{H_d} = m_{H_u}$, which means in other words that supersymmetry breaking is a necessary condition for electroweak symmetry breaking to happen. Performing the following perturbative expansion around the ground-states

$$\begin{aligned} H_d^0 &\longrightarrow \frac{1}{\sqrt{2}} \left[v_d + \text{Re}(H_d^0) + i \text{Im}(H_d^0) \right], \\ H_u^0 &\longrightarrow \frac{1}{\sqrt{2}} \left[v_u + \text{Re}(H_u^0) + i \text{Im}(H_u^0) \right], \end{aligned}$$

in the neutral part of the Higgs potential, we get

$$\begin{aligned} V_{\text{neutral}} &= \frac{1}{2} \begin{pmatrix} \text{Im}(H_d^0) & \text{Im}(H_u^0) \end{pmatrix} \begin{pmatrix} B\mu \tan \beta & B\mu \\ B\mu & B\mu \cotan \beta \end{pmatrix} \begin{pmatrix} \text{Im}(H_d^0) \\ \text{Im}(H_u^0) \end{pmatrix} \\ &+ \frac{1}{2} \begin{pmatrix} \text{Re}(H_d^0) & \text{Re}(H_u^0) \end{pmatrix} \begin{pmatrix} M_Z^2 \cos^2 \beta + B\mu \tan \beta & -M_Z^2 \cos \beta \sin \beta - B\mu \\ -M_Z^2 \cos \beta \sin \beta - B\mu & M_Z^2 \sin^2 \beta + B\mu \cotan \beta \end{pmatrix} \begin{pmatrix} \text{Re}(H_d^0) \\ \text{Re}(H_u^0) \end{pmatrix}, \end{aligned} \quad (2.78)$$

where we have used

$$M_Z^2 = \frac{1}{4} (g^2 + g'^2) (v_u^2 + v_d^2), \quad M_W^2 = \frac{1}{4} g^2 (v_u^2 + v_d^2), \quad (2.79)$$

$$\cos 2\beta = \frac{v_d^2 - v_u^2}{v_d^2 + v_u^2}, \quad \tan \beta + \cotan \beta = \frac{2}{\sin 2\beta}, \quad (2.80)$$

$$\cos \beta = \frac{v_d}{\sqrt{v_d^2 + v_u^2}} \equiv c_\beta, \quad \sin \beta = \frac{v_u}{\sqrt{v_d^2 + v_u^2}} \equiv s_\beta \quad (2.81)$$

$$\cos \theta_W = \frac{g}{\sqrt{g^2 + g'^2}} \equiv c_W, \quad \sin \theta_W = \frac{g'}{\sqrt{g^2 + g'^2}} \equiv s_W. \quad (2.82)$$

The first term in (2.78) corresponds to pseudo-scalar mass terms, and the second one represents scalar mass terms. Both of them are expressed in terms of their gauge eigenstates, namely $(\text{Im}(H_d^0), \text{Im}(H_u^0))$ and $(\text{Re}(H_d^0), \text{Re}(H_u^0))$ for the pseudo-scalar and scalar part respectively. After electroweak symmetry breaking, gauge eigenstates with the same quantum numbers mix one with another, it is thus necessary to diagonalize their respective mass matrix in order to determine the true physical eigenstates and their associated mass eigenvalues.

CP-odd Higgs sector

The diagonalization of the pseudo-scalar 2×2 mass matrix gives

$$G^0 = -\cos \beta \text{Im}(H_d^0) + \sin \beta \text{Im}(H_u^0), \quad (2.83)$$

$$A^0 = \sin \beta \text{Im}(H_d^0) + \cos \beta \text{Im}(H_u^0), \quad (2.84)$$

with

$$M_{G^0} = 0, \quad (2.85)$$

$$M_{A^0}^2 = \frac{2B\mu}{\sin 2\beta} = 2|\mu|^2 + m_{H_d}^2 + m_{H_u}^2. \quad (2.86)$$

CP-even Higgs sector

Using (2.86), it is possible to rewrite the scalar 2×2 mass matrix as

$$M_S^2 = \begin{pmatrix} M_Z^2 \cos^2 \beta + M_{A^0}^2 \sin^2 \beta & -(M_Z^2 + M_{A^0}^2) \cos \beta \sin \beta \\ -(M_Z^2 + M_{A^0}^2) \cos \beta \sin \beta & M_Z^2 \sin^2 \beta + M_{A^0}^2 \cos^2 \beta \end{pmatrix}.$$

The diagonalization leads to

$$H^0 = \cos \alpha \text{Re}(H_d^0) + \sin \alpha \text{Re}(H_u^0), \quad (2.87)$$

$$h^0 = -\sin \alpha \text{Re}(H_d^0) + \cos \alpha \text{Re}(H_u^0), \quad (2.88)$$

with

$$M_{H^0}^2 = \frac{1}{2} \left[M_Z^2 + M_{A^0}^2 + \sqrt{(M_Z^2 - M_{A^0}^2)^2 + 4M_Z^2 M_{A^0}^2 \sin^2 2\beta} \right], \quad (2.89)$$

$$M_{h^0}^2 = \frac{1}{2} \left[M_Z^2 + M_{A^0}^2 - \sqrt{(M_Z^2 - M_{A^0}^2)^2 + 4M_Z^2 M_{A^0}^2 \sin^2 2\beta} \right], \quad (2.90)$$

$$\tan 2\alpha = \tan 2\beta \frac{M_{A^0}^2 + M_Z^2}{M_{A^0}^2 - M_Z^2}, \quad (2.91)$$

which gives the following sum rule when adding (2.89) and (2.90)

$$M_{H^0}^2 + M_{h^0}^2 = M_Z^2 + M_{A^0}^2. \quad (2.92)$$

The light Higgs mass in the decoupling limit

The decoupling limit is the limit for which $M_{A^0} \gg M_Z$. It is called the decoupling limit because in this particular case the mass of the lightest Higgs M_{h^0} , can be re-expressed independently of the mass of the pseudo-scalar M_{A^0} . Starting from (2.90), it is possible to rewrite M_{h^0} such that

$$\begin{aligned} M_{h^0}^2 &= \frac{1}{2} \left[M_Z^2 + M_{A^0}^2 - \sqrt{M_Z^4 + M_{A^0}^4 - 2M_Z^2 M_{A^0}^2 + 4M_Z^2 M_{A^0}^2 (1 - \cos^2 2\beta)} \right] \\ &= \frac{1}{2} \left[M_Z^2 + M_{A^0}^2 - \sqrt{(M_Z^2 + M_{A^0}^2)^2 - 4M_Z^2 M_{A^0}^2 \cos^2 2\beta} \right]. \end{aligned}$$

Factorizing $M_{A^0}^2$ out of the previous equation gives

$$M_{h^0}^2 = \frac{1}{2}M_{A^0}^2 \left(1 + \frac{M_Z^2}{M_{A^0}^2}\right) \left[1 - \sqrt{1 - \frac{4M_Z^2 M_{A^0}^2 \cos^2 2\beta}{M_{A^0}^4 (1 + M_Z^2/M_{A^0}^2)^2}}\right]. \quad (2.93)$$

After performing a series expansion in terms of $M_Z^2/M_{A^0}^2$, taking the limit $M_{A^0} \gg M_Z$, and a few practical manipulations, we obtain for the light CP-even Higgs mass

$$M_{h^0}^2 \simeq M_Z^2 \cos^2 2\beta. \quad (2.94)$$

Thus, at tree level in the MSSM one always has

$$M_{h^0}^2 \lesssim M_Z^2 \cos^2 2\beta. \quad (2.95)$$

This theoretical upper bound on $M_{h^0}^2$, which openly conflicts with the recent observation of a 125 GeV Higgs boson at the LHC, and older LEP constraints [104, 105], can still be evaded by taking into account large one-loop corrections involving especially the stops (top superpartners).

Charged Higgs sector

Using a similar method, it is possible to derive the potential in the charged sector from (2.69). Once again, we make use of (2.69), (2.79), (2.74), (2.80), (2.72), (2.73), and (2.86), and we yield in the basis (H_d^-, H_u^+) the following mass matrix for the charged Higgs bosons

$$M_{\pm} = \begin{pmatrix} (M_W^2 + M_{A^0}^2) \sin^2 \beta & (M_W^2 + M_{A^0}^2) \cos \beta \sin \beta \\ (M_W^2 + M_{A^0}^2) \cos \beta \sin \beta & (M_W^2 + M_{A^0}^2) \cos^2 \beta \end{pmatrix}.$$

The diagonalization gives

$$G^- = -\cos \beta H_d^- + \sin \beta H_u^{+\dagger}, \quad (2.96)$$

$$H^- = \sin \beta H_d^- + \cos \beta H_u^{+\dagger}, \quad (2.97)$$

$$G^+ = -\cos \beta H_d^{-\dagger} + \sin \beta H_u^+, \quad (2.98)$$

$$H^+ = \sin \beta H_d^{-\dagger} + \cos \beta H_u^+, \quad (2.99)$$

with

$$M_{H^\pm} = M_W^2 + M_{A^0}^2 = M_W^2 + 2|\mu|^2 + m_{H_d}^2 + m_{H_u}^2, \quad (2.100)$$

$$M_{G^\pm} = 0, \quad (2.101)$$

where (2.100) is the equivalent of the sum rule (2.92) in the charged Higgs sector.

2.10 Gaugino and Higgsino sector

After the electroweak symmetry breaking, all the particles with the same quantum numbers mix one with another. The electroweak gauginos, and the Higgsinos form a mixing system whose mass eigenstates are collectively denoted as charginos and neutralinos. Charginos ($\tilde{\chi}_i^\pm$) are Dirac fermions which consist of an admixture of the two charged winos (\tilde{W}^\pm) and Higgsinos ($\tilde{H}_u^\pm, \tilde{H}_d^\pm$), while neutralinos ($\tilde{\chi}_i^0$) are Majorana fermions, and amount to a linear combination of the bino (\tilde{B}), the neutral wino (\tilde{W}^3) and the neutral Higgsinos ($\tilde{H}_u^0, \tilde{H}_d^0$), where in this notation the chargino index $i \in \{1, 2\}$, and the neutralino index $i \in \{1, 2, 3, 4\}$.

The contributions to the gaugino and Higgsino mass terms originate from three distinct sources, the Higgs-Higgsino-wino interactions, the Higgs/Higgsino bilinear term of the MSSM superpotential, and the gaugino mass terms of the soft SUSY-breaking potential

Higgs-Higgsino-wino interactions:

$$\begin{aligned} \Delta\mathcal{L}_1 = & -\frac{i}{2}g v_d \left(\sqrt{2}\tilde{H}_d^- \cdot \tilde{W}^+ + \tilde{H}_d^0 \cdot \tilde{W}_3 \right) + \frac{i}{2}g' v_d \tilde{H}_d^0 \cdot \tilde{B} \\ & -\frac{i}{2}g v_u \left(\sqrt{2}\tilde{H}_u^+ \cdot \tilde{W}^- - \tilde{H}_u^0 \cdot \tilde{W}_3 \right) - \frac{i}{2}g' v_u \tilde{H}_u^0 \cdot \tilde{B} + \text{h.c.} , \end{aligned} \quad (2.102)$$

Higgs/Higgsino bilinear term of the MSSM superpotential:

$$\Delta\mathcal{L}_2 = \mu \tilde{H}_d^0 \tilde{H}_u^0 - \mu \tilde{H}_d^- \tilde{H}_u^+ + \text{h.c.} , \quad (2.103)$$

Gaugino mass terms of the soft SUSY-breaking potential:

$$\Delta\mathcal{L}_3 = \frac{1}{2}M_1 \tilde{B} \cdot \tilde{B} + \frac{1}{2}M_2 \tilde{W}^3 \cdot \tilde{W}_3 + M_2 \tilde{W}^+ \cdot \tilde{W}^- + \frac{1}{2}M_3 \tilde{g}^a \cdot \tilde{g}_a + \text{h.c.} . \quad (2.104)$$

As a final remark, let us note that since the $SU(3)_C$ gauge group remains unbroken in the MSSM, the gluino \tilde{g} (which is a color octet Majorana fermion) cannot mix with any other particle in the theory, and thus is simultaneously a gauge and a physical mass eigenstate. The soft-SUSY breaking gluino mass parameter M_3 of (2.104) is in general complex and defined as

$$M_3 = |M_3| e^{i\varphi_{\tilde{g}}} \quad (\text{with the gluino mass } m_{\tilde{g}} = |M_3|) , \quad (2.105)$$

where $\varphi_{\tilde{g}}$ corresponds to the gluino phase.

Chargino sector

Extracting out of (2.102), (2.103), and (2.104), the charged winos and Higgsinos contributions, one obtains the following tree level mass term for the charginos

$$\begin{aligned} \mathcal{L}_{\chi^\pm} = & -\frac{i}{2}g v_d \sqrt{2}\tilde{H}_d^- \cdot \tilde{W}^+ - \frac{i}{2}g v_u \sqrt{2}\tilde{H}_u^+ \cdot \tilde{W}^- - \mu \tilde{H}_d^- \tilde{H}_u^+ + M_2 \tilde{W}^+ \cdot \tilde{W}^- + \text{h.c.} \\ = & -\left(\tilde{W}^- \quad \tilde{H}_d^- \right) \begin{pmatrix} -M_2 & \frac{i}{2}g v_u \sqrt{2} \\ \frac{i}{2}g v_d \sqrt{2} & \mu \end{pmatrix} \begin{pmatrix} \tilde{W}^+ \\ \tilde{H}_u^+ \end{pmatrix} + \text{h.c.} . \end{aligned}$$

A factor of i can be absorbed into the redefinition of the charged winos [103] such that the tree level chargino mass matrix only contains real entries. This gives

$$\mathcal{L}_{\chi^\pm} = -\left(i\tilde{W}^- \quad \tilde{H}_d^- \right) \begin{pmatrix} M_2 & \sqrt{2}M_W \sin \beta \\ \sqrt{2}M_W \cos \beta & \mu \end{pmatrix} \begin{pmatrix} i\tilde{W}^+ \\ \tilde{H}_u^+ \end{pmatrix} + \text{h.c.} , \quad (2.106)$$

which can be also re-expressed as

$$\mathcal{L}_{\chi^\pm} = -\frac{1}{2} \left((\psi^+)^T \quad (\psi^-)^T \right) \begin{pmatrix} 0 & X^T \\ X & 0 \end{pmatrix} \begin{pmatrix} \psi^+ \\ \psi^- \end{pmatrix} + \text{h.c.} , \quad (2.107)$$

with

$$X = \begin{pmatrix} M_2 & \sqrt{2}M_W \sin \beta \\ \sqrt{2}M_W \cos \beta & \mu \end{pmatrix} , \quad \text{and } \psi^\pm = (i\tilde{W}^\pm, \tilde{H}_{u,d}^\pm)^T .$$

Since X is not symmetric, it must be diagonalized by two unitary matrices U and V satisfying

$$U^* X V^{-1} = \text{diag}(m_{\tilde{\chi}_1^\pm}, m_{\tilde{\chi}_2^\pm}) , \quad (2.108)$$

where $m_{\tilde{\chi}_1^\pm} < m_{\tilde{\chi}_2^\pm}$ are the masses of the charginos, and where the gauge eigenstates ψ^\pm are related to the physical mass eigenstates χ_i^\pm by

$$\chi_i^+ = V_{ij} \psi_j^+, \quad \chi_j^- = U_{ij} \psi_j^-,$$

with $i, j = 1, 2$. The mixing matrix V can be obtained after diagonalization of the hermitian matrix $X^\dagger X$. From (2.108), one thus has

$$V X^\dagger X V^{-1} = \text{diag}(m_{\tilde{\chi}_1^\pm}^2, m_{\tilde{\chi}_2^\pm}^2), \quad (2.109)$$

which gives the following charginos masses after diagonalization

$$m_{\tilde{\chi}_1^\pm, \tilde{\chi}_2^\pm}^2 = \frac{1}{2} \left[M_2^2 + 2M_W^2 + \mu^2 \pm \sqrt{(M_2^2 + 2M_W^2 + \mu^2)^2 - 4(M_2\mu + M_W^2 \sin 2\beta)^2} \right].$$

Neutralino sector

In a very similar manner, extracting out of (2.102), (2.103), and (2.104), the neutral bino, wino, and Higgsinos contributions, one obtains the following tree level mass term for the neutralinos

$$\begin{aligned} \mathcal{L}_{\chi^0} &= -\frac{i}{2} g v_d \tilde{H}_d^0 \cdot \tilde{W}_3 + \frac{i}{2} g' v_d \tilde{H}_d^0 \cdot \tilde{B} + \frac{i}{2} g v_u \tilde{H}_u^0 \cdot \tilde{W}_3 - \frac{i}{2} g' v_u \tilde{H}_u^0 \cdot \tilde{B} + \mu \tilde{H}_d^0 \tilde{H}_u^0 \\ &\quad + \frac{1}{2} M_1 \tilde{B} \cdot \tilde{B} + \frac{1}{2} M_2 \tilde{W}^3 \cdot \tilde{W}_3 + \text{h.c.} \\ &= -\frac{1}{2} \begin{pmatrix} \tilde{B} & \tilde{W}^3 & \tilde{H}_d^0 & \tilde{H}_u^0 \end{pmatrix} \begin{pmatrix} -M_1 & 0 & -\frac{i}{2} g' v_d & \frac{i}{2} g' v_u \\ 0 & -M_2 & \frac{i}{2} g v_d & -\frac{i}{2} g v_u \\ -\frac{i}{2} g' v_d & \frac{i}{2} g v_d & 0 & -\mu \\ \frac{i}{2} g' v_u & -\frac{i}{2} g v_u & -\mu & 0 \end{pmatrix} \begin{pmatrix} \tilde{B} \\ \tilde{W}^3 \\ \tilde{H}_d^0 \\ \tilde{H}_u^0 \end{pmatrix} + \text{h.c.} . \end{aligned}$$

Just like for the charginos, a factor of i can be absorbed into the redefinition of the neutral gauginos [103], so that the tree level neutralino mass matrix only contains real entries

$$\mathcal{L}_{\chi^0} = -\frac{1}{2} \begin{pmatrix} i\tilde{B} & i\tilde{W}^3 & \tilde{H}_d^0 & \tilde{H}_u^0 \end{pmatrix} \begin{pmatrix} M_1 & 0 & -M_Z s_W c_\beta & M_Z s_W s_\beta \\ 0 & M_2 & M_Z c_W c_\beta & -M_Z c_W s_\beta \\ -M_Z s_W c_\beta & M_Z c_W c_\beta & 0 & -\mu \\ M_Z s_W c_\beta & -M_Z c_W s_\beta & -\mu & 0 \end{pmatrix} \begin{pmatrix} i\tilde{B} \\ i\tilde{W}^3 \\ \tilde{H}_d^0 \\ \tilde{H}_u^0 \end{pmatrix}.$$

The neutralino mass matrix $M_{\tilde{\chi}^0}$ is moreover completely symmetric, which means that it can be diagonalized with the help of only one unitary mixing matrix N , such that

$$N^* M_{\tilde{\chi}^0} N^{-1} = \text{diag}(m_{\tilde{\chi}_1^0}, m_{\tilde{\chi}_2^0}, m_{\tilde{\chi}_3^0}, m_{\tilde{\chi}_4^0}), \quad (2.110)$$

where $m_{\tilde{\chi}_1^0} < m_{\tilde{\chi}_2^0} < m_{\tilde{\chi}_3^0} < m_{\tilde{\chi}_4^0}$ are the neutralino masses, which are chosen real and positive according to the Supersymmetry Les Houches Accord 2 (SLHA2) conventions, and where the gauge eigenstates ψ^0 are related to the physical mass eigenstates $\tilde{\chi}^0$ by

$$\tilde{\chi}_i^0 = N_{ij} \psi_j^0, \quad (2.111)$$

with $i, j = 1, 2, 3, 4$. Neutralinos are electrically-neutral and color-neutral, massive weakly interacting particles. The lightest neutralino $\tilde{\chi}_1^0$ is usually assumed to be the Lightest Supersymmetric Particle (LSP) and as a consequence provide a potentially viable candidate for Dark Matter, as long as R -parity is preserved.

2.11 Sfermion sector

After the electroweak symmetry breaking, the Higgsinos and the gauginos are not the only states to form a mixing system, the right-handed and left-handed sfermions (with the same quantum numbers) do mix as well. The squark and slepton mass eigenstates are obtained after diagonalization of their respective mass matrix. In the most general case, *i.e.* Non-Minimal Flavour Violation (NMFV), this diagonalization requires the introduction of three 6×6 unitary matrices, namely $R^{\tilde{u}}$, $R^{\tilde{d}}$ and $R^{\tilde{e}}$, respectively for the up-type squarks, down-type squarks, and for the charged sleptons. In the super-CKM and super-PMNS basis, those mixing matrices, which allow for rotations between gauge and physical mass eigenstates, are defined such that

$$\begin{pmatrix} \tilde{u}_1 \\ \tilde{u}_2 \\ \tilde{u}_3 \\ \tilde{u}_4 \\ \tilde{u}_5 \\ \tilde{u}_6 \end{pmatrix} = R^{\tilde{u}} \begin{pmatrix} \tilde{u}_L \\ \tilde{c}_L \\ \tilde{t}_L \\ \tilde{u}_R \\ \tilde{s}_R \\ \tilde{t}_R \end{pmatrix}, \quad \begin{pmatrix} \tilde{d}_1 \\ \tilde{d}_2 \\ \tilde{d}_3 \\ \tilde{d}_4 \\ \tilde{d}_5 \\ \tilde{d}_6 \end{pmatrix} = R^{\tilde{d}} \begin{pmatrix} \tilde{d}_L \\ \tilde{s}_L \\ \tilde{b}_L \\ \tilde{d}_R \\ \tilde{s}_R \\ \tilde{b}_R \end{pmatrix}, \quad \begin{pmatrix} \tilde{e}_1 \\ \tilde{e}_2 \\ \tilde{e}_3 \\ \tilde{e}_4 \\ \tilde{e}_5 \\ \tilde{e}_6 \end{pmatrix} = R^{\tilde{e}} \begin{pmatrix} \tilde{e}_L \\ \tilde{\mu}_L \\ \tilde{\tau}_L \\ \tilde{e}_R \\ \tilde{\mu}_R \\ \tilde{\tau}_R \end{pmatrix}, \quad (2.112)$$

$$R^{\tilde{u}} \mathcal{M}_{\tilde{u}}^2 R^{\tilde{u}\dagger} = \text{diag}(\tilde{u}_1, \dots, \tilde{u}_6), \quad R^{\tilde{d}} \mathcal{M}_{\tilde{d}}^2 R^{\tilde{d}\dagger} = \text{diag}(\tilde{d}_1, \dots, \tilde{d}_6), \\ R^{\tilde{e}} \mathcal{M}_{\tilde{e}}^2 R^{\tilde{e}\dagger} = \text{diag}(\tilde{e}_1, \dots, \tilde{e}_6),$$

where \tilde{u}_i , \tilde{d}_i , and \tilde{e}_i , with $i = 1, \dots, 6$, denote sfermion mass eigenstates, and where the vectors $(\tilde{u}_L, \tilde{c}_L, \tilde{t}_L, \tilde{u}_R, \tilde{s}_R, \tilde{t}_R)$, $(\tilde{d}_L, \tilde{s}_L, \tilde{b}_L, \tilde{d}_R, \tilde{s}_R, \tilde{b}_R)$, and $(\tilde{e}_L, \tilde{\mu}_L, \tilde{\tau}_L, \tilde{e}_R, \tilde{\mu}_R, \tilde{\tau}_R)$ respectively contain up-type squarks, down-type squarks, and charged sleptons gauge eigenstates. By convention, sfermion mass eigenstates are ordered from the lightest to the heaviest one,

$$m_{\tilde{u}_1} < \dots < m_{\tilde{u}_6}, \quad m_{\tilde{d}_1} < \dots < m_{\tilde{d}_6}, \quad m_{\tilde{e}_1} < \dots < m_{\tilde{e}_6}.$$

The generic 6×6 sfermion mixing matrices of (2.112) naturally induce inter-generational mixing. This inter-generational mixing can in turn generate large Flavour Changing Neutral Currents (FCNCs) which are tightly constrained from an experimental point of view. A possible solution to avoid the appearance of large FCNCs consists in practice in imposing Minimal Flavour Violation (MFV), *i.e.* imposing that Yukawa couplings are the only source of flavour violation, and neglecting inter-generational mixing. In this context, the three 6×6 sfermion mixing matrices, reduce to a set of nine 2×2 unitary mixing matrices of the form,

$$\begin{pmatrix} \tilde{f}_1 \\ \tilde{f}_2 \end{pmatrix} = S^{\tilde{f}} \begin{pmatrix} \tilde{f}_L \\ \tilde{f}_R \end{pmatrix}, \quad \text{with} \quad S^{\tilde{f}} = \begin{pmatrix} \cos \theta_f & \sin \theta_f \\ -\sin \theta_f & \cos \theta_f \end{pmatrix}, \quad (2.113)$$

where $S^{\tilde{f}}$ is the flavour diagonal sfermion mixing matrix, where θ_f denotes the associated sfermion mixing angle, and where \tilde{f}_1, \tilde{f}_2 and \tilde{f}_L, \tilde{f}_R are respectively the sfermion mass and gauge eigenstates. In the MSSM, the sfermion mass terms originate from the F -terms, the D -terms, and the soft SUSY-breaking potential (through scalar mass terms and trilinear scalar couplings), such that

F -terms

$$V_F = m_f^2 \tilde{f}_R \tilde{f}_R^\dagger + m_f^2 \tilde{f}_L \tilde{f}_L^\dagger - \mu m_f (\tan \beta)^{-2T_3^f} \tilde{f}_L^\dagger \tilde{f}_R - \mu m_f (\tan \beta)^{-2T_3^f} \tilde{f}_L \tilde{f}_R^\dagger, \quad (2.114)$$

D-terms

$$V_D = M_Z^2 \cos 2\beta \left(T_3^f - Q_f \sin^2 \theta_W \right) \tilde{f}_L^\dagger \tilde{f}_L + Q_f M_Z^2 \cos 2\beta \sin^2 \theta_W \tilde{f}_R^\dagger \tilde{f}_R, \quad (2.115)$$

Soft SUSY-breaking potential

$$V_{soft} = m_L^2 \tilde{f}_L^\dagger \tilde{f}_L + m_R^2 \tilde{f}_R^\dagger \tilde{f}_R + m_f A_f \tilde{f}_L \tilde{f}_R^\dagger + m_f A_f \tilde{f}_L^\dagger \tilde{f}_R. \quad (2.116)$$

Putting together (2.114), (2.115), and (2.116), we obtain the following tree level mass matrix

$$\begin{pmatrix} \tilde{f}_L^\dagger & \tilde{f}_R^\dagger \end{pmatrix} \begin{pmatrix} m_f^2 + m_L^2 + M_Z^2 \cos 2\beta \left(T_3^f - Q_f \sin^2 \theta_W \right) & m_f \left(A_f - \mu (\tan \beta)^{-2T_3^f} \right) \\ m_f \left(A_f - \mu (\tan \beta)^{-2T_3^f} \right) & m_f^2 + m_R^2 + Q_f M_Z^2 \cos 2\beta \sin^2 \theta_W \end{pmatrix} \begin{pmatrix} \tilde{f}_L \\ \tilde{f}_R \end{pmatrix}.$$

The off-diagonal terms of the 2×2 sfermion mass matrix are proportional to the fermion mass m_f . The mixing between sfermions of the same type is therefore of particular significance for the third generation in general, *i.e.* stops, sbottoms and staus, and even more important in the case of the stops, as the top mass is much larger than any of the other SM fermion mass. If we now introduce the compact notation

$$\begin{aligned} m_{\tilde{f}_L}^2 &= m_f^2 + m_L^2 + M_Z^2 \cos 2\beta \left(T_3^f - Q_f \sin^2 \theta_W \right), \\ m_{\tilde{f}_R}^2 &= m_f^2 + m_R^2 + Q_f M_Z^2 \cos 2\beta \sin^2 \theta_W, \\ a_f &= A_f - \mu (\tan \beta)^{-2T_3^f}, \end{aligned}$$

we can rewrite the previous sfermion mass matrix as

$$\mathcal{M}_f^2 = \begin{pmatrix} m_{\tilde{f}_L}^2 & a_f m_f \\ a_f m_f & m_{\tilde{f}_R}^2 \end{pmatrix}. \quad (2.117)$$

Using the sfermion mixing angle of (2.113) to diagonalize (2.117), we obtain the following results for the sfermion mass eigenstates $m_{\tilde{f}_1}$, $m_{\tilde{f}_2}$, and the sfermion mixing angle

$$m_{\tilde{f}_{1,2}}^2 = \frac{1}{2} \left[m_{\tilde{f}_L}^2 + m_{\tilde{f}_R}^2 \mp \sqrt{(m_{\tilde{f}_L}^2 - m_{\tilde{f}_R}^2)^2 + 4 a_f^2 m_f^2} \right], \quad (2.118)$$

$$\cos \theta_f = - \frac{a_f m_f}{\sqrt{(m_{\tilde{f}_L}^2 - m_{\tilde{f}_1}^2)^2 + a_f^2 m_f^2}} \quad (0 \leq \theta_f < \pi) \quad (2.119)$$

Summary:

In this chapter, we have provided a short introduction to $\mathcal{N} = 1$ supersymmetry, which constitutes the theoretical basis of this manuscript. More specifically, we have first recalled some basic facts about SUSY (history, motivations, superalgebra and properties of the supermultiplets), before introducing the superspace formalism, and detailing the various steps inherent to the construction of supersymmetric Lagrangians. In the second part of this chapter, we have then focused on one particular implementation of $\mathcal{N} = 1$ supersymmetry, namely the Minimal Supersymmetric Standard Model, for which we have described the mechanism of electroweak symmetry breaking, and detailed the various sectors of the theory at tree level. In the coming chapters, we are going to apply the concepts, and the notations, we have just introduced to the case of phenomenological studies at leading order, and next-to-leading in perturbation theory.

Chapter 3

Leading Order phenomenology at polarized hadron colliders

In this chapter, we intend to show how polarized proton beams colliding at 14 TeV and 100 TeV could help us to disentangle various new physics models exhibiting the same final-state signature. For the sake of illustration, we focus on the recently proposed monotop signature [106,107], which corresponds to the production of a single top in association with missing transverse energy. Monotops naturally appear in several extensions of the Standard Model, like for example in the MSSM (discussed in the previous chapter) with R -parity violation (RPV), where they are issued from the decay of a singly-produced top squark [108–111]. Besides this RPV mode, monotops can also be produced in various dark matter models [112–115], where the monotop state originates either from the decay of a vector resonance, or from tree-level flavour-changing neutral interactions, with a particle giving rise to missing transverse energy. In the following, we discuss how the measurements of single-spin and double-spin asymmetries at a polarized LHC, or at a polarized FCC, would allow us to get additional information on the nature of the initial partons at the origin of the monotop signal, and show how this could be used in order to constrain the underlying new physics scenario.

This chapter is organized as follows: in Section 3.1, we review the status of new physics searches at the LHC, and motivate the use of polarized beams at LHC-14, and at an hypothetical FCC operating at 100 TeV. In Section 3.2, we perform a detailed study of the PDFs and the parton luminosities for polarized proton-proton collisions at 14 TeV and 100 TeV, showing the ability of spin asymmetries to discriminate among different initial states. Then, we assume the observation of a monotop excess in unpolarized proton-proton collisions, and illustrate in Section 3.3 how spin asymmetries would possibly allow one to get information on the new physics scenarios that have yielded the signal. Finally, we draw our conclusions in Section 3.4.

3.1 Motivations

After 3 years of data-taking, no experimental evidence of New Physics has been found at the LHC, while both the ATLAS and CMS collaborations have probed quite extensively energies up to the TeV scale. The mass exclusion limits of several BSM particles have been pushed higher and higher in energy, and this together with the discovery of a 125 GeV Standard Model-like Higgs boson has led to the exclusion of large fractions of the parameter space of many simplified models. With the current Run II of the Large Hadron Collider, and its proposed high-luminosity upgrade, searches for new phenomena, particles, and interactions, promise to survey an even wider portion of the parameter space of a huge variety of BSM scenarios. If New Physics has to be discovered in the coming years, the main goal of the high energy physics program will be to

fully characterize the newly discovered degrees of freedom, *i.e.* to determine the mass, spin and couplings of the latter.

In most studies performed at unpolarized hadron colliders such as the LHC, experimental (and phenomenological) analyses are motivated by theoretical arguments implying some key new final-state signatures that should be looked for. Those signatures are however neither typical of a given theory, nor of a given benchmark scenario of a specific model. One of the most famous example illustrating this fact is the case of the MSSM [44, 116] and Universal Extra Dimensions (UED) [117], which both predict the pair production of Standard Model partners followed by their cascade decay into a final state enriched in charged leptons and jets, and containing in addition a large amount of missing transverse energy. Beyond discovery, the task of disentangling BSM theories (and even different scenarios within a specific theory) that share a common final-state signature is therefore known to be far from trivial.

In addition to the LHC, there is another high-energy hadron collider that has been providing an impressive wealth of results. The RHIC collider at the Brookhaven National Laboratory (BNL) has successfully operated in its polarized proton-proton mode at 200 GeV and 500 GeV, collecting data with an integrated luminosity of more than 1 fb^{-1} . Although these polarized collisions are mainly dedicated to spin physics, pioneering BSM studies have shown the non-negligible impact of beam polarization to get a handle on (some of) the model parameters of specific theories [118–124]. In addition to the existing RHIC polarized proton collider, most of the aforementioned studies have also considered possible polarization upgrades of both the Tevatron [125] and the LHC. However, although those upgrades have been already discussed in the past and are perfectly feasible [126, 127], they are quite unlikely to be realized. In contrast, first discussions on a Future Circular Collider (FCC) with a center-of-mass energy of 100 TeV are now starting. Therefore, this is the right time to begin to present the physics cases motivating different operating options of such a machine, including a possible polarized mode.

3.2 Spin asymmetries at polarized hadron colliders

As mentioned in the introduction, polarized beams at high-energy hadron colliders would provide a unique opportunity to characterize any new physics signal that might have been previously observed in unpolarized collisions. This appealing possibility relies on the fact that polarized and unpolarized parton-parton luminosities show quite different behaviours for a given flavour combination. Therefore, single- and double-spin asymmetries in polarized hadron collisions can provide information on the initial partonic state of any given process, thus allowing one to disentangle different BSM scenarios that lead to the same final state signatures.

In the next section, we will exploit these remarkable properties to distinguish between new physics scenarios for monotop production at the LHC, characterized by different initial state production mechanisms and thus by different single- and double-spin asymmetries in polarized collisions. However, before discussing specific models, it is instructive to first evaluate a variety of single- and double-spin asymmetries at the level of parton luminosities rather than at the full hadronic cross section level. This approximation is useful since in many cases of interest the polarized and unpolarized matrix elements are similar, and thus the spin asymmetries computed from the partonic luminosities only already carry the bulk of the relevant physics which is accessible experimentally via the hadron-level asymmetries.

First of all, we compare polarized and unpolarized PDFs. To fix the notation, we define unpolarized and polarized parton distributions as usual,

$$f_{i/p}(x, Q^2) \equiv f_{i/p}^{\uparrow}(x, Q^2) + f_{i/p}^{\downarrow}(x, Q^2), \quad (3.1)$$

$$\Delta f_{i/p}(x, Q^2) \equiv f_{i/p}^{\uparrow}(x, Q^2) - f_{i/p}^{\downarrow}(x, Q^2), \quad (3.2)$$

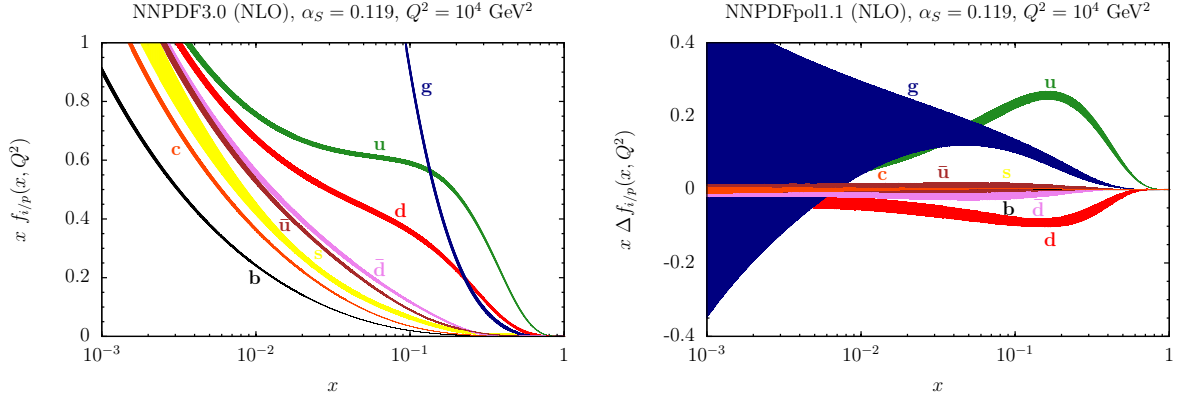


Figure 3.1: Comparison between unpolarized (left) and polarized (right) PDFs from the most up-to-date sets of the NNPDF family, NNPDF3.0 and NNPDFpol1.1 respectively. PDFs have been evaluated at a typical high-energy hadron collider scale of $Q^2 = 10^4 \text{ GeV}^2$.

in terms of the two possible longitudinal polarization states of partons within the nucleon,

$$f_{i/p}^\uparrow(x, Q^2) = f_{i/p}(x, Q^2) + \Delta f_{i/p}(x, Q^2), \quad (3.3)$$

$$f_{i/p}^\downarrow(x, Q^2) = f_{i/p}(x, Q^2) - \Delta f_{i/p}(x, Q^2). \quad (3.4)$$

In Figure 3.1, we present a comparison between the different PDFs of the most up-to-date unpolarized and polarized sets from the NNPDF Collaboration¹, NNPDF3.0 [128] and NNPDF-pol1.1 [129, 130] respectively. The various PDFs have been evaluated at a typical hadron collider scale of $Q^2 = 10^4 \text{ GeV}^2$ using the LHAPDF interface [131]. As an example, the source code that has been used to generate the graphs of Figure 3.1 can be found in Appendix C.

There are various interesting features to remark in Figure 3.1. The first one is that polarized PDFs are always smaller (in absolute value) than their unpolarized counterparts. This is a consequence of the positivity condition of polarized PDFs [132], which at Born level reads,

$$|\Delta f_{i/p}(x, Q^2)| \leq f_{i/p}(x, Q^2). \quad (3.5)$$

At next-to-leading order, similar relations hold but only for physical observables like polarized structure functions. The second feature is that at small- x the growth of the polarized PDFs $x\Delta f_{i/p}(x, Q^2)$ is largely suppressed with respect to that of the unpolarized ones $x f_{i/p}(x, Q^2)$ [133]. As will be shown below, these two features have the important implication that spin asymmetries will be sizable, and thus experimentally accessible, only for final states with large invariant masses. This indeed probes the polarized PDFs at medium and large values of x , two regions where their magnitude is comparable to the one of the unpolarized parton densities.

In addition, and this is of particular importance for the problem at hand, a specific flavour leads to different qualitative behaviours for the polarized and unpolarized PDFs. For instance, Δu and Δd have the opposite sign, while u and d have both the same sign and the same shape. This will translate into qualitatively different behaviours for the various spin asymmetries depending on the underlying initial partonic state.

After comparing PDFs at the unpolarized and polarized level, we move to the study of partonic luminosities [134] and the corresponding single- and double-spin asymmetries. We

¹The polarized and unpolarized sets of parton densities NNPDFpol1.1 and NNPDF3.0 are available from the webpage <https://nnpdf.hepforge.org>.

define the partonic luminosity for the scattering of two partons i and j in unpolarized hadronic collisions, leading to a final state of mass m_X , as

$$\mathcal{L}_{ij} = \frac{1}{s} \int_{\tau}^1 \frac{dx}{x} \frac{1}{1 + \delta_{ij}} \left[f_{i/p}(x, m_X) f_{j/p}\left(\frac{\tau}{x}, m_X\right) + f_{i/p}\left(\frac{\tau}{x}, m_X\right) f_{j/p}(x, m_X) \right], \quad (3.6)$$

where the δ_{ij} factor removes the double counting in the case of a same PDF combination $i = j$, and the collider center-of-mass energy squared $s = E_{\text{cm}}^2$ enters through the variable $\tau = \hat{s}/s$. We can also define corresponding quantities involving polarized parton distributions and thus relevant for polarized collisions. The partonic luminosity relevant for single-spin asymmetries is

$$\mathcal{L}_{ij}^L = \frac{1}{s} \int_{\tau}^1 \frac{dx}{x} \frac{1}{1 + \delta_{ij}} \left[f_{i/p}(x, m_X) \Delta f_{j/p}\left(\frac{\tau}{x}, m_X\right) + f_{i/p}\left(\frac{\tau}{x}, m_X\right) \Delta f_{j/p}(x, m_X) \right], \quad (3.7)$$

while for double-spin asymmetries, we use

$$\mathcal{L}_{ij}^{LL} = \frac{1}{s} \int_{\tau}^1 \frac{dx}{x} \frac{1}{1 + \delta_{ij}} \left[\Delta f_{i/p}(x, m_X) \Delta f_{j/p}\left(\frac{\tau}{x}, m_X\right) + \Delta f_{i/p}\left(\frac{\tau}{x}, m_X\right) \Delta f_{j/p}(x, m_X) \right]. \quad (3.8)$$

In our notation, the L and LL superscripts indicate that these luminosities enter the description of single- and double-spin asymmetries in polarized collisions, respectively. We now define unpolarized and polarized hadron-level cross sections by

$$\sigma_0 = \frac{1}{4} \left[\sigma^{\uparrow\uparrow} + \sigma^{\downarrow\downarrow} + \sigma^{\uparrow\downarrow} + \sigma^{\downarrow\uparrow} \right], \quad (3.9)$$

$$\sigma_L = \frac{1}{4} \left[\sigma^{\uparrow\uparrow} - \sigma^{\downarrow\downarrow} - \sigma^{\uparrow\downarrow} + \sigma^{\downarrow\uparrow} \right], \quad (3.10)$$

$$\sigma_{LL} = \frac{1}{4} \left[\sigma^{\uparrow\uparrow} + \sigma^{\downarrow\downarrow} - \sigma^{\uparrow\downarrow} - \sigma^{\downarrow\uparrow} \right]. \quad (3.11)$$

Here σ_0 stands for the unpolarized cross sections and σ_L and σ_{LL} for singly and doubly-polarized cross sections, respectively, where an up-arrow denotes a helicity $h = +1$ and a down-arrow a helicity $h = -1$ of longitudinally polarized hadrons in the initial state. We recall that in the case of singly-polarized cross sections, only one of the hadrons (the second one here) is polarized. Experimentally, it is useful to consider ratios of these cross sections, or spin asymmetries, because in this case systematic uncertainties are expected to cancel to a good degree. If a single beam is polarized, the experimentally relevant quantity is the single-spin asymmetry, defined as

$$A_L = \frac{\sigma_L}{\sigma_0}, \quad (3.12)$$

whereas if both beams are polarized, the relevant quantity is the double-spin asymmetry

$$A_{LL} = \frac{\sigma_{LL}}{\sigma_0}. \quad (3.13)$$

Eqs. (3.9)–(3.11) define experimentally accessible observables since they are expressed in terms of polarized hadrons. In order to compare data with theoretical predictions, in perturbative QCD the factorization theorem allows one to write hadronic cross sections as convolutions of parton distribution functions with parton level cross sections,

$$\sigma_0 = f_{i/p} \otimes f_{j/p} \otimes \hat{\sigma}_{0,ij} = \mathcal{L}_{ij} \otimes [\hat{s} \hat{\sigma}_{0,ij}], \quad (3.14)$$

$$\sigma_L = f_{i/p} \otimes \Delta f_{j/p} \otimes \hat{\sigma}_{L,ij} = \mathcal{L}_{ij}^L \otimes [\hat{s} \hat{\sigma}_{L,ij}], \quad (3.15)$$

$$\sigma_{LL} = \Delta f_{i/p} \otimes \Delta f_{j/p} \otimes \hat{\sigma}_{LL,ij} = \mathcal{L}_{ij}^{LL} \otimes [\hat{s} \hat{\sigma}_{LL,ij}]. \quad (3.16)$$

The polarized partonic cross sections are here defined in complete analogy to the polarized hadron-level expressions of Eqs. (3.9)–(3.11), namely

$$\hat{\sigma}_0 = \frac{1}{4} \left[\hat{\sigma}^{\uparrow\uparrow} + \hat{\sigma}^{\downarrow\downarrow} + \hat{\sigma}^{\uparrow\downarrow} + \hat{\sigma}^{\downarrow\uparrow} \right], \quad (3.17)$$

$$\hat{\sigma}_L = \frac{1}{4} \left[\hat{\sigma}^{\uparrow\uparrow} - \hat{\sigma}^{\downarrow\downarrow} - \hat{\sigma}^{\uparrow\downarrow} + \hat{\sigma}^{\downarrow\uparrow} \right], \quad (3.18)$$

$$\hat{\sigma}_{LL} = \frac{1}{4} \left[\hat{\sigma}^{\uparrow\uparrow} + \hat{\sigma}^{\downarrow\downarrow} - \hat{\sigma}^{\uparrow\downarrow} - \hat{\sigma}^{\downarrow\uparrow} \right], \quad (3.19)$$

where now the helicities are those of the incoming quarks and gluons in the partonic collision. Furthermore, a sum over all relevant partonic subprocesses is implied (*i.e.*, over i, j) and we refer to Eqs. (3.6)–(3.8) for the definition of the partonic luminosities.

For many cases of physical interest, the expressions in Eqs. (3.14)–(3.16) and consequently the asymmetries in Eqs. (3.12) and (3.13) can be further simplified. Firstly, the dimensionless cross sections $\hat{s}\hat{\sigma}_{ij}$ are often either constant far above the production threshold (see, *e.g.*, Figure 70 in Ref. [134]), or in the case of a narrow s -channel resonance, they are peaked at threshold, that is, $\hat{s} \simeq m_X^2$. In the latter case, we end up having simple expressions of the hadron-level asymmetries in terms of (ratios of weighted sums of) parton luminosities. Secondly, the absolute values of the polarized and unpolarized parton-level matrix elements are often the same or very similar, leading to further simplifications. In cases where there is a single dominant particular sub-channel, the hadronic asymmetries are just simple ratios of parton luminosities, as can be deduced from the single-spin and double-spin asymmetries of Eqs. (3.14)–(3.16),

$$A_L^{ij} = \frac{\mathcal{L}_{ij}^L}{\mathcal{L}_{ij}} \quad \text{and} \quad A_{LL}^{ij} = \frac{\mathcal{L}_{ij}^{LL}}{\mathcal{L}_{ij}}. \quad (3.20)$$

In the rest of this section, we focus on results for single and double-spin asymmetries computed from Eq. (3.20) for different initial state partonic sub-channels. We have calculated these asymmetries for the LHC collider operating at a center-of-mass energy of 14 TeV (LHC 14 TeV), assuming a possible future polarized upgrade, as well as for the polarized mode of an hypothetical Future Circular Collider with a center-of-mass energy of 100 TeV (FCC 100 TeV). As polarized PDFs we use the NNPDFpol1.1 [129, 130] and DSSV08 [135] sets, together with the corresponding unpolarized counterparts, NNPDF2.3 [136] and MRST01 [137]. Comparing the predictions of NNPDFpol1.1 with those of DSSV08 is useful in order to verify which features of the spin asymmetries are generic irrespective of the specific details of the particular polarized PDF set used.

It is clear from the definition of Eqs. (3.6)–(3.8) that to first approximation, luminosities are invariant if the center-of-mass energy is modified, $\sqrt{S'} = k\sqrt{S}$, provided that the final state mass is also modified in the same way, $m'_X = km_X$, since in this case the variable τ is invariant. However, logarithmic corrections to the DGLAP evolution of the PDFs modify this picture, though they should not change any qualitative conclusion. This property will be explicitly verified below when comparing the spin asymmetries at LHC 14 TeV and at FCC 100 TeV.

First of all, we compare the single-spin asymmetries at LHC 14 TeV for the production of a final state with invariant mass m_X assuming different partonic initial states. We compare the consistency of the asymmetries obtained with NNPDF with those obtained with DSSV/MRST. In all cases, the uncertainty band on the asymmetries corresponds to that of the polarized PDFs, since in this respect the unpolarized PDF uncertainties can be neglected. We show the asymmetries for gg , uu and dd initial states in the upper row Figure 3.2 and for the ds , db and sb initial states in the bottom row of the figure. The DSSV08 densities consist of a PDF set obtained in the fixed-flavor-number scheme, and therefore the polarized bottom PDF $\Delta b = \Delta \bar{b} = 0$. While

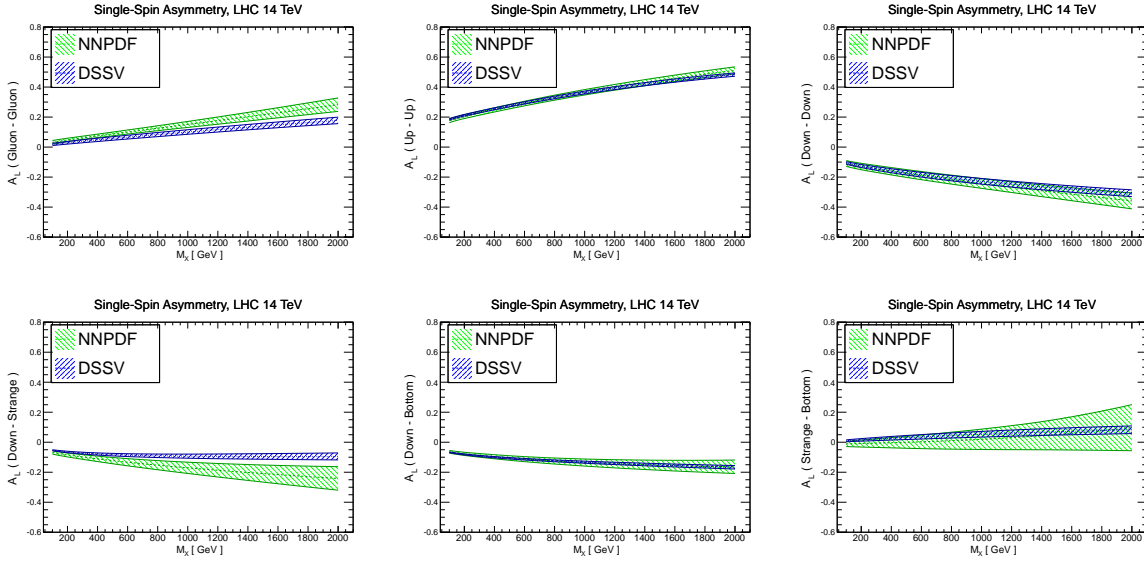


Figure 3.2: The single-spin asymmetry A_L at the parton luminosity level at LHC 14 TeV, and for various initial-state partonic combinations. We compare results obtained using NNPDF-pol1.1/NNPDF2.3 with those obtained using DSSV/MRST and present them as function of the invariant mass of the final state m_X . The bands correspond to the polarized PDF uncertainties.

differences between fixed-flavor-number and variable-flavor-number schemes lead to substantial differences for unpolarized PDFs [138], this is considered less important for polarized PDFs in the region with available experimental data where the contribution from heavy quarks is small. However, this is no longer true when evolving upwards in Q^2 to the region relevant for collider physics, where heavy quark PDFs are not negligible even in the polarized case.

In general there is a reasonable qualitative agreement between the results from NNPDF-pol1.1 and those of DSSV, with some quantitative differences, for instance in asymmetries that involve the polarized strange PDF. This is expected since NNPDFpol1.1 and DSSV08 generally agree well for all PDFs but for $\Delta s(x, Q^2)$, where even the sign is opposite [138]. Larger PDF uncertainties are obtained using NNPDFpol1.1, partially due to the more flexible functional form of the input PDFs as compared to DSSV08. Results for the single spin asymmetries for a 100 TeV FCC are qualitatively similar once the value of the final state mass is properly rescaled as discussed above, so that results are not shown explicitly.

Results for the single-spin asymmetries in the gg , uu , dd and ds partonic sub-channels for LHC 14 TeV and FCC 100 TeV are summarized in Figure 3.3. It is apparent that the property which we have discussed above, namely that if the final state mass range is suitably scaled, the qualitative features of the spin asymmetries are the same at center-of-mass energies of 14 TeV and 100 TeV. The most striking property is that different partonic sub-channels lead to very different asymmetries. In this particular case, just a measurement of the sign of the asymmetry would indicate which are the dominant partonic initial states, and measurements of A_L with a few percent experimental uncertainty would even distinguish between gg and qq initiated final states.

Double-spin asymmetries are experimentally more challenging since their absolute values are smaller. The reason for this is because they involve the convolution of two polarized PDFs in the numerator, instead of just one as for single-spin asymmetries. The results for various partonic channels are summarized in Figure 3.4. Again reasonable agreement between NNPDFpol1.1 and DSSV08 is found. Asymmetries involving quarks are larger than those involving gluons,

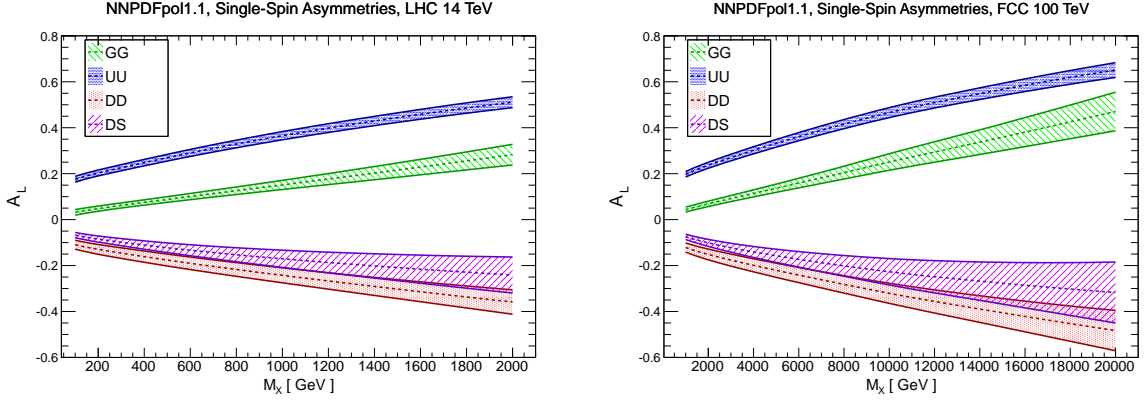


Figure 3.3: Summary of the single-spin asymmetries A_L for a variety of initial state partonic combinations as a function of the invariant mass of the produced final state m_X at the LHC 14 TeV (left panel) and at an FCC 100 TeV (right panel). The asymmetries have been obtained using NNPDFpol1.1/NNPDF2.3.

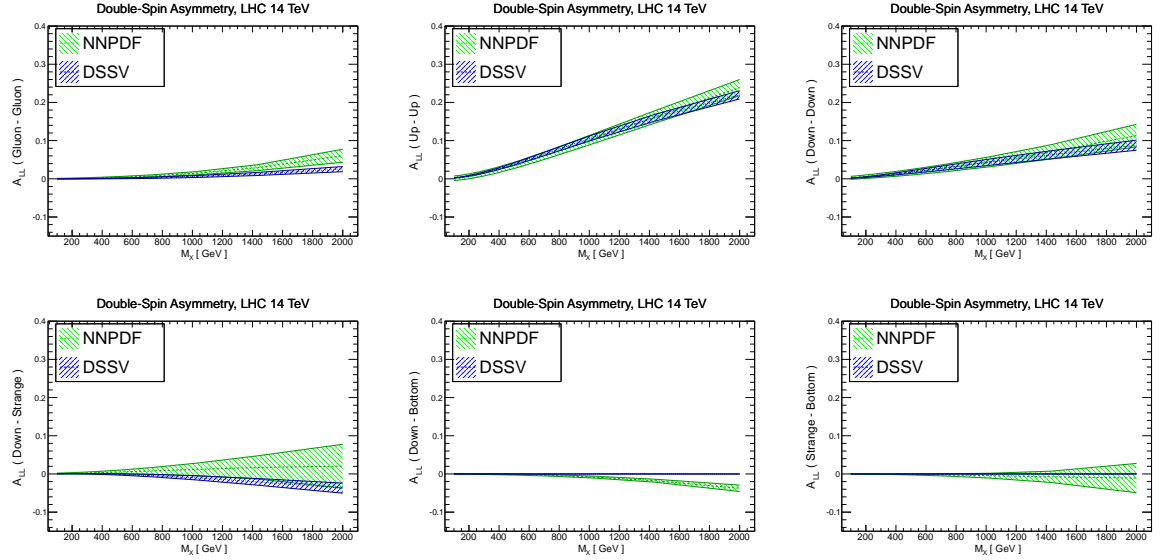


Figure 3.4: The double-spin asymmetry A_{LL} at the PDF level, Eq. (3.20), at LHC 14 TeV for various initial-state partonic combinations, comparing the results obtained using NNPDF-pol1.1/NNPDF2.3 with those obtained using DSSV/MRST.

reflecting that the Δq densities are larger than the Δg one at large- x , as shown in Figure 3.1. Moreover, large final state masses are required to yield spin asymmetries that are larger than a few percent.

The final comparison is provided by double-spin asymmetry calculations for the gg , uu , dd and ds partonic sub-channels for LHC 14 TeV and FCC 100 TeV and we collect the results in Figure 3.5. The PDF uncertainties are found to be very large, since there is far less experimental information in the determinations of the $\Delta f_{i/p}$ densities than in the unpolarized case. However, if the measurement of a vanishing double-spin asymmetry could be performed, this would be a valuable piece of information since it would exclude that the final state is dominantly produced from uu scattering. Moreover, double-spin asymmetry measurements could nevertheless be used

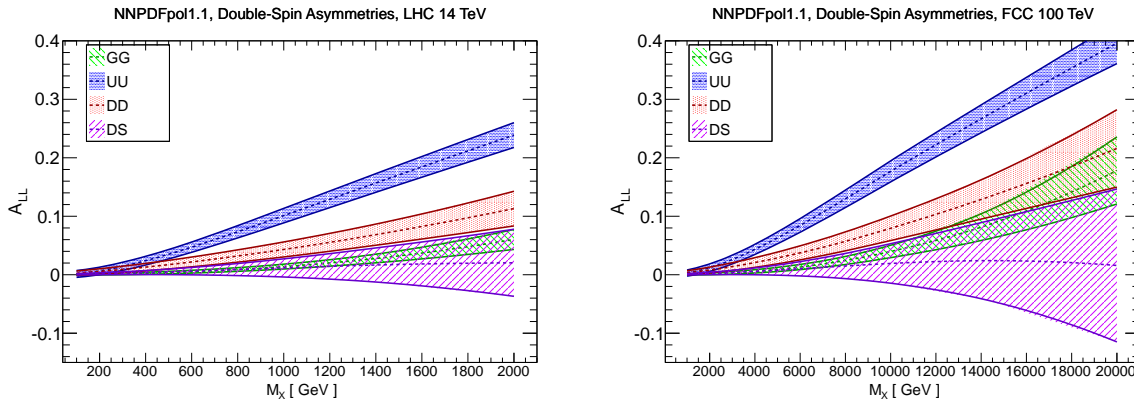


Figure 3.5: Summary of the double-spin asymmetries A_{LL} for a variety of initial state partonic combinations as a function of the invariant mass of the produced final state m_X at the LHC 14 TeV (left panel) and at an FCC 100 TeV (right panel). The asymmetries have been obtained using NNPDFpol1.1.

to verify the results obtained from single-spin asymmetries.

After this discussion at the PDF level only, in the next section we will present predictions for hadron-level asymmetries in various scenarios for BSM monotop production. From now on we will neglect for clarity the polarized PDF uncertainties. It has already been shown in this section that they are large, however, the availability of a polarized hadron collider would also provide a large set of polarized PDF-sensitive measurements that should substantially reduce these uncertainties. In addition, in the short term, additional constraints from a variety of polarized measurements from fixed target and collider experiments like HERMES, COMPASS and RHIC will allow to further pin down the polarized PDFs. In the medium term, important constraints on polarized PDFs could also be provided by a Electron-Ion Collider (EIC) [139–142], currently under study.

3.3 Physics case: monotop production

In order to illustrate the power of spin asymmetries for the characterization of new physics, we focus on one particular BSM signature, dubbed monotop, that has recently been proposed [106, 107]. The monotop signature is characterized by the production of a single top quark in association with missing transverse energy and no other particle. The choice of such a process is driven by several considerations.

First of all, the sector of the top quark is widely believed to be one of the key candidates for coupling in an enhanced way to new physics particles, due to the vicinity of the top mass to the electroweak scale. Second, monotop production is negligible in the Standard Model, where the top quark is produced in association with a Z -boson and no extra jet. This process is indeed loop-induced, GIM-suppressed and further reduced by the branching ratio of the Z -boson to neutrinos. This ensures that the observation of a monotop system at the LHC (or at an FCC) could be safely considered as a clear tell-tale sign of new physics. Third, there is a wide variety of new physics theories that can lead to monotop production (see, *e.g.*, Refs. [106–115]). Monotops therefore offer a good way to illustrate how single-spin and double-spin asymmetries could provide a unique handle to extract information on the (hypothetical) new physics sector.

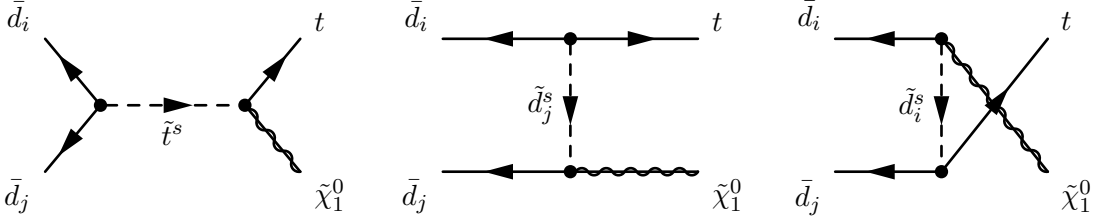


Figure 3.6: Feynman diagrams for monotop production in the R -parity violating MSSM with Minimal Flavour Violation (MFV), where i, j are flavour indices, and s is the squark index.

3.3.1 Monotop production in the RPV MSSM

We begin by considering the MSSM after supplementing its R -parity conserving superpotential by one single RPV operator, the so-called UDD term. As it will be shown below, this simple setup includes three distinct monotop production mechanisms hardly distinguishable in unpolarized proton-proton collisions, apart from the differences in total rates that are however dependent on unknown couplings. This contrasts with the situation where additional polarized observables are available since in this case, discriminating between the different initial states becomes possible. We model the supersymmetric interactions among the matter sector by adding to the R -parity conserving MSSM superpotential W_{MSSM} the RPV UDD operator,

$$W = W_{\text{MSSM}} + \frac{1}{2} \lambda''_{ijk} U_R^i D_R^j D_R^k, \quad (3.21)$$

where U_R and D_R are the chiral superfields associated with the up-type and down-type right-handed (s)quark supermultiplets, the color indices are implicit for clarity and the flavour indices being explicitly indicated. Monotop production is induced by non-vanishing λ''_{3jk} couplings together with enforcing the lightest neutralino to be long-lived, a setup almost unconstrained by experimental data [143]. If at least one of these λ'' couplings is non-vanishing, top squarks of mass $m_{\tilde{t}}$ can be resonantly produced from the scattering of two down-type antiquarks of different flavors and further decay into a top quark and a lightest neutralino which, if lighter than the top quark, is long-lived enough to escape detection and gives rise to missing transverse energy in a detector [144]. The same final state could also be produced through t/u -channel down-type squark exchanges as depicted in Figure 3.6. We however neglect, in the following, these non-resonant contributions with respect to the resonant s -channel diagram, that we have explicitly verified to be largely dominant.

In the RPV supersymmetric framework described above, the fully polarized partonic cross-section for monotop production from a $\bar{q}\bar{q}'$ initial-state is given by

$$\hat{\sigma}_{RPV}^{h_1 h_2}(\bar{q}_j \bar{q}_k \rightarrow t \tilde{\chi}_1^0) = \frac{(1 - h_1)(1 - h_2)\pi |\lambda''_{3jk} \sin \theta_{\tilde{t}}|^2}{6} \text{BR}(\tilde{t} \rightarrow t \tilde{\chi}_1^0) \delta(\hat{s} - m_{\tilde{t}}^2), \quad (3.22)$$

where \hat{s} denotes the partonic center-of-mass energy and h_1 and h_2 the helicities of the initial antiquarks. Results for the charge-conjugate process can be obtained by replacing $h_i \rightarrow -h_i$. Moreover, we have assumed that only one of the two stop mass-eigenstates is light enough to significantly contribute to the cross-section and kept the associated dependence on the stop mixing angle $\theta_{\tilde{t}}$ explicit. Finally, we have adopted the narrow-width approximation to model the resonant behavior of the squared matrix element by a Breit-Wigner lineshape. Although non-general, such an approximation holds when the width of the resonance is small with respect to its mass, which allows one to neglect off-shell effects, when the resonance decays into much lighter particles and when its mass is much smaller than the center-of-mass energy, which avoids important distortions of the Breit-Wigner lineshape [145].

Scenario	σ_0	σ_L	σ_{LL}
MSSM RPV	$ds + \bar{d}\bar{s}$	$d\Delta s + s\Delta d + \bar{d}\Delta\bar{s} + \bar{s}\Delta\bar{d}$	$\Delta d\Delta s + \Delta\bar{d}\Delta\bar{s}$
	$db + \bar{d}\bar{b}$	$d\Delta b + b\Delta d + \bar{d}\Delta\bar{b} + \bar{b}\Delta\bar{d}$	$\Delta d\Delta b + \Delta\bar{d}\Delta\bar{b}$
	$sb + \bar{s}\bar{b}$	$s\Delta b + b\Delta s + \bar{s}\Delta\bar{b} + \bar{b}\Delta\bar{s}$	$\Delta s\Delta b + \Delta\bar{s}\Delta\bar{b}$
Hylogenesis	$dd + \bar{d}\bar{d}$	$d\Delta d + \bar{d}\Delta\bar{d}$	$\Delta d\Delta d + \Delta\bar{d}\Delta\bar{d}$
	$ss + \bar{s}\bar{s}$	$s\Delta s + \bar{s}\Delta\bar{s}$	$\Delta s\Delta s + \Delta\bar{s}\Delta\bar{s}$
	$bb + \bar{b}\bar{b}$	$b\Delta b + \bar{b}\Delta\bar{b}$	$\Delta b\Delta b + \Delta\bar{b}\Delta\bar{b}$
X -model	$gu + g\bar{u}$	$g\Delta u + u\Delta g + g\Delta\bar{u} + \bar{u}\Delta g$	$\Delta g\Delta u + \Delta g\Delta\bar{u}$
	$gc + g\bar{c}$	$g\Delta c + c\Delta g + g\Delta\bar{c} + \bar{c}\Delta g$	$\Delta g\Delta c + \Delta g\Delta\bar{c}$

Table 3.1: Parton luminosities that contribute to the unpolarized cross-section, the single- and the double-spin asymmetries in the three different scenarios for monotop production that are discussed in this paper. For each model, the first row corresponds to the dominant production channel. In singly-polarized collisions, the second hadron is the one that is chosen to be polarized.

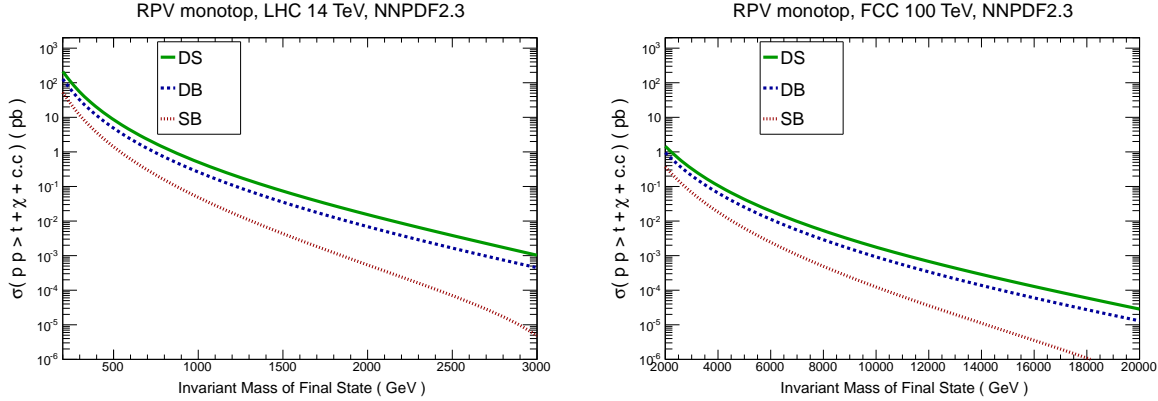


Figure 3.7: RPV monotop production total cross sections at the LHC 14 TeV (left panel) and at an FCC 100 TeV (right panel) as a function of the invariant mass of the final state. We fix the stop mixing angle to $\pi/4$, consider the branching ratio $\text{BR}(\tilde{t} \rightarrow t\tilde{\chi}_1^0) = 1$ and address three distinct benchmark scenarios where one single RPV coupling is non-vanishing at a time: λ''_{312} (green), λ''_{313} (blue) and λ''_{323} (red). Cross-sections have been obtained using the NNPDF2.3 unpolarized parton set.

Because of the symmetry properties of the RPV superpotential of Eq. (3.21), the couplings of quarks or antiquarks of the same flavor to the stop \tilde{t} vanish so that only three different flavour combinations can yield a non-zero cross-section, namely the $ds + \bar{d}\bar{s}$, $db + \bar{d}\bar{b}$ and $sb + \bar{s}\bar{b}$ initial states. Here we are implicitly summing over both monotop and anti-monotop production, while later in the section, we will explore the potential of tagging the charge of the final-state monotop. The parton luminosities that contribute to the unpolarized cross-section, the single- and the double-spin asymmetries in the various different scenarios for monotop production that are discussed in this paper are summarized in Table 3.1.

In Figure 3.7, we present total cross-sections for RPV monotop production at the LHC 14 TeV (left panel) and at an FCC 100 TeV (right panel) as a function of the mass of the lightest top squark. We compute our results by making use of Eq. (3.14) with the NNPDF2.3 set of parton densities, and for the sake of the example, we consider maximal stop mixing ($\theta_{\tilde{t}} = \pi/4$), the branching ratio of the stop resonance into a monotop state equal to unity ($\text{BR}(\tilde{t} \rightarrow t\tilde{\chi}_1^0) = 1$) and all the three possible different initial states. We however assume that only one of the three

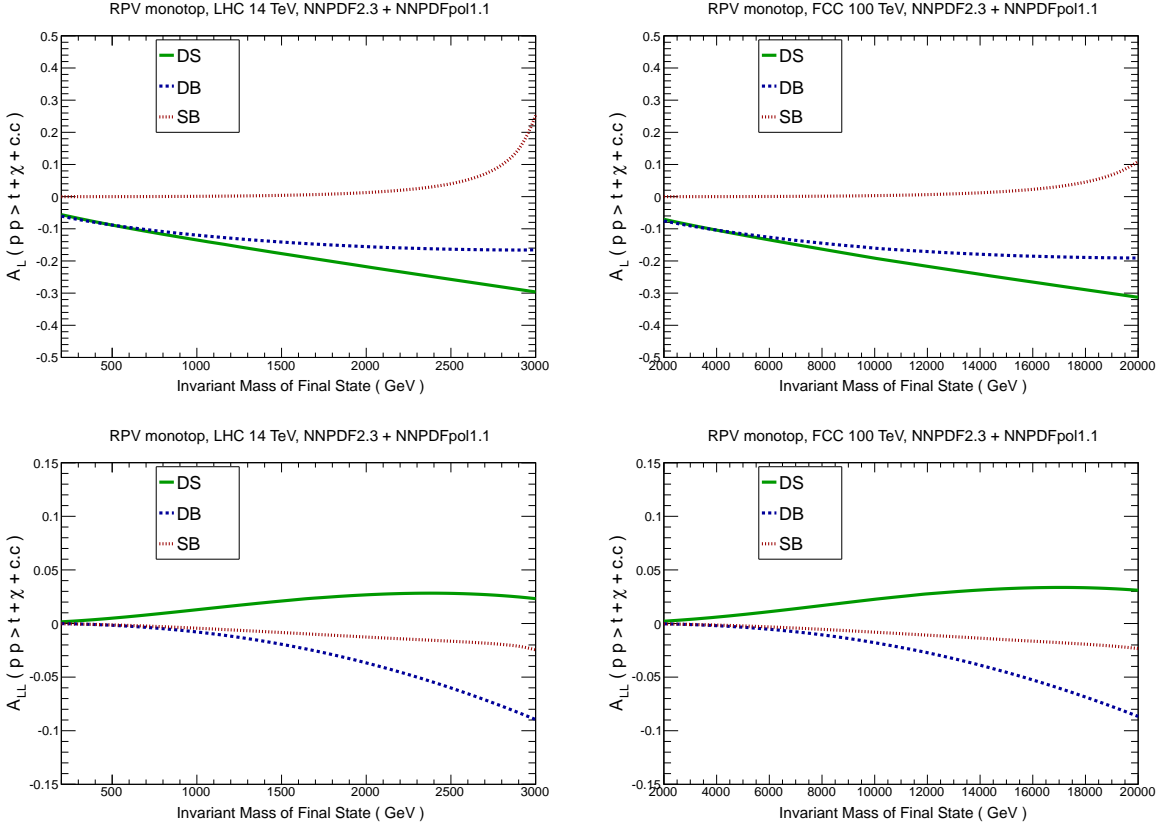


Figure 3.8: Single-spin (upper panel) and double-spin (lower panel) asymmetries for RPV monotop production at the LHC 14 TeV (left panel) and at an FCC 100 TeV (right panel) as function of the stop (or monotop) mass. We fix the stop mixing angle to $\pi/4$, consider the branching ratio $\text{BR}(\bar{t} \rightarrow t\tilde{\chi}_1^0) = 1$ and address three distinct benchmark scenarios where one single RPV coupling is non-vanishing at a time: λ''_{312} (green), λ''_{313} (blue) and λ''_{323} (red). Asymmetries have been obtained using NNPDFpol1.1 and NNPDF2.3.

RPV couplings is non-zero at a time and that its value is fixed to $\lambda'' = 0.2$. With a quadratic dependence on the λ'' -parameters, RPV monotop production could in principle be expected both at the LHC and at an FCC. However, characterizing which partonic initial state would be (dominantly) responsible for the possible observation of an excess is far more complicated than measuring a total cross-section. The standard approach would then be to probe differential distributions sensible, *e.g.*, to the presence of valence or sea quarks in the initial state. However, in the rest of this section we focus on a complementary approach to characterize the initial state of monotop production by means of spin asymmetry measurements in polarized pp collisions.

In the RPV context, there is only one single combination of quark helicities that gives rise to a monotop final state, as indicated in Eq. (3.22). Consequently, partonic spin asymmetries turn out to be equal to ± 1 and hadronic asymmetries reduce to ratios of partonic luminosities. Therefore, in the approximation in which there is a single dominant coupling λ'' , hadron-level spin-asymmetries can be expressed in terms of a ratio of linear combinations of polarized and unpolarized PDFs and the results of Section 3.2 hold. For instance, for the case of monotop production in the dominant channel $\bar{d}\bar{s}+ds$ we have

$$A_L^{\bar{d}\bar{s}+ds} = \frac{\mathcal{L}_{ds}^L - \mathcal{L}_{\bar{d}\bar{s}}^L}{\mathcal{L}_{ds} + \mathcal{L}_{\bar{d}\bar{s}}} \quad \text{and} \quad A_{LL}^{\bar{d}\bar{s}+ds} = \frac{\mathcal{L}_{ds}^{LL} + \mathcal{L}_{\bar{d}\bar{s}}^{LL}}{\mathcal{L}_{ds} + \mathcal{L}_{\bar{d}\bar{s}}}, \quad (3.23)$$

and likewise for other initial states. We collect the results for the relevant channels in Fig-

ure 3.8 for both the LHC 14 TeV (left panel) and the FCC 100 TeV (right panel), after summing over both monotop and anti-monotop production modes, and show single-spin (upper row) and double-spin (lower row) asymmetries.

It is clear from Figure 3.8 that polarized asymmetries can be sizable, and moreover depend strongly on the partonic initial state. For instance, at the LHC 14 TeV and $m_X = 3$ TeV, A_L varies from 20% for the sb initial state to -30% for the ds combination. The different behaviors of A_{LL} and A_L for the same partonic initial state has also discrimination power. Therefore, it can be seen that the availability of polarized beams at high energy hadron colliders allows to disentangle the different possible scenarios leading to monotop production, especially for large final-state masses, where the polarized asymmetries are larger.

3.3.2 Other scenarios for monotop production

In addition to the RPV MSSM scenario, several other models predict monotop production at hadron colliders. Therefore, in the event of observation of the monotop signature, determining which is the correct underlying model will be a difficult task. In particular, even disentangling a resonant monotop production from a non-resonant one might be non-trivial due to detector effects distorting typical resonant shapes expected, for instance, in the missing energy spectrum [107]. In Section 3.3.1, we have investigated monotop production in the context of RPV supersymmetry and have shown how spin asymmetries could help characterizing the type of RPV interactions relevant for the production of a monotop state. We now investigate two additional scenarios predicting the production of a top quark in association with missing energy, and illustrate the strengths of measuring spin asymmetries in polarized collisions in order to obtain information on the underlying model.

We first focus on the so-called Hylogenesis models for dark matter where a monotop state can be produced from the decay of a heavy vector resonance V_μ of mass m_V that couples to down-type quarks [112, 113]. The leading order Feynman diagram for monotop production in this scenario is shown in Figure 3.9. The heavy vector resonance V_μ decays into an associated pair comprised of a top quark and a spin-1/2 dark matter particle, carrying missing energy, that we generically denote by χ . We further describe the couplings of down-type quarks to the colored resonance V_μ with charge $\pm 2/3$ by the Lagrangian²

$$\mathcal{L}_{\text{hylo}} = \frac{1}{2} \kappa_{ij} \bar{d}_i^c \gamma^\mu d_j V_\mu + \text{h.c.} , \quad (3.24)$$

where again a sum over color indices is understood, i and j are flavor indices and κ_{ij} denotes the 3×3 (symmetric) matrix of interaction strengths in flavour space. As in Eq. (3.22) for the RPV case, we will rewrite any dependence on the interactions of the dark matter state χ in terms of the branching ratio of V_μ to a monotop final state, so that the corresponding Lagrangian contributions are unnecessary and have been omitted. The constraints on the parameters of this scenario from collider and flavour physics have been studied in Ref. [146], which shows that they are model dependent and can be easily avoided, specially in the case of third generation quarks. In the rest of this section, we restrict ourselves to the dominant $dd + \bar{d}\bar{d}$ production channel, again summing over monotop and anti-monotop production. As stated above, a discussion on the information that can be obtained by tagging the charge of the final-state top quark, and thus disentangling monotop and anti-monotop production, will be carried out later in this section.

The third model for monotop production that we consider in this work will be denoted by the name ‘ X -Model’. It is motivated by models of dark matter where the top quark couples to a new neutral vector boson X_μ strongly interacting with invisible particles of a hidden sector [114, 115].

²The Lagrangian choice is not unique and we focus on one particular example among others that induces large differences compared to the RPV case.

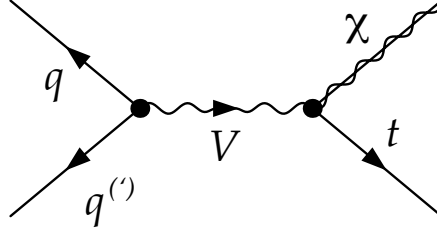
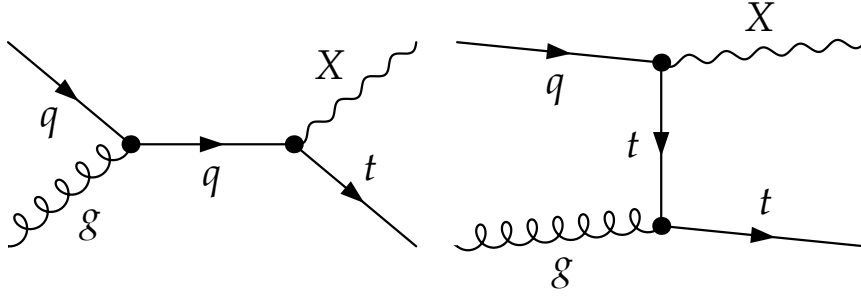


Figure 3.9: Feynman diagram associated with Hylogenesis monotop production.

Figure 3.10: Feynman diagrams associated with monotop production from flavor-changing interactions associated with an extra vector boson X in the X -model.

The Feynman diagrams for monotop production in this scenario are shown in Figure 3.10. In this case, the associated production of the new X -boson, which typically decays into particles of the hidden sector and thus escapes detection, with a top quark leads to a monotop signature. Adopting a simplified approach, we fix the part of the Lagrangian relevant for monotop production to

$$\mathcal{L}_X = g_X^i \bar{u}_i \gamma^\mu P_R t X_\mu + \text{h.c.} , \quad (3.25)$$

where P_R denotes the right-handed chirality projector and g_X the associated vector of coupling constants in generation space. In the following, we focus on the dominant production channel where the X -boson couples to an up quark and a top quark (see Table 3.1). The experimental constraints on the new physics mass scale in this scenario have been studied in Ref. [114]. Their findings indicate that the mass of the X field can be as low as 100 GeV without conflicting with current bounds, such as $B_{d,s} - \bar{B}_{d,s}$ mixing or rare top decays.

The two Lagrangians of Eqs. (3.24) and (3.25) allow us to calculate the corresponding fully polarized partonic cross-sections. We obtain, using the narrow width approximation for the Hylogenesis case and providing the differential cross-section with respect to the Mandelstam t -variable for the X -model,

$$\begin{aligned} \hat{\sigma}_{\text{hylo}}^{h_1 h_2}(\bar{q}_j \bar{q}_k \rightarrow t\chi) &= \frac{2(1 - h_1 h_2)\pi |\kappa_{jk}|^2}{3} \times \text{BR}(V \rightarrow t\chi) \times \delta(\hat{s} - m_V^2) , \\ \frac{d\hat{\sigma}_X^{h,\lambda}}{d\hat{t}}(u_i g \rightarrow tX) &= \frac{1}{16\pi\hat{s}^2} \frac{g_s^2 g_X^{i2}}{12\hat{s}m_X^2(\hat{t} - m_t^2)^2} (1 + h) [C_1 + C_2\lambda] . \end{aligned} \quad (3.26)$$

In the Hylogenesis model, h_1, h_2 are the helicities of the initial partons and the results for the charge-conjugate processes are obtained by replacing $h_i \rightarrow -h_i$. It is clear from the fully polarized partonic cross-section of Eq. (3.26) that in this case, the single-spin asymmetries vanish exactly. In contrast, for the double-polarized asymmetries, we have a similar situation as for

RPV monotop production and the hadron-level asymmetries can be written in terms of ratios of the partonic luminosities discussed in Section 3.2. To be explicit, for the dominant production channel $\bar{d}\bar{d}+dd$ we have

$$A_L^{\bar{d}\bar{d}+dd} = 0, \quad A_{LL}^{\bar{d}\bar{d}+dd} = -\frac{\mathcal{L}_{dd}^{LL} + \mathcal{L}_{\bar{d}\bar{d}}^{LL}}{\mathcal{L}_{dd} + \mathcal{L}_{\bar{d}\bar{d}}}, \quad (3.27)$$

and likewise for other initial states.

In the X -model calculation, we have kept the dependence on the gluon and initial quark polarizations λ and h explicit and have introduced the kinematical factors

$$\begin{aligned} C_1(\hat{s}, \hat{t}) &= m_t^8 - m_t^6 [2\hat{s} + \hat{t}] + m_t^4 [(\hat{s} + \hat{t})^2 - 2m_X^2(\hat{t} + m_X^2)] \\ &\quad + m_t^2 [4m_X^6 - 2m_X^4\hat{t} + 2m_X^2(\hat{s}^2 - \hat{s}\hat{t} + 2\hat{t}^2) - \hat{t}(\hat{s} + \hat{t})^2] \\ &\quad - 2m_X^2\hat{t}(2m_X^4 + \hat{s}^2 + \hat{t}^2 - 2m_X^2(\hat{s} + \hat{t})), \\ C_2(\hat{s}, \hat{t}) &= [m_t^4 + m_t^2(2m_X^2 - \hat{s} - \hat{t}) + 2m_X^2(\hat{s} - \hat{t})] [m_t^4 + \hat{t}(2m_X^2 - \hat{s} - \hat{t}) - m_t^2(2m_X^2 + \hat{s})]. \end{aligned} \quad (3.28)$$

The main feature of this class of models with respect to the RPV case lies in the various helicity combinations contributing to the polarized cross-section. Important differences are consequently expected in spin asymmetries when comparing RPV monotop production to Hylogenesis or dark matter X -model predictions.

This is illustrated in Figure 3.11 where we compare, for illustrative purposes, single-spin and double-spin asymmetries as predicted in RPV scenarios where the monotop system originates from a $ds + \bar{d}\bar{s}$ initial state, in Hylogenesis models where it is produced from $dd + \bar{d}\bar{d}$ scattering and in dark matter X -models where the X -boson arises from the $g(u + \bar{u})$ initial state. We present our results as functions of the monotop system mass being defined as the resonance mass for both the RPV and the Hylogenesis scenarios, and as the sum of the X -boson and top quark masses for the X -model case³.

Figure 3.11 is the main result of this work. It tells us that, assuming polarized PDF uncertainties are improved by a series of dedicated measurements, a measurement of the single-spin asymmetry with 5% precision would allow one to discriminate between the three production mechanisms for states with sufficiently large invariant mass, approximately above 2 TeV at the LHC and above 10 TeV at the FCC. Even a measurement of the sign of the single spin asymmetries would be very valuable to discriminate between different scenarios. Double-spin asymmetries would provide a complementary cross-check of the single-spin results, though their measurement is rather more challenging both because of the reduced rates and because of the smaller values of the asymmetries. The qualitative behavior of A_L and A_{LL} is also found to be rather different in some scenarios. In RPV monotop production, for instance, A_L is large and negative, while A_{LL} is small and positive. It is thus clear that a simultaneous measurement of A_L and A_{LL} would provide stringent constraints on the underlying production dynamics.

3.3.3 Impact of monotop charge tagging

In the final part of this section, we study what we can learn if the charge of the final-state top quark is tagged, that is, if we are able to disentangle the monotop signature (a top quarks of charge $+2/3$ and missing transverse energy) from the anti-monotop signature (same with a top antiquark). This charge tagging could be potentially relevant because in these two cases, the

³The numerical values of all other model parameters are irrelevant as canceling in the ratios of polarized and unpolarized cross-sections.

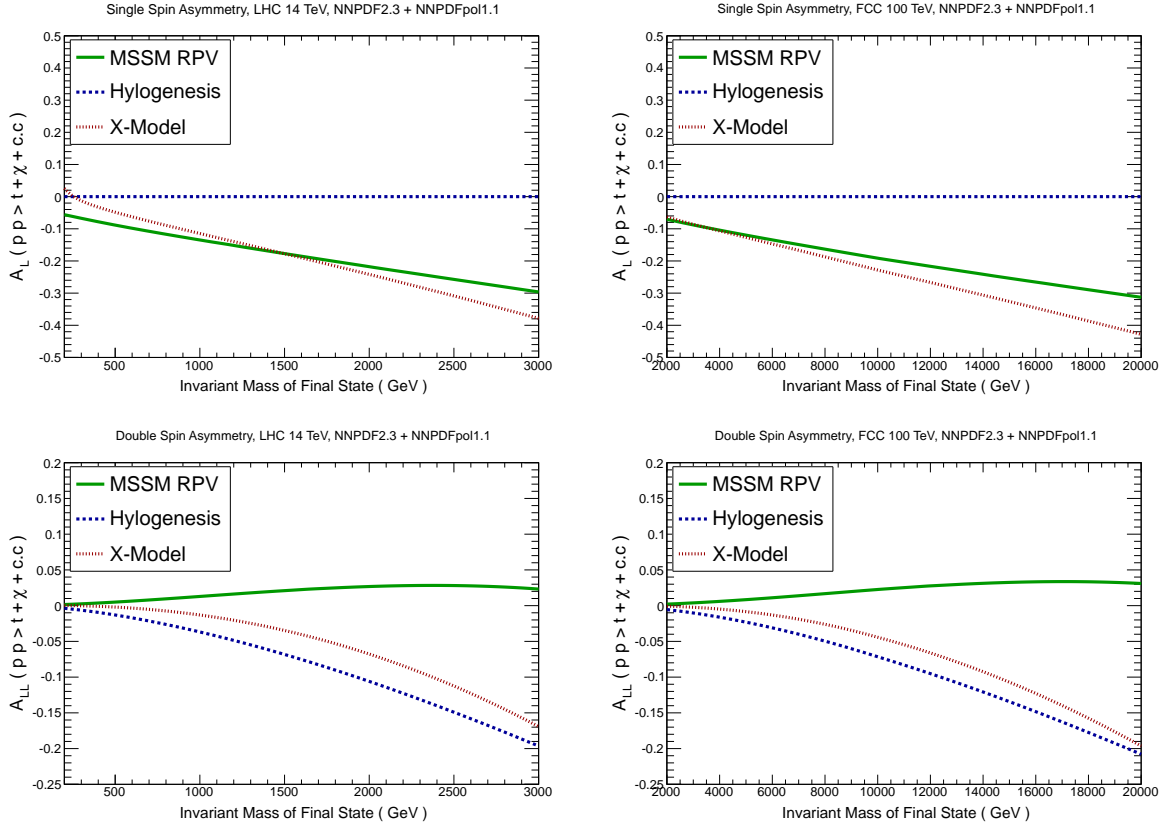


Figure 3.11: Single-spin (upper panel) and double-spin (lower panel) asymmetries for monotop production at the LHC 14 TeV (left panel) and at an FCC 100 TeV (right panel) as function of the monotop system mass for the various new physics scenarios described in the text. Asymmetries have been obtained using NNPDFpol1.1 and NNPDF2.3. Sum over monotop and anti-monotop production is implicit.

polarized PDFs that are relevant according to the nature of the initial state can show quite different behaviors. Tagging the charge of the top quark can thus provide another handle on the underlying BSM scenario that has induced monotop production⁴.

We show in Figure 3.12 the single-spin asymmetries for LHC 14 TeV and FCC 100 TeV, this time separating monotop from anti-monotop production, for the three models under consideration. The relevant initial states for monotop production are $d\bar{s}$, $d\bar{d}$ and ug in the RPV, Hylogenesis and X-model scenarios respectively, and the corresponding charge-conjugate ones for anti-monotop production. It is clear from the differences between the left and right columns of Figure 3.12 that tagging the top quark charge provides important information about the underlying production model, with the differences particularly striking in the case of the RPV scenario, where at large masses a different sign of the asymmetry is predicted in the two cases.

We recall that the results of Figure 3.11 cannot be retrieved by a trivial average of the asymmetries of Figure 3.12 over monotop and anti-monotop production, as the full singly-polarized and unpolarized cross sections need to be averaged first, before evaluating the ratios.

3.3.4 Summary

In this section, we have shown how, using polarized collisions, it is possible to discriminate among different models that lead to the same final-state signature, in this case monotop production.

⁴Charge asymmetries are also interesting observables in the context of unpolarized collisions.

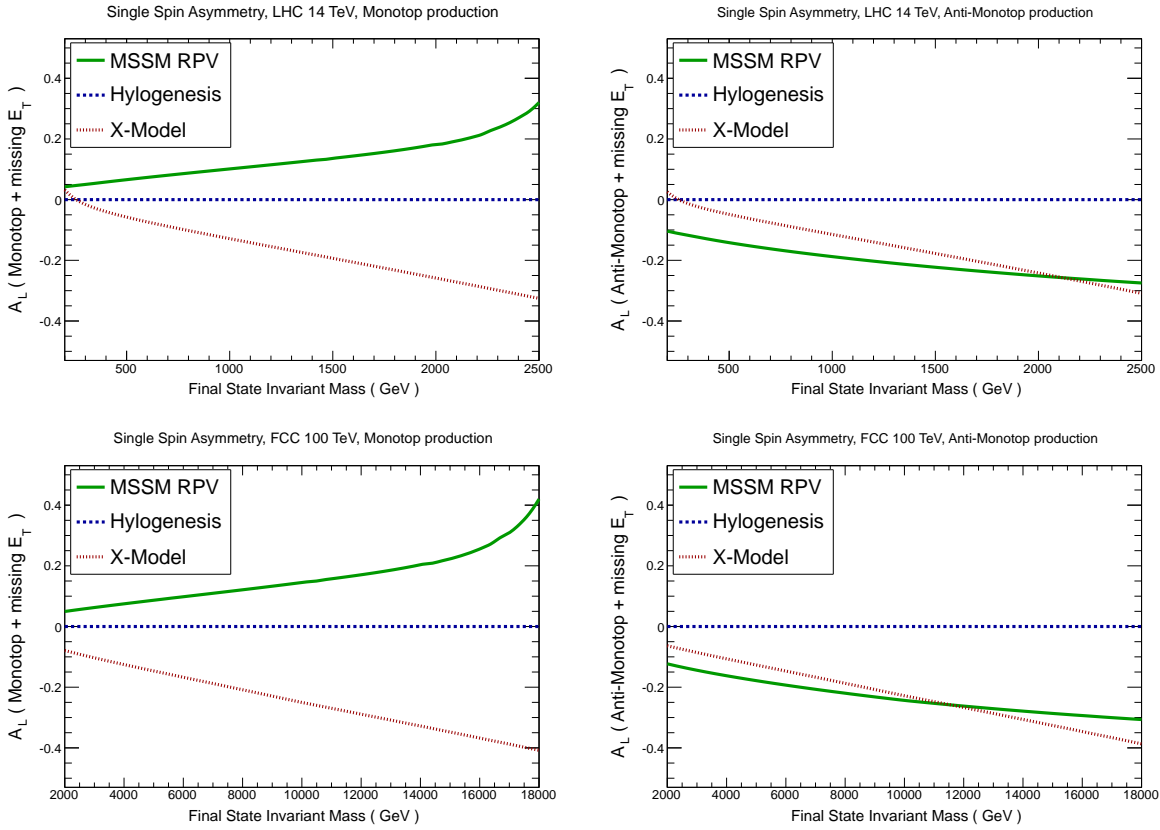


Figure 3.12: Single-spin asymmetries for monotonop (left panel) and anti-monotonop (right panel) production at the LHC 14 TeV (upper row) and at an FCC 100 TeV (lower row) as function of the invariant mass of the final state for the different new physics scenarios discussed in this work.

While we have considered this specific benchmark scenario, it is clear that our results/our considerations apply to a wide variety of other BSM models where the availability of polarized beams would provide a unique handle for their characterization.

3.4 Conclusions

In this chapter, we have shown how the availability of polarized beams at high-energy hadron colliders provides a unique handle on the discrimination between different beyond the Standard Model scenarios that lead to the same final-state signatures in unpolarized collisions. First of all, we have discussed in a model-independent way why single and double-spin asymmetries in polarized collisions allow us for the separation between different initial-state production mechanisms. Then we have considered different benchmark scenarios for monotonop production and shown how the measurement of spin asymmetries in polarized collisions could help to discriminate between different models. Therefore, while polarized beams are certainly not required for BSM discoveries, they can provide very useful information on the properties of the hypothetical BSM sector, in particular in the determination of its couplings to Standard Model particles.

While technically feasible, the likelihood of a future polarized mode at the LHC is very small, requiring a complete modification of the full injector chain. The situation might however be different for the recently proposed Future Circular Collider (FCC) at a center-of-mass energy of 100 TeV: if there is a strong physics case, the polarized option should be considered seriously. In any case this is the right time to begin to think of the feasibility of such an option, now

that various studies for the planning of this machine have just started. In particular, if new physics is discovered at the LHC during the proton-proton runs at center-of-mass energies of 13 TeV, 14 TeV, or at the future high-luminosity upgrade of the LHC, there will be a very strong motivation for a polarized mode of the FCC in order to characterize and understand the properties of this new sector.

Future studies, along similar directions as the ones explored in this thesis, should be performed in two different and complementary directions. First, other BSM scenarios should be studied. These studies should focus on the production of high-mass particles, since it is the only region where single- and double-spin asymmetries are relatively large, and thus experimentally accessible. Second, one should also perform more detailed feasibility studies for the measurement of single- and double-spin asymmetries, trying to estimate the luminosities in the polarized mode that a 100 TeV FCC could deliver and how the rates would be affected by the finite polarization of the beams. Quantifying the statistical uncertainties of the spin asymmetries at the FCC would also allow one to better understand what is the reach of BSM characterization of the polarized collision mode.

As an intriguing final remark, it should be noted that at a 100 TeV FCC it might be possible to access polarized collisions without the need of using polarized beams. Indeed, at the scale of 10-20 TeV, the electroweak W - and Z -bosons are effectively massless and should be included in the DGLAP evolution, which leads at this point to an intrinsic polarization of the quarks and gluons via mixing. This is an interesting possibility to study further, since in any case PDFs with electroweak corrections are mandatory for the physics of a 100 TeV hadron collider.

Chapter 4

Regularization and Renormalization

Tree-level calculations discussed in the previous chapter might be sufficient (in some specific situations) to discover New Physics at the LHC. However, if one aims at checking the internal consistency of a given model, and desires to probe the total rates with a higher level of accuracy, it is necessary to amend leading order calculations by higher order corrections. Next-to-Leading Order (NLO) predictions reduce theoretical uncertainties due to unphysical scales dependence, describe more precisely the shape of the differential distributions (by taking into account for instance new partonic channels opening-up at NLO), allow to assess the convergence of the perturbative series expansion, and provide a better estimate of the various background sources contaminating the different signal regions. These accurate predictions are particularly needed for searches of signal events in large background samples.

In a general manner, NLO corrections are of two types, real and virtual. Real contributions involve the emission of one extra parton compared to the Born process, and are obtained by interfering the corresponding graphs (channel by channel), before summing over all possible channels. Virtual contributions, on the other hand, are characterized by the internal exchange of particles inside closed loops, and are obtained by interfering the one-loop diagrams with the tree-level graphs (channel by channel), before summing over all possible channels. Virtual corrections (for a given channel) can be further decomposed into various sub-categories, that are defined according to the number of external legs contained in the corresponding topologies. The topologies that are most frequently encountered at one-loop for a $2 \rightarrow 2$ process are depicted in Fig. 4.1. The first type of diagram corresponds to one-point graphs, while the second type is usually referred to as bubble graphs (due to its shape). The third, and fourth topologies are finally known as vertex corrections, and box diagrams respectively.

Two major complications are essentially encountered at next-to-leading order *i*) the number of Feynman diagrams involved *ii*) the appearance of divergent integrals at the intermediate stages of the calculation. If the first difficulty can be tackled by means of a suitable computer program generating automatically the relevant Feynman diagrams, such as FEYNARTS [147] or QGRAF [148], the second problem however requires more care. The divergences encountered at the intermediate stages of the one-loop calculations can be of the following types: UV, soft, collinear, and soft-collinear. UV divergences originate from virtual contributions¹, and constitute the main concern of this chapter. Soft divergences come from the emission of a parton of small momentum between two on-shell particles, and can be understood as resulting from the fact that particles with almost vanishing transverse momenta cannot be detected.

¹Because particles entering into the loops are virtual, and because the loop momentum q , over which we integrate loop integrals is left unconstrained by momentum conservation, it is possible for q to get arbitrarily large values. If the power of q in the denominator of the loop integral (assuming no power of q in the numerator) is lower or equal to the number of space-time dimensions, UV-divergences can appear.

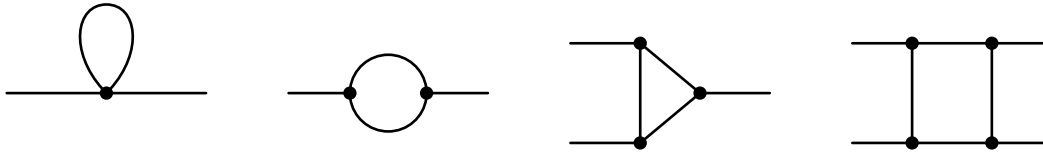


Figure 4.1: Main one-loop topologies encountered at next-to-leading order. Straight lines can denote any field.

Collinear divergences appear when a massless particles splits into two other massless particles, and reflect the fact that particles emitted collinearly one to another cannot be resolved. Finally, soft-collinear divergences arise from kinematical regions where there is an overlap between soft and collinear singularities. Soft, collinear, and soft-collinear divergences are here collectively denoted as infrared (IR) divergences.

The predictive power of a renormalizable theory should not be spoiled by higher order corrections, therefore UV and IR divergences appearing at the intermediate stages of the calculation should ultimately cancel², leaving only finite corrections. In this chapter, we provide a short introduction to one-loop calculations, and detail the procedure of renormalization, which essentially aims at treating UV-divergences. For completeness, note that in order to obtain a result which is also infrared-finite, one still has *i)* to make sure that, according to the Kinoshita-Lee-Nauenberg (KLN) theorem³, all the IR divergences, but the pure collinear poles of the initial state, cancel between the real and the virtual contributions *ii)* to absorb the remaining collinear singularities into the redefinition of the PDFs by means of the mass factorization procedure [151].

This chapter is organized as follows: in Sections 4.1 and 4.2 we provide a consistent definition of Dimensional Regularization (DREG), and Dimensional Reduction (DRED) respectively. DREG and DRED are the two regularization schemes used in this thesis to make singularities manifest. In Section 4.3, we review some one-loop techniques that are used to evaluate frequently encountered scalar integrals, and to isolate divergences from finite terms. In Section. 4.4, we present the Passarino-Veltman decomposition which is used to simplify tensor loop integrals. Finally, in Section 4.5, we explain how UV-divergences can be absorbed into the redefinition of all the bare fields and parameters by means of the procedure of multiplicative renormalization.

4.1 Regularization scheme

The regularization procedure aims at providing a consistent way of adding, subtracting and multiplying potentially divergent quantities, and requires in practice the introduction of an object called the regulator. The purpose of this regulator is to make singularities manifest, so that it becomes possible to practically manipulate them, and to keep track of them all along the calculation. At the end of the calculation, the goal is to have all the divergent terms (related to the regulator) separated out from the finite ones, and eventually, taking the physical limit will confine the divergences to the aforementioned terms. There exists several implementations of the regularization procedure in QFT, all having their own virtues and shortcomings. In a generic manner, the more the symmetries of the theory are preserved by the regularization scheme, the easier the calculations are expected to be. In what follows, we focus more specifically on one particular technique called Dimensional Regularization, which is nowadays one of the most popular and convenient technique to perform loop calculations in perturbation theory.

²For sufficiently inclusive physical observables.

³In a non-Abelian gauge theory with massless fields, transition rates are free of infrared divergences, if the summation over the initial and final degenerate states is carried out [149, 150].

Dimensional regularization:

Dimensional regularization (DREG) is a method originally introduced in 1972 by 't Hooft and Veltman [152], Bollini and Gambiagi [153], Cicuta and Montaldi [154], and Ashmore [155] to regularize divergent integrals. Among many virtues, DREG has the appealing properties of preserving gauge symmetries as well as Poincaré invariance, and allows for a simultaneous regularization of both UV and IR soft/collinear divergences. The basic idea of DREG consists in analytically continuing the loop momenta from 4 to $D = 4 - 2\varepsilon^4$ dimensions, so that the divergences appear as poles in $1/\varepsilon$ and $1/\varepsilon^2$ at the intermediate stages of the calculations. From a formal point of view, the analytic continuation of the loop integrals requires the construction of an infinite dimensional vector space Q_D on which all the D -dimensional integrals are well-defined. This vector space Q_D has to include the usual Minkowski space Q_4 as a vector subspace, and can be decomposed as a direct sum of Q_4 and a residual infinite-dimensional vector subspace Q_{D-4}

$$Q_D = Q_4 \oplus Q_{D-4} , \quad (4.1)$$

where Q_{D-4} and Q_4 are orthogonal to one another. This constructivist formulation of DREG originally developed by Wilson [156] and Collins [157] actually ensures the algebraic consistency of the regularization procedure inasmuch as all the objects, like the metric tensors or the Dirac matrices, are being given an explicit representation in the Q_D space. Analogously to the four-dimensional case, D -dimensional integrals defined over Q_D satisfy the following properties [158]

Linearity: for any complex number a and b , and any function f and g of the momentum q

$$\int d^D q [a f(q) + b g(q)] = a \int d^D q f(q) + b \int d^D q g(q) . \quad (4.2)$$

Translational invariance: for any momentum p , and any function $f(q)$

$$\int d^D q f(q + p) = \int d^D q f(q) . \quad (4.3)$$

Scaling law: for any complex number λ , and any function $f(q)$

$$\int d^D q f(\lambda q) = \lambda^{-D} \int d^D q f(q) . \quad (4.4)$$

Lorentz invariance: for any element Λ of the Lorentz group, and any function $f(q)$

$$\int d^D q f(\Lambda q) = \int d^D q f(q) . \quad (4.5)$$

A proof of uniqueness and existence of such a definition of DREG, as well as a detailed study of all its properties is far beyond the scope of this manuscript, the reader is therefore referred to [157] and references therein for more details on the constructive approach of DREG.

Conventions, subtleties and prescriptions in DREG

Although particularly convenient, the technique of dimensional regularization is not entirely free of ambiguities and requires additional prescriptions to be made unequivocal. The goals of this subsection are *i)* to review the nature and the origin of those ambiguities/subtleties *ii)* to fix the conventions used in the rest of this thesis so that there is no ambiguity left in the calculations.

⁴The regulator ε can be a non-integer or even a complex number.

Conventions

In DREG, the normalization of the D -dimensional integrals can be equivalently chosen to be $1/(2\pi)^D$ or $1/(2\pi)^4$, since what ultimately matters is that the D -dimensional integration measure allows us to recover the four-dimensional one when taking the limit $D \rightarrow 4$. In this thesis, we choose (by convention) the normalization of the D -dimensional integrals to be $1/(2\pi)^D$.

Similarly, in DREG, the normalization of the trace of γ matrices can be equivalently chosen to be $2^{D/2}$ or 4. More specifically, since the representation of γ matrices in D dimensions corresponds to a set of $2^{D/2} \times 2^{D/2}$ matrices, we would expect the trace of the unit matrix to be

$$\text{Tr}(\mathbb{1}) = 2^{D/2} . \quad (4.6)$$

This solution is however unnecessarily complicated for two reasons *i)* Clifford algebras behave differently in even and odd-dimensions, so there is no natural continuation of the algebra in arbitrary D dimensions *ii)* no algebraic manipulation depends on the value of the trace, thus any value of the trace ensuring a smooth transition around $D = 4$ can provide a satisfactory answer [159]. In this manuscript, we choose to define the trace of the unit matrix in complete analogy to the four-dimensional case by taking

$$\text{Tr}(\mathbb{1}) = 4 . \quad (4.7)$$

Subtleties

In DREG, the first subtlety is related to the necessity of shifting the dimensionality of all the fields and couplings when performing the analytic continuation from the standard Minkowski space into the infinite D -dimensional vector space Q_D . The action, which is the integral of the classical Lagrangian density, is by definition a dimensionless quantity in four-dimensions, and has to remain dimensionless in arbitrary D -dimensions. In order to preserve the renormalizability of the theory, the associated Lagrangian density thus has to become D -dimensional. The dimensionality of the fields and the couplings is therefore expected to be affected by the procedure of analytic continuation. For a generic Standard Model-like Lagrangian, we obtain

$$\begin{aligned} [A_\mu] &= \frac{D-2}{2} = 1 - \varepsilon , & [\phi] &= \frac{D-2}{2} = 1 - \varepsilon , & [g] &= \frac{4-D}{2} = \varepsilon , \\ [\Psi] &= \frac{D-1}{2} = \frac{3}{2} - \varepsilon , & [\lambda] &= 4 - D = 2\varepsilon , & [Y] &= \frac{4-D}{2} = \varepsilon , \end{aligned}$$

where A_μ , ϕ , Ψ , g , λ and Y generically denote gauge fields, scalar fields, Dirac fermions, gauge coupling constants, quartic coupling constants for scalar fields, and Yukawa couplings. The notation $[x]$ here refers to the mass-dimension of the argument x . At this point it is important to note that all the couplings that were originally dimensionless for $D = 4$ have become dimensionful in arbitrary D dimensions. For all the couplings of the theory to retain the mass-dimension they had in $D = 4$, it is found necessary to modify the integration measure of loop integrals such that

$$\int \frac{d^D q}{(2\pi)^D} \longrightarrow \mu_R^{2\varepsilon} \int \frac{d^D q}{(2\pi)^D} , \quad (4.8)$$

where q is the loop momentum, and where μ_R is the renormalization scale.

The second subtlety in DREG is linked to the simultaneous regularization of UV and IR divergences. As highlighted before in this section, the concept of dimensional regularization is based on the fundamental property that divergent integrals in four dimensions can become convergent in D dimensions. More specifically, UV divergences encountered in loops are better behaved for $\varepsilon > 0$, while their IR counterpart tend to favour $\varepsilon < 0$. Seeing that it is not possible

to have $\text{Re}(D) > 4$ and $\text{Re}(D) < 4$ at the same time, what is done in practice is *i)* assume that there are no IR divergences (or at least that the latter are regulated in some other way) *ii)* take $\varepsilon > 0$, so that loop integrals become convergent in the UV *iii)* use analytic continuation to the complex D -plane to make the integrals infrared-convergent. Eventually the IR divergences will appear as $1/\varepsilon$ and $1/\varepsilon^2$ poles at one-loop.

Prescriptions

The first prescription needed concerns the analytic continuation of γ^5 in DREG. γ^5 is by definition a four-dimensional object, and as such can only be well-defined on Q_4 . Extending its definition to Q_D is intrinsically bound to generate mathematical inconsistencies (for more details see Appendix E). Several prescriptions have been designed to handle γ^5 in DREG, in this thesis we adopt the Naive Dimensional Regularization (NDR) scheme.

The second prescription required is related to the analytic continuation of the external four-momenta and spin degrees of freedom. More specifically, the convergence of the loop integrals only requires the loop momenta to be D -dimensional, but does not tell us anything about the way the analytic continuation of the external momenta and spin degrees of freedom has to be performed. This additional ambiguity has led to the emergence of different schemes, which are all based on the original formulation of 't Hooft and Veltman. In the following, we review the basic properties of each of the four schemes that are commonly employed in modern calculations.

The 't Hooft-Veltman (HV) scheme:

The 't Hooft-Veltman scheme [152] is historically the first scheme that has been worked-out. In this scheme, external fields have their momenta and spin degrees of freedom kept four-dimensional, while virtual particles entering in the loops have their momenta and spin degrees of freedom continued into D -dimensions. In the HV scheme, on-shell fermions have two degrees of freedom, and massless (resp. massive) internal gauge bosons have $D-2$ (resp. $D-1$) degrees of freedom. It has been proven that the HV scheme preserves unitarity of the S -matrix [152].

The Conventional Dimensional Regularization (CDR) scheme:

Conventional Dimensional Regularization [157] is a slight variation of the HV scheme and differs only from the latter by the fact that external momenta and external fields are also considered D -dimensional. In CDR, everything is D -dimensional. The CDR scheme is the natural scheme for quantities computed using the optical theorem, and thus preserves unitarity.

The Dimensional Reduction (DRED) scheme:

Another variation of the HV scheme is called Dimensional Reduction, and was originally introduced by Siegel [160] at the end of the seventies as a manifestly SUSY-preserving regularization scheme. In a nutshell, DRED consists in lowering the dimensionality of the loop momenta from 4 to $D = 4 - 2\varepsilon$, while keeping all the fields and all external momenta four dimensional. For more details, see next section.

The Four-Dimensional Helicity (FDH) scheme:

The Four-Dimensional Helicity [161, 162] scheme was originally developed to construct one-loop amplitudes from unitarity cuts, and is frequently used in the context of massless NLO QCD calculations, where it can drastically simplify calculations. The FDH scheme, like DRED, continues loop-momenta to D -dimensions while keeping the fields four-dimensional. In this scheme, gauge invariance of the full theory is broken by the restriction of the loop momenta to have a smaller dimensionality than the spin degrees of freedom, Ward identities are therefore not satisfied for the additional spin degrees of freedom and the FDH scheme starts to become inconsistent beyond NLO for non-supersymmetric theories [163]. The ills of FDH at higher orders can however be cured by means of Dimensional reconstruction [164].

4.2 Dimensional Reduction

Although DREG (*i.e.* the HV or the CDR scheme) has been successfully applied to a huge variety of QCD and electroweak processes at next-to-leading order and beyond, this technique is however not suited for supersymmetric extensions of the Standard Model. Dimensional regularization indeed introduces a mismatch between bosonic and fermionic degrees of freedom within vector supermultiplets⁵, resulting into a manifest breaking of supersymmetry. As mentioned in the previous section, a good regularization scheme, is a scheme that preserves as many symmetries as possible at the quantum level. Resorting to DREG in the context of supersymmetric theories, although still possible, is certainly not the optimal choice as it would require an additional prescription to restore the fundamental Ward-Takahashi and Slavnov-Taylor identities in the final step of the renormalization procedure. In the case of our interest, this would for instance entail the introduction of SUSY restoring counter-terms⁶ that do not stem from the original Lagrangian by multiplicative renormalization [165, 166]. The determination of the structure of those counter-terms and their subsequent evaluation would hence be the source of additional complications that would make the use of DREG particularly inconvenient.

In order to avoid the aforementioned troubles, a manifestly SUSY-preserving regularization scheme called Dimensional Reduction (DRED) has been proposed by Siegel in [160]. The original idea of DRED [167] is to start from a standard four-dimensional space-time and to compactify it to a smaller vector space of dimension $D = 4 - 2\varepsilon < 4$, where only loop momenta take values so that UV singularities can still be dimensionally regularized. However, in contrast to DREG, spin degrees of freedom of both external and internal fields are kept four-dimensional⁷. From a formal point of view, the original version of DRED consists in decomposing the standard Minkowski space Q_4 as direct sum of orthogonal vector subspaces such that

$$Q_4 = Q_D \oplus Q_{4-D} , \quad (4.9)$$

where Q_D is the infinite dimensional vector space of DREG, and where Q_{4-D} is its infinite dimensional complement. As outlined by Siegel himself in the early 80's [168], this formulation of DRED however suffers from mathematical inconsistencies, which arise when considering the following product of antisymmetric tensors

$$\varepsilon_{\mu\nu\rho\sigma}^{(D)} \varepsilon^{\alpha\beta\gamma\delta(4-D)} \varepsilon^{(D)} \mu\nu\rho\sigma \varepsilon_{\alpha\beta\gamma\delta}^{(4-D)} , \quad (4.10)$$

where $\varepsilon_{\mu\nu\rho\sigma}^{(D)}$ is a Levi-Civita tensor living in the D -dimensional space, and $\varepsilon_{\alpha\beta\gamma\delta}^{(4-D)}$ is the associated rank-four antisymmetric tensor of the complementary vector space Q_{4-D} . If we contract antisymmetric tensors living in the same vector space, we obtain

$$\varepsilon_{\mu\nu\rho\sigma}^{(D)} \varepsilon^{\alpha\beta\gamma\delta(4-D)} \varepsilon^{(D)} \mu\nu\rho\sigma \varepsilon_{\alpha\beta\gamma\delta}^{(4-D)} = D(D-1)(D-2)(D-3)(4-D)(3-D)(2-D)(1-D) ,$$

which can be rewritten as

$$\varepsilon_{\mu\nu\rho\sigma}^{(D)} \varepsilon^{\alpha\beta\gamma\delta(4-D)} \varepsilon^{(D)} \mu\nu\rho\sigma \varepsilon_{\alpha\beta\gamma\delta}^{(4-D)} = D(D-1)^2(D-2)^2(D-3)^2(D-4) . \quad (4.11)$$

In contrast, if we contract antisymmetric tensors living in two different (orthogonal) vector spaces, then the product (4.10) has to be zero, which gives

$$0 = D(D-1)^2(D-2)^2(D-3)^2(D-4) . \quad (4.12)$$

⁵An on-shell gluino has two fermionic degrees of freedom, while an on-shell gluon in D dimensions has $D-2$ degrees of freedom.

⁶The existence of such counter-terms is guaranteed by renormalizability of supersymmetric theories [165].

⁷All Dirac algebra can thus be treated as four-dimensional.

The previous equation becomes inconsistent if *i*) D is a complex number *ii*) D is a real non-integer number *iii*) D is a strictly positive integer with $D > 4$. A generalization of this mathematical inconsistency can be formulated in terms of the determinant of the metric tensor of each vector space without using Levi-Civita tensors [169]. The authors of the aforementioned study have moreover correlated this inconsistency with the impossibility of decomposing the standard (finite) Minkowski space Q_4 into a direct sum of two infinite dimensional vector subspaces, Q_D and Q_{4-D} . To get a rid of the inconsistencies of the original definition of DRED, the same authors have also introduced the concept of quasi-four dimensional vector space Q_{4S} [169,170], whose existence has been formally demonstrated by construction in [171].

The peculiarity of this quasi-four dimensional vector space resides in the fact that it retains most of the four-dimensional properties of the Minkowski space⁸, while being infinite dimensional at the same time. It is shown in [171] that Q_{4S} can be decomposed as the direct sum of the D -dimensional space Q_D , and a residual Q_{4S-D} vector space such that

$$Q_{4S} = Q_D \oplus Q_{4S-D} , \quad (4.13)$$

where Q_D and Q_{4S-D} are completely orthogonal one to another, and where

$$Q_D = Q_4 \oplus Q_{D-4} . \quad (4.14)$$

One can respectively define over Q_{4S} , Q_D , Q_{4S-D} , Q_4 and Q_{D-4} , the associated metric tensors $\eta^{\mu\nu}$, $\hat{\eta}^{\mu\nu}$, $\tilde{\eta}^{\mu\nu}$, $\bar{\eta}^{\mu\nu}$ and $\tilde{\tilde{\eta}}^{\mu\nu}$, which satisfy the following properties

$$\begin{aligned} \eta^{\mu\nu} &= \hat{\eta}^{\mu\nu} + \tilde{\eta}^{\mu\nu} , & \eta^{\mu\nu} \eta_{\mu\nu} &= 4 , & \hat{\eta}^{\mu\nu} \hat{\eta}_{\mu\nu} &= D , & \tilde{\eta}^{\mu\nu} \tilde{\eta}_{\mu\nu} &= 2\varepsilon \\ \eta^{\mu\nu} \hat{\eta}_{\nu}{}^{\rho} &= \hat{\eta}^{\mu\rho} , & \eta^{\mu\nu} \tilde{\eta}_{\nu}{}^{\rho} &= \tilde{\eta}^{\mu\rho} , & \hat{\eta}^{\mu\nu} \tilde{\eta}_{\nu}{}^{\rho} &= 0 , & \hat{\eta}^{\mu\nu} &= \bar{\eta}^{\mu\nu} + \tilde{\tilde{\eta}}^{\mu\nu} , \\ \bar{\eta}^{\mu\nu} \bar{\eta}_{\mu\nu} &= 4 , & \tilde{\tilde{\eta}}^{\mu\nu} \tilde{\tilde{\eta}}_{\mu\nu} &= D - 4 = -2\varepsilon , & \hat{\eta}^{\mu\nu} \bar{\eta}_{\nu}{}^{\rho} &= \bar{\eta}^{\mu\rho} , & \hat{\eta}^{\mu\nu} \tilde{\tilde{\eta}}_{\nu}{}^{\rho} &= \tilde{\tilde{\eta}}^{\mu\rho} , \\ & & \bar{\eta}^{\mu\nu} \tilde{\tilde{\eta}}_{\nu}{}^{\rho} &= 0 . \end{aligned} \quad (4.15)$$

In the previous set of equations it is important to realize that, except for the case of the standard Minkowski space Q_4 , index counting is no longer possible. As a matter of fact, in infinite-dimensional vector spaces Lorentz indices can take infinitely many different values, whereas they are formally limited to 0, 1, 2 and 3 in the usual Minkowski space Q_4 . Using dimensional splitting, it is possible to define any four-vector p^μ living in Q_{4S} such that

$$p^\mu = \hat{p}^\mu + \tilde{p}^\mu , \quad \hat{p}^\mu = \hat{\eta}^{\mu\nu} p_\nu , \quad \tilde{p}^\mu = \tilde{\eta}^{\mu\nu} p_\nu , \quad (4.16)$$

where \hat{p}^μ and \tilde{p}^μ are respectively the D and $4S - D$ component of p^μ . Imposing the Dirac algebra in Q_{4S}

$$\{\gamma^\mu, \gamma^\nu\} = 2\eta^{\mu\nu} \mathbb{1} , \quad (4.17)$$

gives the following relations for the Q_{4S-D} and Q_D components

$$\{\hat{\gamma}^\mu, \hat{\gamma}^\nu\} = 2\hat{\eta}^{\mu\nu} \mathbb{1} , \quad \{\tilde{\gamma}^\mu, \tilde{\gamma}^\nu\} = 2\tilde{\eta}^{\mu\nu} \mathbb{1} , \quad \{\hat{\gamma}^\mu, \tilde{\gamma}^\nu\} = 0 . \quad (4.18)$$

Since the introduction of the infinite-dimensional vector spaces Q_{4S} , Q_D and Q_{4S-D} requires the spinor indices to range over an infinite number of values, one must work with infinite-dimensional γ -matrices to realize the Dirac algebra. However, this means that the genuinely four-dimensional Fierz identities, which are supposed to ensure the invariance of the Lagrangian under SUSY transformations, cannot be satisfied anymore. The lack of Fierz identities in Q_{4S} in principle entails a loss of supersymmetry even at the one-loop level. Fortunately it was shown in [169] that such effects only arise at higher orders, where traces of at least ten γ -matrices are encountered. The consistent formulation of DRED thus breaks supersymmetry just like DREG, but only starting from higher orders. DRED is therefore perfectly legitimate in the context of supersymmetric one-loop calculations, and can be safely applied to the cases of our interest.

⁸But the Fierz identities that are genuinely four-dimensional.

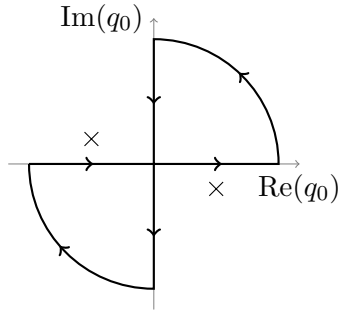


Figure 4.2: Integration contour in the q_0 complex plane. The crosses correspond to the location of the poles displaced from the real axis by means of the Feynman prescription.

4.3 Evaluation of scalar one-loop integrals

Now that we have a consistent definition of DREG (and DRED), we would like to evaluate some scalar integrals that are commonly encountered in the context of one-loop calculations. In this section, we first derive the analytical form of the one-point function, before doing the same for the two-point function. The case of the three-point and four-point function is not detailed in the present manuscript, here we simply provide a general expression for each of those integrals, their complete analytical expression can however be found in [172–174].

Scalar one-point function $A_0(m^2)$

The scalar one-point function $A_0(m^2)$ is defined as

$$A_0(m^2) := \int \frac{d^D q}{i\pi^2} (2\pi\mu_R)^{2\epsilon} \frac{1}{[q^2 - m^2 + i\epsilon]}, \quad (4.19)$$

where q , m , μ_R , and $i\epsilon$ are respectively the loop momentum, the mass of the particle entering in the loop, the renormalization scale, and the Feynman prescription in charge of ensuring causality of the propagator. More specifically, the integral (4.19) contains an integration over the q^0 real axis running from $-\infty$ to $+\infty$ which exhibits the following poles

$$q^0 = \pm \sqrt{|\vec{q}|^2 + m^2 - i\epsilon} = \pm \sqrt{|\vec{q}|^2 + m^2} \mp \frac{i\epsilon}{2\sqrt{|\vec{q}|^2 + m^2}} + \mathcal{O}(\epsilon^2). \quad (4.20)$$

The Feynman prescription $i\epsilon$ previously introduced aims at shifting the poles above and below the real axis (see Fig. 4.2) such that it is possible to define a closed integration contour in the q^0 complex plane that do not enclose the poles. Thanks to the Cauchy theorem⁹, the integral over this closed contour has to be zero. For $D < 2$, the originally divergent integral (4.19) becomes convergent, and the integrand vanishes fast enough so that the contribution of the arcs drops-out for $|q^0| \rightarrow \infty$. Consequently, it is then possible to replace the q^0 integration over the real axis by a q^0 integration over the imaginary axis. This procedure is called Wick rotation and from a conceptual point of view strictly amounts to transforming the Minkowski space into an Euclidean space. In practice, Wick rotation is achieved by performing the following substitution

$$q^0 = iq_E^0, \quad \vec{q} = \vec{q}_E, \quad q^2 = (q^0)^2 - \vec{q}^2 = -(q_E^0)^2 - \vec{q}_E^2 = -q_E^2. \quad (4.21)$$

⁹The integral of an holomorphic function over a closed contour that do not enclosed any pole vanishes.

The genuine virtue of this technique resides in the fact that it is always possible in the Euclidean space to use rotational invariance to decompose the integrand into a radial and an angular part by introducing the following spherical coordinates

$$d^D q = (idq_E^0)d^{D-1}\vec{q}_E = id^D q_E = iq_E^{D-1}dq_E d\Omega_D, \quad (4.22)$$

thus making the evaluation of loop integrals simpler than in the case of the regular Minkowski space, where one has to use the residue theorem instead. Recalling that $D = 4 - 2\varepsilon$, we obtain

$$A_0(m^2) = -\frac{(4\pi^2\mu_R^2)^\varepsilon}{i\pi^2} \int_0^\infty \frac{iq_E^{D-1}dq_E d\Omega_D}{[q_E^2 + m^2 - i\varepsilon]} \stackrel{(D.11)}{=} -\frac{(4\pi\mu_R^2)^\varepsilon}{\Gamma(D/2)} \int_0^\infty dq_E^2 \frac{(q_E^2)^{D/2-1}}{[q_E^2 + m^2 - i\varepsilon]}$$

If we perform the following change of variable

$$T = \frac{(m^2 - i\varepsilon)}{q_E^2 + (m^2 - i\varepsilon)} \longrightarrow q_E^2 = (m^2 - i\varepsilon)(1 - T)T^{-1}, \quad (4.23)$$

$$dT = -\frac{(m^2 - i\varepsilon) dq_E^2}{[q_E^2 + (m^2 - i\varepsilon)]^2} \longrightarrow dq_E^2 = -(m^2 - i\varepsilon)T^{-2}dT, \quad (4.24)$$

the scalar one-point function reduces to

$$A_0(m^2) = -\frac{(4\pi\mu_R^2)^\varepsilon}{\Gamma(D/2)} \int_0^1 dT (1 - T)^{D/2-1} T^{(1-D/2)-1} (m^2 - i\varepsilon)^{D/2-1}. \quad (4.25)$$

Using the definition (D.8) of the Euler-Beta function, the previous expression simplifies to

$$A_0(m^2) = -\Gamma(\varepsilon - 1)(m^2 - i\varepsilon) \left(\frac{m^2 - i\varepsilon}{4\pi\mu_R^2} \right)^{-\varepsilon}.$$

Using the property (D.3) of the Euler-Gamma function, the previous equation gives

$$A_0(m^2) = -\frac{\Gamma(\varepsilon + 1)}{\varepsilon(\varepsilon - 1)} (m^2 - i\varepsilon) \left(\frac{m^2 - i\varepsilon}{4\pi\mu_R^2} \right)^{-\varepsilon}. \quad (4.26)$$

The regularization procedure aims at identifying and isolating singularities so that it becomes possible to practically manipulate them. Eq.(4.26) is in this respect not very useful as the pole structure of the scalar one-point function is not made explicit. The pole structure can only be made manifest by performing a Laurent series expansion around $\varepsilon = 0$. At one-loop we obtain

$$A_0(m^2) = -\frac{m^2}{\varepsilon} \left[-1 - \varepsilon + \mathcal{O}(\varepsilon^2) \right] \left[1 - \varepsilon\gamma_E + \mathcal{O}(\varepsilon^2) \right] \left[1 - \varepsilon \ln \left(\frac{m^2}{4\pi\mu_R^2} \right) + \mathcal{O}(\varepsilon^2) \right],$$

which thus gives

$$A_0(m^2) = m^2 \left[\frac{1}{\varepsilon} + 1 - \ln \left(\frac{m^2}{\mu_R^2} \right) + \mathcal{O}(\varepsilon) \right], \quad (4.27)$$

with

$$\frac{1}{\varepsilon} = \frac{1}{\varepsilon} + \ln(4\pi) - \gamma_E. \quad (4.28)$$

At this level, two comments are in order *i*) the choice of including or not the universal constant $\ln(4\pi) - \gamma_E$ into the definition of the pole is purely conventional, and is related to the choice of the renormalization scheme, in this thesis we choose to include those terms, this the so-called $\overline{\text{MS}}/\overline{\text{DR}}$ scheme *ii*) according to (4.27), a massless scalar one-point function is exactly zero.

Scalar two-point function $B_0(p^2, m_1^2, m_2^2)$

The scalar two-point function $B_0(p^2, m_1^2, m_2^2)$ is defined as

$$B_0(p^2, m_1^2, m_2^2) := \int \frac{d^D q}{i\pi^2} (2\pi\mu_R)^{2\varepsilon} \frac{1}{[q^2 - m_1^2 + i\epsilon][(p+q)^2 - m_2^2 + i\epsilon]}, \quad (4.29)$$

where p is the external momentum, q is the internal loop momentum, and m_1 and m_2 are the masses of the virtual particles. Note in addition that $B_0(p^2, m_1^2, m_2^2)$ is symmetric under the permutation of m_1 and m_2 such that $B_0(p^2, m_1^2, m_2^2) = B_0(p^2, m_2^2, m_1^2)$. Using the Feynman trick

$$\frac{1}{AB} = \int_0^1 \frac{dx}{[Ax + (1-x)B]^2}, \quad (4.30)$$

it is possible to rewrite (4.29) as follows

$$B_0(p^2, m_1^2, m_2^2) = \frac{(4\pi^2\mu_R^2)^\varepsilon}{i\pi^2} \int_0^1 dx \int \frac{d^D q}{[(p+q)^2 x + (1-x)q^2 - (1-x)m_1^2 - xm_2^2 + i\epsilon]^2}.$$

If we *i*) use translational invariance to perform the momentum transformation $q \rightarrow q = q + xp$
ii) introduce the variable $M^2 = x^2 p^2 - x(p^2 + m_1^2 - m_2^2) + m_1^2 - i\epsilon$ *iii*) perform a Wick rotation
iv) use (D.11) to simplify the angular part of the loop integral, we obtain the following expression

$$B_0(p^2, m_1^2, m_2^2) = \frac{(4\pi^2\mu_R^2)^\varepsilon}{\pi^2} \frac{\sqrt{\pi}^D}{\Gamma(D/2)} \int_0^1 dx \int_0^{+\infty} dq_E^2 \frac{(q_E^2)^{D/2-1}}{[q_E^2 + M^2]^2}. \quad (4.31)$$

With the following change of variable

$$X = \frac{M^2}{q_E^2 + M^2} \rightarrow q_E^2 = M^2 \frac{(1-X)}{X}, \quad (4.32)$$

$$dX = -\frac{M^2 dq_E^2}{[q_E^2 + M^2]^2} \rightarrow dq_E^2 = -\frac{M^2 dX}{X^2}, \quad (4.33)$$

the scalar two-point function can be rewritten as

$$B_0(p^2, m_1^2, m_2^2) = (4\pi^2\mu_R^2)^\varepsilon \frac{\pi^{-\varepsilon}}{\Gamma(D/2)} \int_0^1 dx \int_0^1 dX (1-X)^{D/2-1} X^{1-D/2} (M^2)^{D/2-2}. \quad (4.34)$$

Using the definition (D.8) of the Euler-beta function, and the property (D.3) of the Euler-Gamma function the previous expression reduces to

$$B_0(p^2, m_1^2, m_2^2) = \int_0^1 dx \frac{\Gamma(1+\varepsilon)}{\varepsilon} \left(\frac{M^2}{4\pi\mu_R^2} \right)^{-\varepsilon}. \quad (4.35)$$

To make the pole structure of the two-point function $B_0(p^2, m_1^2, m_2^2)$ explicit, we finally perform a Laurent series expansion around $\varepsilon = 0$, and obtain at one-loop

$$B_0(p^2, m_1^2, m_2^2) = \int_0^1 dx \frac{1}{\varepsilon} [1 - \varepsilon\gamma_E + \mathcal{O}(\varepsilon^2)] \left[1 - \varepsilon \ln \left(\frac{M^2}{4\pi\mu_R^2} \right) + \mathcal{O}(\varepsilon^2) \right], \quad (4.36)$$

which finally simplifies to

$$B_0(p^2, m_1^2, m_2^2) = \frac{1}{\varepsilon} - \int_0^1 dx \ln \left(\frac{x^2 p^2 - x(p^2 + m_1^2 - m_2^2) + m_1^2 - i\epsilon}{\mu_R^2} \right) + \mathcal{O}(\varepsilon). \quad (4.37)$$

The argument of the logarithm in (4.37) can be rewritten in terms of the roots of the polynomial equation $x^2 p^2 - x(p^2 + m_1^2 - m_2^2) + m_1^2 - i\epsilon = 0$. Those roots are

$$x_{1,2} = \frac{p^2 + m_1^2 - m_2^2 \pm \sqrt{(p^2 + m_1^2 - m_2^2)^2 - 4p^2(m_1^2 - i\epsilon)}}{2p^2}, \quad (4.38)$$

such that

$$B_0(p^2, m_1^2, m_2^2) = \frac{1}{\bar{\epsilon}} - \int_0^1 dx \ln \left(\frac{p^2(x - x_1)(x - x_2)}{\mu_R^2} \right) + \mathcal{O}(\epsilon). \quad (4.39)$$

After integrating by part the previous expression, one obtains

$$B_0(p^2, m_1^2, m_2^2) = \frac{1}{\bar{\epsilon}} + 2 - \ln \left(\frac{p^2}{\mu_R^2} \right) - \sum_{i=1}^2 \left[\ln(1 - x_i) + x_i \ln \left(\frac{x_i}{x_i - 1} \right) \right] + \mathcal{O}(\epsilon),$$

which eventually reduces to

$$B_0(p^2, m_1^2, m_2^2) = \frac{1}{\bar{\epsilon}} + 2 - \ln \left(\frac{m_2^2}{\mu_R^2} \right) - \sum_{i=1}^2 x_i \ln \left(\frac{x_i}{x_i - 1} \right) + \mathcal{O}(\epsilon). \quad (4.40)$$

From the generic expression (4.37), one can also deduce the following special cases

$$\begin{aligned} B_0(0, 0, 0) &= \frac{1}{\bar{\epsilon}} - \frac{1}{\bar{\epsilon}_{IR}}, \\ B_0(p^2, 0, 0) &= \frac{1}{\bar{\epsilon}} + 2 - \ln \left(\frac{-p^2 - i\epsilon}{\mu_R^2} \right) + \mathcal{O}(\epsilon), \\ B_0(0, m^2, 0) &= \frac{1}{\bar{\epsilon}} + 1 - \ln \left(\frac{m^2}{\mu_R^2} \right) + \mathcal{O}(\epsilon), \\ B_0(0, m^2, m^2) &= \frac{1}{\bar{\epsilon}} - \ln \left(\frac{m^2}{\mu_R^2} \right) + \mathcal{O}(\epsilon), \\ B_0(m^2, m^2, 0) &= \frac{1}{\bar{\epsilon}} + 2 - \ln \left(\frac{m^2}{\mu_R^2} \right) + \mathcal{O}(\epsilon), \\ B_0(0, m_1^2, m_2^2) &= \frac{1}{\bar{\epsilon}} + 1 - \frac{1}{m_1^2 - m_2^2} \left[m_1^2 \ln \left(\frac{m_1^2}{\mu_R^2} \right) - m_2^2 \ln \left(\frac{m_2^2}{\mu_R^2} \right) \right] + \mathcal{O}(\epsilon), \\ B_0(p^2, m^2, 0) &= \frac{1}{\bar{\epsilon}} + 2 - \ln \left(\frac{m^2}{\mu_R^2} \right) + \frac{m^2 - p^2}{p^2} \ln \left(\frac{m^2 - p^2 - i\epsilon}{m^2} \right) + \mathcal{O}(\epsilon), \\ B_0(m^2, m^2, m^2) &= \frac{1}{\bar{\epsilon}} + 2 - \ln \left(\frac{m^2}{\mu_R^2} \right) - \frac{\pi}{\sqrt{3}} + \mathcal{O}(\epsilon), \\ B_0(p^2, m^2, m^2) &= \frac{1}{\bar{\epsilon}} + 2 - \ln \left(\frac{m^2}{\mu_R^2} \right) + \beta \ln \left(\frac{\beta - 1}{\beta + 1} \right) + \mathcal{O}(\epsilon), \quad \beta = \sqrt{1 - \frac{4(m^2 - i\epsilon)}{p^2}}. \end{aligned}$$

Analogously, the derivative of the scalar two-point function $B'_0(p^2, m_1^2, m_2^2)$ is defined such that

$$B'_0(p^2, m_1^2, m_2^2) = \frac{\partial B_0(p^2, m_1^2, m_2^2)}{\partial p^2}. \quad (4.41)$$

Its analytical form can be obtained by applying the previous definition to (4.37), which gives

$$B'_0(p^2, m_1^2, m_2^2) = \int_0^1 dx \frac{x(1-x)}{[x^2 p^2 - x(p^2 + m_1^2 - m_2^2) + m_1^2 - i\epsilon]} + \mathcal{O}(\epsilon). \quad (4.42)$$

Note that (4.42) is UV-finite, but can potentially contain infrared singularities as shown below

$$\begin{aligned}
B'_0(0, 0, 0) &= 0, \\
B'_0(p^2, 0, 0) &= -\frac{1}{p^2} + \mathcal{O}(\varepsilon), \\
B'_0(0, m^2, 0) &= \frac{1}{2m^2} + \mathcal{O}(\varepsilon), \\
B'_0(0, m^2, m^2) &= \frac{1}{6m^2} + \mathcal{O}(\varepsilon), \\
B'_0(m^2, m^2, 0) &= -\frac{1}{2m^2} \left[\frac{1}{\varepsilon_{IR}} + 2 - \ln \left(\frac{m^2}{\mu_R^2} \right) \right] + \mathcal{O}(\varepsilon), \\
B'_0(0, m_1^2, m_2^2) &= \frac{1}{(m_2^2 - m_1^2)^2} \left[\frac{m_2^2 + m_1^2}{2} - \frac{m_2^2 m_1^2}{(m_2^2 - m_1^2)} \ln \left(\frac{m_2^2}{m_1^2} \right) \right] + \mathcal{O}(\varepsilon), \\
B'_0(p^2, m^2, 0) &= -\frac{1}{p^2} \left[1 + \frac{m^2}{p^2} \ln \left(\frac{m^2 - p^2 - i\epsilon}{m^2} \right) \right] + \mathcal{O}(\varepsilon), \\
B'_0(m^2, m^2, m^2) &= \frac{1}{m^2} \left[\frac{2\pi}{3\sqrt{3}} - 1 \right] + \mathcal{O}(\varepsilon), \\
B'_0(p^2, m_1^2, m_2^2) &= \frac{1}{p^2(x_1 - x_2)} \left[x_1(x_1 - 1) \ln \left(\frac{x_1}{x_1 - 1} \right) - x_2(x_2 - 1) \ln \left(\frac{x_2}{x_2 - 1} \right) \right] - \frac{1}{p^2} + \mathcal{O}(\varepsilon).
\end{aligned}$$

Scalar three-point function $C_0(p_1^2, p_2^2, m_1^2, m_2^2, m_3^2)$

The scalar three-point function $C_0(p_1^2, p_2^2, m_1^2, m_2^2, m_3^2)$ is defined as

$$C_0 := \int \frac{d^D q}{i\pi^2} (2\pi\mu_R)^{2\varepsilon} \frac{1}{[q^2 - m_1^2 + i\epsilon][(p_1 + q)^2 - m_2^2 + i\epsilon][(p_1 + p_2 + q)^2 - m_3^2 + i\epsilon]}, \quad (4.43)$$

where p_1, p_2 , and p_3 are the external momenta, q is the internal loop momentum, m_1, m_2 , and m_3 are the masses of the virtual particles, and where the arguments of C_0 on the left-hand side of (4.43) have been omitted for brevity. Note in addition that (4.43) is UV-finite, but can potentially contain infrared divergences. The exact analytical expression of (4.43), where the pole structure is made explicit, and where the finite terms are detailed, is given in [172–174].

Scalar four-point function $D_0(p_1^2, p_2^2, p_3^2, m_1^2, m_2^2, m_3^2, m_4^2)$

The scalar four-point function $D_0(p_1^2, p_2^2, p_3^2, m_1^2, m_2^2, m_3^2, m_4^2)$ is defined as

$$\begin{aligned}
D_0 &:= \int \frac{d^D q}{i\pi^2} \frac{(2\pi\mu_R)^{2\varepsilon}}{[q^2 - m_1^2 + i\epsilon][(p_1 + q)^2 - m_2^2 + i\epsilon][(p_1 + p_2 + q)^2 - m_3^2 + i\epsilon]} \\
&\quad \times \frac{1}{[(p_1 + p_2 + p_3 + q)^2 - m_4^2 + i\epsilon]}, \quad (4.44)
\end{aligned}$$

where p_1, p_2, p_3 , and p_4 are the external momenta, q is the internal loop momentum, m_1, m_2, m_3 , and m_4 are the masses of the virtual particles, and where the arguments of D_0 on the left-hand side of (4.44) have been omitted for brevity. Analogously to (4.43), (4.44) is UV-finite but can contain infrared divergences. Similarly, the analytical expression of (4.44), where the pole structure is made manifest, and where the finite terms are detailed, can be found in [172–174].

4.4 Passarino-Veltman reduction

The Passarino-Veltman (PV) reduction scheme was originally introduced in 1978 [175], and is historically the first systematic procedure that has been developed to decompose tensor and vector integrals over a basis of scalar integrals. More specifically, the main reason why the PV decomposition allows us to reduce any tensor/vector integral to a linear combination of scalar integrals is Lorentz invariance. According to Lorentz invariance, the tensor structure of the loop integrals can be expressed in terms of Lorentz-invariant quantities, *i.e.* the external momenta p_i^μ , and the metric tensor $\eta^{\mu\nu}$. At one-loop, we can perform the following form-factor expansion

$$\begin{aligned}
B^\mu &= p^\mu B_1, \\
B^{\mu\nu} &= p^\mu p^\nu B_{21} + \eta^{\mu\nu} B_{22}, \\
\\
C^\mu &= p_1^\mu C_{11} + p_2^\mu C_{12}, \\
C^{\mu\nu} &= p_1^\mu p_1^\nu C_{21} + p_2^\mu p_2^\nu C_{22} + \{p_1 p_2\}^{\mu\nu} C_{23} + \eta^{\mu\nu} C_{24}, \\
C^{\mu\nu\rho} &= p_1^\mu p_1^\nu p_1^\rho C_{31} + p_2^\mu p_2^\nu p_2^\rho C_{32} + \{p_1 p_1 p_2\}^{\mu\nu\rho} C_{33} + \{p_1 p_2 p_2\}^{\mu\nu\rho} C_{34} \\
&\quad + \{p_1 \eta\}^{\mu\nu\rho} C_{35} + \{p_2 \eta\}^{\mu\nu\rho} C_{36}, \\
\\
D^\mu &= p_1^\mu D_{11} + p_2^\mu D_{12} + p_3^\mu D_{13}, \\
D^{\mu\nu} &= p_1^\mu p_1^\nu D_{21} + p_2^\mu p_2^\nu D_{22} + p_3^\mu p_3^\nu D_{23} + \{p_1 p_2\}^{\mu\nu} D_{24} + \{p_1 p_3\}^{\mu\nu} D_{25} \\
&\quad + \{p_2 p_3\}^{\mu\nu} D_{26} + \eta^{\mu\nu} D_{27},
\end{aligned} \tag{4.45}$$

where $B_1, B_{21}, B_{22}, C_{11}, C_{12}, \dots, D_{27}$ are some scalar integrals, the so-called form factors, whose arguments have been omitted for brevity, and where the notation $\{\dots\}^{\mu\nu\rho}$ corresponds to a sum over all possible permutations of Lorentz indices. The PV reduction is here performed up to $D^{\mu\nu}$, because, in the context of squark-antisquark pair production, and gluino pair production, this is the highest rank four-point function that is needed (at one-loop).

Vector integral $B_\mu(p^2, m_1^2, m_2^2)$

The vector integral $B_\mu(p^2, m_1^2, m_2^2)$ is defined as

$$B_\mu(p^2, m_1^2, m_2^2) = \int \frac{d^D q}{i\pi^2} (2\pi\mu_R)^{2\varepsilon} \frac{q_\mu}{[q^2 - m_1^2 + i\epsilon][(p+q)^2 - m_2^2 + i\epsilon]}. \tag{4.46}$$

Using the Feynman trick (4.30), and translational invariance, we obtain

$$B_\mu(p^2, m_1^2, m_2^2) = \int_0^1 dx \int \frac{d^D q}{i\pi^2} (2\pi\mu_R)^{2\varepsilon} \frac{q_\mu - xp_\mu}{[q^2 - M^2]^2}, \tag{4.47}$$

with $M^2 = x^2 p^2 - x(p^2 + m_1^2 - m_2^2) + m_1^2 - i\epsilon$. Note that the first term of (4.47) has to be zero because *i*) the function is odd in q *ii*) the domain of integration of this function is symmetric, so

$$B_\mu(p^2, m_1^2, m_2^2) = p_\mu \left[- \int_0^1 dx \int \frac{d^D q}{i\pi^2} (2\pi\mu_R)^{2\varepsilon} \frac{x}{[q^2 - M^2]^2} \right] = p_\mu B_1(p^2, m_1^2, m_2^2). \tag{4.48}$$

Following the procedure detailed in the case of $B_0(p, m_1^2, m_2^2)$, we obtain for $B_1(p, m_1^2, m_2^2)$,

$$B_1(p^2, m_1^2, m_2^2) = -\frac{1}{2\varepsilon} + \int_0^1 x dx \ln \left(\frac{x^2 p^2 - x(p^2 + m_1^2 - m_2^2) + m_1^2 - i\epsilon}{\mu_R^2} \right) + \mathcal{O}(\varepsilon). \tag{4.49}$$

If we contract (4.48) with the external momentum p^μ , we obtain

$$p^\mu B_\mu(p^2, m_1^2, m_2^2) = \int_0^1 dx \int \frac{d^D q}{i\pi^2} (2\pi\mu_R)^{2\varepsilon} \frac{p \cdot q}{[q^2 - m_1^2 + i\varepsilon][(p+q)^2 - m_2^2 + i\varepsilon]} . \quad (4.50)$$

In addition to Lorentz invariance, the PV reduction scheme also relies on the assumption that it is always possible to decompose (at one-loop) any scalar product of loop momenta with external momenta as a linear combination of inverse propagator (plus an invariant). For $p \cdot q$ we have

$$p \cdot q = \frac{1}{2} \left[[(p+q)^2 - m_2^2 + i\varepsilon] - [q^2 - m_1^2 + i\varepsilon] + (m_2^2 - p^2 - m_1^2) \right] , \quad (4.51)$$

where the third term of (4.51) is the so-called invariant. Injecting (4.51) into (4.50) then gives

$$p^\mu B_\mu(p^2, m_1^2, m_2^2) = \frac{1}{2} \left[A_0(m_1^2) - A_0(m_2^2) + f_1(p, m_1^2, m_2^2) B_0(p^2, m_1^2, m_2^2) \right] , \quad (4.52)$$

with

$$f_1(p^2, m_1^2, m_2^2) = (m_2^2 - p^2 - m_1^2) . \quad (4.53)$$

Therefore, according to (4.48), the scalar integral $B_1(p^2, m_1^2, m_2^2)$ can be rewritten as

$$B_1(p^2, m_1^2, m_2^2) = \frac{1}{2p^2} \left[A_0(m_1^2) - A_0(m_2^2) + f_1(p^2, m_1^2, m_2^2) B_0(p^2, m_1^2, m_2^2) \right] . \quad (4.54)$$

Note that *i*) the previous definition of B_1 is only useful as long as $p^2 \neq 0$, if in some specific cases $p^2 = 0$, one has to go back to the generic definition of (4.49) to derive the analytical form of the B_1 function *ii*) in contrast to $B_0(p^2, m_1^2, m_2^2)$, $B_1(p^2, m_1^2, m_2^2)$ is not symmetric under the permutation of m_1 and m_2 . The permutation of the second and third argument indeed gives

$$B_1(p^2, m_2^2, m_1^2) = -B_1(p^2, m_1^2, m_2^2) - B_0(p^2, m_1^2, m_2^2) . \quad (4.55)$$

Similarly to $B'_0(p^2, m_1^2, m_2^2)$, the derivative of $B_1(p^2, m_1^2, m_2^2)$ is defined as

$$B'_1(p^2, m_1^2, m_2^2) = \frac{\partial B_1(p^2, m_1^2, m_2^2)}{\partial p^2} . \quad (4.56)$$

The analytical form of $B'_1(p^2, m_1^2, m_2^2)$ is obtained after applying (4.56) to (4.49), this gives

$$B'_1(p^2, m_1^2, m_2^2) = \int_0^1 dx \frac{x^2(x-1)}{[x^2 p^2 - x(p^2 + m_1^2 - m_2^2) + m_1^2 - i\varepsilon]} + \mathcal{O}(\varepsilon) . \quad (4.57)$$

Tensor integral $B_{\mu\nu}(p^2, m_1^2, m_2^2)$

The tensor integral $B_{\mu\nu}(p^2, m_1^2, m_2^2)$ is defined as

$$B_{\mu\nu}(p^2, m_1^2, m_2^2) = \int \frac{d^D q}{i\pi^2} (2\pi\mu_R)^{2\varepsilon} \frac{q_\mu q_\nu}{[q^2 - m_1^2 + i\varepsilon][(p+q)^2 - m_2^2 + i\varepsilon]} , \quad (4.58)$$

Using the Feynman trick (4.30), and translational invariance, we obtain

$$B_{\mu\nu}(p^2, m_1^2, m_2^2) = \int_0^1 dx \int \frac{d^D q}{i\pi^2} (2\pi\mu_R)^{2\varepsilon} \frac{q_\mu q_\nu - x(p_\mu q_\nu + q_\mu p_\nu) + x^2 p_\mu p_\nu}{[q^2 - M^2]^2} , \quad (4.59)$$

with $M^2 = x^2 p^2 - x(p^2 + m_1^2 - m_2^2) + m_1^2 - i\epsilon$. Note that the second term of (4.59) has to be zero because *i*) the function is odd in q *ii*) the domain of integration of this function is symmetric, so

$$B_{\mu\nu}(p^2, m_1^2, m_2^2) = \int_0^1 dx \int \frac{d^D q}{i\pi^2} (2\pi\mu_R)^{2\epsilon} \frac{x^2 p_\mu p_\nu + \frac{1}{4} q^2 \eta_{\mu\nu}}{[q^2 - M^2]^2}. \quad (4.60)$$

If we define the following integrals

$$B_{21}(p^2, m_1^2, m_2^2) = \int_0^1 dx \int \frac{d^D q}{i\pi^2} (2\pi\mu_R)^{2\epsilon} \frac{x^2}{[q^2 - M^2]^2}, \quad (4.61)$$

$$B_{22}(p^2, m_1^2, m_2^2) = \frac{1}{4} \int_0^1 dx \int \frac{d^D q}{i\pi^2} (2\pi\mu_R)^{2\epsilon} \frac{q^2}{[q^2 - M^2]^2}, \quad (4.62)$$

and inject them into (4.60), we recover the expected Lorentz decomposition

$$B_{\mu\nu}(p^2, m_1^2, m_2^2) = p_\mu p_\nu B_{21}(p^2, m_1^2, m_2^2) + \eta_{\mu\nu} B_{22}(p^2, m_1^2, m_2^2). \quad (4.63)$$

Following the same procedure as detailed before, B_{21} and B_{22} can be re-expressed as

$$B_{21}(p^2, m_1^2, m_2^2) = \frac{1}{3\bar{\epsilon}} - \int_0^1 dx x^2 \ln \left(\frac{x^2 p^2 - x(p^2 + m_1^2 - m_2^2) + m_1^2 - i\epsilon}{\mu_R^2} \right) + \mathcal{O}(\epsilon), \quad (4.64)$$

$$B_{22}(p^2, m_1^2, m_2^2) = -\frac{1}{4\bar{\epsilon}} \left[\frac{p^2}{3} - m_1^2 - m_2^2 \right] + \frac{1}{4} \int_0^1 dx M^2 \left[1 - 2 \ln \left(\frac{M^2}{\mu_R^2} \right) \right] + \mathcal{O}(\epsilon). \quad (4.65)$$

If we now contract the tensor two-point function with all the possible Lorentz invariants, *i.e.* we apply the metric tensor $\eta^{\mu\nu}$ and the external momentum p^μ to (4.63) and (4.58), we obtain

$$\eta^{\mu\nu} B_{\mu\nu} = D B_{22} + p^2 B_{21} = A_0(m_2^2) + m_1^2 B_0(p^2, m_1^2, m_2^2), \quad (4.66)$$

$$p^\mu B_{\mu\nu} = [B_{22} + p^2 B_{21}] p_\nu = \frac{1}{2} [A_0(m_2^2) + f_1(p^2, m_1^2, m_2^2) B_1(p^2, m_1^2, m_2^2)] p_\nu, \quad (4.67)$$

which simplifies to the the following system of equations

$$D B_{22} + p^2 B_{21} = A_0(m_2^2) + m_1^2 B_0(p^2, m_1^2, m_2^2), \quad (4.68)$$

$$B_{22} + p^2 B_{21} = \frac{1}{2} [A_0(m_2^2) + f_1(p^2, m_1^2, m_2^2) B_1(p^2, m_1^2, m_2^2)]. \quad (4.69)$$

Subtracting (4.69) from (4.68) ultimately gives

$$B_{22}(p^2, m_1^2, m_2^2) = \frac{1}{D-1} \left[m_1^2 B_0(p^2, m_1^2, m_2^2) - \frac{1}{2} f_1(p^2, m_1^2, m_2^2) B_1(p^2, m_1^2, m_2^2) + \frac{1}{2} A_0(m_2^2) \right],$$

which can in turn be injected into (4.69) to deduce B_{21}

$$B_{21}(p^2, m_1^2, m_2^2) = \frac{1}{p^2} \left[\frac{1}{2} A_0(m_2^2) + \frac{1}{2} f_1(p^2, m_1^2, m_2^2) B_0(p^2, m_1^2, m_2^2) - B_{22}(p^2, m_1^2, m_2^2) \right].$$

Note that the previous definitions of B_{21} and B_{22} are only useful as long as $p^2 \neq 0$, if $p^2 = 0$ one has to go back to (4.64) and (4.65) to derive the analytical form of B_{21} and B_{22} .

Vector integral $C^\mu(p_1^2, p_2^2, m_1^2, m_2^2, m_3^2)$

The vector three-point function $C^\mu(p_1^2, p_2^2, m_1^2, m_2^2, m_3^2)$ is defined as

$$C^\mu(p_1^2, p_2^2, m_1^2, m_2^2, m_3^2) = \int \frac{d^D q}{i\pi^2} (2\pi\mu_R)^{2\epsilon} \frac{q^\mu}{[q^2 - m_1^2] [(p_1 + q)^2 - m_2^2] [(p_1 + p_2 + q)^2 - m_3^2]}, \quad (4.70)$$

where the Feynman prescription $i\epsilon$ has been omitted for brevity. Lorentz invariance allows for the following Passarino-Veltman decomposition of the vector three-point function C^μ

$$C^\mu = p_1^\mu C_{11} + p_2^\mu C_{12} . \quad (4.71)$$

If we respectively apply the external momenta $p_{1,\mu}$ and $p_{2,\mu}$ on (4.71), we obtain

$$p_{1\mu} C^\mu = p_1^2 C_{11} + p_1 \cdot p_2 C_{12} , \quad (4.72)$$

$$p_{2\mu} C^\mu = p_1 \cdot p_2 C_{11} + p_2^2 C_{12} . \quad (4.73)$$

If we now apply the external momenta $p_{1,\mu}$ and $p_{2,\mu}$ on (4.70), we obtain on the other hand

$$p_{1\mu} C^\mu = \int \frac{d^D q}{i\pi^2} (2\pi\mu_R)^{2\varepsilon} \frac{p_1 \cdot q}{[1][2][3]} , \quad (4.74)$$

$$p_{2\mu} C^\mu = \int \frac{d^D q}{i\pi^2} (2\pi\mu_R)^{2\varepsilon} \frac{p_2 \cdot q}{[1][2][3]} , \quad (4.75)$$

where we have introduced the following handy notation

$$[q^2 - m_1^2] = [1] , \quad [(p_1 + q)^2 - m_2^2] = [2] , \quad [(p_1 + p_2 + q)^2 - m_3^2] = [3] . \quad (4.76)$$

Since

$$p_1 \cdot q = \frac{1}{2} \left[[(p_1 + q)^2 - m_2^2] - [q^2 - m_1^2] + f_1(p_1, m_1^2, m_2^2) \right] , \quad (4.77)$$

$$p_2 \cdot q = \frac{1}{2} \left[[(p_1 + p_2 + q)^2 - m_3^2] - [(p_1 + q)^2 - m_1^2] + f_2(p_1, p_2, m_2^2, m_3^2) \right] , \quad (4.78)$$

with

$$f_1(p_1^2, m_1^2, m_2^2) = (m_2^2 - m_1^2 - p_1^2) , \quad (4.79)$$

$$f_2(p_1^2, p_2^2, m_2^2, m_3^2) = [m_3^2 - m_2^2 - (p_1 + p_2)^2 + p_1^2] , \quad (4.80)$$

then the equations (4.74) and (4.75) can be rewritten as

$$p_{1\mu} C^\mu = \frac{1}{2} \int \frac{d^D q}{i\pi^2} (2\pi\mu_R)^{2\varepsilon} \left[\frac{1}{[1][3]} - \frac{1}{[2][3]} \right] + \frac{1}{2} f_1 C_0 , \quad (4.81)$$

$$p_{2\mu} C^\mu = \frac{1}{2} \int \frac{d^D q}{i\pi^2} (2\pi\mu_R)^{2\varepsilon} \left[\frac{1}{[1][2]} - \frac{1}{[1][3]} \right] + \frac{1}{2} f_2 C_0 , \quad (4.82)$$

where the arguments of the functions f_1 , f_2 , C_0 and C_μ have been omitted for brevity. Equating the previous expressions with (4.72) and (4.73) respectively, gives eventually

$$R_1 = p_1^2 C_{11} + p_1 \cdot p_2 C_{12} = \frac{1}{2} [B_0(1, 3) - B_0(2, 3) + f_1 C_0] , \quad (4.83)$$

$$R_2 = p_1 \cdot p_2 C_{11} + p_2^2 C_{12} = \frac{1}{2} [B_0(1, 2) - B_0(1, 3) + f_2 C_0] , \quad (4.84)$$

where the notation $B_0(i, j)$ corresponds to

$$B_0(i, j) = \int \frac{d^D q}{i\pi^2} (2\pi\mu_R)^{2\varepsilon} \frac{1}{[i][j]} , \quad \text{with } i, j = 1, 2, 3 \text{ and } i \neq j . \quad (4.85)$$

Note that because $B_0(1, 3) - B_0(2, 3)$, $B_0(1, 2) - B_0(1, 3)$, and C_0 are UV-finite, the integrals C_{11} and C_{12} must also be UV-finite. The equations (4.83) and (4.84) can then be rewritten as

$$\begin{pmatrix} R_1 \\ R_2 \end{pmatrix} = \underbrace{\begin{pmatrix} p_1^2 & p_1 \cdot p_2 \\ p_1 \cdot p_2 & p_2^2 \end{pmatrix}}_X \begin{pmatrix} C_{11} \\ C_{12} \end{pmatrix}, \quad (4.86)$$

where the 2×2 matrix X is the so-called Gram matrix. If the Gram matrix is invertible, it is possible to decompose the form factors C_{11} and C_{12} over a basis of scalar integrals. The inverse of the Gram matrix then takes the following analytical form

$$X^{-1} = \frac{1}{p_1^2 p_2^2 - (p_1 \cdot p_2)^2} \begin{pmatrix} p_2^2 & -p_1 \cdot p_2 \\ -p_1 \cdot p_2 & p_1^2 \end{pmatrix}. \quad (4.87)$$

In the case where the Gram matrix is not invertible, the system cannot be solved, and therefore the PV reduction becomes inefficient. We finally obtain the solution

$$\begin{pmatrix} C_{11} \\ C_{12} \end{pmatrix} = X^{-1} \begin{pmatrix} R_1 \\ R_2 \end{pmatrix}. \quad (4.88)$$

Tensor integral $C^{\mu\nu}(p_1^2, p_2^2, m_1^2, m_2^2, m_3^2)$

The tensor three-point function $C^{\mu\nu}(p_1^2, p_2^2, m_1^2, m_2^2, m_3^2)$ is defined as

$$C^{\mu\nu}(p_1^2, p_2^2, m_1^2, m_2^2, m_3^2) = \int \frac{d^D q}{i\pi^2} (2\pi\mu_R)^{2\varepsilon} \frac{q^\mu q^\nu}{[q^2 - m_1^2][(p_1 + q)^2 - m_2^2][(p_1 + p_2 + q)^2 - m_3^2]}, \quad (4.89)$$

where the Feynman prescription has been omitted for simplicity. Lorentz invariance allows for the following decomposition of the tensor integral $C^{\mu\nu}$

$$C^{\mu\nu} = p_1^\mu p_1^\nu C_{21} + p_2^\mu p_2^\nu C_{22} + (p_1^\mu p_2^\nu + p_2^\mu p_1^\nu) C_{23} + \eta^{\mu\nu} C_{24}. \quad (4.90)$$

If we apply the external momenta $p_{1,\mu}$ and $p_{2,\mu}$, and the metric tensor $\eta_{\mu\nu}$ on (4.90), we obtain

$$p_{1\mu} C^{\mu\nu} = [p_1^2 C_{21} + p_1 \cdot p_2 C_{23} + C_{24}] p_1^\nu + [p_1 \cdot p_2 C_{22} + p_1^2 C_{23}] p_2^\nu, \quad (4.91)$$

$$p_{2\mu} C^{\mu\nu} = [p_1 \cdot p_2 C_{21} + p_2^2 C_{23}] p_1^\nu + [p_2^2 C_{22} + p_1 \cdot p_2 C_{23} + C_{24}] p_2^\nu, \quad (4.92)$$

$$\eta_{\mu\nu} C^{\mu\nu} = D C_{24} + p_1^2 C_{21} + p_2^2 C_{22} + 2p_1 \cdot p_2 C_{23}. \quad (4.93)$$

If we now apply $p_{1,\mu}$, $p_{2,\mu}$, and $\eta_{\mu\nu}$ on (4.89), and use (4.77) and (4.78), this gives

$$p_{1\mu} C^{\mu\nu} = \int \frac{d^D q}{i\pi^2} (2\pi\mu_R)^{2\varepsilon} \frac{p_1 \cdot q q^\nu}{[1][2][3]} = \int \frac{d^D q}{i\pi^2} (2\pi\mu_R)^{2\varepsilon} \frac{q^\nu}{2} \left[\frac{1}{[1][3]} - \frac{1}{[2][3]} + \frac{f_1}{[1][2][3]} \right],$$

$$p_{2\mu} C^{\mu\nu} = \int \frac{d^D q}{i\pi^2} (2\pi\mu_R)^{2\varepsilon} \frac{p_2 \cdot q q^\nu}{[1][2][3]} = \int \frac{d^D q}{i\pi^2} (2\pi\mu_R)^{2\varepsilon} \frac{q^\nu}{2} \left[\frac{1}{[1][2]} - \frac{1}{[1][3]} + \frac{f_2}{[1][2][3]} \right],$$

$$\eta_{\mu\nu} C^{\mu\nu} = \int \frac{d^D q}{i\pi^2} (2\pi\mu_R)^{2\varepsilon} \frac{q^2}{[1][2][3]} = \int \frac{d^D q}{i\pi^2} (2\pi\mu_R)^{2\varepsilon} \left[\frac{1}{[2][3]} + \frac{m_1^2}{[1][2][3]} \right].$$

With the help of the notation introduced in (4.85), this system of equations can be rewritten as

$$p_{1\mu} C^{\mu\nu} = \frac{1}{2} \left[B^\nu(1, 3) + f_1 C^\nu - \int \frac{d^D q}{i\pi^2} (2\pi\mu_R)^{2\varepsilon} \frac{q^\nu - p_1^\nu}{[q^2 - m_2^2][(p_2 + q)^2 - m_3^2]} \right], \quad (4.94)$$

$$p_{2\mu} C^{\mu\nu} = \frac{1}{2} \left[B^\nu(1, 2) - B^\nu(1, 3) + f_2 C^\nu \right], \quad (4.95)$$

$$\eta_{\mu\nu} C^{\mu\nu} = B_0(2, 3) + m_1^2 C_0, \quad (4.96)$$

where we have performed the momentum transformation $q \rightarrow q - p_1$ in (4.94), and where

$$\begin{aligned} B^\nu(1, 2) &= B^\nu(p_1^2, m_1^2, m_2^2) = p_1^\nu B_1(p_1^2, m_1^2, m_2^2) = p_1^\nu B_1(1, 2) , \\ B^\nu(1, 3) &= B^\nu((p_1 + p_2)^2, m_1^2, m_3^2) = (p_1 + p_2)^\nu B_1(1, 3) , \\ B_0(2, 3) &= B_0(p_2^2, m_2^2, m_3^2) . \end{aligned}$$

Using the previous definitions and Lorentz invariance we obtain

$$\begin{aligned} p_{1\mu} C^{\mu\nu} &= \frac{1}{2} \left[(p_1 + p_2)^\nu B_1(1, 3) + f_1 [p_1^\nu C_{11} + p_2^\nu C_{12}] - p_2^\nu B_1(p_2^2, m_2^2, m_3^2) + p_1^\nu B_0(2, 3) \right] , \\ p_{2\mu} C^{\mu\nu} &= \frac{1}{2} \left[p_1^\nu B_1(1, 2) - (p_1 + p_2)^\nu B_1(1, 3) + f_2 [p_1^\nu C_{11} + p_2^\nu C_{12}] \right] , \\ \eta_{\mu\nu} C^{\mu\nu} &= B_0(2, 3) + m_1^2 C_0 . \end{aligned}$$

Combining (4.91), and the first line of the previous system of equations gives

$$p_1^2 C_{21} + p_1 \cdot p_2 C_{23} + C_{24} = \frac{1}{2} [B_1(1, 3) + B_0(2, 3) + f_1 C_{11}] = R_3 , \quad (4.97)$$

$$p_1 \cdot p_2 C_{22} + p_1^2 C_{23} = \frac{1}{2} [B_1(1, 3) - B_1(p_2^2, m_2^2, m_3^2) + f_1 C_{12}] = R_5 . \quad (4.98)$$

Similarly combining (4.92), and the second line of the same system of equations gives

$$p_1 \cdot p_2 C_{21} + p_2^2 C_{23} = \frac{1}{2} [B_1(1, 2) - B_1(1, 3) + f_2 C_{11}] = R_4 , \quad (4.99)$$

$$p_2^2 C_{22} + p_1 \cdot p_2 C_{23} + C_{24} = \frac{1}{2} [-B_1(1, 3) + f_2 C_{12}] = R_6 . \quad (4.100)$$

Combining (4.97) with (4.99), and (4.98) with (4.100), and solving the two systems by inverting the 2×2 Gram matrix gives the following results for the form factors C_{21} , C_{22} , and C_{23}

$$\begin{pmatrix} C_{21} \\ C_{23} \end{pmatrix} = X^{-1} \begin{pmatrix} R_3 - C_{24} \\ R_4 \end{pmatrix} , \quad \begin{pmatrix} C_{23} \\ C_{22} \end{pmatrix} = X^{-1} \begin{pmatrix} R_5 \\ R_6 - C_{24} \end{pmatrix} . \quad (4.101)$$

The last step of the reduction procedure of the tensor integral $C^{\mu\nu}$ consists in finding an analytical solution for the remaining form factor C_{24} . This can be done by equating (4.93) and (4.96), and assembling the resulting equation with (4.97) and (4.99) such that we have

$$DC_{24} + p_1^2 C_{21} + p_2^2 C_{22} + 2p_1 \cdot p_2 C_{23} = m_1^2 C_0 + B_0(2, 3) , \quad (4.102)$$

$$p_1^2 C_{21} + p_1 \cdot p_2 C_{23} + C_{24} = \frac{1}{2} [B_1(1, 3) + B_0(2, 3) + f_1 C_{11}] , \quad (4.103)$$

$$p_2^2 C_{22} + p_1 \cdot p_2 C_{23} + C_{24} = \frac{1}{2} [-B_1(1, 3) + f_2 C_{12}] . \quad (4.104)$$

Subtracting (4.103) and (4.104) from (4.102) then directly gives

$$C_{24} = \frac{1}{(D-2)} \left[m_1^2 C_0 - \frac{1}{2} [f_1 C_{11} + f_2 C_{12} - B_0(2, 3)] \right] . \quad (4.105)$$

As a final remark let us note that because C_0 , C_{11} and C_{12} are UV-finite, C_{24} has to be UV-divergent. C_{24} is moreover the only UV-divergent form factor of $C^{\mu\nu}$, this result can be deduced after plugging (4.105) into (4.101). The UV-divergent piece of C_{24} more specifically reads

$$\text{UV}[C_{24}] = \frac{1}{4\epsilon} . \quad (4.106)$$

Tensor integral $C^{\mu\nu\rho}(p_1^2, p_2^2, m_1^2, m_2^2, m_3^2)$

The tensor three-point function $C^{\mu\nu}(p_1^2, p_2^2, m_1^2, m_2^2, m_3^2)$ is defined as

$$C^{\mu\nu\rho}(p_1^2, p_2^2, m_1^2, m_2^2, m_3^2) = \int \frac{d^D q}{i\pi^2} (2\pi\mu_R)^{2\varepsilon} \frac{q^\mu q^\nu q^\rho}{[q^2 - m_1^2] [(p_1 + q)^2 - m_2^2] [(p_1 + p_2 + q)^2 - m_3^2]}, \quad (4.107)$$

where the Feynman prescription has been omitted for simplicity. Lorentz invariance allows for the following decomposition of the tensor integral $C^{\mu\nu\rho}$

$$\begin{aligned} C^{\mu\nu\rho} &= p_1^\mu p_1^\nu p_1^\rho C_{31} + p_2^\mu p_2^\nu p_2^\rho C_{32} + \{p_1 p_1 p_2\}^{\mu\nu\rho} C_{33} + \{p_1 p_2 p_2\}^{\mu\nu\rho} C_{34} \\ &+ \{p_1 \eta\}^{\mu\nu\rho} C_{35} + \{p_2 \eta\}^{\mu\nu\rho} C_{36}, \end{aligned} \quad (4.108)$$

with

$$\{p_1 p_1 p_2\}^{\mu\nu\rho} = p_1^\mu p_1^\nu p_2^\rho + p_1^\nu p_1^\rho p_2^\mu + p_1^\rho p_1^\mu p_2^\nu, \quad \{p_1 \eta\}^{\mu\nu\rho} = p_1^\mu \eta^{\nu\rho} + p_1^\nu \eta^{\rho\mu} + p_1^\rho \eta^{\mu\nu}, \quad (4.109)$$

$$\{p_1 p_2 p_2\}^{\mu\nu\rho} = p_1^\mu p_2^\nu p_2^\rho + p_1^\nu p_2^\rho p_2^\mu + p_1^\rho p_2^\mu p_2^\nu, \quad \{p_2 \eta\}^{\mu\nu\rho} = p_2^\mu \eta^{\nu\rho} + p_2^\nu \eta^{\rho\mu} + p_2^\rho \eta^{\mu\nu}. \quad (4.110)$$

Apart from the increasing complexity of the calculations, the reduction procedure of $C^{\mu\nu\rho}$ remains the same as for $C^{\mu\nu}$. The procedure is summarized as follows *i*) contract (4.108) with the external momenta $p_{1,\rho}$ and $p_{2,\rho}$ *ii*) construct a set of linear equations by first selecting in both $p_{1,\rho} C^{\mu\nu\rho}$ and $p_{2,\rho} C^{\mu\nu\rho}$ the scalar coefficient appearing in front of a given tensor component and assume that each of those coefficients is equal to a scalar function R_i *iii*) the analytic form of each R_i (expressed in terms of scalar integrals) is obtained after contraction of (4.107) with the external momenta $p_{1,\rho}$ and $p_{2,\rho}$ and the extraction of the relevant tensor component *iv*) as soon as all the R_i are known, each system of equations is then solved by inverting the Gram matrix. The scalar products $p_{1,\rho} C^{\mu\nu\rho}$ and $p_{2,\rho} C^{\mu\nu\rho}$ have four possible tensor components in total, namely $\eta^{\mu\nu}$, $p_1^\mu p_1^\nu$, $p_2^\mu p_2^\nu$, and $(p_1^\mu p_2^\nu + p_1^\nu p_2^\mu)$. Following the procedure detailed above gives

$$\begin{pmatrix} C_{35} \\ C_{36} \end{pmatrix} = X^{-1} \begin{pmatrix} R_{10} \\ R_{11} \end{pmatrix},$$

for the $\eta^{\mu\nu}$ component, with the scalar functions R_{10} and R_{11} defined such that

$$\begin{aligned} R_{10} &= \frac{1}{2} [f_1 C_{24} + B_{22}(1, 3) - B_{22}(p_2^2, m_2^2, m_3^2)], \\ R_{11} &= \frac{1}{2} [f_2 C_{24} + B_{22}(1, 2) - B_{22}(1, 3)], \end{aligned}$$

and

$$\begin{pmatrix} C_{31} \\ C_{33} \end{pmatrix} = X^{-1} \begin{pmatrix} R_{12} - 2C_{35} \\ R_{13} \end{pmatrix},$$

for the $p_1^\mu p_1^\nu$ component, with the scalar functions R_{12} and R_{13} defined such that

$$\begin{aligned} R_{12} &= \frac{1}{2} [f_1 C_{21} + B_{21}(1, 3) - B_0(2, 3)], \\ R_{13} &= \frac{1}{2} [f_2 C_{21} + B_{21}(1, 2) - B_{21}(1, 3)], \end{aligned}$$

and

$$\begin{pmatrix} C_{34} \\ C_{32} \end{pmatrix} = X^{-1} \begin{pmatrix} R_{14} \\ R_{15} - 2C_{36} \end{pmatrix},$$

for the $p_2^\mu p_2^\nu$ component, with the scalar functions R_{14} and R_{15} defined such that

$$\begin{aligned} R_{14} &= \frac{1}{2} \left[f_1 C_{22} + B_{21}(1, 3) - B_{21}(p_2^2, m_2^2, m_3^2) \right], \\ R_{15} &= \frac{1}{2} \left[f_2 C_{22} - B_{21}(1, 3) \right], \end{aligned}$$

and

$$\begin{pmatrix} C_{33} \\ C_{34} \end{pmatrix} = X^{-1} \begin{pmatrix} R_{16} - C_{36} \\ R_{17} - C_{35} \end{pmatrix},$$

for the $(p_1^\mu p_2^\nu + p_1^\nu p_2^\mu)$ component, with the scalar functions R_{16} and R_{17} defined such that

$$\begin{aligned} R_{16} &= \frac{1}{2} \left[f_1 C_{23} + B_{21}(1, 3) + B_1(p_2^2, m_2^2, m_3^2) \right], \\ R_{17} &= \frac{1}{2} \left[f_2 C_{23} - B_{21}(1, 3) \right]. \end{aligned}$$

Four-point vector integral $D^\mu(p_1^2, p_2^2, p_3^2, m_1^2, m_2^2, m_3^2, m_4^2)$

The four-point vector integral D^μ is defined as

$$D^\mu = \int \frac{d^D q}{i\pi^2} \frac{(2\pi\mu_R)^{2\varepsilon} q^\mu}{[q^2 - m_1^2] [(p_1 + q)^2 - m_2^2] [(p_1 + p_2 + q)^2 - m_3^2] [(p_1 + p_2 + p_3 + q)^2 - m_4^2]}, \quad (4.111)$$

where the arguments of D^μ , and the Feynman prescription $i\epsilon$ have been omitted for brevity. Lorentz covariance allows us to decompose the four-point function D^μ such that

$$D^\mu = p_1^\mu D_{11} + p_2^\mu D_{12} + p_3^\mu D_{13}. \quad (4.112)$$

If we respectively contract (4.112) with the external momenta $p_{1,\mu}$, $p_{2,\mu}$, and $p_{3,\mu}$ we obtain

$$p_{1,\mu} D^\mu = p_1^2 D_{11} + p_1 \cdot p_2 D_{12} + p_1 p_3 D_{13} = R_{20}, \quad (4.113)$$

$$p_{2,\mu} D^\mu = p_1 \cdot p_2 D_{11} + p_2^2 D_{12} + p_2 p_3 D_{13} = R_{21}, \quad (4.114)$$

$$p_{3,\mu} D^\mu = p_1 \cdot p_3 D_{11} + p_2 p_3 D_{12} + p_3^2 D_{13} = R_{22}. \quad (4.115)$$

This system of equations can be rewritten in terms of the 3×3 Gram matrix X such that

$$\underbrace{\begin{pmatrix} p_1^2 & p_1 \cdot p_2 & p_1 \cdot p_3 \\ p_1 \cdot p_2 & p_2^2 & p_2 \cdot p_3 \\ p_1 \cdot p_3 & p_2 \cdot p_3 & p_3^2 \end{pmatrix}}_X \begin{pmatrix} D_{11} \\ D_{12} \\ D_{13} \end{pmatrix} = \begin{pmatrix} R_{20} \\ R_{21} \\ R_{22} \end{pmatrix}, \quad (4.116)$$

and therefore,

$$\begin{pmatrix} D_{11} \\ D_{12} \\ D_{13} \end{pmatrix} = X^{-1} \begin{pmatrix} R_{20} \\ R_{21} \\ R_{22} \end{pmatrix}. \quad (4.117)$$

Similarly, if we now contract (4.111) with the external momenta $p_{1,\mu}$, $p_{2,\mu}$, and $p_{3,\mu}$, this gives

$$p_{1\mu} D^\mu = \int \frac{d^D q}{i\pi^2} (2\pi\mu_R)^{2\varepsilon} \frac{p_1 \cdot q}{[1][2][3][4]} = \frac{1}{2} \int \frac{d^D q}{i\pi^2} (2\pi\mu_R)^{2\varepsilon} \left[\frac{1}{[1][3][4]} - \frac{1}{[2][3][4]} \right] + \frac{1}{2} f_1 D_0, \quad (4.118)$$

$$p_{2\mu} D^\mu = \int \frac{d^D q}{i\pi^2} (2\pi\mu_R)^{2\varepsilon} \frac{p_2 \cdot q}{[1][2][3][4]} = \frac{1}{2} \int \frac{d^D q}{i\pi^2} (2\pi\mu_R)^{2\varepsilon} \left[\frac{1}{[1][2][4]} - \frac{1}{[1][3][4]} \right] + \frac{1}{2} f_2 D_0, \quad (4.119)$$

$$p_{3\mu} D^\mu = \int \frac{d^D q}{i\pi^2} (2\pi\mu_R)^{2\varepsilon} \frac{p_3 \cdot q}{[1][2][3][4]} = \frac{1}{2} \int \frac{d^D q}{i\pi^2} (2\pi\mu_R)^{2\varepsilon} \left[\frac{1}{[1][2][3]} - \frac{1}{[1][2][4]} \right] + \frac{1}{2} f_3 D_0 \quad (4.120)$$

where we have introduced the convenient notations

$$\begin{aligned} [1] &= [q^2 - m_1^2], & [2] &= [(p_1 + q)^2 - m_2^2], \\ [3] &= [(p_1 + p_2 + q)^2 - m_3^2], & [4] &= [(p_1 + p_2 + p_3 + q)^2 - m_4^2], \end{aligned}$$

and where f_1 and f_2 have already been defined in (4.79) and (4.80), and f_3 is given by

$$f_3(p_1^2, p_2^2, p_3^2, m_2^2, m_3^2, m_4^2) = \left[m_4^2 - m_3^2 - (p_1 + p_2 + p_3)^2 + (p_1 + p_2)^2 \right]. \quad (4.121)$$

Equating (4.113), (4.114), and (4.115) with (4.118), (4.119), and (4.120) respectively leads to

$$R_{20} = \frac{1}{2} \left[f_1 D_0 + C_0(1, 3, 4) - C_0(2, 3, 4) \right], \quad (4.122)$$

$$R_{21} = \frac{1}{2} \left[f_2 D_0 + C_0(1, 2, 4) - C_0(1, 3, 4) \right], \quad (4.123)$$

$$R_{22} = \frac{1}{2} \left[f_3 D_0 + C_0(1, 2, 3) - C_0(1, 2, 4) \right], \quad (4.124)$$

and

$$\begin{pmatrix} D_{11} \\ D_{12} \\ D_{13} \end{pmatrix} = X^{-1} \begin{pmatrix} R_{20} \\ R_{21} \\ R_{22} \end{pmatrix}.$$

Four-point tensor integral $D^{\mu\nu}(p_1^2, p_2^2, p_3^2, m_1^2, m_2^2, m_3^2, m_4^2)$

The four-point tensor integral $D^{\mu\nu}$ is defined as

$$D^{\mu\nu} = \int \frac{d^D q}{i\pi^2} \frac{(2\pi\mu_R)^{2\epsilon} q^\mu q^\nu}{[q^2 - m_1^2][(p_1 + q)^2 - m_2^2][(p_1 + p_2 + q)^2 - m_3^2][(p_1 + p_2 + p_3 + q)^2 - m_4^2]}, \quad (4.125)$$

where the arguments of $D^{\mu\nu}$, and the Feynman prescription $i\epsilon$ have been omitted for brevity. Lorentz covariance allows us to decompose the four-point function $D^{\mu\nu}$ such that

$$\begin{aligned} D^{\mu\nu} &= p_1^\mu p_1^\nu D_{21} + p_2^\mu p_2^\nu D_{22} + p_3^\mu p_3^\nu D_{23} + \{p_1 p_2\}^{\mu\nu} D_{24} + \{p_1 p_3\}^{\mu\nu} D_{25} \\ &+ \{p_2 p_3\}^{\mu\nu} D_{26} + \eta^{\mu\nu} D_{27}. \end{aligned} \quad (4.126)$$

The procedure to derive the analytical expression of the form factors D_{21} , D_{22} , D_{23} , D_{24} , D_{25} , D_{26} , and D_{27} has already been detailed when reviewing the $C^{\mu\nu\rho}$ function, we do not repeat it here. The only difference comes from the fact that the exact form of D_{27} can be obtained by contracting (4.125) and (4.126) with the metric tensor, equating the two resulting equations, and then subtracting from the latter R_{30} , R_{34} , and R_{38} . Following this procedure, we obtain

$$\begin{pmatrix} D_{21} \\ D_{24} \\ D_{25} \end{pmatrix} = X^{-1} \begin{pmatrix} R_{30} - D_{27} \\ R_{31} \\ R_{32} \end{pmatrix},$$

for the p_1^ν component, with the scalar functions R_{30} , R_{31} , and R_{32} defined such that

$$\begin{aligned} R_{30} &= \frac{1}{2} \left[f_1 D_{11} + C_0(2, 3, 4) + C_{11}((p_1 + p_2)^2, p_3^2, m_1^2, m_3^2, m_4^2) \right], \\ R_{31} &= \frac{1}{2} \left[f_2 D_{11} + C_{11}(p_1^2, (p_2 + p_3)^2, m_1^2, m_2^2, m_4^2) - C_{11}((p_1 + p_2)^2, p_3^2, m_1^2, m_3^2, m_4^2) \right], \\ R_{32} &= \frac{1}{2} \left[f_3 D_{11} + C_{11}(p_1^2, p_2^2, m_1^2, m_2^2, m_3^2) - C_{11}(p_1^2, (p_2 + p_3)^2, m_1^2, m_2^2, m_4^2) \right], \end{aligned}$$

and

$$\begin{pmatrix} D_{24} \\ D_{22} \\ D_{26} \end{pmatrix} = X^{-1} \begin{pmatrix} R_{33} \\ R_{34} - D_{27} \\ R_{35} \end{pmatrix},$$

for the p_2^ν component, with the scalar functions R_{33} , R_{34} and R_{35} defined such that

$$\begin{aligned} R_{33} &= \frac{1}{2} \left[f_1 D_{12} + C_{11}((p_1 + p_2)^2, p_3^2, m_1^2, m_3^2, m_4^2) - C_{11}(p_2^2, p_3^2, m_2^2, m_3^2, m_4^2) \right], \\ R_{34} &= \frac{1}{2} \left[f_2 D_{12} + C_{12}(p_1^2, (p_2 + p_3)^2, m_1^2, m_2^2, m_4^2) - C_{11}((p_1 + p_2)^2, p_3^2, m_1^2, m_3^2, m_4^2) \right], \\ R_{35} &= \frac{1}{2} \left[f_3 D_{12} + C_{12}(p_1^2, p_2^2, m_1^2, m_2^2, m_3^2) - C_{12}(p_1^2, (p_2 + p_3)^2, m_1^2, m_2^2, m_4^2) \right], \end{aligned}$$

and

$$\begin{pmatrix} D_{25} \\ D_{26} \\ D_{23} \end{pmatrix} = X^{-1} \begin{pmatrix} R_{36} \\ R_{37} \\ R_{38} - D_{27} \end{pmatrix},$$

for the p_3^ν component, with the scalar functions R_{36} , R_{37} and R_{38} defined such that

$$\begin{aligned} R_{36} &= \frac{1}{2} \left[f_1 D_{13} + C_{12}((p_1 + p_2)^2, p_3^2, m_1^2, m_3^2, m_4^2) - C_{12}(p_2^2, p_3^2, m_2^2, m_3^2, m_4^2) \right], \\ R_{37} &= \frac{1}{2} \left[f_2 D_{13} + C_{12}(p_1^2, (p_2 + p_3)^2, m_1^2, m_2^2, m_4^2) - C_{12}((p_1 + p_2)^2, p_3^2, m_1^2, m_3^2, m_4^2) \right], \\ R_{38} &= \frac{1}{2} \left[f_3 D_{13} - C_{12}(p_1^2, (p_2 + p_3)^2, m_1^2, m_2^2, m_4^2) \right], \end{aligned}$$

where D_{27} is defined as

$$D_{27} = \frac{1}{(D-3)} \left[m_1^2 D_0 - \frac{1}{2} \left[f_1 D_{11} + f_2 D_{12} + f_3 D_{13} - C_0(2, 3, 4) \right] \right]. \quad (4.127)$$

Limitations of the Passarino-Veltman reduction method

The Passarino-Veltman (PV) decomposition is an efficient reduction technique employed in many modern loop calculations. Yet, this procedure still exhibits some intrinsic limitations that make its use highly inadvisable, if not impossible, in certain cases. In the following, we detail some pathological cases for which an alternative to the PV reduction has to be found to carry out the reduction program.

The validity of the PV algorithm first depends on the assumption that the Gram matrix is invertible, *i.e.* the Gram determinant is non-zero. However, there exists some specific kinematical configurations, called exceptional phase-space points, for which the Gram determinant exactly vanishes, this is the case for instance when two external momenta are collinear one to another. In such configurations, the PV algorithm is bounded to fail. Besides, even if the Gram determinant is not exactly zero, but close to zero, the brute-force application of the PV algorithm can generate numerical instabilities¹⁰. Second, the Passarino-Veltman algorithm relies on the idea that the scalar product of a loop momentum with an external momentum can always be expressed as a linear combination of inverse propagators. This statement is true at one-loop, but not necessarily at higher orders. The PV reduction scheme is therefore not the optimal choice for calculations beyond one-loop. Third, the iterative nature of the PV algorithm directly implies a rapid growth in the number of terms when evaluating high-rank tensor integrals. The PV reduction is therefore not the best choice when dealing with loop integrals exhibiting many Lorentz indices.

¹⁰The numerical instabilities are due to a loss of significance which occurs when subtracting two nearly equal numbers, such as $p_1^2 p_2^2 - (p_1 \cdot p_2)^2$ for instance when p_1 , and p_2 are (almost) collinear.

4.5 Renormalization

Now that the poles have been isolated from the finite terms, the last step of the procedure consists in absorbing UV divergences into the redefinition of all the fields and parameters of the original tree-level Lagrangian, the so-called bare fields and bare parameters, by means of a technique called multiplicative renormalization. This technique is called multiplicative renormalization because it amounts to re-expressing each bare quantity, usually denoted by the subscript "0", as a product between its renormalized counterpart and a multiplicative factor Z_i such that

$$\phi_0 = Z_\phi^{1/2} \phi, \quad g_0 = Z_g g, \quad (4.128)$$

where ϕ , and g respectively correspond to generic renormalized fields, and coupling constants, and where the Z_i are the renormalization constants (RCs). In perturbation theory, it is possible to perform a series expansion around unity for each RC. At one-loop, this gives in our notations

$$Z_\phi^{1/2} = 1 + \frac{1}{2} \delta Z_\phi, \quad Z_g = 1 + \delta Z_g. \quad (4.129)$$

With the help of (4.129), it is possible to split the original tree-level Lagrangian $\mathcal{L}(\phi_0, g_0)$ into a renormalized part $\mathcal{L}(\phi, g)$, and a part containing the counter-terms (CT),

$$\mathcal{L}(\phi_0, g_0) = \mathcal{L}(\phi, g) + \mathcal{L}_{ct}(\phi, g, \delta Z_\phi, \delta Z_g). \quad (4.130)$$

The first term on the right-hand side of (4.130) is similar to the original tree-level Lagrangian, except that all the bare fields and parameters have been replaced by their renormalized counterpart. The second term on the other hand introduces new interactions (and hence new Feynman diagrams), whose aim is to cancel UV-divergences originating from the renormalized Lagrangian $\mathcal{L}(\phi, g)$ (through loop calculations). If the divergent part of each counter-term is fixed by the requirement that it should cancel against the UV poles of the loops, the finite part depends on the other hand on the choice of the renormalization scheme. There are several renormalization schemes available on the market, in this thesis, we employ the on-shell (OS) scheme, and the modified minimal subtraction scheme $\overline{\text{MS}}$ (resp. $\overline{\text{DR}}^{11}$ for SUSY loop calculations).

The on-shell scheme consists in fixing the counter-terms such that the renormalized parameters are set equal to their physical value at all orders in perturbation theory. Renormalization constants being fixed at physical scales, physical observables and parameters are consequently scale independent in this scheme, *i.e.* they do not run with the energy. The OS scheme is a scheme that is frequently encountered in the literature, however its use, in the context of perturbative QCD, for the renormalization of the gluon wave-function (WF), the strong coupling constant, and the light-quark masses and WFs is made ambiguous by the fact at low-energies quarks and gluons are screened inside hadrons. More specifically, this ambiguity can be traced back to the fact that UV-divergences are subtracted from the aforementioned quantities at scales where perturbation theory is no longer reliable, while we assume perturbativity in the first place. In this case, a more suitable choice is the $\overline{\text{MS}}$ scheme (resp. $\overline{\text{DR}}$ scheme for supersymmetric loop calculations¹²) where the only requirement is that the counter-terms should cancel the UV-part of the loop contributions.

In this section, we will apply the procedure of multiplicative renormalization detailed above to the case of the free Lagrangian describing the dynamics of a set of generic massive complex scalar fields, massive fermions, and massive gauge fields with mixing. The goal of this section is to determine the analytical expressions of all the RCs needed to obtain a UV-finite result.

¹¹ $\overline{\text{DR}}$ is defined as the combined use of DRED and modified minimal subtraction.

¹²At one-loop, the $\overline{\text{MS}}$ and $\overline{\text{DR}}$ scheme only differ by finite terms, consequently counter-terms calculated in the $\overline{\text{MS}}$ or in the $\overline{\text{DR}}$ scheme are completely equivalent.



Figure 4.3: One-particle irreducible two-point function for generic scalar fields \tilde{f}_i with mixing. $\hat{\Gamma}$ denotes the matrix of inverse propagators, $\hat{\Pi}_{ij}(p^2)$ is the renormalized self-energy, and p is the momentum of the external particles. The momentum p flows from the left to the right.

Renormalization of generic scalar fields with mixing

At tree-level, the free Lagrangian for a set of massive complex scalar fields \tilde{f}_i reads

$$\mathcal{L} = (\partial_\mu \tilde{f}_{0,i}^* \partial^\mu \tilde{f}_{0,j} - m_{\tilde{f}_{i,0}}^2 \tilde{f}_{0,i}^* \tilde{f}_{0,j}) \delta_{ij} . \quad (4.131)$$

Knowing that, at one-loop, the scalar fields $\tilde{f}_{0,i}$ and their masses $m_{\tilde{f}_{i,0}}^2$ are renormalized as

$$\begin{aligned} \tilde{f}_{0,j} &= \left[\delta_{jk} + \frac{1}{2} (\delta Z_{\tilde{f}})_{jk} \right] \tilde{f}_k , & \tilde{f}_{0,i}^* &= \tilde{f}_\ell^* \left[\delta_{i\ell} + \frac{1}{2} (\delta Z_{\tilde{f}}^*)_{i\ell} \right] , \\ m_{\tilde{f}_{i,0}}^2 &= m_{\tilde{f}_i}^2 + \delta m_{\tilde{f}_i}^2 , \end{aligned}$$

we obtain the following expression for the renormalized self-energy $\hat{\Pi}_{ij}(p^2)$

$$\hat{\Pi}_{ij}(p^2) = \Pi_{ij}(p^2) + \frac{1}{2} (p^2 - m_{\tilde{f}_i}^2) (\delta Z_{\tilde{f}})_{ij} + \frac{1}{2} (p^2 - m_{\tilde{f}_j}^2) (\delta Z_{\tilde{f}}^*)_{ji} - \delta_{ij} \delta m_{\tilde{f}_i}^2 . \quad (4.132)$$

In the previous expression, $\Pi_{ij}(p^2)$ denotes to the unrenormalized self-energy, which originates from the calculation of loop diagrams, and p is the momentum of the external particles. The renormalized self-energy $\hat{\Pi}_{ij}(p^2)$ is linked to the matrix of inverse propagators $\hat{\Gamma}$ by the relation given in Fig. 4.3. The next step of the procedure then consists in fixing the counter-terms by means of the renormalization conditions. In the on-shell scheme, those conditions read

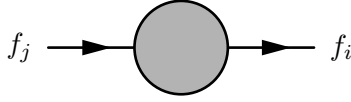
$$\widetilde{\text{Re}} \hat{\Gamma}_{ij}(p^2) \Big|_{p^2=m_{\tilde{f}_j}^2} = 0 , \quad (4.133)$$

$$\lim_{p^2 \rightarrow m_{\tilde{f}_i}^2} \frac{1}{p^2 - m_{\tilde{f}_i}^2} \widetilde{\text{Re}} \hat{\Gamma}_{ii}(p^2) = 1 , \quad (4.134)$$

which means that we simultaneously require the real part of the pole of the propagator to be the renormalized mass, *i.e.* the physical mass, and the residue of the pole to be one. The mass counter-term $\delta m_{\tilde{f}_i}^2$ can be obtained from (4.133), in the case where $i = j$. The expression of the off-diagonal Wave-Function Renormalization Constants (WFRCs) δZ_{ij} can also be derived from (4.133), but for $i \neq j$. Finally, the diagonal WFRCs δZ_{ii} can be determined from (4.134), after having injected the definition of $\delta m_{\tilde{f}_i}^2$ into the previous equation. Eventually, the counter-terms for a set of complex scalar fields take the following form

$$\begin{aligned} \delta m_{\tilde{f}_i}^2 &= \widetilde{\text{Re}} \left[\Pi_{ii}(m_{\tilde{f}_i}^2) \right] , \\ (\delta Z_{\tilde{f}})_{ij} &= \frac{2}{m_{\tilde{f}_i}^2 - m_{\tilde{f}_j}^2} \widetilde{\text{Re}} \left[\Pi_{ij}(m_{\tilde{f}_j}^2) \right] \quad \text{with} \quad i \neq j , \\ (\delta Z_{\tilde{f}})_{ii} &= - \widetilde{\text{Re}} \left[\dot{\Pi}_{ii}(m_{\tilde{f}_i}^2) \right] \quad \text{with} \quad \dot{\Pi}_{ii}(m_{\tilde{f}_i}^2) = \frac{\partial \Pi_{ii}(p^2)}{\partial p^2} \Big|_{p^2=m_{\tilde{f}_i}^2} . \end{aligned}$$

The WFRCs and the mass counter-terms are consequently expressed in terms of the unrenormalized self-energy, which is calculable order by order in perturbation theory.



$$\begin{aligned}\mathcal{M} &= i \bar{u}_i(p) \hat{\Gamma}_{ij} u_j(p) \\ \hat{\Gamma}_{ij} &= \delta_{ij}(\not{p} - m_{f_i}) + \hat{\Sigma}_{ij}(p)\end{aligned}$$

Figure 4.4: The one-particle irreducible two-point function for generic fermions f_i with mixing. $\hat{\Gamma}$ denotes the matrix of inverse propagators, $\hat{\Sigma}_{ij}(p^2)$ is the renormalized self-energy, and p is the momentum of the external particles. The momentum p flows from the left to the right.

Renormalization of generic fermion fields with mixing

At tree-level, the free Lagrangian for a set of massive four-components fermions f_i reads

$$\mathcal{L} = \bar{f}_{0,i}(i\gamma^\mu\partial_\mu - m_{f_i,0})f_{0,j} \delta_{ij} . \quad (4.135)$$

At one-loop, the Dirac spinors $f_{0,i}$, and their mass $m_{f_i,0}$ are reparameterized as follows

$$\begin{aligned}f_{0,j} &= \left[\delta_{jk} + \frac{1}{2} (\delta Z_f^L)_{jk} P_L + \frac{1}{2} (\delta Z_f^R)_{jk} P_R \right] f_k , \\ \bar{f}_{0,i} &= \bar{f}_l \left[\delta_{li} + \frac{1}{2} (\delta Z_f^{R\dagger})_{li} P_L + \frac{1}{2} (\delta Z_f^{L\dagger})_{li} P_R \right] , \\ m_{f_i,0} &= m_{f_i} + \delta m_{f_i} ,\end{aligned}$$

where P_L and P_R are the chiral projectors defined in Appendix A, and δZ_f^L and δZ_f^R are the left-handed, and right-handed WFRCs of the fermions. Injecting the previous equations into the tree-level Lagrangian, leads to the following expression for the renormalized self-energy $\hat{\Sigma}_{ij}(p)$

$$\hat{\Sigma}_{ij}(p) = \hat{\Sigma}_{ij}^{V,L}(p) \not{p} P_L + \hat{\Sigma}_{ij}^{V,R}(p) \not{p} P_R + \hat{\Sigma}_{ij}^{S,L}(p) P_L + \hat{\Sigma}_{ij}^{S,R}(p) P_R , \quad (4.136)$$

with

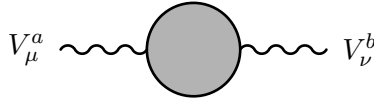
$$\begin{aligned}\hat{\Sigma}_{ij}^{V,L/R}(p) &= \Sigma_{ij}^{V,L/R}(p) + \frac{1}{2} [(\delta Z_f^{L/R})_{ij} + (\delta Z_f^{L/R\dagger})_{ij}] , \\ \hat{\Sigma}_{ij}^{S,L/R}(p) &= \Sigma_{ij}^{S,L/R}(p) - \frac{1}{2} [m_{f,i}(\delta Z_f^{L/R})_{ij} + (\delta Z_f^{R/L\dagger})_{ij} m_{f,j}] - \delta m_{f,i} \delta_{ij} ,\end{aligned}$$

where $\Sigma_{ij}^{V,L}$ and $\Sigma_{ij}^{V,R}$ respectively denote the left-, and right-handed vector part of the unrenormalized self-energy, $\Sigma_{ij}^{S,L}$ and $\Sigma_{ij}^{S,R}$ respectively correspond to the left-, and right-handed scalar part of the unrenormalized self-energy, and p is the momentum of the external particles. $\Sigma_{ij}^{V,L/R}$, and $\Sigma_{ij}^{S,L/R}$ are the so-called vector, and scalar parts of the unrenormalized self-energy $\hat{\Sigma}_{ij}(p)$ because they are respectively proportional to \not{p} , and m_f . The renormalized self-energy $\hat{\Sigma}_{ij}(p)$ is linked to the matrix of inverse propagators $\hat{\Gamma}$ by the relation given in Fig. 4.4. Then, we fix the counter-terms with the help of the on-shell renormalization conditions, which are in this case

$$\widetilde{\text{Re}} \hat{\Gamma}_{ij}(p) u_j(p) \Big|_{p^2=m_{f_j}^2} = 0 , \quad (4.137)$$

$$\lim_{p^2 \rightarrow m_{f_i}^2} \frac{1}{\not{p} - m_{f_i}} \widetilde{\text{Re}} \hat{\Gamma}_{ii}(p) u_i(p) = u_i(p) . \quad (4.138)$$

The mass counter-term δm_{f_i} is obtained from (4.137), by taking $i = j$. The derivation works as follows *i*) rewrite the condition (4.137) as a system of two equations (one for each chiral component) *ii*) add those two equations to cancel the WFRCs dependence *iii*) re-express δm_{f_i}



$$\mathcal{M} = -i \epsilon^\mu(p) \hat{\Gamma}_{\mu\nu}^{ab} \epsilon^{*\nu}(p)$$

$$\hat{\Gamma}_{\mu\nu}^{ab} = -(p^2 - m_{V^a}^2) \delta_{ab} \eta_{\mu\nu} - \hat{\Pi}_{\mu\nu}(p)$$

Figure 4.5: The one-particle irreducible two-point function for vector fields V with mixing. $\hat{\Gamma}$ denotes the matrix of inverse propagators, $\hat{\Sigma}_{ij}(p^2)$ is the renormalized self-energy, and p is the momentum of the external particles. The momentum p flows from the left to the right.

in terms of the various components of the unrenormalized self-energy, and the mass m_{f_i} . The off-diagonal Wave-Function Renormalization Constants (WFRCs) δZ_{ij} are also derived from (4.137), but for $i \neq j$. Finally, the diagonal WFRCs δZ_{ii} are determined by injecting the definition of δm_{f_i} into (4.138). Eventually, the counter-terms take the following form

$$\begin{aligned} \delta m_{f_i} &= \frac{1}{2} \widetilde{\text{Re}} \left[m_i \left(\Sigma_{ii}^{V,L}(m_{f_i}) + \Sigma_{ii}^{V,R}(m_{f_i}) \right) + \Sigma_{ii}^{S,L}(m_{f_i}) + \Sigma_{ii}^{S,R}(m_{f_i}) \right], \\ (\delta Z_f^{L/R})_{ij} &= \frac{2}{m_{f_i}^2 - m_{f_j}^2} \times \widetilde{\text{Re}} \left[m_j^2 \Sigma_{ij}^{V,L/R}(m_{f_j}) + m_i m_j \Sigma_{ij}^{V,R/L}(m_{f_j}) \right. \\ &\quad \left. + m_i \Sigma_{ij}^{S,L/R}(m_{f_j}) + m_j \Sigma_{ij}^{S,R/L}(m_{f_j}) \right], \\ (\delta Z_f^{L/R})_{ii} &= -\widetilde{\text{Re}} \left[\Sigma_{ii}^{V,L/R}(m_{f_i}) \right] + \frac{1}{2m_{f_i}} \widetilde{\text{Re}} \left[\Sigma_{ii}^{S,L/R}(m_{f_i}) - \Sigma_{ii}^{S,R/L}(m_{f_i}) \right] \\ &\quad - m_{f_i} \widetilde{\text{Re}} \left[m_{f_i} \left(\dot{\Sigma}_{ii}^{V,L/R}(m_{f_i}) + \dot{\Sigma}_{ii}^{V,R/L}(m_{f_i}) \right) + \dot{\Sigma}_{ii}^{S,L/R}(m_{f_i}) + \dot{\Sigma}_{ii}^{S,R/L}(m_{f_i}) \right]. \end{aligned}$$

Renormalization of generic vector bosons with mixing

At tree-level, the free Lagrangian for a set of massive vector fields V reads

$$\mathcal{L} = -\frac{1}{2} \left(\partial^\rho V_{0,a}^\mu \partial_\rho V_{0,b}^\nu \eta_{\mu\nu} - \partial^\rho V_{0,a}^\mu \partial_\mu V_{0,b}^\nu \eta_{\rho\nu} \right) \delta_{ab} + m_{V^a,0}^2 V_{0,a}^\mu V_{0,b}^\nu \delta_{ab} \eta_{\mu\nu}. \quad (4.139)$$

At one-loop, the fields and mass parameters can be renormalized as

$$V_{0,a}^\mu = \left[\delta_{ac} + \frac{1}{2} (\delta Z_V)_{ac} \right] V_c^\mu, \quad V_{0,b}^\nu = \left[\delta_{bd} + \frac{1}{2} (\delta Z_V)_{bd} \right] V_d^\nu, \quad (4.140)$$

$$m_{V^a,0}^2 = m_{V^a}^2 + \delta m_{V^a}^2. \quad (4.141)$$

The renormalized self-energy $\hat{\Pi}_{\mu\nu}(p^2)$ can be split into a transverse and a longitudinal part

$$\hat{\Pi}_{\mu\nu}^{ab}(p) = \left(\eta_{\mu\nu} - \frac{p_\mu p_\nu}{p^2} \right) \hat{\Pi}_T^{ab}(p) + \frac{p_\mu p_\nu}{p^2} \hat{\Pi}_L^{ab}(p), \quad (4.142)$$

respectively denoted as $\hat{\Pi}_T^{ab}(p)$ and $\hat{\Pi}_L^{ab}(p)$. Gauge invariance of the renormalized self-energy $\hat{\Pi}_{\mu\nu}(p)$ directly fixes the longitudinal component to be zero, *i.e.* $\hat{\Pi}_L^{ab}(p) = 0$. In the following, we therefore suppress all subscripts T , as it is understood that we are systematically referring to the transverse part of the renormalized self-energy anyway. Injecting (4.140), and (4.141) into (4.139) leads to the following expression for $\hat{\Pi}^{ab}(p)$

$$\hat{\Pi}^{ab}(p) = \Pi_{ab}(p) + \frac{1}{2} (p^2 - m_{V^a}^2) (\delta Z_V)_{ab} + \frac{1}{2} (p^2 - m_{V^b}^2) (\delta Z_V)_{ba} - \delta_{ab} \delta m_{V^a}^2. \quad (4.143)$$

In the previous expression, $\Pi_{ab}(p)$ denotes to the unrenormalized self-energy, which originates from the calculation of loop diagrams, and p is the momentum of the external particles. The

renormalized self-energy $\widehat{\Pi}_{\mu\nu}^{ab}(p)$ is linked to the matrix of inverse propagators $\widehat{\Gamma}_{\mu\nu}$ by the relation given in Fig. 4.5. The counter-terms are then fixed by applying the on-shell renormalization conditions, which read as follows for a set of generic vector fields

$$\widetilde{\text{Re}} \widehat{\Gamma}_{\mu\nu}^{ab}(p)\epsilon^\nu(p) \Big|_{p^2=m_{V_b}^2} = 0, \quad (4.144)$$

$$\lim_{p^2 \rightarrow m_{V_a}^2} \frac{1}{p^2 - m_{V_a}^2} \widetilde{\text{Re}} \widehat{\Gamma}_{\mu\nu}^{aa}(p^2)\epsilon^\nu(p) = -\epsilon_\mu(p). \quad (4.145)$$

The mass counter-term $\delta m_{V_a}^2$ can be obtained from (4.144), by taking $a = b$. The off-diagonal WFRs $(\delta Z_V)_{ab}$ can also be derived from (4.144), but for $a \neq b$. Finally, the diagonal WFRs $(\delta Z_V)_{aa}$ are fixed by (4.145), after having injected the definition of $\delta m_{V_a}^2$ into the previous equation. Eventually, the counter-terms take the following form

$$\begin{aligned} \delta m_{V_a}^2 &= \widetilde{\text{Re}} \left[\Pi_{aa}(m_{V_a}^2) \right], \\ (\delta Z_V)_{ab} &= \frac{2}{m_{V_a}^2 - m_{V_b}^2} \widetilde{\text{Re}} \left[\Pi_{ab}(m_{V_b}^2) \right], \\ (\delta Z_V)_{aa} &= -\widetilde{\text{Re}} \left[\dot{\Pi}_{aa}(m_{V_a}^2) \right]. \end{aligned}$$

In practice, only the last counter-term will be needed in the calculations reported in Chapters 5 and 6. This is due to the fact that the gauge symmetry $SU(3)_C$ forbids mass corrections to the gluon, and to the fact that even if the gauge group of QCD were broken, gluons could not mix with any other vector field whatsoever¹³. So, neither the off-diagonal WFRs, nor the mass counter-terms are needed for the gluon in QCD or SUSY-QCD.

Renormalization of the strong coupling constant

The renormalization of the strong coupling constant g_s proceeds exactly as detailed before for the two-point functions. We start from the tree-level Lagrangian of SUSY-QCD, and renormalize the gluon field, the quark, gluino, and squark fields and masses, and the coupling constant g_s such that $g_{s,0} = g_s + \delta g_s$. In the case of the quark-quark-gluon interaction, this gives for instance the following counter-term Lagrangian at one-loop

$$\begin{aligned} \mathcal{L}_{CT} &= \bar{q}_i^{c_m} g_\mu^a \gamma^\mu \left[\delta g_s \delta_{ij} + \frac{g_s}{2} \left([(\delta Z_q^L)_{ij} + (\delta Z_q^{L\dagger})_{ij}] P_L + [(\delta Z_q^R)_{ij} \right. \right. \\ &\quad \left. \left. + (\delta Z_q^{R\dagger})_{ij}] P_R + \delta Z_g \delta_{ij} \right) \right] T_{c_m c_n}^a q_j^{c_n}. \end{aligned}$$

Then, we impose that the sum of this counter-term and the vertex corrections V_{gqq} associated to triangle graphs involving two external quarks and one external gluon is UV-finite. Seeing that the WFRs have been defined in the previous step of the renormalization procedure, the expression of the counter-term δg_s directly ensue from the previous requirement. The same procedure has to be carried out for each term of the interaction Lagrangian, so that UV-finiteness is ensured at one-loop in every sector of the theory. We will give more details on that step when discussing the squark-antisquark pair production in SUSY-QCD with NMFV in the next chapter.

Renormalization of the squark mixing angles

In the case of our interest, supersymmetric QCD, the only scalars that can mix are the squarks. More specifically, from (2.112), we know that squark gauge eigenstates $\tilde{q}_{0,j}^g$ and mass eigenstates

¹³Because gluons are the only spin-1 coloured particles of the theory.

$\tilde{q}_{0,k}^g$ are related by the following equation at tree-level

$$\tilde{q}_{0,j}^g = R_{0,kj}^{\tilde{q}*} \tilde{q}_{0,k} , \quad (4.146)$$

where the superscript g denotes gauge eigenstates, and $R^{\tilde{q}}$ corresponds to the squark mixing matrix. At one-loop, the mass eigenstates and the elements of $R^{\tilde{q}}$ are reparameterized as follows

$$\tilde{q}_{0,k} = \left[\delta_{ki} + \frac{1}{2} (\delta Z_{\tilde{q}})_{ki} \right] \tilde{q}_i , \quad R_{0,kj}^{\tilde{q}*} = R_{kj}^{\tilde{q}*} + \delta R_{kj}^{\tilde{q}*} , \quad (4.147)$$

which gives for the gauge eigenstates

$$\tilde{q}_{0,j}^g = \left[R_{kj}^{\tilde{q}*} + \delta R_{kj}^{\tilde{q}*} \right] \left[\delta_{ki} + \frac{1}{2} (\delta Z_{\tilde{q}})_{ki} \right] \tilde{q}_i = R_{ij}^{\tilde{q}*} \tilde{q}_i + \delta R_{ij}^{\tilde{q}*} \tilde{q}_i + \frac{1}{2} R_{kj}^{\tilde{q}*} (\delta Z_{\tilde{q}})_{ki} \tilde{q}_i .$$

The squarks WFRs can then be split into an hermitian, and anti-hermitian part such that

$$\tilde{q}_{0,j}^g = R_{ij}^{\tilde{q}*} \tilde{q}_i + \delta R_{ij}^{\tilde{q}*} \tilde{q}_i + \frac{1}{4} R_{kj}^{\tilde{q}*} \left[(\delta Z_{\tilde{q}})_{ki} + (\delta Z_{\tilde{q}}^*)_{ik} \right] \tilde{q}_i + \frac{1}{4} R_{kj}^{\tilde{q}*} \left[(\delta Z_{\tilde{q}})_{ki} - (\delta Z_{\tilde{q}}^*)_{ik} \right] \tilde{q}_i ,$$

which is equivalent to

$$\tilde{q}_{0,j}^g = \left[R_{kj}^{\tilde{q}*} + \frac{1}{4} R_{ij}^{\tilde{q}*} \left[(\delta Z_{\tilde{q}})_{ik} + (\delta Z_{\tilde{q}}^*)_{ki} \right] \right] \tilde{q}_k + \left[\delta R_{ij}^{\tilde{q}*} + \frac{1}{4} R_{kj}^{\tilde{q}*} \left[(\delta Z_{\tilde{q}})_{ki} - (\delta Z_{\tilde{q}}^*)_{ik} \right] \right] \tilde{q}_i .$$

In the previous equation, the mixing angle counter-term $\delta R_{ij}^{\tilde{q}}$ can be chosen so that it cancels the anti-hermitian part of the squark WFRs [176]. The motivation behind this choice is that it is highly desirable to preserve the form of the rotation (4.146) at one-loop. This leads to

$$\delta R_{ij}^{\tilde{q}} = \frac{1}{4} \sum_{k=1}^6 \left[(\delta Z_{\tilde{q}})_{ik} - (\delta Z_{\tilde{q}}^*)_{ki} \right] R_{kj}^{\tilde{q}} . \quad (4.148)$$

Additional prescriptions:

Because of the $SU(2)_L$ symmetry, the soft-SUSY breaking mass parameters of the left-handed squarks of the same isodoublet must be identical at tree-level. This feature is preserved at one-loop in the $\overline{\text{DR}}$ scheme. This is however not the case in the on-shell scheme, where the finite terms differ. By convention, an additional (finite) shift must therefore be performed on the OS soft-SUSY mass parameter of the left-handed down-type squarks, so that the equality mentioned above is restored. If this prescription has been discussed in the case of MFV [177–179], its generalization to NMFV is currently under study. The renormalization of the off-diagonal elements of the squark mass matrix in the gauge eigenstate basis is also currently under study.

Summary:

In this chapter, we have provided a short introduction to one-loop calculation techniques. More specifically, we have first recalled the various challenges of NLO calculations, before giving a constructive (and mathematically consistent) definition of both Dimensional Regularization, and Dimensional Reduction. Then, we have detailed how to evaluate scalar integrals that are frequently encountered in the context of one-loop calculations, and introduce the Passarino-Veltman reduction scheme designed to decompose each vector and tensor loop integral into a linear combination of simpler scalar integrals multiplied by Lorentz invariants. The last part of this chapter has been dedicated to the procedure of multiplicative renormalization, which aims at absorbing UV divergences into the redefinition of all the bare fields and parameters of the original tree-level Lagrangian. In this last section, we have derived all the renormalization constants that are necessary to ensure the UV-finiteness of the theory at one-loop (for generic scalar, fermions, and vector fields with mixing), and provided our results in the on-shell scheme.

Chapter 5

Squark-antisquark production at NLO with NMFV

In the previous chapter, we have detailed the procedure of renormalization for a set of generic scalar, fermion, and vector fields (with mixing) and derived the expression of all the counter-terms that are necessary to ensure the UV-finiteness of the final result. In this chapter, we are going to apply this procedure, for the first time, to the case of squark-antisquark production at next-to-leading order in supersymmetric QCD with Non-Minimal Flavour Violation.

Accurate theoretical predictions for squark-antisquark hadroproduction are essential for the derivation of the squark masses exclusion limits at the LHC, can possibly help to refine the experimental search strategies in some specific regions of the parameter space, and in case of discovery, can be used to characterize the properties of the observed particles [180–182]. The inclusive cross section for squark-antisquark hadroproduction at leading order in SUSY-QCD, in the limit of mass degenerate squarks, has been known for more than thirty years [183–185]. The next-to-leading order SUSY-QCD corrections have been obtained ten years later [186–188], also in the limit where all the squarks, but the stops, are mass degenerate. Those corrections have been found to be positive, and large, more than 30% of the tree-level contribution (depending on the detail of the considered SUSY scenario), and their inclusion has been shown to significantly reduce the factorization and renormalization scale dependence of the total cross section. The previous results have been subsequently implemented in the publicly available FORTRAN code PROSPINO [189], which allows for the computation of inclusive and differential cross section of squark and gluino hadroproduction, at leading order, and next-to-leading order in SUSY-QCD.

A significant part of the large NLO SUSY-QCD corrections originates from the energy region near the (partonic) production threshold [187]. In this region, the NLO corrections are essentially dominated by the contributions coming from soft gluon emission in the initial and final state, and by Coulomb corrections due to the exchange of (long-range) gluons between massive particles in the final state. The soft-gluon corrections can be taken into account to all orders in perturbation theory by means of threshold resummation techniques [190,191]. Recently, a substantial amount of work has been dedicated to the inclusion of threshold effects at the next-to-leading logarithmic (NLL) [192–199], and next-to-next-to-leading logarithmic (NNLL) accuracy [200–203]. These corrections typically result into a small increase of the total cross section, 5 to 15 % depending on the SUSY scenario, and lead to a further reduction of the renormalization and factorization scale dependence.

In addition to the large SUSY-QCD corrections, the leading order electroweak (EW) contributions have also been considered [204,205], and the NLO-EW corrections to squark-antisquark hadroproduction have been studied in [206–209]. The latter have been shown to be sizeable, depending on the model, and on the flavour and chirality of the produced squarks in the final

state. The squark-antisquark production and decay matched with parton showers at NLO has been investigated in [210,211], and recently, a lot of efforts have been devoted to the automation of precision calculations for squark-antisquark hadroproduction [88,212,213].

In all the aforementioned studies, Minimal Flavour Violation has been systematically assumed, and in most cases, the 2×2 squark mixing matrices have been considered to be diagonal, except for the top squarks. The inclusion of Non-Minimal Flavour Violating effects for squark-antisquark hadroproduction at NLO in SUSY-QCD has however never been investigated in the literature so far. In this chapter, we provide the first preliminary (analytical) results for the virtual contributions, *i.e.* the loop amplitudes and the renormalization constants, and report on the status of this on-going calculation. The analytical results obtained and summarized in the present manuscript have been cross-checked with the help of the MATHEMATICA packages FEYNARTS-3.9 and FORMCALC-8.4. More specifically, the Feynman diagrams and their associated amplitudes have been generated via the FEYNARTS package by means of the tree-level model file FVMSSM.mod, which is an implementation of the MSSM Lagrangian including Non-Minimal Flavour Violating effects. The Feynman rules implemented in the FEYNARTS model file FVMSSM.mod, do not contain the SUSY-QCD counter-terms that are needed to ensure the UV-finiteness of the virtual contribution. Those counter-terms have been implemented into a new model file. The generated amplitudes have been then be calculated with the help of FORMCALC.

This chapter is organized as follows: in Section 5.1, we fix our conventions, define our model, and provide the expression of the MSSM SUSY-QCD Lagrangian, where Non-Minimal Flavour Violating effects have been included. In Section 5.2, we provide the first necessary ingredient of the next-to-leading order cross-section, namely the leading order matrix element for squark-antisquark hadroproduction. In Section 5.3, we detail the renormalization program, and specify all the renormalization constants that need to be calculated to yield a UV-finite result. In Section 5.4, we calculate the self-energies of all the fields appearing in the tree-level diagrams, *i.e.* quarks, gluons, squarks, and gluinos, and provide their respective renormalization constants in the On-Shell (OS) scheme, and/or in the $\overline{\text{MS}}/\overline{\text{DR}}$ scheme. In Section 5.5, we consider the case of the vertex corrections, and calculate the renormalization constant of the strong coupling constant. In Section 5.6, we focus on the box contributions, and provide all the Feynman diagrams contributing to this last piece of the one-loop calculation.

5.1 Theoretical set-up

In the most general version of the Minimal Supersymmetric Standard Model (MSSM), soft supersymmetry breaking induces the mixing of all left- and right-handed squark gauge eigenstates (with the same quantum numbers). Because the squark mass eigenstates, that are obtained after the diagonalization of the two squark mass matrices by means of the 6×6 unitary matrices $R^{\tilde{u}}$ and $R^{\tilde{d}}$ respectively (see Section 2.11 for more details), are an admixture of left- and right-handed squark gauge eigenstates of all generations, flavour violations can arise even in the SUSY-QCD sector of the usual MSSM Lagrangian. In the squark mass-eigenstate basis, the Lagrangian of our interest (in the four-component spinor formalism) reads

$$\begin{aligned} \mathcal{L} = & -\frac{1}{4}g_{\mu\nu}g^{\mu\nu} - \frac{1}{2}(\partial_\mu g^\mu)^2 - \bar{u}_g \partial_\mu D^\mu u_g + \frac{i}{2}\bar{g}\not{D}g - \frac{1}{2}m_{\tilde{g}}\bar{g}g + D_\mu \tilde{q}_i^\dagger D^\mu \tilde{q}_i - m_{\tilde{q}_i}^2 \tilde{q}_i^\dagger \tilde{q}_i \\ & + i\bar{q}_i \not{D}q_i - m_{q_i} \bar{q}_i q_i - \frac{g_s^2}{2} \left[\tilde{q}_i^\dagger (R^{\tilde{q}})_{if} T^a (R^{\tilde{q}})_{jf}^* \tilde{q}_j - \tilde{q}_i^\dagger (R^{\tilde{q}})_{i(f+3)} T^a (R^{\tilde{q}})_{j(f+3)}^* \tilde{q}_j \right]^2 \\ & + \sqrt{2}g_s \left[(\bar{q}_f P_L e^{-\frac{i\varphi_{\tilde{g}}}{2}} \tilde{g}^a) T^a (R^{\tilde{q}})_{i(f+3)}^* \tilde{q}_i - \tilde{q}_i^\dagger (R^{\tilde{q}})_{if} T^a (e^{-\frac{i\varphi_{\tilde{g}}}{2}} g^a P_L q_f) + \text{h.c.} \right]. \end{aligned} \quad (5.1)$$

All color indices have been understood, except when attached to the matrices of the fundamental representation of $SU(3)_C$, that we denote by T^a . The first line of the previous Lagrangian includes kinetic and gauge interaction terms for the gluon (g), the gluino (\tilde{g}), and the squarks (\tilde{q}), as well as the soft SUSY-breaking gluino and squark mass terms, where $m_{\tilde{g}}$ and $m_{\tilde{q}_i}$ respectively correspond to the gluino and squarks masses. Note that we have also added to the Lagrangian the necessary ghost (u_g), and gauge-fixing terms related to our choice of working in the Feynman gauge. The second line of the Lagrangian includes kinetic, mass, and gauge interaction terms for the quarks (q_i), and describes the quartic interactions of the squarks. Finally, the last line corresponds to trilinear quark-squark-gluino interactions. For completeness, we have kept explicit the dependence of the squark-quark-gluino vertices on the gluino phase $\varphi_{\tilde{g}}$ (see Section 2.10).

In order to write Eq. (5.1) under a compact form, we have employed $SU(3)_C$ covariant derivatives D_μ and the gluon field strength tensor $g_{\mu\nu}$. These objects are defined such that

$$g_{\mu\nu}^a = \partial_\mu g_\nu^a - \partial_\nu g_\mu^a + g_s f^a_{bc} g_\mu^b g_\nu^c \quad \text{and} \quad D_\mu = \partial_\mu - ig_s \mathcal{T}^a g_\mu^a, \quad (5.2)$$

where we denote the strong coupling constant by g_s , and the antisymmetric structure constants of $SU(3)_C$ by f_{abc} . The matrices \mathcal{T}^a are taken in the appropriate representation of $SU(3)_c$, *i.e.*, the fundamental one for (s)quarks and the adjoint for gluinos and ghosts. The Feynman rules relevant for the calculations performed in this work have been extracted from the Lagrangian (5.1), and are summarized in Appendix F.

The momenta associated to the initial-state particles of the original $2 \rightarrow 2$ process are labelled p_1 , and p_2 , those of the final-state particles are called p_3 and p_4 . The Mandelstam variable \hat{s} , \hat{t} , and \hat{u} are defined such that

$$\hat{s} = (p_1 + p_2)^2 = (p_3 + p_4)^2, \quad \hat{t} = (p_1 - p_3)^2 = (p_2 - p_4)^2, \quad (5.3)$$

$$\hat{u} = (p_1 - p_4)^2 = (p_2 - p_3)^2, \quad (5.4)$$

and the reduced Mandelstam variables \hat{t}_X and \hat{u}_X correspond to

$$\hat{t}_X = \hat{t} - m_X^2, \quad \hat{u}_X = \hat{u} - m_X^2. \quad (5.5)$$

Note finally, that the matrix elements detailed below are evaluated in the approximation of massless quarks in the initial state, and that the final-state squarks are assumed to be produced on-shell, *i.e.* $\hat{s} > (m_{\tilde{q}_i} + m_{\tilde{q}_j})$.

5.2 Tree-level matrix element

Before starting to compute loops, it is first necessary to derive the full matrix element for the $2 \rightarrow 2$ process at tree-level. The diagrams contributing to squark-antisquark pair production at leading order in SUSY-QCD are represented on Fig. 5.1. The first two diagrams correspond to the quark-antiquark channel, and are interfered coherently to produce the correct matrix element, which reads as follows

$$\begin{aligned} |M_{q,s}^B|^2 &= (n_c^2 - 1) \frac{2g_s^4}{\hat{s}^2} (\hat{u}\hat{t} - m_{\tilde{q}_i}^2 m_{\tilde{q}_j}^2) \delta_{qq'} \delta_{ij} \delta_{mn}, \\ |M_{q,t}^B|^2 &= (n_c^2 - 1) \frac{g_s^4}{\hat{t}_{\tilde{g}}^4} \left[(|R_{im}^{\tilde{q}} R_{jn}^{\tilde{q}'}|^2 + |R_{i(m+3)}^{\tilde{q}} R_{j(n+3)}^{\tilde{q}'}|^2) (\hat{u}\hat{t} - m_{\tilde{q}_i}^2 m_{\tilde{q}_j}^2) \right. \\ &\quad \left. + m_{\tilde{g}}^2 \hat{s} (|R_{im}^{\tilde{q}} R_{j(n+3)}^{\tilde{q}'}|^2 + |R_{i(m+3)}^{\tilde{q}} R_{jn}^{\tilde{q}'}|^2) \right], \\ 2 \operatorname{Re}\{M_{q,s}^B M_{q,t}^{B*}\} &= -\frac{n_c^2 - 1}{n_c} \frac{2g_s^4}{\hat{s}\hat{t}_{\tilde{g}}} (\hat{u}\hat{t} - m_{\tilde{q}_i}^2 m_{\tilde{q}_j}^2) \operatorname{Re}\{R_{im}^{\tilde{q}} R_{jn}^{\tilde{q}'*} + R_{i(m+3)}^{\tilde{q}} R_{j(n+3)}^{\tilde{q}'*}\} \delta_{qq'} \delta_{ij} \delta_{mn}. \end{aligned} \quad (5.6)$$

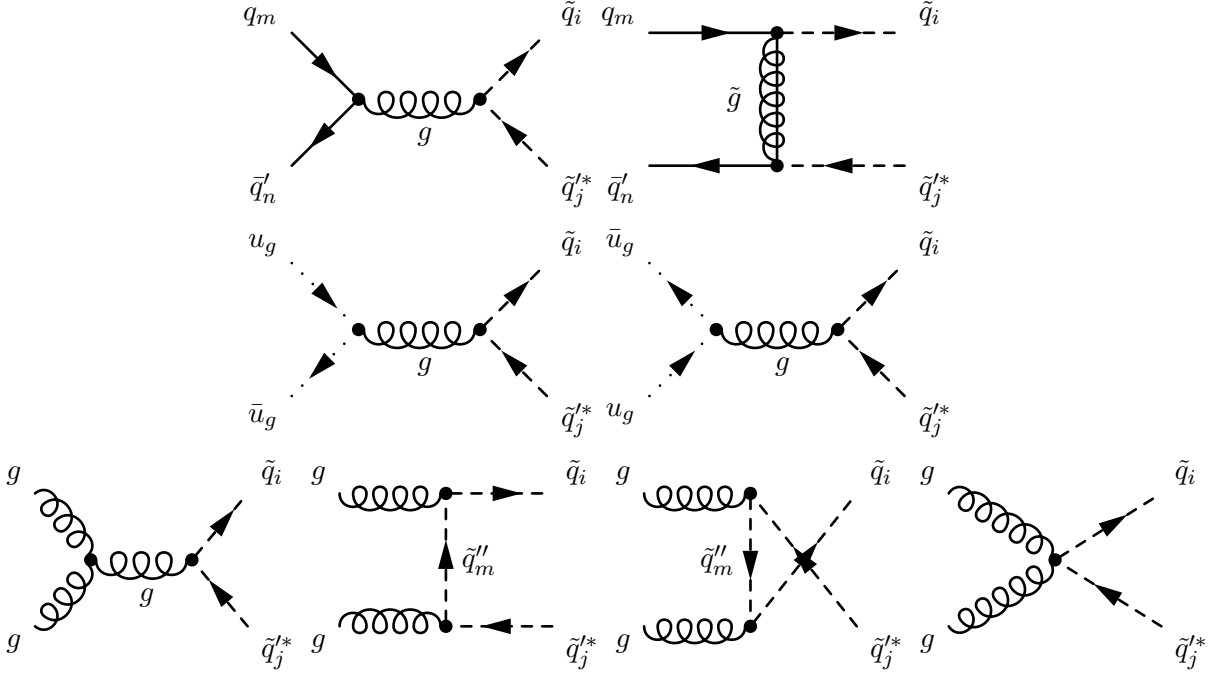


Figure 5.1: Feynman diagrams for squark-antisquark pair production at leading order in SUSY-QCD. The quark-antiquark channel (top), the gluon-gluon channel (bottom), and the ghost channel (middle), mandatory for calculations performed in Feynman gauge, are depicted here.

In the previous expressions, \tilde{q} and \tilde{q}' denote the squark-type indices, m and n correspond to quark flavour indices, i and j are the squark flavour indices, and n_c is the number of colours. Analogously, the various contributions associated to the gluon-gluon sub-process are given by

$$|M_{g,s}^B|^2 = (n_c^2 - 1)n_c \frac{g_s^4}{4\hat{s}^2} [32m_{\tilde{q}_i}^4 - 3(\hat{t}^2 + \hat{u}^2) - 26\hat{t}\hat{u}] \delta_{qq'} \delta_{ij} , \quad (5.7)$$

$$|M_{g,t}^B|^2 = \frac{(n_c^2 - 1)^2}{n_c} \frac{g_s^4}{\hat{t}_{\tilde{q}_i}^2} (\hat{t} + m_{\tilde{q}_i}^2)^2 \delta_{qq'} \delta_{ij} , \quad (5.8)$$

$$|M_{g,u}^B|^2 = \frac{(n_c^2 - 1)^2}{n_c} \frac{g_s^4}{\hat{u}_{\tilde{q}_i}^2} (\hat{u} + m_{\tilde{q}_i}^2)^2 \delta_{qq'} \delta_{ij} , \quad (5.9)$$

$$|M_{g,4}^B|^2 = 2 \frac{(n_c^2 - 1)(n_c^2 - 2)}{n_c} g_s^4 \delta_{qq'} \delta_{ij} ,$$

$$2\text{Re}\{M_{g,s}^B M_{g,t}^{B*}\} = -(n_c^2 - 1)n_c \frac{g_s^4}{4\hat{s}\hat{t}_{\tilde{q}_i}} [4(\hat{t}^2 + m_{\tilde{q}_i}^4) + \hat{s}^2 - 8m_{\tilde{q}_i}^2(\hat{s} + \hat{t})] \delta_{qq'} \delta_{ij} , \quad (5.10)$$

$$2\text{Re}\{M_{g,s}^B M_{g,u}^{B*}\} = -(n_c^2 - 1)n_c \frac{g_s^4}{4\hat{s}\hat{u}_{\tilde{q}_i}} [4(\hat{u}^2 + m_{\tilde{q}_i}^4) + \hat{s}^2 - 8m_{\tilde{q}_i}^2(\hat{s} + \hat{u})] \delta_{qq'} \delta_{ij} , \quad (5.11)$$

$$2\text{Re}\{M_{g,s}^B M_{g,4}^{B*}\} = 0 , \quad (5.12)$$

$$2\text{Re}\{M_{g,t}^B M_{g,u}^{B*}\} = \frac{n_c^2 - 1}{n_c} \frac{-g_s^4}{2\hat{t}_{\tilde{q}_i}\hat{u}_{\tilde{q}_i}} (\hat{s} - 4m_{\tilde{q}_i}^2)^2 \delta_{qq'} \delta_{ij} , \quad (5.13)$$

$$2\text{Re}\{M_{g,t}^B M_{g,4}^{B*}\} = \frac{(n_c^2 - 1)(n_c^2 - 2)}{n_c} \frac{g_s^4}{4\hat{t}_{\tilde{q}_i}} [\hat{s} - 4(\hat{t} + m_{\tilde{q}_i}^2)] \delta_{qq'} \delta_{ij} , \quad (5.14)$$

$$2\text{Re}\{M_{g,u}^B M_{g,4}^{B*}\} = \frac{(n_c^2 - 1)(n_c^2 - 2)}{n_c} \frac{g_s^4}{4\hat{u}_{\tilde{q}_i}} [\hat{s} - 4(\hat{u} + m_{\tilde{q}_i}^2)] \delta_{qq'} \delta_{ij} , \quad (5.15)$$

from which we have to subtract the two squared ghost contributions,

$$|M_{u_g,1}^B|^2 = |M_{u_g,2}^B|^2 = (n_c^2 - 1)n_c \frac{g_s^4}{8\hat{s}^2} (\hat{t} - \hat{u})^2 \delta_{\tilde{q}_i \tilde{q}'_j} . \quad (5.16)$$

Summing-up all the contributions, the squared matrix element we obtain agrees with [214–216]. The gluon channel is numerically the dominant channel at the LHC, due to the large PDF of the gluon, and is completely independent of the flavour structure of the theory, *i.e.* of the squark mixing angle. In this channel, the produced squarks are bounded to exhibit the same fermion type and sfermion index. Similar considerations also hold for the s -channel diagram of the $q\bar{q}$ -channel. As a matter of fact, only the t -channel of the quark-antiquark channel exhibit a dependence on the squark mixing angles, due to presence of gluino-squark-quark vertices, and can lead to the production of squarks of different types, and with different sfermion index.

The matrix elements detailed above have also been checked against the results obtained with FEYNARTS/FORMCALC, for each contribution separately in the case of the $q\bar{q}$ -channel, and at the level of the total matrix element for the gg -channel (out of which the ghost contributions must be subtracted). This fact more specifically originates from the fact that in FEYNARTS/FORMCALC only the (physical) transverse polarization modes of the gluon are taken into account, *i.e.* gluons are expressed in the axial gauge.

5.3 Renormalization set-up

As explained in Section 4.5, the original tree-level Lagrangian (5.1) must be renormalized to absorb UV-divergences appearing when evaluating loop integrals. In this study, we renormalize multiplicatively all the bare fields and parameters, before expanding each renormalization constant perturbatively. Since, we focus in this chapter on next-to-leading order calculations in SUSY-QCD, this expansion can be restricted to the first order in α_s . This gives the following replacement rules for all the bare fields (denoted by the subscript "0") appearing in (5.1)

$$\begin{aligned} g_0^\mu &= \sqrt{Z_g} g^\mu = (1 + \frac{1}{2} \delta Z_g) g^\mu , \\ q_{0,i} &= (\sqrt{Z_q})_{ij} q_j = \left[\delta_{ij} + \frac{1}{2} (\delta Z_q^L)_{ij} P_L + \frac{1}{2} (\delta Z_q^R)_{ij} P_R \right] q_j , \\ \tilde{g}_0 &= \sqrt{Z_{\tilde{g}}} \tilde{g} = \left[1 + \frac{1}{2} \delta Z_{\tilde{g}}^L P_L + \frac{1}{2} \delta Z_{\tilde{g}}^R P_R \right] \tilde{g} , \\ \tilde{q}_{0,i} &= (\sqrt{Z_{\tilde{q}}})_{ij} \tilde{q}_j = \left[\delta_{ij} + \frac{1}{2} (\delta Z_{\tilde{q}})_{ij} \right] \tilde{q}_j , \end{aligned} \quad (5.17)$$

where the generation indices for quarks (resp. squarks) are ranging from one to three (resp. from one to six). The previous expressions include a dependence on the renormalization constants δZ that are extracted by requiring the ultraviolet-finiteness of the renormalized self-energies of the various fields (see Section 5.4 below). The remaining ultraviolet divergences, that may still arise after field renormalization, are absorbed by renormalizing all the parameters of the Lagrangian (5.1). For the quark, squark, and gluino masses we have

$$m_{q_i,0} = m_{q_i} + \delta m_{q_i} , \quad m_{\tilde{g},0} = m_{\tilde{g}} + \delta m_{\tilde{g}} , \quad (5.18)$$

$$m_{\tilde{q}_i,0}^2 = m_{\tilde{q}_i}^2 + \delta m_{\tilde{q}_i}^2 . \quad (5.19)$$

Similarly, for the squark mixing angles we obtain

$$(R^{\tilde{q}})_{ij} = (R^{\tilde{q}})_{ij} + (\delta R^{\tilde{q}})_{ij} . \quad (5.20)$$

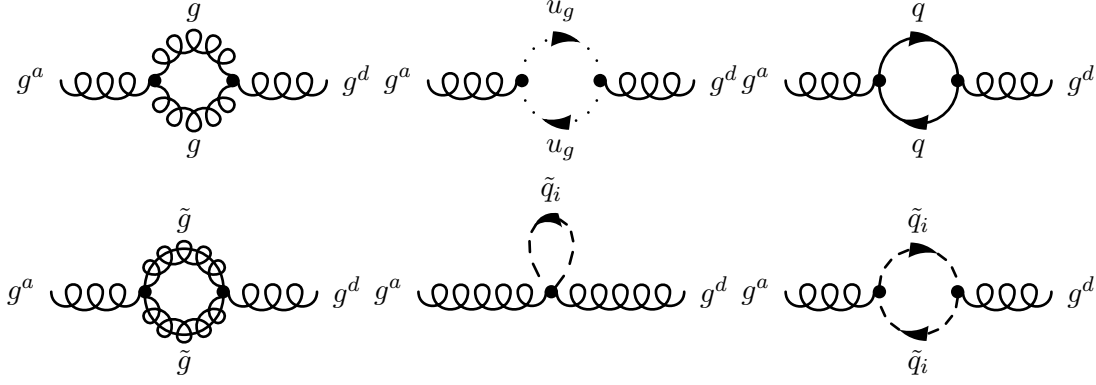


Figure 5.2: Virtual QCD (top) and SUSY-QCD (bottom) corrections to the gluon self-energy. The momentum p flows from the left to the right, and the indices a and d correspond to the colour indices of the external gluons. The vanishing tadpole diagrams are not depicted here.

Finally, the strong coupling constant is reparameterized as follows at one-loop

$$g_{s,0} = g_s + \delta g_s . \quad (5.21)$$

Applying (5.17), (5.19), Eq. (5.20) and Eq. (5.21) to the original tree-level Lagrangian (5.1) allows us to derive the counter-term Lagrangian, whose Feynman rules are summarized in Section 5.4, and Appendix F. All counter-terms, such as the one induced by the quartic squark interaction term, that are irrelevant for squark-antisquark pair production at the LHC have been omitted.

5.4 Self-energies

In this section, we are going to *i*) calculate the one-loop corrections to the propagator of the gluon, quarks, gluino and squarks *ii*) derive the counter-term associated to each propagator *iii*) determine the various renormalization constants associated to each field appearing in the diagrams of the tree-level process. All the self energies, and RCs, have been cross-checked with the help of FEYNARTS [147] and FORMCALC [217, 218] via the FVMSSM.mod model file.

Gluon self-energy

At next-to-leading order in SUSY-QCD, the gluon propagator receives contributions from gluon, ghost, and quark loops (first row of Fig. 5.2), and from gluino, and squark loops (second row of Fig. 5.2). There also exists another possible diagram, a one-point graph with a gluon running into the loop, however its contribution can be omitted, inasmuch as a massless A_0 function is identically zero. The amplitudes corresponding to the gluon and ghost diagrams are

$$\begin{aligned}
i\Pi_{ad}^{\mu\nu (g)}(p) &= \frac{1}{2} \int \frac{d^D q}{(2\pi)^D} \mu_R^{2\epsilon} g_s f_{abc} \left[(2p+q)^\sigma \eta^{\mu\rho} + (q-p)^\rho \eta^{\mu\sigma} - (2q+p)^\mu \eta^{\sigma\rho} \right] \\
&\quad \times g_s f_{acb} \left[(q-p)_\rho \delta^\nu_\sigma - (2q+p)^\nu \eta_{\rho\sigma} + (2p+q)_\sigma \delta^\nu_\rho \right] \frac{-i}{(p+q)^2} \frac{-i}{q^2} \\
&= -\frac{ig_s^2 \delta_{ad}}{32\pi^2} n_c \left[\left((6-D)p^\mu p^\nu - 5p^2 \eta^{\mu\nu} \right) B_0(p^2, 0, 0) + (3-2D) \left(p^\mu B^\nu(p^2, 0, 0) \right. \right. \\
&\quad \left. \left. + p^\nu B^\mu(p^2, 0, 0) \right) - 2\eta^{\mu\nu} p_\rho B^\rho(p^2, 0, 0) - (4D-6) B^{\mu\nu}(p^2, 0, 0) \right] , \quad (5.22) \\
i\Pi_{ad}^{\mu\nu (u_g)}(p) &= \int \frac{d^D q}{(2\pi)^D} \mu_R^{2\epsilon} (-1) \left[-g_s f_{abc}(-p^\mu - q^\mu) \right] \left[-g_s f_{dbc}(-q^\nu) \right] \frac{i}{q^2} \frac{i}{(p+q)^2} \\
&= -\frac{ig_s^2 \delta_{ad}}{32\pi^2} n_c \left[2B^{\mu\nu}(p^2, 0, 0) + 2p^\mu B^\nu(p^2, 0, 0) \right] ,
\end{aligned}$$

where n_c denotes for the number of colours, μ_R is the renormalization scale, and where the factor of $1/2$ appearing in front of the gluon amplitude is a symmetry factor needed to account for the fact that identical particles are running into the loop. In order to stay as generic as possible, the previous results are expressed in terms of $D = 4 - 2r\varepsilon$, with the r -parameter defined as

$$r = \begin{cases} 1 & \text{for HV and CDR ,} \\ 0 & \text{for DRED and FDH .} \end{cases} \quad (5.23)$$

The fermion loops, can be divided into three categories, $n_f = 5$ massless quark loops, a massive top quark loop, and a massive gluino loop. The corresponding amplitudes read

$$\begin{aligned} i\Pi_{ad}^{\mu\nu (q)}(p) &= n_f \int \frac{d^D q}{(2\pi)^D} \mu_R^{2\varepsilon} (-1) \text{Tr} \left\{ \left[ig_s T_{mn}^a \gamma^\mu \right] \frac{i\not{q}}{q^2} \left[ig_s T_{nm}^d \gamma^\nu \right] \frac{i(\not{p} + \not{q})}{(q+p)^2} \right\} \\ &= -\frac{in_f g_s^2 \delta_{ad}}{8\pi^2} \left[2B^{\mu\nu}(p^2, 0, 0) + p^\nu B^\mu(p^2, 0, 0) + p^\mu B^\nu(p^2, 0, 0) - \eta^{\mu\nu} p_\rho B^\rho(p^2, 0, 0) \right], \\ i\Pi_{ad}^{\mu\nu (t)}(p) &= \int \frac{d^D q}{(2\pi)^D} \mu_R^{2\varepsilon} (-1) \text{Tr} \left\{ \left[ig_s T_{mn}^a \gamma^\mu \right] \frac{i(\not{q} + m_t)}{q^2 - m_t^2} \left[ig_s T_{nm}^d \gamma^\nu \right] \frac{i(\not{p} + \not{q} + m_t)}{(q+p)^2 - m_t^2} \right\} \\ &= -\frac{ig_s^2 \delta_{ad}}{8\pi^2} \left[2B^{\mu\nu}(p^2, m_t^2, m_t^2) + p^\nu B^\mu(p^2, m_t^2, m_t^2) + p^\mu B^\nu(p^2, m_t^2, m_t^2) \right. \\ &\quad \left. - \eta^{\mu\nu} (p_\rho B^\rho(p^2, m_t^2, m_t^2) + A_0(m_t^2)) \right], \end{aligned} \quad (5.24)$$

$$\begin{aligned} i\Pi_{ad}^{\mu\nu (\tilde{g})}(p) &= \frac{1}{2} \int \frac{d^D q}{(2\pi)^D} \mu_R^{2\varepsilon} (-1) \text{Tr} \left\{ \left[g_s f_{abc} \gamma^\mu \right] \frac{i(\not{q} + m_{\tilde{g}})}{q^2 - m_{\tilde{g}}^2} \left[g_s f_{dcb} \gamma^\nu \right] \frac{i(\not{p} + \not{q} + m_{\tilde{g}})}{(q+p)^2 - m_{\tilde{g}}^2} \right\} \\ &= -\frac{in_c g_s^2 \delta_{ad}}{8\pi^2} \left[2B^{\mu\nu}(p^2, m_{\tilde{g}}^2, m_{\tilde{g}}^2) + p^\nu B^\mu(p^2, m_{\tilde{g}}^2, m_{\tilde{g}}^2) + p^\mu B^\nu(p^2, m_{\tilde{g}}^2, m_{\tilde{g}}^2) \right. \\ &\quad \left. - \eta^{\mu\nu} (p_\rho B^\rho(p^2, m_{\tilde{g}}^2, m_{\tilde{g}}^2) + A_0(m_{\tilde{g}}^2)) \right]. \end{aligned} \quad (5.25)$$

Note that the top and gluino contributions are similar, up to a symmetry factor (due to identical particle in the loop), and to the general color structure of the loop diagrams. The remaining contributions, *i.e.* the squark bubble and the one-point graph presented in the lower panel of Fig. 5.2, read, after summing over all squark species,

$$\begin{aligned} i\Pi_{ad}^{\mu\nu (\tilde{q},t)}(p) &= \sum_{\tilde{q}} \left\{ \int \frac{d^D q}{(2\pi)^D} \mu_R^{2\varepsilon} ig_s^2 \text{Tr} \{ T_a T_d + T_d T_a \} \eta^{\mu\nu} \frac{i}{q^2 - m_{\tilde{q}}^2} \right\} \\ &= \frac{-ig_s^2 \delta_{ad}}{16\pi^2} \eta^{\mu\nu} \sum_{\tilde{q}} A_0(m_{\tilde{q}}^2), \\ i\Pi_{ad}^{\mu\nu (\tilde{q},b)}(p) &= \sum_{\tilde{q}} \left\{ \int \frac{d^D q}{(2\pi)^D} \mu_R^{2\varepsilon} \left[ig_s (p+2q)^\mu T_{mn}^a \right] \left[ig_s (p+2q)^\nu T_{nm}^d \right] \right. \\ &\quad \left. \frac{i}{q^2 - m_{\tilde{q}}^2} \frac{i}{(q+p)^2 - m_{\tilde{q}}^2} \right\} \\ &= \frac{ig_s^2 \delta_{ad}}{32\pi^2} \sum_{\tilde{q}} \left\{ 4B^{\mu\nu}(p^2, m_{\tilde{q}}^2, m_{\tilde{q}}^2) + 2p^\mu B^\nu(p^2, m_{\tilde{q}}^2, m_{\tilde{q}}^2) + 2p^\nu B^\mu(p^2, m_{\tilde{q}}^2, m_{\tilde{q}}^2) \right. \\ &\quad \left. + p^\mu p^\nu B_0(p^2, m_{\tilde{q}}^2, m_{\tilde{q}}^2) \right\}. \end{aligned} \quad (5.26)$$

$$g_\mu^a(p) \text{ (diagram of a gluon loop with a cross) } g_\nu^d(p) = -i\delta_{ad} \delta Z_g (p^2 \eta^{\mu\nu} - p^\mu p^\nu) .$$

Figure 5.3: Feynman rule associated to the gluon kinetic counter-term. The indices μ, ν and a, d respectively correspond to Lorentz and colour indices.

As explained in Section 4.4, Lorentz covariance allows us to decompose each vector and tensor integral in (5.22), (5.24), (5.25), and (5.26) as a linear combination of scalar integrals such that,

$$\begin{aligned} B_\mu(p^2, m_1^2, m_2^2) &= p_\mu B_1(p^2, m_1^2, m_2^2) , \\ B_{\mu\nu}(p^2, m_1^2, m_2^2) &= p_\mu p_\nu B_{21}(p^2, m_1^2, m_2^2) + \eta_{\mu\nu} B_{22}(p^2, m_1^2, m_2^2) , \end{aligned} \quad (5.27)$$

where the scalar integrals B_1 and B_{21} , and B_{22} can be further reduced to A_0 and B_0 functions. Eventually, we obtain for the total unrenormalized self-energy

$$i\Pi_{ab}^{\mu\nu}(p) = i\delta_{ab} (p^2 \eta^{\mu\nu} - p^\mu p^\nu) \Pi(p) , \quad (5.28)$$

with $\Pi(p)$

$$\begin{aligned} \Pi(p) &= \frac{g_s^2}{32(3-2\varepsilon)\pi^2} \left[(10+2(r-4)\varepsilon) n_c B_0(p^2, 0, 0) + 4(\varepsilon-1) n_f B_0(p^2, 0, 0) + 8(1-\varepsilon) \frac{A_0(m_t^2)}{p^2} \right. \\ &\quad + 4\left(\varepsilon-1-2\frac{m_t^2}{p^2}\right) B_0(p^2, m_t^2, m_t^2) + 4n_c \left(\varepsilon-1-2\frac{m_g^2}{p^2}\right) B_0(p^2, m_g^2, m_g^2) \\ &\quad \left. + 8(1-\varepsilon) n_c \frac{A_0(m_g^2)}{p^2} + \sum_{\bar{q}} \left\{ 4(\varepsilon-1) \frac{A_0(m_{\bar{q}}^2)}{p^2} + \left(\frac{4m_{\bar{q}}^2}{p^2} - 1 \right) B_0(p^2, m_{\bar{q}}^2, m_{\bar{q}}^2) \right\} \right] , \end{aligned} \quad (5.29)$$

As detailed in Section 4.5, the gluon counter-term is obtained after applying the procedure of multiplicative renormalization to the bare kinetic Lagrangian

$$\mathcal{L} = -\frac{1}{4} g_0^{a,\mu\nu} g_{0,\mu\nu}^d \delta_{ad} , \quad (5.30)$$

where we recall that the bare quantities are denoted by the subscript "0". From the gluon kinetic CT Lagrangian, one can deduce the associated Feynman rule, which is given in Fig. 5.3. After factorizing out the color structure, the counter-term contribution to the gluon self-energy reads,

$$i\Pi_{ad}^{\mu\nu(x)}(p) = -i\delta_{ad} \delta Z_g (p^2 \eta^{\mu\nu} - p^\mu p^\nu) , \quad (5.31)$$

where δZ_g is the gluon WFRC. In order to determine δZ_g , we still need to fix the renormalization conditions. As mentioned in the previous chapter, renormalizing the gluon on-shell is not an optimal choice, because *i*) it amounts to subtracting UV-divergences at scales where QCD is no longer perturbative *ii*) parton distributions (including the one of the gluon) are usually provided in the $\overline{\text{MS}}$ scheme, not in the OS scheme¹. Seeing that, when convoluting the NLO partonic cross section with the PDFs in the very last step of the calculation, every single quantity needs to be expressed in the same scheme (for consistency of the final result), it is therefore tempting renormalize the gluon WFRC in the $\overline{\text{MS}}/\overline{\text{DR}}$ scheme. However, because it is a mass-independent renormalization scheme, the $\overline{\text{MS}}/\overline{\text{DR}}$ scheme explicitly violates the

¹Note however that it is still possible to use translation rules to go from one scheme to another.

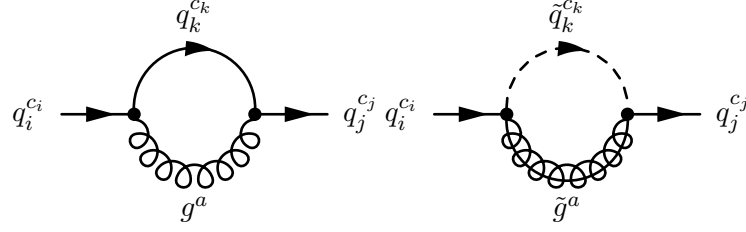


Figure 5.4: Virtual QCD (left) and SUSY-QCD (right) corrections to the quark self-energy. The momentum p flows from the left to the right, and the indices c_j and c_i correspond to the colour indices of the external quarks. The vanishing tadpole diagrams are not depicted here.

Appelquist-Carazzone decoupling theorem [219], which stipulates that heavy fields should ultimately decouple from low-energy physics. So, instead of just the $\overline{\text{MS}}/\overline{\text{DR}}$ scheme, we are going to apply the Collins-Wilczek-Zee (CWZ) prescription [220] to derive the gluon WFRG. The CWZ prescription consists in using *i*) the $\overline{\text{MS}}/\overline{\text{DR}}$ scheme for the light flavours *ii*) a zero-momentum subtraction for heavy particle graphs, and gives in practice

$$\delta Z_g = -\frac{g_s^2}{8\pi^2} \left[\frac{1}{2\bar{\epsilon}} (n_f + 1 - n_c) - \frac{1}{3} \ln \frac{m_t^2}{\mu_R^2} - \frac{n_c}{3} \ln \frac{m_{\tilde{g}}^2}{\mu_R^2} - \frac{1}{12} \sum_{\tilde{q}} \ln \frac{m_{\tilde{q}}^2}{\mu_R^2} \right], \quad (5.32)$$

and

$$\delta Z_g = \frac{1}{\bar{\epsilon}} \frac{g_s^2}{16\pi^2} (n_c - (n_f + 1)), \quad (5.33)$$

in the $\overline{\text{MS}}/\overline{\text{DR}}$ scheme, with

$$\frac{1}{\bar{\epsilon}} = \frac{1}{\epsilon} + \ln 4\pi - \gamma_E. \quad (5.34)$$

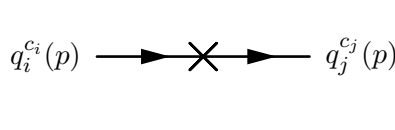
Finally, let us note that keeping only the QCD diagrams, we recover the well-known expression

$$\delta Z_g^{\text{QCD}} = \frac{1}{\bar{\epsilon}} \frac{g_s^2}{48\pi^2} (5n_c - 2n_f). \quad (5.35)$$

Quark self-energy

As illustrated in Fig. 5.4, the quark self-energy $i\Sigma$ gets contributions, at next-to-leading order in SUSY-QCD, from gluon (left) and gluino (right) loop-diagrams. The amplitudes related to the gluon and gluino bubbles read

$$\begin{aligned} i\Sigma_{c_j c_i}^{(g)}(p) &= \int \frac{d^D q}{(2\pi)^D} \mu_R^{2\bar{\epsilon}} \left[i g_s T_{c_j c_k}^a \gamma^\mu \delta_{jk} \right] \frac{i(-\not{q} + m_{q_k})}{q^2 - m_{q_k}^2} \left[i g_s T_{c_k c_i}^a \gamma_\mu \delta_{ik} \right] \frac{-i}{(q+p)^2} \\ &= \frac{i g_s^2 C_F \delta_{c_j c_i}}{16\pi^2} \delta_{ij} \left[(2-D) \gamma^\mu B_\mu(p^2, m_{q_i}^2, 0) - D B_0(p^2, m_{q_i}^2, 0) \right], \\ i\Sigma_{c_j c_i}^{(\tilde{g})}(p) &= \sum_{k=1}^6 \left\{ \int \frac{d^D q}{(2\pi)^D} \mu_R^{2\bar{\epsilon}} \left[i \sqrt{2} g_s T_{c_j c_k}^a \left((R^{\tilde{q}})_{k(j+3)}^* e^{-i\varphi_{\tilde{g}}/2} P_L - (R^{\tilde{q}})_{kj}^* e^{i\varphi_{\tilde{g}}/2} P_R \right) \right] \right. \\ &\quad \left. \frac{i(-\not{q} + m_{\tilde{g}})}{q^2 - m_{\tilde{g}}^2} \left[i \sqrt{2} g_s T_{c_k c_i}^a \left((R^{\tilde{q}})_{k(i+3)} e^{i\varphi_{\tilde{g}}/2} P_R - (R^{\tilde{q}})_{ki} e^{-i\varphi_{\tilde{g}}/2} P_L \right) \right] \frac{i}{(p+q)^2 - m_{\tilde{q}_k}^2} \right\} \\ &= \frac{i g_s^2 C_F \delta_{c_j c_i}}{8\pi^2} \sum_{k=1}^6 \left\{ -\gamma^\mu B_\mu(p^2, m_{\tilde{g}}^2, m_{\tilde{q}_k}^2) \mathcal{P}_{1,kij} - m_{\tilde{g}} B_0(p^2, m_{\tilde{g}}^2, m_{\tilde{q}_k}^2) \mathcal{P}_{2,kij} \right\}, \end{aligned} \quad (5.36)$$



$$i\delta_{c_i c_j} \left[\frac{1}{2} (\delta Z_q^L + \delta Z_q^{L\dagger}) \not{p} P_L + \frac{1}{2} (\delta Z_q^R + \delta Z_q^{R\dagger}) \not{p} P_R - \delta m_q - \frac{1}{2} (\delta Z_q^{R\dagger} m_q + m_q \delta Z_q^L) P_L - \frac{1}{2} (\delta Z_q^{L\dagger} m_q + m_q \delta Z_q^R) P_R \right]_{ji} .$$

Figure 5.5: Feynman rule for the counter-term associated to the quark propagator. The indices i , j , and c_i and c_j respectively correspond to flavour and colour indices of the external quarks.

where c_i and c_j are the external fundamental color indices, where we recall that the $SU(3)_c$ group invariant $C_F = (n_c^2 - 1)/(2n_c)$, and where the quantities $\mathcal{P}_{1,kij}$ and $\mathcal{P}_{2,kij}$ are defined as

$$\mathcal{P}_{1,kij} = (R^{\bar{q}})_{ki} (R^{\bar{q}})_{kj}^* P_L + (R^{\bar{q}})_{k(i+3)} (R^{\bar{q}})_{k(j+3)}^* P_R , \quad (5.37)$$

$$\mathcal{P}_{2,kij} = (R^{\bar{q}})_{ki} (R^{\bar{q}})_{k(j+3)}^* e^{-i\varphi_{\bar{g}}} P_L + (R^{\bar{q}})_{k(i+3)} (R^{\bar{q}})_{kj}^* e^{i\varphi_{\bar{g}}} P_R . \quad (5.38)$$

The total unrenormalized amplitude can in a general manner be rewritten as

$$i\Sigma_{ji}^{c_j c_i}(p) = i\delta_{c_j c_i} \left[\Sigma_{ji}^{V,L}(p^2) \not{p} P_L + \Sigma_{ji}^{V,R}(p^2) \not{p} P_R + \Sigma_{ji}^{S,L}(p^2) P_L + \Sigma_{ji}^{S,R}(p^2) P_R \right] , \quad (5.39)$$

where $\Sigma^{V,L/R}$ is its left-handed (resp. right-handed) vector component, and $\Sigma^{S,L}$ is its left-handed (resp. right-handed) scalar component. The vector integrals appearing in (5.36) can be reduced to a basis of scalar integrals by means of (5.27). The various components of the unrenormalized amplitude hence read as follows

$$\begin{aligned} \Sigma_{ji}^{V,L}(p) &= -\frac{g_s^2 C_F}{8\pi^2} \left[(1-r\varepsilon) B_1(p^2, m_{q_i}^2, 0) \delta_{ij} + \sum_{k=1}^6 (R^{\bar{q}})_{kj}^* (R^{\bar{q}})_{ki} B_1(p^2, m_{\bar{g}}^2, m_{\bar{q}_k}^2) \right] , \\ \Sigma_{ji}^{V,R}(p) &= -\frac{g_s^2 C_F}{8\pi^2} \left[(1-r\varepsilon) B_1(p^2, m_{q_i}^2, 0) \delta_{ij} + \sum_{k=1}^6 (R^{\bar{q}})_{k(j+3)}^* (R^{\bar{q}})_{k(i+3)} B_1(p^2, m_{\bar{g}}^2, m_{\bar{q}_k}^2) \right] , \\ \Sigma_{ji}^{S,L}(p) &= -\frac{g_s^2 C_F}{8\pi^2} \left[(2-r\varepsilon) m_{q_i} B_0(p^2, m_{q_i}^2, 0) \delta_{ij} + m_{\bar{g}} \sum_{k=1}^6 \left\{ (R^{\bar{q}})_{ki} (R^{\bar{q}})_{k(j+3)}^* e^{-i\varphi_{\bar{g}}} B_0(p^2, m_{\bar{g}}^2, m_{\bar{q}_k}^2) \right\} \right] , \\ \Sigma_{ji}^{S,R}(p) &= -\frac{g_s^2 C_F}{8\pi^2} \left[(2-r\varepsilon) m_{q_i} B_0(p^2, m_{q_i}^2, 0) \delta_{ij} + m_{\bar{g}} \sum_{k=1}^6 \left\{ (R^{\bar{q}})_{k(i+3)} (R^{\bar{q}})_{kj}^* e^{i\varphi_{\bar{g}}} B_0(p^2, m_{\bar{g}}^2, m_{\bar{q}_k}^2) \right\} \right] . \end{aligned} \quad (5.40)$$

The free massive quark counter-term is obtained, as explained in Section 4.5, after applying the procedure of multiplicative renormalization to the bare Lagrangian

$$\mathcal{L} = (\bar{q}_{j,0} i \not{D} q_{i,0} - m_{q_i,0} \bar{q}_{j,0} q_{i,0}) \delta_{ij} \quad (5.41)$$

where we recall that the subscript "0" denotes bare quantities. From the corresponding CT Lagrangian, it is possible to deduce the Feynman rule given in Fig. 5.5. Since only light quarks can contribute to the quark-antiquark channel at the LHC, the quark WFRCs can be expressed directly in the $\overline{\text{MS}}/\overline{\text{DR}}$ scheme. Using unitarity of the mixing matrices $R^{\bar{q}}$, and retaining only the UV-divergent part, we obtain

$$(\delta Z_q^{L/R})_{ij} = -\frac{g_s^2 C_F}{8\pi^2 \bar{\varepsilon}} \delta_{ij} . \quad (5.42)$$

Similarly, we obtain for the light quark mass corrections

$$\delta m_{q_i} = -\frac{g_s^2 C_F}{8\pi^2 \bar{\varepsilon}} m_{q_i} . \quad (5.43)$$

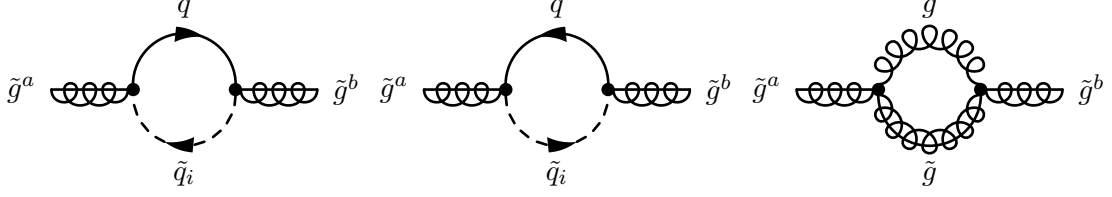


Figure 5.6: Virtual one-loop contributions to the gluino self-energy. The momentum p flows from the left to the right, and the indices a and d correspond to the colour indices of the external gluinos. The vanishing tadpole diagrams are not depicted here.

Gluino self-energy

At the one-level, the gluino propagator receives contributions from two quark/squark loop diagrams and one gluon/gluino loop diagram, as shown in Fig. 5.6,

$$\begin{aligned}
i\Sigma_{ba}^{(\tilde{g})}(p) &= \int \frac{d^D q}{(2\pi)^D} \mu_R^{2\epsilon} \left[g_s f^{cbd} \gamma^\mu \right] \frac{i(-\not{q} + m_{\tilde{g}})}{q^2 - m_{\tilde{g}}^2} \left[g_s f^{cda} \gamma_\mu \right] \frac{-i}{(q+p)^2} \\
&= \frac{ig_s^2 n_c}{16\pi^2} \delta_{ab} \left[(2-D) \gamma^\mu B_\mu(p^2, m_{\tilde{g}}^2, 0) - DB_0(p^2, m_{\tilde{g}}^2, 0) \right], \\
i\Sigma_{ba}^{(\tilde{q})}(p) &= \int \frac{d^D q}{(2\pi)^D} \mu_R^{2\epsilon} \sum_{q_i, \tilde{q}_j} \left\{ \left[i\sqrt{2} g_s T_{c_j c_i}^b \left((R^{\tilde{q}})_{j(i+3)} e^{i\varphi_{\tilde{g}}/2} P_R - (R^{\tilde{q}})_{j_i} e^{-i\varphi_{\tilde{g}}/2} P_L \right) \right] \right. \\
&\quad \frac{i(-\not{q} + m_{q_i})}{q^2 - m_{q_i}^2} \left[i\sqrt{2} g_s T_{c_i c_j}^a \left((R^{\tilde{q}})_{j(i+3)}^* e^{-i\varphi_{\tilde{g}}/2} P_L - (R^{\tilde{q}})_{j_i}^* e^{i\varphi_{\tilde{g}}/2} P_R \right) \right] \frac{i}{(p+q)^2 - m_{\tilde{q}_j}^2} \\
&\quad + \left[i\sqrt{2} g_s T_{c_i c_j}^b \left((R^{\tilde{q}})_{j(i+3)}^* e^{-i\varphi_{\tilde{g}}/2} P_L - (R^{\tilde{q}})_{j_i}^* e^{i\varphi_{\tilde{g}}/2} P_R \right) \right] \frac{i(-\not{q} + m_{q_i})}{q^2 - m_{q_i}^2} \\
&\quad \left. \left[i\sqrt{2} g_s T_{c_j c_i}^a \left((R^{\tilde{q}})_{j(i+3)} e^{i\varphi_{\tilde{g}}/2} P_R - (R^{\tilde{q}})_{j_i} e^{-i\varphi_{\tilde{g}}/2} P_L \right) \right] \frac{i}{(p+q)^2 - m_{\tilde{q}_j}^2} \right\}, \\
&= \frac{ig_s^2 \delta_{ab}}{16\pi^2} \sum_{q_i, \tilde{q}_j} \left\{ -\gamma^\mu B_\mu(p^2, m_{q_i}^2, m_{\tilde{q}_j}^2) \mathcal{C}_{ji} - 2m_{q_i} B_0(p^2, m_{q_i}^2, m_{\tilde{q}_j}^2) \left[\mathcal{S}_{ji} P_L + \mathcal{S}_{ji}^* P_R \right] \right\},
\end{aligned} \tag{5.44}$$

where a and b are the color indices associated to the external gluinos, and where the coefficients \mathcal{C}_{ji} , and \mathcal{S}_{ji} are defined such that


$$\mathcal{C}_{ji} = |(R^{\tilde{q}})_{ji}|^2 + |(R^{\tilde{q}})_{j(i+3)}|^2, \quad \mathcal{S}_{ji} = (R^{\tilde{q}})_{ji} (R^{\tilde{q}})_{j(i+3)}^* e^{-i\varphi_{\tilde{g}}}, \tag{5.45}$$

The total unrenormalized amplitude can in a general manner be rewritten as

$$i\Sigma^{ab}(p) = i\delta_{ab} \left[\Sigma^{V,L}(p^2) \not{p} P_L + \Sigma^{V,R}(p^2) \not{p} P_R + \Sigma^{S,L}(p^2) P_L + \Sigma^{S,R}(p^2) P_R \right], \tag{5.46}$$

The vector integrals B_μ in (5.44) can be reduced to a basis of scalar integrals by means of (5.27), such that the various components of the unrenormalized amplitude read as follows

$$\begin{aligned}
\Sigma^{V,L}(p) &= -\frac{g_s^2}{16\pi^2} \left[2(1-r\epsilon) n_c B_1(p^2, m_{\tilde{g}}^2, 0) + \sum_{q_i, \tilde{q}_j} \left\{ \mathcal{C}_{ji} B_1(p^2, m_{q_i}^2, m_{\tilde{q}_j}^2) \right\} \right], \\
\Sigma_{ji}^{V,R}(p) &= -\frac{g_s^2}{16\pi^2} \left[2(1-r\epsilon) n_c B_1(p^2, m_{\tilde{g}}^2, 0) + \sum_{q_i, \tilde{q}_j} \left\{ \mathcal{C}_{ji} B_1(p^2, m_{q_i}^2, m_{\tilde{q}_j}^2) \right\} \right], \\
\Sigma_{ji}^{S,L}(p) &= -\frac{g_s^2}{16\pi^2} \left[2(2-r\epsilon) n_c m_{\tilde{g}} B_0(p^2, m_{\tilde{g}}^2, 0) + 2 \sum_{q_i, \tilde{q}_j} \left\{ m_{q_i} \mathcal{S}_{ji} B_0(p^2, m_{q_i}^2, m_{\tilde{q}_j}^2) \right\} \right], \\
\Sigma_{ji}^{S,R}(p) &= -\frac{g_s^2}{16\pi^2} \left[2(2-r\epsilon) n_c m_{\tilde{g}} B_0(p^2, m_{\tilde{g}}^2, 0) + 2 \sum_{q_i, \tilde{q}_j} \left\{ m_{q_i} \mathcal{S}_{ji}^* B_0(p^2, m_{q_i}^2, m_{\tilde{q}_j}^2) \right\} \right].
\end{aligned} \tag{5.47}$$



$$i\delta_{ab} \left[\Re\{\delta Z_{\tilde{g}}^L\} \not{p} P_L + \Re\{\delta Z_{\tilde{g}}^R\} \not{p} P_R - \delta m_{\tilde{g}} - \frac{m_{\tilde{g}}}{2} (\delta Z_{\tilde{g}}^{*R} + \delta Z_{\tilde{g}}^L) P_L - \frac{m_{\tilde{g}}}{2} (\delta Z_{\tilde{g}}^{*L} + \delta Z_{\tilde{g}}^R) P_R \right].$$

Figure 5.7: Feynman rule for the counter-term associated to the gluino propagator. The indices a and b correspond to the colour indices of the external gluinos.

The free massive gluino counter-term is obtained, as explained in Section 4.5, after applying the procedure of multiplicative renormalization to the bare Lagrangian

$$\mathcal{L} = \left(\frac{i}{2} \bar{\tilde{g}}_0^b \not{p} \tilde{g}_0^a - \frac{1}{2} m_{\tilde{g}} \bar{\tilde{g}}^b \tilde{g}^a \right) \delta_{ab}, \quad (5.48)$$

where we recall that the subscript "0" denotes bare quantities. From the corresponding CT Lagrangian, it is possible to deduce the Feynman rule given in Fig. 5.7. The diagonal WFRCs of the gluino can be written in the OS scheme as

$$\begin{aligned} (\delta Z_{\tilde{g}}^{L/R})_{ij} &= \frac{g_s^2}{16\pi^2} \left[2(1-r\varepsilon) n_c B_1(m_{\tilde{g}}^2, m_{\tilde{g}}^2, 0) + \sum_{q_i, \tilde{q}_j} \left\{ \mathcal{C}_{ji} B_1(m_{\tilde{g}}^2, m_{q_i}^2, m_{\tilde{q}_j}^2) \right\} \right. \\ &\quad + 2m_{\tilde{g}}^2 \left[2n_c(1-r\varepsilon) B_1'(m_{\tilde{g}}^2, m_{\tilde{g}}^2, 0) + 2n_c(2-r\varepsilon) B_0'(m_{\tilde{g}}^2, m_{\tilde{g}}^2, 0) \right. \\ &\quad \left. \left. + \sum_{q_f, \tilde{q}_i} \left\{ \mathcal{C}_{ji} B_1'(m_{\tilde{g}}^2, m_{q_i}^2, m_{\tilde{q}_j}^2) + 2 \frac{m_{q_i}}{m_{\tilde{g}}} \Re(\mathcal{S}_{ji}) B_0'(m_{\tilde{g}}^2, m_{q_i}^2, m_{\tilde{q}_j}^2) \right\} \right] \right]. \end{aligned} \quad (5.49)$$

The WFRCs can alternatively be expressed in the $\overline{\text{MS}}/\overline{\text{DR}}$ scheme by retaining only the UV-divergent part of the B_0 , and B_1 functions. In this case, the WFRCs take the following form

$$\delta Z_{\tilde{g}}^{L/R} = -\frac{g_s^2}{16\pi^2 \varepsilon} (n_c + n_f + 1). \quad (5.50)$$

The gluino mass is renormalized on-shell so that it corresponds to the gluino physical mass,

$$\begin{aligned} \delta m_{\tilde{g}} &= -\frac{g_s^2 m_{\tilde{g}}}{16\pi^2} \left[2n_c \left[(1-r\varepsilon) B_1(m_{\tilde{g}}^2, m_{\tilde{g}}^2, 0) + (2-r\varepsilon) B_0(m_{\tilde{g}}^2, m_{\tilde{g}}^2, 0) \right] \right. \\ &\quad \left. + \sum_{q_f, \tilde{q}_i} \left\{ \mathcal{C}_{ji} B_1(m_{\tilde{g}}^2, m_{q_i}^2, m_{\tilde{q}_j}^2) + 2 \frac{m_{q_i}}{m_{\tilde{g}}} \widetilde{\text{Re}}(\mathcal{S}_{ji}) B_0(m_{\tilde{g}}^2, m_{q_i}^2, m_{\tilde{q}_j}^2) \right\} \right]. \end{aligned} \quad (5.51)$$

Squark self-energy

The one-loop contributions to the squark self-energy in SUSY-QCD, noted $i\Pi^{ij}$ where the indices i and j specify the outgoing and incoming squark mass-eigenstates, consist in the three diagrams depicted in Fig. 5.8. The corresponding amplitudes read, using the Feynman rules of Appendix F,

$$\begin{aligned} i\Pi_{c_i c_j}^{(g)}(p) &= \int \frac{d^D q}{(2\pi)^D} \mu_R^{2\varepsilon} \left[ig_s T_{c_i c_k}^a (p_\mu - q_\mu) \right] \frac{i}{q^2 - m_{\tilde{q}_i}^2} \frac{-i}{(q+p)^2} \left[ig_s T_{c_k c_j}^a (p^\mu - q^\mu) \right] \delta_{ij} \\ &= \frac{ig_s^2 C_F \delta_{c_i c_j}}{16\pi^2} \delta_{ij} \left[4p^\mu B_\mu(p^2, m_{\tilde{q}_i}^2, 0) - A_0(m_{\tilde{q}_i}^2) \right], \end{aligned} \quad (5.52)$$

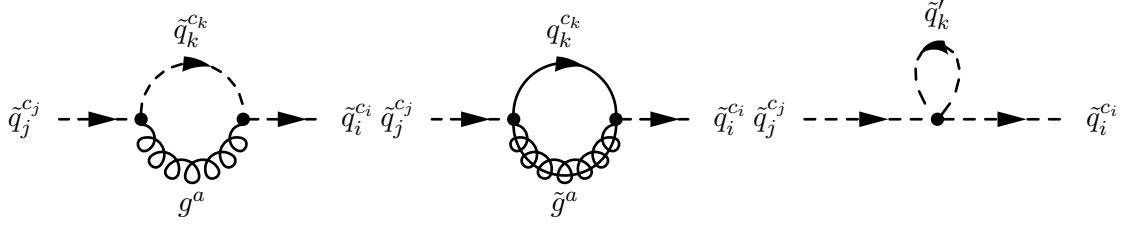


Figure 5.8: Virtual one-loop contributions to the squark self-energy. The momentum p flows from the left to the right, and the indices c_j , c_i and i , j respectively correspond to colour and flavour indices of the external squarks. The vanishing tadpole diagrams are not depicted here.

$$\begin{aligned}
i\Pi_{c_i c_j}^{(q)}(p) &= - \int \frac{d^D q}{(2\pi)^D} \mu_R^{2\epsilon} \sum_{l=1}^3 \text{Tr} \left\{ \left[i\sqrt{2}g_s T_{c_i c_l}^a \left((R^{\tilde{q}})_{i(l+3)} e^{i\varphi_{\tilde{g}}/2} P_R - (R^{\tilde{q}})_{il} e^{-i\varphi_{\tilde{g}}/2} P_L \right) \right] \right. \\
&\quad \left. \frac{i(-\not{q} + m_{q_l})}{q^2 - m_{q_l}^2} \left[i\sqrt{2}g_s T_{c_l c_j}^a \left((R^{\tilde{q}})_{j(l+3)}^* e^{-i\varphi_{\tilde{g}}/2} P_L - (R^{\tilde{q}})_{jl}^* e^{i\varphi_{\tilde{g}}/2} P_R \right) \right] \frac{i(-\not{q} - \not{p} + m_{\tilde{g}})}{(q+p)^2 - m_{\tilde{g}}^2} \right\} \\
&= \frac{ig_s^2 C_F \delta_{c_i c_j}}{16\pi^2} \sum_{l=1}^3 \left\{ 4m_{\tilde{g}} m_{q_l} \mathcal{S}_{2,ijl} B_0(p^2, m_{q_l}^2, m_{\tilde{g}}^2) - 4\mathcal{S}_{1,ijl} \left[A_0(m_{\tilde{g}}^2) \right. \right. \\
&\quad \left. \left. + m_{q_l}^2 B_0(p^2, m_{q_l}^2, m_{\tilde{g}}^2) + p^\mu B_\mu(p^2, m_{q_l}^2, m_{\tilde{g}}^2) \right] \right\}, \tag{5.53}
\end{aligned}$$

$$\begin{aligned}
i\Pi_{c_i c_j}^{(\tilde{q})}(p) &= \int \frac{d^D q}{(2\pi)^D} \mu_R^{2\epsilon} \sum_{k=1}^6 \left\{ \frac{i}{q^2 - m_{\tilde{q}_k}^2} \times (-ig_s^2) \left[R(\tilde{q}_k^{c_k}, \tilde{q}_k^{c_k}) R(\tilde{q}_j^{c_j}, \tilde{q}_i^{c_i}) + R(\tilde{q}_k^{c_k}, \tilde{q}_i^{c_i}) R(\tilde{q}_j^{c_j}, \tilde{q}_k^{c_k}) \right] \right\}, \\
&= \frac{ig_s^2 C_F \delta_{c_i c_j}}{16\pi^2} \sum_{k=1}^6 \sum_{l=1}^3 \left\{ \left[(R^{\tilde{q}})_{kl}^* (R^{\tilde{q}})_{il} - (R^{\tilde{q}})_{k(l+3)}^* (R^{\tilde{q}})_{i(l+3)} \right] \right. \\
&\quad \left. \left[(R^{\tilde{q}})_{jl}^* (R^{\tilde{q}})_{kl} - (R^{\tilde{q}})_{j(l+3)}^* (R^{\tilde{q}})_{k(l+3)} \right] A_0(m_{\tilde{q}_k}^2) \right\},
\end{aligned}$$

where c_i and c_j are the color indices associated to the external squarks, where the coefficients $R(\tilde{q}_a^{c_a}, \tilde{q}_b^{c_b})$ are given in Appendix F, and where for simplicity we have defined

$$\mathcal{S}_{1,ijl} = (R^{\tilde{q}})_{il} (R^{\tilde{q}})_{jl}^* + (R^{\tilde{q}})_{i(l+3)} (R^{\tilde{q}})_{j(l+3)}^*, \tag{5.54}$$

$$\mathcal{S}_{2,ijl} = (R^{\tilde{q}})_{il} (R^{\tilde{q}})_{j(l+3)}^* e^{-i\varphi_{\tilde{g}}} + (R^{\tilde{q}})_{i(l+3)} (R^{\tilde{q}})_{jl}^* e^{i\varphi_{\tilde{g}}}. \tag{5.55}$$

The B_μ integrals of (5.53) can be reduced to a basis of scalar integrals by means of (5.27). After factorizing out the colour structure, the total unrenormalized self-energy reads

$$\begin{aligned}
\Pi_{ij}(p^2) &= \frac{g_s^2 C_F}{16\pi^2} \left[\left\{ A_0(m_{\tilde{q}_i}^2) - 2(p^2 + m_{\tilde{q}_i}^2) B_0(p^2, m_{\tilde{q}_i}^2, 0) \right\} \delta_{ij} + \sum_{k=1}^6 \sum_{l=1}^3 \left\{ \left[(R^{\tilde{q}})_{kl}^* (R^{\tilde{q}})_{il} \right. \right. \right. \\
&\quad \left. \left. - (R^{\tilde{q}})_{k(l+3)}^* (R^{\tilde{q}})_{i(l+3)} \right] \left[(R^{\tilde{q}})_{jl}^* (R^{\tilde{q}})_{kl} - (R^{\tilde{q}})_{j(l+3)}^* (R^{\tilde{q}})_{k(l+3)} \right] A_0(m_{\tilde{q}_k}^2) \right\} \\
&\quad + 2 \sum_{l=1}^3 \left\{ \mathcal{S}_{1,ijl} \left[(p^2 - m_{q_l}^2 - m_{\tilde{g}}^2) B_0(p^2, m_{q_l}^2, m_{\tilde{g}}^2) - A_0(m_{\tilde{g}}^2) - A_0(m_{q_l}^2) \right] \right. \\
&\quad \left. + 2m_{\tilde{g}} m_{q_l} \mathcal{S}_{2,ijl} B_0(p^2, m_{q_l}^2, m_{\tilde{g}}^2) \right\}. \tag{5.56}
\end{aligned}$$

The free massive squark counter-term is obtained, as explained in Section 4.5, after applying the procedure of multiplicative renormalization to the bare Lagrangian

$$\mathcal{L} = \left(\partial_\mu \tilde{q}_{i,0}^\dagger \partial^\mu \tilde{q}_{j,0} - m_{\tilde{q}_{i,0}}^2 \tilde{q}_{i,0}^\dagger \tilde{q}_{j,0} \right) \delta_{ij}, \tag{5.57}$$

$$\tilde{q}_j^{c_j}(p) \text{ --- } \text{---} \text{---} \tilde{q}_i^{c_i}(p) \quad i\delta_{c_i c_j} \left[\frac{1}{2} (\delta Z_{\tilde{q}} + \delta Z_{\tilde{q}}^\dagger) p^2 - \frac{1}{2} (m_{\tilde{q}}^2 \delta Z_{\tilde{q}} + \delta Z_{\tilde{q}}^\dagger m_{\tilde{q}}^2) - \delta m_{\tilde{q}}^2 \right]_{ij} .$$

Figure 5.9: Feynman rule for the counter-term associated to the gluino propagator. The indices i , j , and ci and cj respectively correspond to flavour and colour indices of the external squarks.

where we recall that the subscript $_0$ denotes bare quantities. From the corresponding CT Lagrangian, it is possible to deduce the Feynman rule given in Fig. 5.9. In the OS scheme, the squark mass renormalization constants $\delta m_{\tilde{q}_i}^2$ takes the following form

$$\begin{aligned} \delta m_{\tilde{q}_i}^2 = & \frac{g_s^2 C_F}{16\pi^2} \left[\left\{ A_0(m_{\tilde{q}_i}^2) - 4m_{\tilde{q}_i}^2 B_0(m_{\tilde{q}_i}^2, m_{\tilde{q}_i}^2, 0) \right\} + \sum_{k=1}^6 \sum_{l=1}^3 \left\{ \widetilde{\text{Re}} \left[(R^{\tilde{q}})_{kl}^* (R^{\tilde{q}})_{il} \right. \right. \right. \\ & \left. \left. \left. - (R^{\tilde{q}})_{k(l+3)}^* (R^{\tilde{q}})_{i(l+3)} \right] \left[(R^{\tilde{q}})_{il}^* (R^{\tilde{q}})_{kl} - (R^{\tilde{q}})_{i(l+3)}^* (R^{\tilde{q}})_{k(l+3)} \right] \right\} A_0(m_{\tilde{q}_k}^2) \right\} \\ & + 2 \sum_{l=1}^3 \left\{ \widetilde{\text{Re}}(\mathcal{S}_{1,iil}) \left[(m_{\tilde{q}_i}^2 - m_{\tilde{q}_l}^2 - m_{\tilde{g}}^2) B_0(m_{\tilde{q}_i}^2, m_{\tilde{q}_l}^2, m_{\tilde{g}}^2) - A_0(m_{\tilde{g}}^2) - A_0(m_{\tilde{q}_l}^2) \right] \right. \\ & \left. + 2m_{\tilde{g}} m_{\tilde{q}_l} \widetilde{\text{Re}}(\mathcal{S}_{2,iil}) B_0(m_{\tilde{q}_i}^2, m_{\tilde{q}_l}^2, m_{\tilde{g}}^2) \right\} . \end{aligned} \quad (5.58)$$

Similarly, the diagonal squark WFRCS can be written, in the OS scheme, as

$$\begin{aligned} (\delta Z_{\tilde{q}})_{ii} = & -\frac{g_s^2 C_F}{16\pi^2} \left[-4m_{\tilde{q}_i}^2 B'_0(m_{\tilde{q}_i}^2, m_{\tilde{q}_i}^2, 0) - 2B_0(m_{\tilde{q}_i}^2, m_{\tilde{q}_i}^2, 0) + 2 \sum_{l=1}^3 \left\{ \widetilde{\text{Re}}(\mathcal{S}_{1,iil}) \left[\right. \right. \right. \\ & \left. \left. \left. (m_{\tilde{q}_i}^2 - m_{\tilde{q}_l}^2 - m_{\tilde{g}}^2) B'_0(m_{\tilde{q}_i}^2, m_{\tilde{q}_l}^2, m_{\tilde{g}}^2) + B_0(m_{\tilde{q}_i}^2, m_{\tilde{q}_l}^2, m_{\tilde{g}}^2) \right] \right. \right. \\ & \left. \left. \left. + 2m_{\tilde{g}} m_{\tilde{q}_l} \widetilde{\text{Re}}(\mathcal{S}_{2,iil}) B'_0(m_{\tilde{q}_i}^2, m_{\tilde{q}_l}^2, m_{\tilde{g}}^2) \right\} , \end{aligned} \quad (5.59)$$

and, in the $\overline{\text{MS}}/\overline{\text{DR}}$ scheme, as

$$(\delta Z_{\tilde{q}})_{ii} = 0 . \quad (5.60)$$

The off-diagonal squark WFRCS, out of which we construct the $(\delta R^{\tilde{q}})_{ij}$, are given by

$$\begin{aligned} (\delta Z_{\tilde{q}})_{ij} = & \frac{g_s^2 C_F}{8\pi^2} \frac{1}{m_{\tilde{q}_i}^2 - m_{\tilde{q}_j}^2} \left[\sum_{k=1}^6 \sum_{l=1}^3 \left\{ \left[(R^{\tilde{q}})_{kl}^* (R^{\tilde{q}})_{il} - (R^{\tilde{q}})_{k(l+3)}^* (R^{\tilde{q}})_{i(l+3)} \right] \right. \right. \\ & \left. \left. \left[(R^{\tilde{q}})_{jl}^* (R^{\tilde{q}})_{kl} - (R^{\tilde{q}})_{j(l+3)}^* (R^{\tilde{q}})_{k(l+3)} \right] A_0(m_{\tilde{q}_k}^2) \right\} + 2 \sum_{l=1}^3 \left\{ \mathcal{S}_{1,ijl} \left[(m_{\tilde{q}_i}^2 - m_{\tilde{q}_l}^2 - m_{\tilde{g}}^2) \right. \right. \right. \\ & \left. \left. \left. B_0(m_{\tilde{q}_j}^2, m_{\tilde{q}_l}^2, m_{\tilde{g}}^2) - A_0(m_{\tilde{g}}^2) - A_0(m_{\tilde{q}_l}^2) \right] + 2m_{\tilde{g}} m_{\tilde{q}_l} \mathcal{S}_{2,ijl} B_0(m_{\tilde{q}_i}^2, m_{\tilde{q}_l}^2, m_{\tilde{g}}^2) \right\} . \end{aligned} \quad (5.61)$$

5.5 Vertex corrections

In this section, our goals are *i*) to calculate the one-loop corrections to each vertex appearing in the Feynman diagrams of the leading-order process (see Section 5.2) *ii*) to derive the form of the counter-term associated to each vertex *iii*) to determine the renormalization constant δg_s by imposing that the sum of the vertex corrections and the counter-term is UV-finite (for each vertex). Note that the last point require the RCs of Section 5.4 as a necessary input.

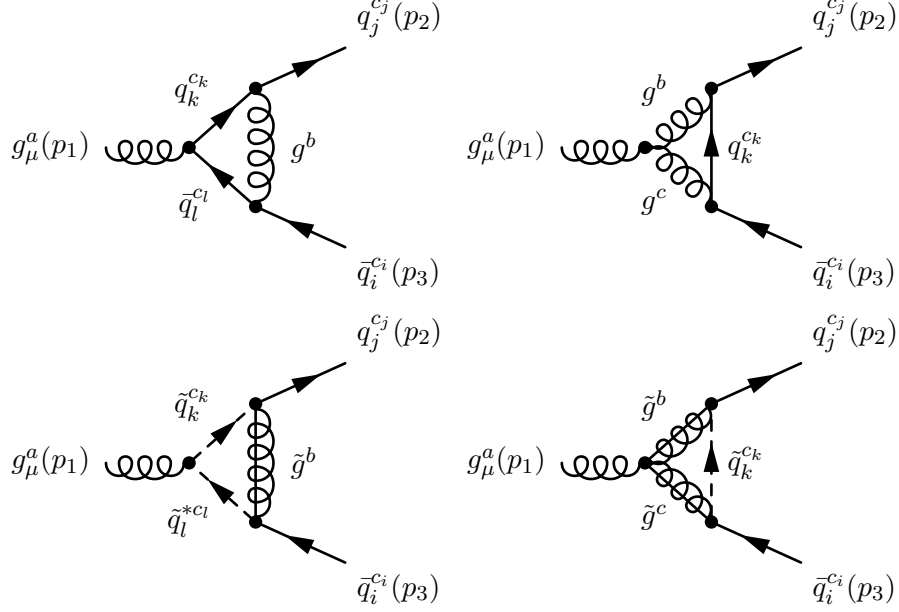


Figure 5.10: One-loop contributions to the gluon-quark-antiquark vertex, where μ denotes the Lorentz index of the external gluon, and a, b, c, c_i, c_j, c_k , and c_l correspond to colour indices. The four-momenta of the gluon (p_1) and the fermions (p_2, p_3) are taken incoming to the loop.

The gluon-quark-antiquark vertex

The gluon-quark-antiquark interactions are derived from the Lagrangian

$$\mathcal{L}_{gqq} = g_{s,0} \bar{q}_{0,j}^{c_j} \gamma^\mu T_{c_j c_i}^a g_{0,\mu}^a q_{0,i}^{c_i}. \quad (5.62)$$

At the one-loop level in supersymmetric QCD, the corresponding vertex, $V_{gqq}^{(0)}$ receives corrections from the four diagrams depicted in Fig. 5.10. For future convenience, we introduce the notation $V_{gqq}^{(xyz)}$ to label the various amplitudes contributing to the corrections of the gluon-quark-antiquark vertex. The letters x, y and z here correspond to the particles entering in the loops. With the help of the Feynman rules of Appendix F, the pure QCD corrections, with only quarks and gluons running into the loops, are given by

$$\begin{aligned} V_{gqq}^{(qqg)} &= \int \frac{d^D q}{(2\pi)^D} \mu_R^{2\epsilon} \left[i g_s T_{c_j c_i}^b \delta_{jl} \gamma^\nu \right] i \frac{\not{q} - \not{p}_2}{(q + p_2)^2} \left[i g_s T_{c_i c_k}^a \delta_{lk} \gamma^\mu \right] i \frac{-\not{q} - \not{p}_1 - \not{p}_2}{(q + p_1 + p_2)^2} \left[i g_s T_{c_k c_i}^b \delta_{ki} \gamma_\nu \right] \frac{-i}{q^2} \\ &= -\frac{i \delta_{ij} g_s^3}{32 n_c \pi^2} T_{c_j c_i}^a \delta_{ij} \left[\left((4 - D) \not{p}_2 \gamma^\mu \not{p}_1 - 2 \not{p}_1 \gamma^\mu \not{p}_2 + (2 - D) \not{p}_2 \gamma^\mu \not{p}_2 \right) C_0 + \left((2 - D) \not{p}_2 \right. \right. \\ &\quad \left. \left. - 2 \not{p}_1 \right) \gamma^\mu \gamma^\beta C_\beta + \gamma^\alpha \gamma^\mu \left((4 - D) \not{p}_1 + (2 - D) \not{p}_2 \right) C_\alpha + (2 - D) \gamma^\alpha \gamma^\mu \gamma^\beta C_{\alpha\beta} \right], \end{aligned}$$

and

$$\begin{aligned} V_{gqq}^{(ggq)} &= \int \frac{d^D q}{(2\pi)^D} \mu_R^{2\epsilon} \left[i g_s \gamma^\nu T_{c_j c_i}^b \delta_{jl} \right] i \frac{\not{q}}{q^2} \left[i g_s \gamma^\rho T_{c_i c_l}^c \delta_{li} \right] \frac{-i}{(q + p_2)^2} \frac{-i}{(q + p_1 + p_2)^2} \times g_s f_{abc} \\ &\quad \times \left[(p_1 - p_2 - q)_\rho \delta^\mu_\nu - (q + 2p_1 + p_2)_\nu \delta^\mu_\rho + (2q + 2p_2 + p_1)^\mu \eta_{\nu\rho} \right] \\ &= \frac{i \delta_{ij} n_c g_s^3}{32 \pi^2} T_{c_j c_i}^a \left[2B_0(p_1^2, 0, 0) \gamma^\mu - \left(\gamma^\mu \gamma^\alpha (\not{p}_1 - \not{p}_2) - (2\not{p}_1 + \not{p}_2) \gamma^\alpha \gamma^\mu \right. \right. \\ &\quad \left. \left. + (2 - D)(2p_2 + p_1)^\mu \gamma^\alpha \right) C_\alpha + (2D - 4) \gamma^\alpha C^\mu_\alpha \right]. \end{aligned}$$

Note that for clarity, we have omitted the arguments of all the three-point functions appearing in the previous expressions. Those arguments can however be recovered by performing the following substitutions

$$\begin{aligned} V_{gq\bar{q}}^{(gq\bar{q})} : C_{\{0,\mu,\mu\nu\}} &\leftrightarrow C_{\{0,\mu,\mu\nu\}}(p_2^2, p_1^2, 0, 0, 0) , \\ V_{gq\bar{q}}^{(gq\bar{q})} : C_{\{0,\mu,\mu\nu\}} &\leftrightarrow C_{\{0,\mu,\mu\nu\}}(p_2^2, p_1^2, 0, 0, 0) . \end{aligned} \quad (5.63)$$

The supersymmetric contributions, with squarks and gluinos running into the loops, can be obtained in a similar manner, and take the following form

$$\begin{aligned} V_{gq\bar{q}}^{(\bar{q}\bar{q}\bar{g})} &= \int \frac{d^D q}{(2\pi)^D} \mu_R^{2\varepsilon} \sum_{k=1}^6 \left\{ \left[i\sqrt{2}g_s T_{c_j c_k}^b \left((R^{\bar{q}})_{k(j+3)}^* e^{-i\varphi_{\bar{g}}/2} P_L - (R^{\bar{q}})_{kj}^* e^{i\varphi_{\bar{g}}/2} P_R \right) \right] \times i \frac{\not{q} + m_{\bar{g}}}{q^2 - m_{\bar{g}}^2} \times \right. \\ &\quad \left[i\sqrt{2}g_s T_{c_i c_l}^b \left((R^{\bar{q}})_{k(i+3)} e^{i\varphi_{\bar{g}}/2} P_R - (R^{\bar{q}})_{ki} e^{-i\varphi_{\bar{g}}/2} P_L \right) \right] \times \frac{i}{(q+p_2)^2 - m_{\bar{q}_k}^2} \times \\ &\quad \left. \frac{i}{(q+p_2+p_1)^2 - m_{\bar{q}_k}^2} \times \left[-ig_s T_{c_k c_l}^a (2p_2 + p_1 + 2q)^\mu \right] \right\} \\ &= -\frac{ig_s^3}{16n_c \pi^2} T_{c_j c_i}^a \sum_{k=1}^6 \left\{ \gamma^\alpha \mathcal{P}_{1,kij} \left[2C_\alpha^\mu + (2p_2 + p_1)^\mu C_\alpha \right] - m_{\bar{g}} \mathcal{P}_{2,kij} \left[2C^\mu + (2p_2 + p_1)^\mu C_0 \right] \right\} , \\ V_{gq\bar{q}}^{(\bar{g}\bar{g}\bar{q})} &= \int \frac{d^D q}{(2\pi)^D} \mu_R^{2\varepsilon} \sum_{k=1}^6 \left\{ \left[i\sqrt{2}g_s T_{c_j c_k}^b \left((R^{\bar{q}})_{k(j+3)}^* e^{-i\varphi_{\bar{g}}/2} P_L - (R^{\bar{q}})_{kj}^* e^{i\varphi_{\bar{g}}/2} P_R \right) \right] \times \frac{i}{q^2 - m_{\bar{q}_i}^2} \times \right. \\ &\quad i \frac{-\not{q} - \not{p}_2 + m_{\bar{g}}}{(q+p_2)^2 - m_{\bar{g}}^2} \times [g_s f_{abc} \gamma^\mu] \times i \frac{-\not{q} - \not{p}_1 - \not{p}_2 + m_{\bar{g}}}{(q+p_1+p_2)^2 - m_{\bar{g}}^2} \times \left[i\sqrt{2}g_s T_{c_k c_i}^c \right. \\ &\quad \left. \left((R^{\bar{q}})_{k(i+3)} e^{i\varphi_{\bar{g}}/2} P_R - (R^{\bar{q}})_{ki} e^{-i\varphi_{\bar{g}}/2} P_L \right) \right] \\ &= -\frac{in_c g_s^3}{16\pi^2} T_{c_j c_i}^a \sum_{k=1}^6 \left\{ \left[(\not{p}_2 \gamma^\mu (\not{p}_1 + \not{p}_2) + m_{\bar{g}}^2 \gamma^\mu) C_0 + (\not{p}_2 \gamma^\mu \gamma^\alpha + \gamma^\alpha \gamma^\mu (\not{p}_1 + \not{p}_2)) C_\alpha \right. \right. \\ &\quad \left. \left. + \gamma^\alpha \gamma^\mu \gamma^\beta C_{\alpha\beta} \right] \mathcal{P}_{1,kij} + m_{\bar{g}} \left[(\not{p}_2 \gamma^\mu + \gamma^\mu (\not{p}_1 + \not{p}_2)) C_0 + 2C^\mu \right] \mathcal{P}_{2,kij} \right\} , \end{aligned}$$

where the arguments of the three-point functions can be recovered by performing the replacements

$$\begin{aligned} V_{gq\bar{q}}^{(\bar{q}\bar{q}\bar{g})} : C_{\{0,\mu,\mu\nu\}} &\leftrightarrow C_{\{0,\mu,\mu\nu\}}(p_2^2, p_1^2, m_{\bar{g}}^2, m_{\bar{q}_k}^2, m_{\bar{q}_k}^2) , \\ V_{gq\bar{q}}^{(\bar{g}\bar{g}\bar{q})} : C_{\{0,\mu,\mu\nu\}} &\leftrightarrow C_{\{0,\mu,\mu\nu\}}(p_2^2, p_1^2, m_{\bar{q}_k}^2, m_{\bar{g}}^2, m_{\bar{g}}^2) . \end{aligned} \quad (5.64)$$

Note for completeness that in the present case, we have considered all quarks massless, inasmuch as top quark loops would imply that we would have a top quark initiated process at leading order². We moreover recall that

$$C_{\{0,\mu,\mu\nu\}}(p_2^2, p_1^2; m_1^2, m_2^2, m_3^2) = \int \frac{d^D q}{i\pi^2} (2\pi\mu_R)^{2\varepsilon} \frac{\{1, q_\mu, q_\mu q_\nu\}}{[q^2 - m_1^2][(q+p_2)^2 - m_2^2][(q+p_1+p_2)^2 - m_3^2]} ,$$

and that the quantities $\mathcal{P}_{1,kij}$ and $\mathcal{P}_{2,kij}$ are defined as

$$\begin{aligned} \mathcal{P}_{1,kij} &= (R^{\bar{q}})_{ki} (R^{\bar{q}})_{kj}^* P_L + (R^{\bar{q}})_{k(i+3)} (R^{\bar{q}})_{k(j+3)}^* P_R , \\ \mathcal{P}_{2,kij} &= (R^{\bar{q}})_{ki} (R^{\bar{q}})_{k(j+3)}^* e^{-i\varphi_{\bar{g}}/2} P_L + (R^{\bar{q}})_{k(i+3)} (R^{\bar{q}})_{kj}^* e^{i\varphi_{\bar{g}}/2} P_R . \end{aligned}$$

As detailed in Section 4.4, Lorentz covariance allows us to decompose each vector and tensor integral as linear combination of scalar integrals such that

$$\begin{aligned} C^\mu(p_2^2, p_1^2, m_1^2, m_2^2, m_3^2) &= p_2^\mu C_{11}(p_2^2, p_1^2, m_1^2, m_2^2, m_3^2) + p_1^\mu C_{12}(p_2^2, p_1^2, m_1^2, m_2^2, m_3^2) , \\ C^{\mu\nu}(p_2^2, p_1^2, m_1^2, m_2^2, m_3^2) &= p_2^\mu p_2^\nu C_{21}(p_2^2, p_1^2, m_1^2, m_2^2, m_3^2) + p_1^\mu p_1^\nu C_{22}(p_2^2, p_1^2, m_1^2, m_2^2, m_3^2) \\ &\quad + (p_2^\mu p_1^\nu + p_1^\mu p_2^\nu) C_{23}(p_2^2, p_1^2, m_1^2, m_2^2, m_3^2) + \eta^{\mu\nu} C_{24}(p_2^2, p_1^2, m_1^2, m_2^2, m_3^2) , \end{aligned} \quad (5.65)$$

²The parton distribution of the top quark is irrelevant at energy scales of a few TeV.

where the C_{ij} can be further reduced to a basis of scalar integrals, namely the A_0 , B_0 , and C_0 functions. The resulting expressions after complete reduction being rather lengthy, we will only rewrite the amplitudes at the level of the C_{ij} . We obtain for the amplitudes of our interest

$$\begin{aligned}
V_{gq\bar{q}}^{(qqg)} &= -\frac{i\delta_{ij}g_s^3}{32n_c\pi^2}\delta_{ij}T_{c_jc_i}^a \left[(2-D)^2C_{24}\gamma^\mu + (2-D)(C_{12}+C_{22})\not{p}_1\gamma^\mu\not{p}_1 + (2-D)(2C_{11} \right. \\
&\quad \left. + C_{21}+C_0)\not{p}_2\gamma^\mu\not{p}_2 + \left((2-D)(C_{12}+C_{23})+(4-D)(C_{11}+C_0) \right)\not{p}_2\gamma^\mu\not{p}_1 \right. \\
&\quad \left. + \left((2-D)(C_{12}+C_{23})-2(C_{11}+C_0) \right)\not{p}_1\gamma^\mu\not{p}_2 \right], \\
V_{gq\bar{q}}^{(ggq)} &= \frac{i\delta_{ij}n_cg_s^3}{32\pi^2}T_{c_jc_i}^a \left[\left(2B_0(p_1; 0, 0)+2(D-2)C_{24}+p_1^2C_{12}+2p_2^2C_{11} \right)\gamma^\mu + (D-2)(C_{12} \right. \\
&\quad \left. + 2C_{22})\not{p}_1p_1^\mu + (D-2)(C_{11}+2C_{23})\not{p}_2p_1^\mu + 2(D-2)(C_{12}+C_{23})\not{p}_1p_2^\mu \right. \\
&\quad \left. + 2(D-2)(C_{11}+C_{21})\not{p}_2p_2^\mu + C_{12}\gamma^\mu\not{p}_1\not{p}_2 + C_{11}\gamma^\mu\not{p}_2\not{p}_1 + 2C_{11}\not{p}_1\not{p}_2\gamma^\mu + C_{12}\not{p}_2\not{p}_1\gamma^\mu \right], \quad (5.66) \\
V_{gq\bar{q}}^{(\bar{q}\bar{q}\bar{g})} &= -\frac{ig_s^3}{16n_c\pi^2}T_{c_jc_i}^a \sum_{k=1}^6 \left\{ \left[2C_{24}\gamma^\mu + (C_{11}+2C_{23})\not{p}_2p_1^\mu + (C_{11}+C_{21})\not{p}_2p_2^\mu + (C_{12} \right. \right. \\
&\quad \left. \left. + 2C_{22})\not{p}_1p_1^\mu + 2(C_{12}+C_{23})\not{p}_1p_2^\mu \right] \mathcal{P}_{1,kij} - m_{\bar{g}} \left[(2C_{12}+C_0)p_1^\mu + 2(C_{11}+C_0)p_2^\mu \right] \mathcal{P}_{2,kij} \right\}, \\
V_{gq\bar{q}}^{(\bar{g}\bar{g}\bar{q})} &= -\frac{in_cg_s^3}{16\pi^2}T_{c_jc_i}^a \sum_{k=1}^6 \left\{ \left[\left((2-D)C_{24}+m_{\bar{g}}^2C_0 \right)\gamma^\mu + (2C_{11}+C_{21}+C_0)\not{p}_2\gamma^\mu\not{p}_2 + (C_{12} \right. \right. \\
&\quad \left. \left. + C_{23})\not{p}_1\gamma^\mu\not{p}_2 + (C_{12}+C_{22})\not{p}_1\gamma^\mu\not{p}_1 + (C_{11}+C_{12}+C_{23}+C_0)\not{p}_2\gamma^\mu\not{p}_1 \right] \mathcal{P}_{1,kij} \right. \\
&\quad \left. + m_{\bar{g}} \left[C_0\gamma^\mu\not{p}_1 + 2C_{12}p_1^\mu + 2(C_{11}+C_0)p_2^\mu \right] \mathcal{P}_{2,kij} \right\}.
\end{aligned}$$

The four one-loop diagrams presented above are all ultraviolet-divergent, their UV-part being

$$\text{UV} \left[V_{gq\bar{q}}^{(qqg)} + V_{gq\bar{q}}^{(ggq)} + V_{gq\bar{q}}^{(\bar{q}\bar{q}\bar{g})} + V_{gq\bar{q}}^{(\bar{g}\bar{g}\bar{q})} \right] = \frac{ig_s^3}{16\pi^2\bar{\epsilon}} \frac{2n_c^2-1}{n_c} \gamma^\mu T_{c_jc_i}^a. \quad (5.67)$$

As explained in Section 4.5, the renormalizability of a theory requires that UV-divergences originating from loops cancel against those coming from the counter-terms. In the case of our interest, the counter-term we need is obtained from the tree-level Lagrangian (5.62) by means of multiplicative renormalization, and according to Fig. 5.11 reads as follows

$$\begin{aligned}
V_{gq\bar{q}}^{(x)} &= i\gamma^\mu \left[\delta g_s \delta_{ji} + \frac{g_s}{2} \left(\left[(\delta Z_q^L)_{ji} + (\delta Z_q^{L\dagger})_{ji} \right] P_L + \left[(\delta Z_q^R)_{ji} + (\delta Z_q^{R\dagger})_{ji} \right] P_R + \delta Z_g \delta_{ij} \right) \right] T_{c_jc_i}^a \\
&= i \left[\delta g_s + \frac{g_s^3}{32\pi^2\bar{\epsilon}} \left[-4C_F + n_c - n_f - 1 \right] \right] \gamma^\mu T_{c_jc_i}^a. \quad (5.68)
\end{aligned}$$

where we recall that in our definitions of the WFRCs, we have factorized out the color structure. Collecting all the contributions to the vertex corrections at order $\mathcal{O}(\alpha_s)$ and imposing the result to be UV-finite, we derive the strong coupling constant renormalization constant,

$$\delta g_s = -\frac{g_s^3}{32\pi^2\bar{\epsilon}} \left[3n_c - n_f - 1 \right] \equiv -\frac{g_s^3}{32\pi^2\bar{\epsilon}} \beta_0, \quad (5.69)$$

where we have introduced the first coefficient of the SUSY-QCD β -function, β_0 . Accounting for five active light flavours, as well as for gluons in the running of the strong coupling constant, we

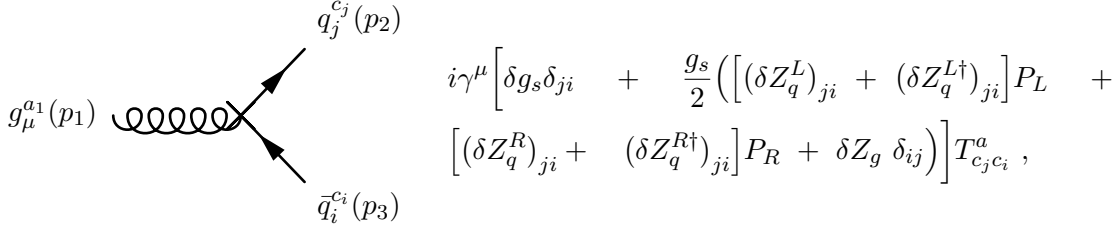


Figure 5.11: Feynman rule of the gluon-quark-antiquark vertex counter-term $V_{gq\bar{q}}^{(x)}$. The indices i , j , and ci and cj respectively correspond to flavour and colour indices of the external quarks

obtain for the strong coupling renormalization constant [220–223],

$$\delta g_s = \frac{g_s^3}{16\pi^2} \left[-\frac{\beta_0}{2\bar{\epsilon}} - \frac{n_c}{3} \log \frac{m_{\tilde{g}}^2}{\mu_R^2} - \frac{1}{12} \sum_{\tilde{q}_i} \log \frac{m_{\tilde{q}_i}^2}{\mu_R^2} - \frac{1}{3} \log \frac{m_t^2}{\mu_R^2} \right], \quad (5.70)$$

where g_s is now evaluated at the renormalization scale μ_R and obeys the evolution equation

$$\frac{dg_s^2(\mu_R^2)}{d \log \mu_R^2} = -\frac{g_s^4(\mu_R^2)}{16\pi^2} \left[\frac{11}{3} n_c - \frac{2}{3} n_f \right]. \quad (5.71)$$

The gluon-squark-antisquark vertex

The gluon-squark-antisquark interactions are described by the tree-level Lagrangian

$$\mathcal{L} = ig_s [\tilde{q}_{i,0}^\dagger g_{0,\mu}^a T^a \partial^\mu \tilde{q}_{j,0} - \partial_\mu \tilde{q}_{i,0}^\dagger g_0^{\mu a} T^a \tilde{q}_{j,0}]. \quad (5.72)$$

At the one-loop level, in SUSY-QCD, the associated vertex $V_{g\tilde{q}\bar{q}}^{(0)}$ receives corrections from six diagrams, which are depicted in Fig. 5.12. With the help of the Feynman rules of Appendix F, we first evaluate the diagrams involving quarks and gluinos in the loops. We obtain

$$\begin{aligned} V_{g\tilde{q}\bar{q}}^{(qq\tilde{g})} &= -\sum_{k=1}^3 \int \frac{d^D q}{(2\pi)^D} \mu_R^{2\bar{\epsilon}} \text{Tr} \left\{ \left[i\sqrt{2}g_s T_{c_i c_k}^b \left((R^{\tilde{q}})_{i(k+3)} e^{i\varphi_{\tilde{g}}/2} P_R - (R^{\tilde{q}})_{ik} e^{-i\varphi_{\tilde{g}}/2} P_L \right) \right. \right. \\ &\quad \left. \frac{-i(\not{p}_2 + \not{q} - m_{q_k})}{(q+p_2)^2 - m_{q_k}^2} \left[ig_s \gamma^\mu T_{c_k c_i}^a \right] \frac{-i(\not{p}_1 + \not{p}_2 + \not{q} - m_{q_k})}{(q+p_1+p_2)^2 - m_{q_k}^2} \right. \\ &\quad \left. \left[i\sqrt{2}g_s T_{c_i c_j}^b \left((R^{\tilde{q}})_{j(k+3)}^* e^{-i\varphi_{\tilde{g}}/2} P_L - (R^{\tilde{q}})_{jk}^* e^{i\varphi_{\tilde{g}}/2} P_R \right) \right] \frac{-i(\not{q} - m_{\tilde{g}})}{q^2 - m_{\tilde{g}}^2} \right\} \\ &= \frac{ig_s^3}{8n_c \pi^2} T_{c_i c_j}^a \sum_{k=1}^3 \left[\left[(p_1+p_2)^\mu B_0(p_1^2, m_{q_k}^2, m_{q_k}^2) + B^\mu(p_1^2, m_{q_k}^2, m_{q_k}^2) + (p_2^\nu (p_1+2p_2)^\mu + p_1^\nu p_2^\mu) C_\nu \right. \right. \\ &\quad \left. \left. + (m_{\tilde{g}}^2 + m_{q_k}^2 - p_2^2 - p_1 \cdot p_2) C^\mu + m_{\tilde{g}}^2 (p_1+2p_2)^\mu C_0 \right] \mathcal{S}_{1,ijk} - m_{\tilde{g}} m_{q_k} \mathcal{S}_{2,ijk} \left[2C^\mu + (p_1+2p_2)^\mu C_0 \right] \right], \\ V_{g\tilde{q}\bar{q}}^{(\tilde{g}\tilde{g}q)} &= -\sum_{k=1}^3 \int \frac{d^D q}{(2\pi)^D} \mu_R^{2\bar{\epsilon}} \text{Tr} \left\{ \left[i\sqrt{2}g_s T_{c_i c_k}^b \left((R^{\tilde{q}})_{i(k+3)} e^{i\varphi_{\tilde{g}}/2} P_R - (R^{\tilde{q}})_{ik} e^{-i\varphi_{\tilde{g}}/2} P_L \right) \right] \frac{i(\not{q} + m_{q_k})}{q^2 - m_{q_k}^2} \right. \\ &\quad \left. \left[i\sqrt{2}g_s T_{c_i c_j}^b \left((R^{\tilde{q}})_{j(k+3)}^* e^{-i\varphi_{\tilde{g}}/2} P_L - (R^{\tilde{q}})_{jk}^* e^{i\varphi_{\tilde{g}}/2} P_R \right) \right] \frac{i(\not{q} + \not{p}_1 + \not{p}_2 + m_{\tilde{g}})}{(q+p_1+p_2)^2 - m_{\tilde{g}}^2} \left[g_s f_{abc} \gamma^\mu \right] \frac{i(\not{q} + \not{p}_2 + m_{\tilde{g}})}{(q+p_2)^2 - m_{\tilde{g}}^2} \right\} \\ &= -\frac{ig_s^3 n_c}{8\pi^2} T_{c_j c_i}^a \sum_{k=1}^3 \left[\left[\left(\frac{1}{2} p_1 + p_2 \right)^\mu B_0(p_1^2, m_{\tilde{g}}^2, m_{\tilde{g}}^2) + m_{q_k}^2 (2p_2+p_1)^\mu C_0 + (m_{\tilde{g}}^2 + m_{q_k}^2 - p_1 \cdot p_2 - p_2^2) C^\mu \right. \right. \\ &\quad \left. \left. + (p_1^\mu p_2^\nu + (2p_2+p_1)^\nu p_2^\mu) C_\nu \right] \mathcal{S}_{1,ijk} - m_{q_k} m_{\tilde{g}} \mathcal{S}_{2,ijk} \left[2C^\mu + (p_1+2p_2)^\mu C_0 \right] \right], \end{aligned}$$

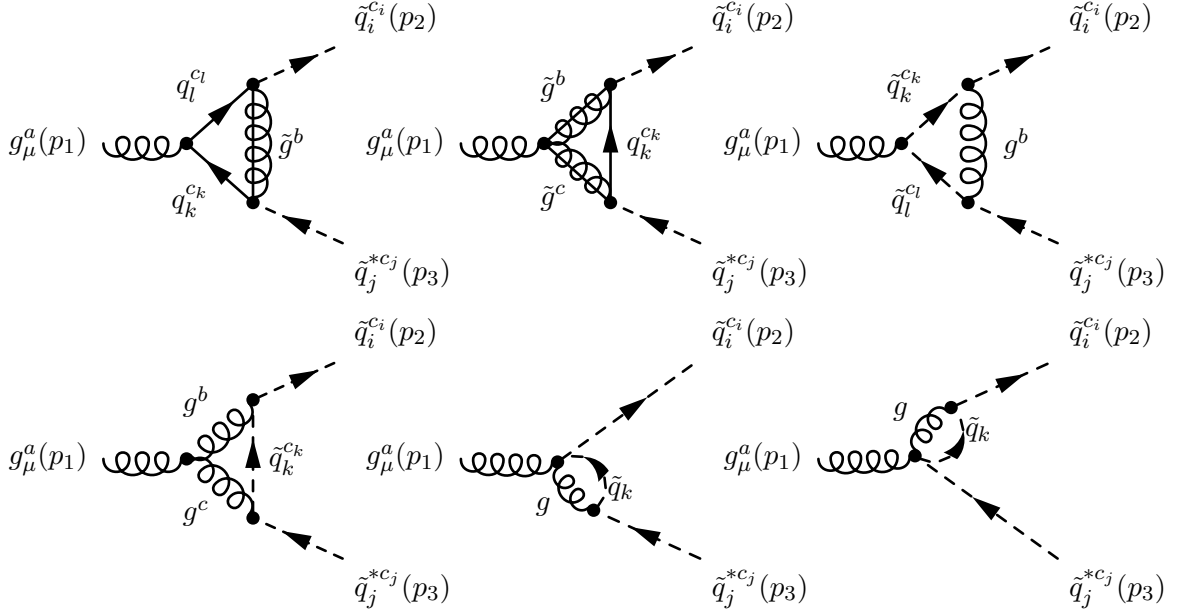


Figure 5.12: Virtual one-loop contributions to the gluon-squark-antisquark vertex. The external Lorentz (μ) and color (a, c_i, c_j) indices are indicated, and the four-momenta of the gluon (p_1) and the fermions (p_2, p_3) are taken incoming to the loop.

where the arguments of the three-point functions can be recovered by means of the substitutions

$$\begin{aligned} V_{g\tilde{q}\tilde{q}}^{(qq\tilde{g})} &: C_{\{0,\mu,\mu\nu\}} \leftrightarrow C_{\{0,\mu,\mu\nu\}}(p_2^2, p_1^2, m_{\tilde{g}}^2, m_{q_k}^2, m_{q_k}^2), \\ V_{g\tilde{q}\tilde{q}}^{(\tilde{g}\tilde{g}q)} &: C_{\{0,\mu,\mu\nu\}} \leftrightarrow C_{\{0,\mu,\mu\nu\}}(p_2^2, p_1^2, m_{q_k}^2, m_{\tilde{g}}^2, m_{\tilde{g}}^2). \end{aligned} \quad (5.73)$$

Analogously, one can evaluate the two flavour-diagonal triangle diagrams, *i.e.* the ones with gluons and squarks running into the loops. This gives

$$\begin{aligned} V_{g\tilde{q}\tilde{q}}^{(\tilde{q}\tilde{q}g)} &= \int \frac{d^D q}{(2\pi)^D} \mu_R^{2\epsilon} \left[-ig_s T_{c_i c_k}^b (2p_2 + q)^\nu \right] \frac{i}{(q + p_2)^2 - m_{\tilde{q}_i}^2} \left[-ig_s T_{c_k c_i}^a (2q + 2p_2 + p_1)^\mu \right] \\ &\quad \frac{i}{(q + p_2 + p_1)^2 - m_{\tilde{q}_i}^2} \left[-ig_s T_{c_i c_j}^b (q + 2p_1 + 2p_2)_\nu \right] \frac{-i}{q^2} \\ &= \frac{ig_s^3 \delta_{ij}}{16n_c \pi^2} T_{c_i c_j}^a \left[2(p_2^2 + p_1 \cdot p_2)(p_1 + 2p_2)^\mu C_0 + 4(p_2^2 + p_1 \cdot p_2)C^\mu + (p_1 + 2p_2)^\nu \right. \\ &\quad \left. (p_1 + 2p_2)^\mu C_\nu + 2(p_1 + 2p_2)^\nu C^\mu \right], \\ V_{g\tilde{q}\tilde{q}}^{(gg\tilde{q})} &= \int \frac{d^D q}{(2\pi)^D} \mu_R^{2\epsilon} \times g_s f_{abc} \left[(p_1 - p_2 - q)_\rho \delta^\mu{}_\nu - (q + 2p_1 + p_2)_\nu \delta^\mu{}_\rho + (2q + 2p_2 + p_1)^\mu \eta_{\nu\rho} \right] \\ &\quad \frac{-i}{(p_2 + q)^2} \left[-ig_s T_{c_i c_k}^b (p_2 - q)^\nu \right] \frac{-i}{(p_1 + p_2 + q)^2} \left[ig_s T_{c_k c_j}^c (q - p_1 - p_2)^\rho \right] \frac{i}{q^2 - m_{\tilde{q}_i}^2} \\ &= -\frac{ig_s^3 n_c \delta_{ij}}{32\pi^2} T_{c_i c_j}^a \left[2(p_1 + 2p_2)^\mu B_0(p_1^2, 0, 0) - (p_1 \cdot p_2 p_1^\mu - p_1^2 p_2^\mu - 2m_{\tilde{q}_i}^2 (p_1 + 2p_2)^\mu) C_0 \right. \\ &\quad \left. - (p_1^2 - 4p_1 \cdot p_2 - 4p_2^2)C^\mu - \left((2p_2 - p_1)^\mu p_1^\nu + (2p_1 + 4p_2)^\mu p_2^\nu \right) C_\nu - (2p_1 + 4p_2)^\nu C^\mu \right], \end{aligned}$$

where the replacement rules

$$\begin{aligned} V_{g\bar{q}\bar{q}}^{(\bar{q}\bar{q}g)} &: C_{\{0,\mu,\mu\nu\}} \leftrightarrow C_{\{0,\mu,\mu\nu\}}(p_2^2, p_1^2, 0, m_{\bar{q}_i}^2, m_{\bar{q}_i}^2), \\ V_{g\bar{q}\bar{q}}^{(g\bar{q}\bar{q})} &: C_{\{0,\mu,\mu\nu\}} \leftrightarrow C_{\{0,\mu,\mu\nu\}}(p_2^2, p_1^2, m_{\bar{q}_i}^2, 0, 0), \end{aligned} \quad (5.74)$$

have to be applied to recover the arguments of the three-point functions. The last two diagrams, the bubble diagrams, are calculated in a similar way, and their sum $V_{g\bar{q}\bar{q}}^{\text{bub}}$ is given by

$$\begin{aligned} V_{g\bar{q}\bar{q}}^{\text{bub}} &= \int \frac{d^D q}{(2\pi)^D} \mu_R^{2\epsilon} \left[\left[ig_s^2 (T^a T^b + T^b T^a)_{c_i c_k} \right] \left[ig_s (q + 2p_3)^\mu T_{c_k c_j}^b \right] \frac{i}{(q + p_3)^2 - m_{\bar{q}_i}^2} \frac{-i}{q^2} \right. \\ &\quad \left. + \left[ig_s^2 (T^a T^b + T^b T^a)_{c_k c_j} \right] \left[-ig_s (q + 2p_2)^\mu T_{c_i c_k}^b \right] \frac{i}{(q + p_2)^2 - m_{\bar{q}_i}^2} \frac{-i}{q^2} \right] \\ &= \frac{ig_s^3 (n_c^2 - 2) \delta_{ij}}{32 n_c \pi^2} T_{c_i c_j}^a \left[B^\mu(p_2^2, 0, m_{\bar{q}_i}^2) - B^\mu(p_3^2, 0, m_{\bar{q}_i}^2) + 2p_2^\mu B_0(p_2^2, 0, m_{\bar{q}_i}^2) - 2p_3^\mu B_0(p_3^2, 0, m_{\bar{q}_i}^2) \right]. \end{aligned}$$

The vector and tensor integrals appearing in the expressions above can be reduced to scalar integrals using (5.27), and (5.65). For loops containing massive quarks and gluinos, we get

$$\begin{aligned} V_{g\bar{q}\bar{q}}^{(q\bar{q}\bar{q})} &= \frac{ig_s^3}{8 n_c \pi^2} T_{c_i c_j}^a \sum_{k=1}^3 \left[\left[\left(\frac{1}{2} p_1^\mu + p_2^\mu \right) B_0(p_1^2, m_{q_k}^2, m_{q_k}^2) + C_0 m_{\bar{g}}^2 (p_1 + 2p_2)^\mu + C_{11} (p_2^2 p_1^\mu \right. \right. \\ &\quad \left. \left. + (m_{\bar{g}}^2 + m_{q_k}^2 + p_2^2) p_2^\mu \right) + C_{12} \left((m_{\bar{g}}^2 + m_{q_k}^2 - p_2^2) p_1^\mu + (p_1^2 + 2p_1 \cdot p_2) p_2^\mu \right) \right] \mathcal{S}_{1,ijk} \\ &\quad \left. - m_{\bar{g}} m_{q_k} \mathcal{S}_{2,ijk} \left[C_0 (p_1 + 2p_2)^\mu + 2C_{11} p_2^\mu + 2C_{12} p_1^\mu \right] \right], \\ V_{g\bar{q}\bar{q}}^{(\bar{g}\bar{g}q)} &= -\frac{ig_s^3 n_c}{8 \pi^2} T_{c_i c_j}^a \left[\left[\left(\frac{1}{2} p_1^\mu + p_2^\mu \right) B_0(p_1^2, m_{\bar{g}}^2, m_{\bar{g}}^2) + C_0 m_{q_k}^2 (p_1 + 2p_2)^\mu + C_{11} (p_2^2 p_1^\mu \right. \right. \\ &\quad \left. \left. + (p_2^2 + m_{q_k}^2 + m_{\bar{g}}^2) p_2^\mu \right) + C_{12} \left((m_{\bar{g}}^2 + m_{q_k}^2 - p_2^2) p_1^\mu + (p_1^2 + 2p_1 \cdot p_2) p_2^\mu \right) \right] \mathcal{S}_{1,ijk} \\ &\quad \left. - m_{\bar{g}} m_{q_k} \mathcal{S}_{2,ijk} \left[C_0 (p_1 + 2p_2)^\mu + 2C_{11} p_2^\mu + 2C_{12} p_1^\mu \right] \right]. \end{aligned} \quad (5.75)$$

Finally, we deduce the contributions of the last two triangles and the bubble diagrams

$$\begin{aligned} V_{g\bar{q}\bar{q}}^{(\bar{q}\bar{q}g)} &= \frac{ig_s^3 \delta_{ij}}{16 n_c \pi^2} T_{c_i c_j}^a \left[2C_0 (p_2^2 + p_1 \cdot p_2) (p_1 + 2p_2)^\mu + C_{11} \left((2p_2^2 + p_1 \cdot p_2) p_1^\mu + (8p_2^2 + 6p_1 \cdot p_2) p_2^\mu \right) \right. \\ &\quad \left. + C_{12} \left((p_1^2 + 4p_2^2 + 6p_1 \cdot p_2) p_1^\mu + (2p_1^2 + 4p_1 \cdot p_2) p_2^\mu \right) + C_{21} \left(4p_2^2 + 2p_1 \cdot p_2 \right) p_2^\mu + C_{22} \left(2p_1^2 \right. \right. \\ &\quad \left. \left. + 4p_1 \cdot p_2 \right) p_1^\mu + C_{23} \left((4p_2^2 + 2p_1 \cdot p_2) p_1^\mu + (2p_1^2 + 4p_1 \cdot p_2) p_2^\mu \right) + C_{24} (2p_1 + 4p_2)^\mu \right], \\ V_{g\bar{q}\bar{q}}^{(g\bar{q}\bar{q})} &= -\frac{ig_s^3 n_c \delta_{ij}}{32 \pi^2} T_{c_i c_j}^a \left[\left(2p_1^\mu + 4p_2^\mu \right) B_0(p_1^2, 0, 0) - C_0 \left((p_1 \cdot p_2 - 2m_{\bar{q}_i}^2) p_1^\mu - (p_1^2 + 4m_{\bar{q}_i}^2) p_2^\mu \right) \right. \\ &\quad \left. + C_{11} \left((p_1 \cdot p_2 - 2p_2^2) p_1^\mu - (p_1^2 - 2p_1 \cdot p_2) p_2^\mu \right) + C_{12} \left((4p_2^2 + 2p_1 \cdot p_2) p_1^\mu - (2p_1^2 + 4p_1 \cdot p_2) p_2^\mu \right) \right. \\ &\quad \left. - C_{21} \left(4p_2^2 + 2p_1 \cdot p_2 \right) p_2^\mu - C_{22} \left(2p_1^2 + 4p_1 \cdot p_2 \right) p_1^\mu - C_{23} \left((4p_2^2 + 2p_1 \cdot p_2) p_1^\mu \right. \right. \\ &\quad \left. \left. + (2p_1^2 + 4p_1 \cdot p_2) p_2^\mu \right) - C_{24} (2p_1 + 4p_2)^\mu \right], \\ V_{g\bar{q}\bar{q}}^{\text{bub}} &= \frac{ig_s^3 (n_c^2 - 2) \delta_{ij}}{64 n_c \pi^2} T_{c_i c_j}^a \left[\left(3 + \frac{m_{\bar{q}_i}^2}{p_2^2} \right) p_2^\mu B_0(p_2^2, 0, m_{\bar{q}_i}^2) - \left(3 + \frac{m_{\bar{q}_i}^2}{p_3^2} \right) p_3^\mu B_0(p_3^2, 0, m_{\bar{q}_i}^2) \right. \\ &\quad \left. - A_0(m_{\bar{q}_i}^2) \left(\frac{p_2^\mu}{p_2^2} - \frac{p_3^\mu}{p_3^2} \right) \right]. \end{aligned} \quad (5.76)$$

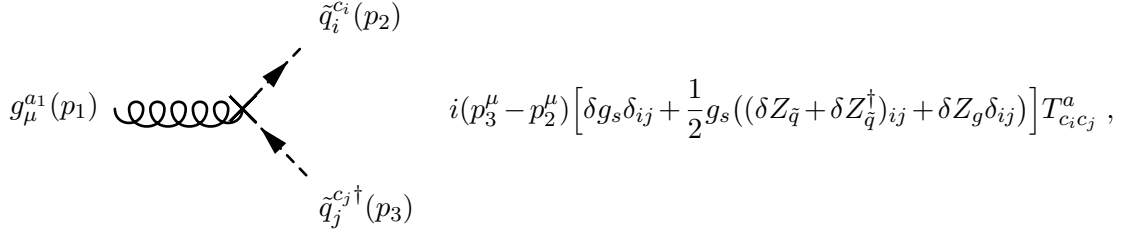


Figure 5.13: Feynman rule of the gluon-squark-antisquark vertex counter-term $V_{g\tilde{q}\tilde{q}}^{(x)}$. The indices i, j , and c_i and c_j correspond to flavour and colour indices of the external squarks.

The one-loop amplitudes presented above are all separately UV-divergent, and their sum gives

$$\text{UV} \left[V_{g\tilde{q}\tilde{q}}^{(qq\tilde{g})} + V_{g\tilde{q}\tilde{q}}^{(\tilde{g}\tilde{q}\tilde{q})} + V_{g\tilde{q}\tilde{q}}^{(\tilde{q}\tilde{q}g)} + V_{g\tilde{q}\tilde{q}}^{(gg\tilde{q})} + V_{g\tilde{q}\tilde{q}}^{\text{bub}} \right] = -\frac{ig_s^3 n_c \delta_{ij}}{16\pi^2 \bar{\epsilon}} (p_2 - p_3)^\mu T_{c_i c_j}^a. \quad (5.77)$$

As explained in Section 4.5, the renormalizability of a theory requires that UV-divergences originating from loops cancel against those coming from the counter-terms. In the case of our interest, the counter-term we need is obtained from the tree-level Lagrangian (5.1) by means of multiplicative renormalization, and according to Fig. 5.13 reads as follows

$$\begin{aligned} V_{g\tilde{q}\tilde{q}}^{(x)} &= i(p_3 - p_2)^\mu \delta_{ij} \left[\delta g_s + \frac{1}{2} g_s \delta Z_g \right] T_{c_i c_j}^a \\ &= \frac{ig_s^3 \delta_{ij}}{16\pi^2} (p_2 - p_3)^\mu T_{c_i c_j}^a \left[\frac{n_c}{\bar{\epsilon}} + \frac{n_c}{3} \log \frac{m_{\tilde{g}}^2}{\mu_R^2} + \frac{1}{12} \sum_{\tilde{q}_i} \log \frac{m_{\tilde{q}_i}^2}{\mu_R^2} + \frac{1}{3} \log \frac{m_t^2}{\mu_R^2} \right], \end{aligned} \quad (5.78)$$

where we have introduced the results of Eqs. (5.33) and (5.70). As expected, the renormalized gluon-squark-antisquark vertex is then ultraviolet-finite.

The gluino-squark-quark vertex

The gluino-quark-squark interactions are described by the tree-level Lagrangian

$$\mathcal{L} = \sqrt{2} g_{s,0} \left[(\tilde{q}_{j,0} P_L e^{-\frac{i\varphi_{\tilde{g}}}{2}} \tilde{g}_0^a) T^a (R_0^{\tilde{q}})_{i(j+3),0}^* \tilde{q}_{i,0} - \tilde{q}_{i,0}^\dagger (R_0^{\tilde{q}})_{ij,0} T^a (e^{-\frac{i\varphi_{\tilde{g}}}{2}} g_0^a P_L q_{j,0}) + \text{h.c.} \right]. \quad (5.79)$$

In what follows, we only detail the calculations related to the gluino-squark-antiquark vertex, inasmuch as corrections to the gluino-antisquark-quark vertex can be deduced by hermitian conjugation. At one-loop in SUSY-QCD, the gluino-squark-antiquark vertex receives corrections from the four diagrams that are depicted in Fig. 5.14. If we compute their respective amplitudes, $V_{\tilde{g}\tilde{q}\tilde{q}}^{(q\tilde{q}\tilde{g})}$, $V_{\tilde{g}\tilde{q}\tilde{q}}^{(\tilde{g}\tilde{q}\tilde{q})}$, $V_{\tilde{g}\tilde{q}\tilde{q}}^{(\tilde{q}\tilde{q}g)}$ and $V_{\tilde{g}\tilde{q}\tilde{q}}^{(g\tilde{q}\tilde{q})}$ with the help of the Feynman rules of Appendix F, and with the help of the following replacement rules for the arguments of the three-point functions,

$$\begin{aligned} V_{\tilde{g}\tilde{q}\tilde{q}}^{(q\tilde{q}\tilde{g})} &: C_{\{0,\mu,\mu\nu\}} \leftrightarrow C_{\{0,\mu,\mu\nu\}}(p_2^2, p_1^2, m_{\tilde{g}}^2, m_{q_k}^2, m_{\tilde{q}_l}^2), \\ V_{\tilde{g}\tilde{q}\tilde{q}}^{(\tilde{g}\tilde{q}\tilde{q})} &: C_{\{0,\mu,\mu\nu\}} \leftrightarrow C_{\{0,\mu,\mu\nu\}}(p_2^2, p_1^2, m_{\tilde{q}_j}^2, m_{\tilde{g}}^2, 0), \\ V_{\tilde{g}\tilde{q}\tilde{q}}^{(\tilde{q}\tilde{q}g)} &: C_{\{0,\mu,\mu\nu\}} \leftrightarrow C_{\{0,\mu,\mu\nu\}}(p_2^2, p_1^2, 0, m_{\tilde{q}_i}^2, m_{q_j}^2), \\ V_{\tilde{g}\tilde{q}\tilde{q}}^{(g\tilde{q}\tilde{q})} &: C_{\{0,\mu,\mu\nu\}} \leftrightarrow C_{\{0,\mu,\mu\nu\}}(p_2^2, p_1^2, m_{\tilde{q}_i}^2, 0, m_{\tilde{g}}^2), \end{aligned} \quad (5.80)$$

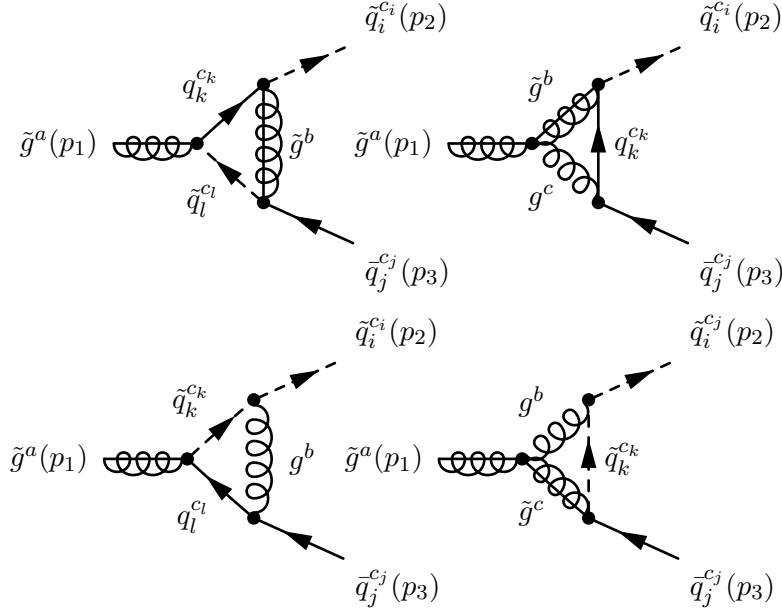


Figure 5.14: Virtual one-loop contributions to the gluino-squark-antisquark vertex. The external color indices (a , c_i , c_j) are indicated, and the four-momenta p_1 , p_2 , and p_3 are all taken incoming to the loop.

the amplitudes read

$$\begin{aligned}
V_{\tilde{g}\tilde{q}\tilde{q}}^{(q\tilde{q}\tilde{g})} &= \int \frac{d^D q}{(2\pi)^D} \mu_R^{2\epsilon} \sum_{k,l} \left\{ \left[i\sqrt{2}g_s T_{c_k c_l}^a \left((R^{\tilde{q}})_{l(k+3)}^* e^{-i\varphi_{\tilde{g}}/2} P_L - (R^{\tilde{q}})_{lk}^* e^{i\varphi_{\tilde{g}}/2} P_R \right) \right] i \frac{\not{q} + \not{p}_2 + m_{q_k}}{(q+p_2)^2 - m_{q_k}^2} \right. \\
&\quad \left[i\sqrt{2}g_s T_{c_i c_k}^b \left((R^{\tilde{q}})_{i(k+3)} e^{i\varphi_{\tilde{g}}/2} P_R - (R^{\tilde{q}})_{ik} e^{-i\varphi_{\tilde{g}}/2} P_L \right) \right] i \frac{\not{q} + m_{\tilde{g}}}{q^2 - m_{\tilde{g}}^2} \\
&\quad \times \left. \left[i\sqrt{2}g_s T_{c_l c_j}^b \left((R^{\tilde{q}})_{l(j+3)} e^{i\varphi_{\tilde{g}}/2} P_R - (R^{\tilde{q}})_{lj} e^{-i\varphi_{\tilde{g}}/2} P_L \right) \right] \frac{i}{(q+p_1+p_2)^2 - m_{\tilde{q}_i}^2} \right\} \\
&= -\frac{i\sqrt{2}g_s^3}{16n_c\pi^2} T_{c_i c_j}^a \sum_{k,l} \left\{ \left[B_0(p_1^2, m_{q_k}^2, m_{\tilde{q}_i}^2) + m_{\tilde{g}}^2 C_0 + \not{p}_2 \gamma^\nu C_\nu \right] P_1 + m_{\tilde{g}} \left[\not{p}_2 C_0 + \gamma^\nu C_\nu \right] P_2 \right. \\
&\quad \left. + m_{q_k} \gamma^\nu C_\nu P_3 + m_{\tilde{g}} m_{q_k} C_0 P_4 \right\}, \\
V_{\tilde{g}\tilde{q}\tilde{q}}^{(\tilde{g}q\tilde{q})} &= \int \frac{d^D q}{(2\pi)^D} \mu_R^{2\epsilon} \left[g_s f_{cab} \gamma^\mu \right] i \frac{\not{q} + \not{p}_2 + m_{\tilde{g}}}{(q+p_2)^2 - m_{\tilde{g}}^2} \left[i\sqrt{2}g_s T_{c_i c_k}^b \left((R^{\tilde{q}})_{i(j+3)} e^{i\varphi_{\tilde{g}}/2} P_R \right. \right. \\
&\quad \left. \left. - (R^{\tilde{q}})_{ij} e^{-i\varphi_{\tilde{g}}/2} P_L \right) \right] i \frac{\not{q} + m_{q_j}}{q^2 - m_{q_j}^2} \left[i g_s \gamma_\mu T_{c_k c_j}^c \right] \frac{-i}{(q+p_1+p_2)^2} \\
&= -\frac{i\sqrt{2}n_c g_s^3}{32\pi^2} T_{c_i c_j}^a \left\{ \left[DB_0(p_1^2, m_{\tilde{g}}^2, 0) + (4p_2^\nu + (D-4)\not{p}_2 \gamma^\nu + (2-D)m_{\tilde{g}} \gamma^\nu) C_\nu \right. \right. \\
&\quad \left. \left. + m_{q_j}^2 DC_0 \right] S_{1,ij} + m_{q_j} \left[(m_{\tilde{g}} + (2-D)\not{p}_2) C_0 + (2-D)\gamma^\nu C_\nu \right] S_{2,ij} \right\}, \\
V_{\tilde{g}\tilde{q}\tilde{q}}^{(\tilde{q}q\tilde{g})} &= \int \frac{d^D q}{(2\pi)^D} \mu_R^{2\epsilon} \left[i\sqrt{2}g_s T_{c_k c_l}^a \left((R^{\tilde{q}})_{i(j+3)} e^{i\varphi_{\tilde{g}}/2} P_R - (R^{\tilde{q}})_{ij} e^{-i\varphi_{\tilde{g}}/2} P_L \right) \right] (-i) \frac{\not{q} + \not{p}_1 + \not{p}_2 - m_{q_j}}{(q+p_1+p_2)^2 - m_{q_j}^2} \\
&\quad \left[i g_s \gamma_\mu T_{c_l c_j}^b \right] \frac{-i}{q^2} \frac{i}{(q+p_2)^2 - m_{\tilde{q}_i}^2} \times \left[-i g_s (2p_2 + q)^\mu T_{c_i c_k}^b \right] \\
&= \frac{i\sqrt{2}g_s^3}{32n_c\pi^2} T_{c_i c_j}^a \left\{ \left[B_0(p_1^2, m_{\tilde{q}_i}^2, m_{q_j}^2) + (\not{p}_1 + \not{p}_2) \gamma^\nu + 2\gamma^\nu \not{p}_2 \right] C_\nu + 2(\not{p}_1 + \not{p}_2) \not{p}_2 C_0 \right\} S_{1,ij} \\
&\quad - m_{q_j} \left[2\not{p}_2 C_0 + \gamma^\nu C_\nu \right] S_{2,ij} \left. \right\},
\end{aligned}$$

$$\begin{aligned}
V_{\tilde{g}\tilde{q}\tilde{q}}^{(g\tilde{g}\tilde{q})} &= \int \frac{d^D q}{(2\pi)^D} \mu_R^{2\epsilon} \left[g_s f_{bca} \gamma^\mu \right] (-i) \frac{\not{q} + \not{p}_1 + \not{p}_2 - m_{\tilde{g}}}{(q+p_1+p_2)^2 - m_{\tilde{g}}^2} \left[i\sqrt{2} g_s T_{c_k c_j}^c \left((R^{\tilde{q}})_{i(j+3)} e^{i\varphi_{\tilde{g}}/2} P_R \right. \right. \\
&\quad \left. \left. - (R^{\tilde{q}})_{ij} e^{-i\varphi_{\tilde{g}}/2} P_L \right) \right] \frac{i}{q^2 - m_{\tilde{q}_i}^2} \frac{-i}{(p_2+q)^2} \left[-i g_s (p_2 - q)_\mu T_{c_i c_k}^b \right] \\
&= \frac{i\sqrt{2} n_c g_s^3}{32\pi^2} T_{c_i c_j}^a \left[B_0(p_1^2, 0, m_{\tilde{g}}^2) + \left(\gamma^\nu (\not{p}_2 + \not{p}_1 - m_{\tilde{g}}) - \not{p}_2 \gamma^\nu \right) C_\nu + \left(m_{\tilde{q}_i}^2 - \not{p}_2 (\not{p}_1 + \not{p}_2 - m_{\tilde{g}}) \right) C_0 \right] S_{1,ij} ,
\end{aligned}$$

where we have introduced the quantities

$$S_{1,ij} = (R^{\tilde{q}})_{ij} e^{-i\varphi_{\tilde{g}}/2} P_L - (R^{\tilde{q}})_{i(j+3)} e^{i\varphi_{\tilde{g}}/2} P_R , \quad (5.81)$$

$$S_{2,ij} = (R^{\tilde{q}})_{ij} e^{-i\varphi_{\tilde{g}}/2} P_R - (R^{\tilde{q}})_{i(j+3)} e^{i\varphi_{\tilde{g}}/2} P_L , \quad (5.82)$$

and

$$P_1 = (R^{\tilde{q}})_{l(k+3)}^* (R^{\tilde{q}})_{i(k+3)} (R^{\tilde{q}})_{lj} e^{-i\varphi_{\tilde{g}}/2} P_L - (R^{\tilde{q}})_{lk}^* (R^{\tilde{q}})_{ik} (R^{\tilde{q}})_{l(j+3)} e^{i\varphi_{\tilde{g}}/2} P_R , \quad (5.83)$$

$$P_2 = (R^{\tilde{q}})_{lk}^* (R^{\tilde{q}})_{ik} (R^{\tilde{q}})_{lj} e^{-i\varphi_{\tilde{g}}/2} P_L - (R^{\tilde{q}})_{l(k+3)}^* (R^{\tilde{q}})_{i(k+3)} (R^{\tilde{q}})_{l(j+3)} e^{i\varphi_{\tilde{g}}/2} P_R , \quad (5.84)$$

$$P_3 = (R^{\tilde{q}})_{l(k+3)}^* (R^{\tilde{q}})_{ik} (R^{\tilde{q}})_{l(j+3)} e^{-i\varphi_{\tilde{g}}/2} P_R - (R^{\tilde{q}})_{lk}^* (R^{\tilde{q}})_{i(k+3)} (R^{\tilde{q}})_{lj} e^{i\varphi_{\tilde{g}}/2} P_L , \quad (5.85)$$

$$P_4 = (R^{\tilde{q}})_{lk}^* (R^{\tilde{q}})_{i(k+3)} (R^{\tilde{q}})_{l(j+3)} e^{3i\varphi_{\tilde{g}}/2} P_R - (R^{\tilde{q}})_{l(k+3)}^* (R^{\tilde{q}})_{ik} (R^{\tilde{q}})_{lj} e^{-3i\varphi_{\tilde{g}}/2} P_L . \quad (5.86)$$

The vector and tensor integrals appearing in the expressions above can be reduced to scalar integrals by means of (5.27), and (5.65). Eventually, one obtains

$$\begin{aligned}
V_{\tilde{g}\tilde{q}\tilde{q}}^{(q\tilde{q}\tilde{g})} &= -\frac{i\sqrt{2} g_s^3}{16 n_c \pi^2} T_{c_i c_j}^a \sum_{k,l} \left\{ \left[B_0(p_1^2, m_{q_k}^2, m_{\tilde{q}_l}^2) + m_{\tilde{g}}^2 C_0 + p_2^2 C_{11} + \not{p}_2 \not{p}_1 C_{12} \right] P_1 + m_{\tilde{g}} \left[\not{p}_2 (C_0 + C_{11}) \right. \right. \\
&\quad \left. \left. + \not{p}_1 C_{12} \right] P_2 + m_{q_k} \left[\not{p}_2 C_{11} + \not{p}_1 C_{12} \right] P_3 + m_{q_k} m_{\tilde{g}} C_0 P_4 \right\} , \\
V_{\tilde{g}\tilde{q}\tilde{q}}^{(\tilde{g}gq)} &= -\frac{i\sqrt{2} n_c g_s^3}{32\pi^2} T_{c_i c_j}^a \left\{ \left[D B_0(p_1^2, m_{\tilde{g}}^2, 0) + (D p_2^2 + (2-D) m_{\tilde{g}} \not{p}_2) C_{11} + (4 p_1 \cdot p_2 + (2-D) m_{\tilde{g}} \not{p}_1 \right. \right. \\
&\quad \left. \left. + (D-4) \not{p}_2 \not{p}_1 \right) C_{12} + m_{q_j}^2 D C_0 \right] S_{1,ij} + m_{q_j} \left[(m_{\tilde{g}} + (2-D) \not{p}_2) C_0 + (2-D) (\not{p}_2 C_{11} + \not{p}_1 C_{12}) \right] S_{2,ij} \right\} , \\
V_{\tilde{g}\tilde{q}\tilde{q}}^{(\tilde{q}qg)} &= \frac{i\sqrt{2} g_s^3}{32 n_c \pi^2} T_{c_i c_j}^a \left\{ \left[B_0(p_1^2, m_{\tilde{q}_i}^2, m_{q_j}^2) + 2(\not{p}_1 + \not{p}_2) \not{p}_2 C_0 + (3 p_2^2 + \not{p}_1 \not{p}_2) C_{11} \right. \right. \\
&\quad \left. \left. + (p_1^2 + 2 p_1 \cdot p_2 + \not{p}_1 \not{p}_2) C_{12} \right] S_{1,ij} - m_{q_j} \left[2 \not{p}_2 C_0 + \not{p}_2 C_{11} + \not{p}_1 C_{12} \right] S_{2,ij} \right\} , \\
V_{\tilde{g}\tilde{q}\tilde{q}}^{(g\tilde{g}\tilde{q})} &= \frac{i\sqrt{2} n_c g_s^3}{32\pi^2} T_{c_i c_j}^a \left[B_0(p_1^2, 0, m_{\tilde{g}}^2) + \left(m_{\tilde{q}_i}^2 - \not{p}_2 (\not{p}_1 + \not{p}_2 - m_{\tilde{g}}) \right) C_0 + \left(\not{p}_2 \not{p}_1 - m_{\tilde{g}} \not{p}_2 \right) C_{11} \right. \\
&\quad \left. + \left(p_1^2 - m_{\tilde{g}} \not{p}_1 + \not{p}_1 \not{p}_2 - \not{p}_2 \not{p}_1 \right) C_{12} \right] S_{1,ij} .
\end{aligned}$$

The previous amplitudes are all UV-divergent, and the sum of their UV-divergent part is

$$\text{UV} \left[V_{\tilde{g}\tilde{q}\tilde{q}}^{(q\tilde{q}\tilde{g})} + V_{\tilde{g}\tilde{q}\tilde{q}}^{(\tilde{g}gq)} + V_{\tilde{g}\tilde{q}\tilde{q}}^{(\tilde{q}qg)} + V_{\tilde{g}\tilde{q}\tilde{q}}^{(g\tilde{g}\tilde{q})} \right] = -\frac{i\sqrt{2} g_s^3}{32\pi^2 \bar{\epsilon}} T_{c_i c_j}^a \frac{5n_c^2 - 1}{n_c} S_{1,ij} . \quad (5.87)$$

Starting from the Lagrangian of (5.79), one can obtain the counter-term Feynman rules summarized in Appendix F by replacing all the bare fields and parameters by their renormalized counter-parts. A specificity of the gluino-squark-quark interactions is that they also involve the squark mixing angles, which must also be renormalized as follows,

$$(R_0^{\tilde{q}})_{ij} = (R^{\tilde{q}})_{ij} + (\delta R^{\tilde{q}})_{ij} . \quad (5.88)$$

The renormalization constants $(\delta R^{\tilde{q}})_{ij}$ are defined such that

$$(\delta R^{\tilde{q}})_{ij} = \frac{1}{4} \sum_{k=1}^6 [(\delta Z_{\tilde{q}})_{ik} - (\delta Z_{\tilde{q}}^*)_{ki}] R_{kj}^{\tilde{q}}. \quad (5.89)$$

Even if there is no canonical definition for the squark mixing matrices renormalization constants, the choice of (5.89) is inspired by the on-shell scheme, where the one-loop corrections to the sfermion mixing angles are imposed to vanish on-shell. In the $\overline{\text{MS}}$ -scheme, the squark renormalization constants being anti-hermitian, the counterterm contribution to the gluino-squark-antisquark vertex simplifies to

$$V_{\hat{g}\tilde{q}\tilde{q}}^{(x)} = \frac{i\sqrt{2}g_s^3}{32\pi^2} T_{c_i c_j}^a \left[\frac{5n_c^2 - 1}{n_c \bar{\epsilon}} + \frac{2n_c}{3} \log \frac{m_{\tilde{g}}^2}{\mu_R^2} + \frac{1}{6} \sum_{\tilde{q}_i} \log \frac{m_{\tilde{q}_i}^2}{\mu_R^2} + \frac{2}{3} \log \frac{m_t^2}{\mu_R^2} \right] S_{1,ij}, \quad (5.90)$$

where the last equality is deduced from the results of (5.33), (5.42), (5.50) and (5.70). Comparing with Eq. (5.87), the renormalized gluino-squark-antisquark vertex is thus finite in the UV.

The triple gluon vertex

The triple gluon interactions are described by the following tree-level Lagrangian

$$\mathcal{L} = -g_{s,0} f_{abc} \partial^\nu g_{0,\mu}^a g_{0,\nu}^b g_0^{\mu c}. \quad (5.91)$$

At one-loop, the associated triple gluon vertex receives (non-vanishing) corrections from the diagrams that are depicted in Fig. 5.15. With the help of the Feynman rules of Appendix F, we obtain for the massive quark loop contributions

$$\begin{aligned} V_{ggg}^{(qqq)} &= \int \frac{d^D q}{(2\pi)^D} \mu^{2\epsilon} \text{Tr} \left\{ [ig_s \gamma^\nu T_{nm}^b] i \frac{-\not{q} - \not{p}_2 + m_q}{(q+p_2)^2 - m_q^2} [ig_s \gamma^\nu T_{mo}^a] i \frac{-\not{q} - \not{p}_2 - \not{p}_1 + m_{qk}}{(q+p_2+p_1)^2 - m_q^2} [ig_s \gamma^\nu T_{on}^c] \right. \\ &\quad \left. i \frac{-\not{q} + m_q}{q^2 - m_q^2} + [ig_s \gamma^\nu T_{mn}^b] i \frac{-\not{q} - \not{p}_2 + m_{qk}}{(q+p_2)^2 - m_q^2} [ig_s \gamma^\nu T_{om}^a] i \frac{-\not{q} - \not{p}_2 - \not{p}_1 + m_q}{(q+p_2+p_1)^2 - m_q^2} [ig_s \gamma^\nu T_{no}^c] i \frac{-\not{q} + m_q}{q^2 - m_q^2} \right\} \\ &= -\frac{g_s^3 n_f}{32\pi^2} f^{abc} \left[\text{Tr} \left\{ \gamma^\nu \gamma^\alpha \gamma^\mu \gamma^\beta \gamma^\rho \gamma^\sigma \right\} \left[C_{\alpha\beta\sigma} + (p_2+p_1)_\beta C_{\alpha\sigma} + p_{2\alpha} C_{\beta\sigma} + p_{2\alpha} (p_2+p_1)_\beta C_\sigma \right] \right. \\ &\quad \left. + 4m_q^2 \left[C^\rho \eta^{\mu\nu} + C^\nu \eta^{\mu\rho} + C^\mu \eta^{\nu\rho} + [p_1^\rho \eta^{\mu\nu} - p_1^\nu \eta^{\mu\rho} + (p_1+2p_2)^\mu \eta^{\nu\rho}] C_0 \right] \right], \end{aligned}$$

where m , n , and o correspond to colour indices of the quarks running into the loops, and k is the flavour index of the quarks. The contribution of the n_f light quarks is directly obtained from the previous expression by taking the massless limit. The arguments of the three-point functions appearing above can be recovered by performing the following substitution

$$V_{ggg}^{(qqq)} : C_{\{0,\mu,\mu\nu,\mu\nu\rho\}} \leftrightarrow C_{\{0,\mu,\mu\nu,\mu\nu\rho\}}(p_2^2, p_1^2, m_q^2, m_q^2, m_q^2). \quad (5.92)$$

The triangle integrals with three Lorentz indices can be reduced to a linear combination of scalar integrals such that

$$\begin{aligned} C^{\mu\nu\rho} &= p_{2\mu} p_{2\nu} p_{2\rho} C_{31} + p_{1\mu} p_{1\nu} p_{1\rho} C_{32} + (p_2^\mu p_2^\nu p_1^\rho + p_2^\mu p_2^\rho p_1^\nu + p_2^\nu p_2^\rho p_1^\mu) C_{33} + (p_1^\mu p_1^\nu p_2^\rho + p_1^\mu p_1^\rho p_2^\nu \\ &\quad + p_1^\nu p_1^\rho p_2^\mu) C_{34} + (p_{2\mu} \eta_{\nu\rho} + p_{2\nu} \eta_{\mu\rho} + p_{2\rho} \eta_{\mu\nu}) C_{35} + (p_{1\mu} \eta_{\nu\rho} + p_{1\nu} \eta_{\mu\rho} + p_{1\rho} \eta_{\mu\nu}) C_{36}. \end{aligned}$$

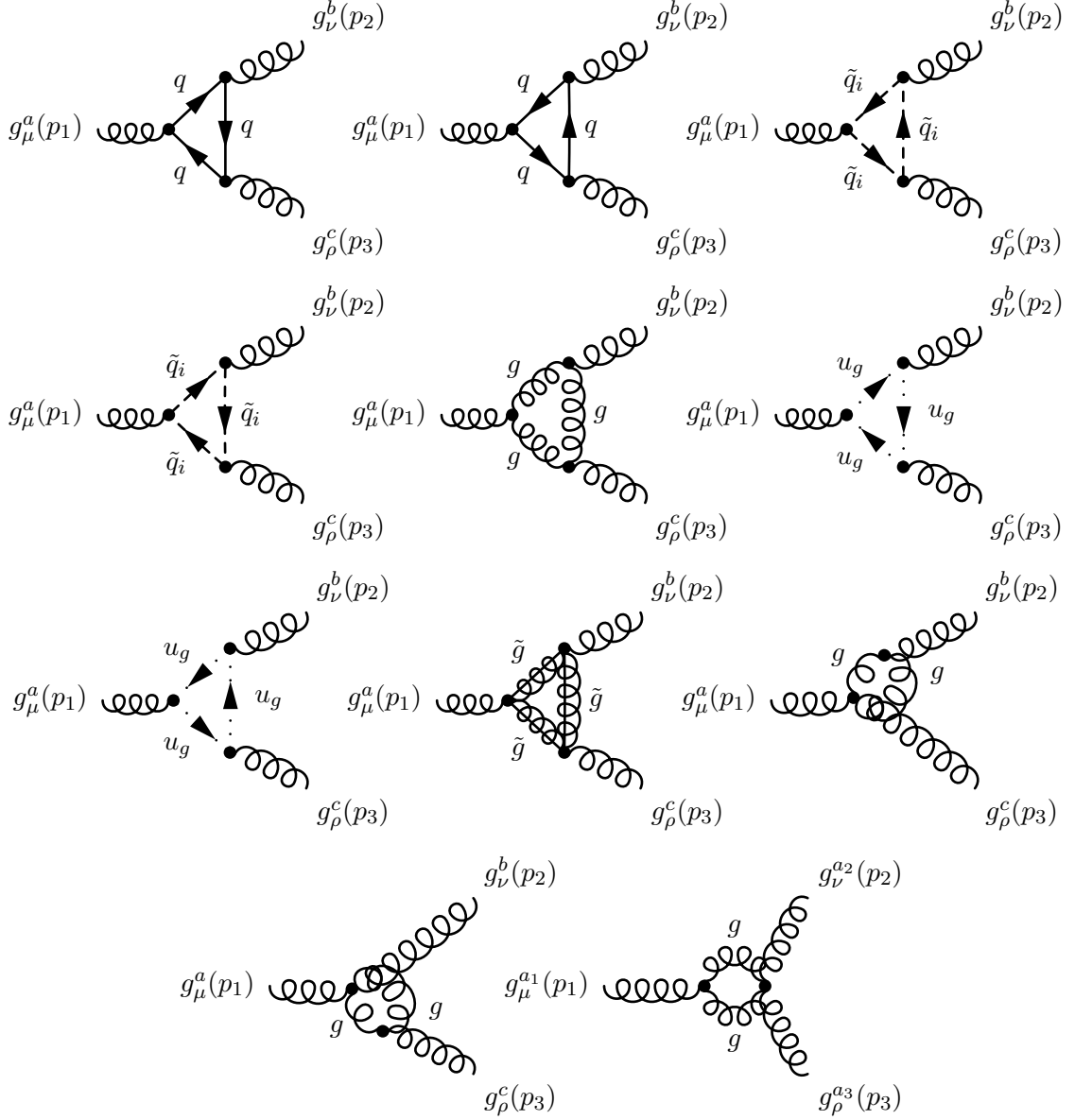


Figure 5.15: Non-vanishing virtual one-loop contributions to the triple gluon vertex. The external color indices (a , b , c) are indicated and the four-momenta p_1 , p_2 , and p_3 are all taken incoming.

where all arguments are understood. The reduction involving large analytical expressions, we do not detail it here. The sum of all diagrams containing a squark loop, $V_{ggg}^{(\tilde{q}\tilde{q}\tilde{q})}$ is given by

$$\begin{aligned}
V_{ggg}^{(\tilde{q}\tilde{q}\tilde{q})} &= \int \frac{d^D q}{(2\pi)^D} \mu_R^{2\epsilon} \sum_{\tilde{q}} \left\{ \left[\left[-ig_s T_{nm}^b (2q+p_2)^\nu \right] \left[-ig_s T_{mo}^a (2q+2p_2+p_1)^\mu \right] \left[-ig_s T_{on}^c (2q+p_1+p_2)^\rho \right] \right. \right. \\
&\quad \left. \left. + \left[-ig_s T_{mn}^b (2q+p_2)^\nu \right] \left[-ig_s T_{om}^a (2q+2p_2+p_1)^\mu \right] \left[-ig_s T_{no}^c (2q+p_1+p_2)^\rho \right] \right] \frac{i}{q-m_{\tilde{q}}^2} \right. \\
&\quad \left. \times \frac{i}{(q+p_2)^2 - m_{\tilde{q}}^2} \frac{i}{(q+p_1+p_2)^2 - m_{\tilde{q}}^2} \right. \\
&= \frac{g_s^3}{32\pi^2} f^{abc} \sum_{\tilde{q}} \left\{ 8C^{\mu\nu\rho} + 4 \left[(p_1+p_2)^\rho C^{\mu\nu} + (p_1+2p_2)^\mu C^{\nu\rho} + p_2^\nu C^{\mu\rho} \right] + 2 \left[(p_1+2p_2)^\mu (p_1 \right. \right. \\
&\quad \left. \left. + p_2)^\rho C^\nu + p_2^\nu (p_1+p_2)^\rho C^\mu + p_2^\nu (p_1+2p_2)^\mu C^\rho \right] + (p_1+2p_2)^\mu p_2^\nu (p_1+p_2)^\rho C_0 \right\},
\end{aligned}$$

where the arguments of the three-point functions read now as

$$V_{ggg}^{(\bar{q}\bar{q}\bar{q})} : C_{\{0,\mu,\mu\nu,\mu\nu\rho\}} \leftrightarrow C_{\{0,\mu,\mu\nu,\mu\nu\rho\}}(p_2^2, p_1^2, m_{\bar{q}}^2, m_{\bar{q}}^2, m_{\bar{q}}^2) . \quad (5.93)$$

The gluon and ghost loops form a gauge invariant subset and read

$$\begin{aligned} V_{ggg}^{(ggg)} &= \int \frac{d^D q}{(2\pi)^D} \mu_R^{2\varepsilon} g_s f^{adf} \left[(p_1 - p_2 - q)^\sigma \eta^{\mu\alpha} - (q + 2p_1 + p_2)^\alpha \eta^{\mu\sigma} + (2q + 2p_2 + p_1)^\mu \eta^{\alpha\sigma} \right] \\ &\quad \times g_s f^{dbe} \left[- (2p_2 + q)^\beta \delta^\nu_\alpha + (2q + p_2)^\nu \delta^\beta_\alpha + (p_2 - q)_\alpha \eta^{\beta\nu} \right] g_s f^{fec} \left[(p_1 + p_2 + 2q)^\rho \eta_{\sigma\beta} \right. \\ &\quad \left. - (q + 2p_1 + 2p_2)_\beta \delta^\rho_\sigma + (p_2 + p_1 - q)_\sigma \delta^{\rho\beta} \right] \frac{-i}{q^2} \frac{-i}{(q+p_2)^2} \frac{-i}{(q+p_1+p_2)^2} \\ &= \frac{g_s^3 n_c}{32\pi^2} f^{abc} \left[(8D-14) C^{\mu\nu\rho} + 2 \left[\eta^{\mu\rho} C^{\nu\alpha}_\alpha + \eta^{\nu\rho} C^{\mu\alpha}_\alpha + \eta^{\mu\nu} C^{\rho\alpha}_\alpha \right] + \left[(3p_1 - p_2)^\rho \eta^{\mu\nu} \right. \right. \\ &\quad \left. \left. - (4p_1 + p_2)^\nu \eta^{\mu\rho} + 3(p_1 + 2p_2)^\mu \eta^{\rho\nu} \right] C^\alpha_\alpha + (4D-7) \left[(p_1 + 2p_2)^\mu C^{\nu\rho} + p_2^\nu C^{\mu\rho} \right. \right. \\ &\quad \left. \left. + (p_1 + p_2)^\rho C^{\mu\nu} \right] + 2 \left[\eta^{\nu\rho} (p_1 + 2p_2)_\alpha C^{\alpha\mu} + \eta^{\mu\rho} p_{2\alpha} C^{\alpha\nu} + \eta^{\mu\nu} (p_1 + p_2)_\alpha C^{\alpha\rho} \right] + \left[3p_1^\nu p_1^\rho \right. \right. \\ &\quad \left. \left. + (2D-1) p_1^\rho p_2^\nu - 13p_1^\nu p_2^\rho + (2D-14) p_2^\nu p_2^\rho + \eta^{\nu\rho} [12p_2^2 + 12p_1 \cdot p_2 - p_1^2] \right] C^\mu + \left[(2D-14) p_1^\mu p_1^\rho \right. \right. \\ &\quad \left. \left. + (4D-20) p_1^\rho p_2^\mu + (2D-1) p_1^\mu p_2^\rho + (4D-4) p_2^\mu p_2^\rho + \eta^{\mu\rho} [10p_1^2 + 10p_1 \cdot p_2 - p_2^2] \right] C^\nu + \left[3p_1^\mu p_1^\nu \right. \right. \\ &\quad \left. \left. + 16p_1^\nu p_2^\mu + (2D-3) p_1^\mu p_2^\nu + (4D-4) p_2^\mu p_2^\nu - \eta^{\mu\nu} [p_1^2 + 12p_1 \cdot p_2 + p_2^2] \right] C^\rho + \left[p_1^\alpha [3(p_1 \right. \right. \\ &\quad \left. \left. + p_2)^\rho \eta^{\mu\nu} - 4(2p_1 + p_2)^\nu \eta^{\mu\rho} + (3p_1 + 2p_2)^\mu \eta^{\nu\rho}] + p_2^\alpha [(7p_1 - p_2)^\rho \eta^{\mu\nu} - (8p_1 + p_2)^\nu \eta^{\mu\rho} + 2(p_1 \right. \right. \\ &\quad \left. \left. + 2p_2)^\mu \eta^{\nu\rho}] \right] C_\alpha + \left[3p_1^\nu p_1^\rho p_2^\mu + (D-7) p_1^\mu p_1^\rho p_2^\nu + (2D-11) p_1^\rho p_2^\nu p_2^\mu + 3p_1^\nu p_2^\mu p_2^\rho + (D-4) p_1^\mu p_2^\nu p_2^\rho \right. \right. \\ &\quad \left. \left. + (2D-8) p_2^\mu p_2^\nu p_2^\rho + \eta^{\mu\nu} [5p_1^\rho p_2^2 - 2p_2^2 p_2^\rho - 8p_1 \cdot p_2 p_2^\rho - p_2^2 p_2^\rho] + \eta^{\mu\rho} [-4p_1 \cdot p_2 p_1^\nu - 6p_2^2 p_1^\nu \right. \right. \\ &\quad \left. \left. + 5p_1^2 p_2^\nu + 6p_1 \cdot p_2 p_2^\nu - p_2^2 p_2^\nu] + \eta^{\nu\rho} [3p_1 \cdot p_2 p_1^\mu + 4p_2^2 p_1^\mu + p_1^2 p_2^\mu + 8p_1 \cdot p_2 p_2^\mu + 8p_2^2 p_2^\mu] \right] C_0 \right] , \\ V_{ggg}^{(u_g u_g u_g)} &= \int \frac{d^D q}{(2\pi)^D} \mu_R^{2\varepsilon} (-) \left[-g_s f^{afd} (p_2 + q)^\mu \right] \left[-g_s f^{bde} q^\nu \right] \left[-g_s f^{cef} (p_1 + p_2 + q)^\rho \right] \\ &\quad + \left[g_s f^{adf} (p_1 + p_2 + q)^\mu \right] \left[g_s f^{bed} (p_2 + q)^\nu \right] \left[g_s f^{efe} q^\rho \right] \frac{i}{q^2} \frac{i}{(q+p_2)^2} \frac{i}{(q+p_1+p_2)^2} \\ &= \frac{g_s^3 n_c}{32\pi^2} f^{abc} \left[2C^{\mu\nu\rho} + \left[(p_1 + 2p_2)^\mu C^{\nu\rho} + p_2^\nu C^{\mu\rho} + (p_1 + p_2)^\rho C^{\mu\nu} \right] \right. \\ &\quad \left. + \left[(p_1^\rho p_2^\mu + p_2^\mu p_2^\rho) C^\nu + p_2^\nu (p_1 + p_2)^\mu C^\rho \right] \right] , \end{aligned}$$

where d , e and f are internal adjoint color indices and the replacement rule for the arguments of the three-point functions is

$$V_{ggg}^{(ggg/u_g u_g u_g)} : C_{\{0,\mu,\mu\nu,\mu\nu\rho\}} \leftrightarrow C_{\{0,\mu,\mu\nu,\mu\nu\rho\}}(p_2^2, p_1^2, 0, 0, 0) . \quad (5.94)$$

The last triangle diagram, *i.e.* the one with gluinos, finally gives the following expression

$$\begin{aligned} V_{ggg}^{(\bar{g}\bar{g}\bar{g})} &= - \int \frac{d^D q}{(2\pi)^D} \mu_R^{2\varepsilon} \text{Tr} \left\{ \left[g_s f^{bde} \gamma^\nu \right] i \frac{\not{q} + m_{\bar{g}}}{q^2 - m_{\bar{g}}^2} \left[g_s f^{cef} \gamma^\rho \right] i \frac{\not{q} + \not{p}_1 + \not{p}_2 + m_{\bar{g}}}{(q+p_1+p_2)^2 - m_{\bar{g}}^2} \left[g_s f^{afd} \gamma^\mu \right] i \frac{\not{q} + \not{p}_2 + m_{\bar{g}}}{(q+p_2)^2 - m_{\bar{g}}^2} \right\} \\ &= - \frac{g_s^3 n_c}{32\pi^2} f^{abc} \left\{ \text{Tr} \left\{ \gamma^\nu \gamma^\alpha \gamma^\rho \gamma^\beta \gamma^\mu \gamma^\delta \right\} \left[C_{\alpha\beta\delta} + (p_1 + p_2)_\beta C_{\alpha\delta} + p_{2\delta} C_{\alpha\beta} + (p_1 + p_2)_\beta p_{2\delta} C_\alpha \right] \right. \\ &\quad \left. + m_{\bar{g}}^2 \left[\text{Tr} \left\{ \gamma^\nu \gamma^\rho \gamma^\mu \gamma^\alpha \right\} \left[C_\alpha + p_{2\alpha} C_0 \right] + \text{Tr} \left\{ \gamma^\nu \gamma^\rho \gamma^\alpha \gamma^\mu \right\} \left[C_\alpha + (p_1 + p_2)_\alpha C_0 \right] + \text{Tr} \left\{ \gamma^\nu \gamma^\alpha \gamma^\rho \gamma^\mu \right\} C_\alpha \right] \right\} , \end{aligned}$$

where the arguments of the loop-integrals read

$$V_{ggg}^{(\bar{g}\bar{g}\bar{g})} : C_{\{0,\mu,\mu\nu,\mu\nu\rho\}} \leftrightarrow C_{\{0,\mu,\mu\nu,\mu\nu\rho\}}(p_2^2, p_1^2, m_{\bar{g}}^2, m_{\bar{g}}^2, m_{\bar{g}}^2) . \quad (5.95)$$

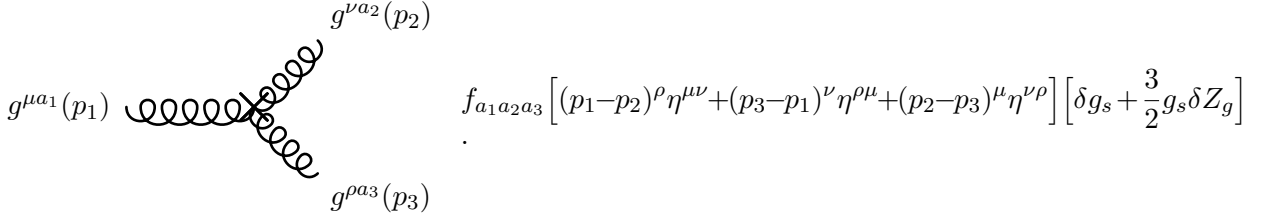


Figure 5.16: Feynman rule of the triple gluon vertex counter-term. All four-momenta are taken incoming to the vertex, and are denoted by p_1 , p_2 and p_3 . The indices a_1 , a_2 and a_3 are adjoint color indices.

We now turn to the calculation of the bubble diagrams included in Fig. 5.15, using the Feynman rules of Appendix F. The amplitude associated to the first diagram (third line of Fig. 5.15) reads

$$\begin{aligned} V_{ggg}^{(gg1)} &= \frac{1}{2} \int \frac{d^D q}{(2\pi)^D} \mu_R^{2\epsilon} g_s f^{abd} \left[-(2p_2 + q)^\alpha \eta^{\beta\nu} + (2q + p_2)^\nu \eta^{\alpha\beta} + (p_2 - q)^\beta \eta^{\alpha\nu} \right] \frac{-i}{q^2} \frac{-i}{(q + p_2)^2} \times i g_s^2 \\ &\quad \left[\delta^\mu_\alpha \delta^\rho_\beta [f^{acf} f^{edf} + f^{aef} f^{cdf}] + \eta^{\mu\nu} \eta_{\alpha\beta} [f^{adf} f^{ecf} - f^{aef} f^{cdf}] + \delta^\mu_\beta \delta^\rho_\alpha [-f^{adf} f^{ecf} - f^{acf} f^{edf}] \right] \\ &= \frac{9n_c g_s^3}{64\pi^2} f^{abc} \left[p_2^\rho \eta^{\mu\nu} - p_2^\mu \eta^{\nu\rho} \right] B_0(p_2^2, 0, 0), \end{aligned}$$

while those associated to the second and third diagrams (last line of Fig. 5.15) are obtained by symmetry,

$$\begin{aligned} V_{ggg}^{(gg2)} &= \frac{9n_c g_s^3}{64\pi^2} f^{abc} \left[p_3^\mu \eta^{\rho\nu} - p_3^\nu \eta^{\mu\rho} \right] B_0(p_3^2, 0, 0), \\ V_{ggg}^{(gg3)} &= \frac{9n_c g_s^3}{64\pi^2} f^{abc} \left[p_1^\nu \eta^{\rho\mu} - p_1^\rho \eta^{\mu\nu} \right] B_0(p_1^2, 0, 0). \end{aligned}$$

Summing up all the contribution, the ultraviolet-divergent piece of the one-loop corrections to the triple gluon vertex is given by

$$\begin{aligned} \text{UV}[V_{ggg}] &= \text{UV} \left[V_{ggg}^{(qqq)} + V_{ggg}^{(\bar{q}\bar{q}\bar{q})} + V_{ggg}^{(ggg)} - V_{ggg}^{(u_g u_g u_g)} + V_{ggg}^{(\bar{g}\bar{g}\bar{g})} + V_{ggg}^{(gg2)} + V_{ggg}^{(gg3)} + V_{ggg}^{(gg3)} \right] \\ &= \frac{g_s^3}{32\pi^2} f^{abc} \left[(p_1 - p_2)^\rho \eta^{\mu\nu} + (p_3 - p_1)^\nu \eta^{\rho\mu} + (p_2 - p_3)^\mu \eta^{\nu\rho} \right] \frac{1}{\epsilon} [2n_f + 2]. \end{aligned} \quad (5.96)$$

As explained in Section 4.5, the renormalizability of a theory requires that UV-divergences originating from loops cancel against those coming from the counter-terms. In the case of our interest, the counter-term we need is obtained from the tree-level Lagrangian (5.91) by means of multiplicative renormalization, and according to Fig. 5.16 reads as follows,

$$\begin{aligned} V_{ggg}^{(x)} &= f^{abc} \left[(p_1 - p_2)^\rho \eta^{\mu\nu} + (p_3 - p_1)^\nu \eta^{\rho\mu} + (p_2 - p_3)^\mu \eta^{\nu\rho} \right] \left[\delta g_s + \frac{3}{2} g_s \delta Z_g \right] \\ &= -\frac{g_s^3}{32\pi^2} f^{abc} \left[(p_1 - p_2)^\rho \eta^{\mu\nu} + (p_3 - p_1)^\nu \eta^{\rho\mu} + (p_2 - p_3)^\mu \eta^{\nu\rho} \right] \times \left[\frac{2n_f + 2}{\epsilon} \right. \\ &\quad \left. + \frac{n_c}{3} \log \frac{m_g^2}{\mu_R^2} + \frac{1}{12} \sum_{\tilde{q}_i} \log \frac{m_{\tilde{q}_i}^2}{\mu_R^2} + \frac{1}{3} \log \frac{m_t^2}{\mu_R^2} \right], \end{aligned} \quad (5.97)$$

where we have used the results of (5.33) and (5.70) to derive the analytical expression of $V_{ggg}^{(x)}$. Comparing $\text{UV}[V_{ggg}]$, and $V_{ggg}^{(x)}$, we conclude that the renormalized vertex is UV-finite, .

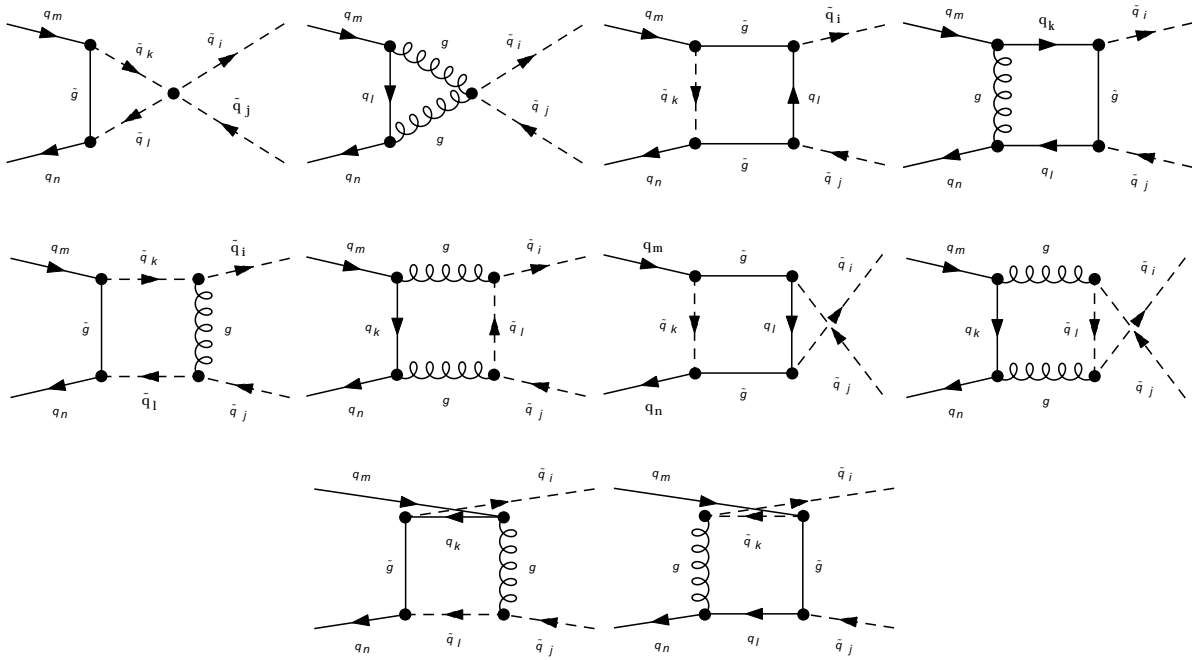


Figure 5.17: The ten box diagrams contributing to the quark-antiquark channel. The flavour indices of the external quarks and squarks are respectively denoted by m, n , and i, j , while k , and l correspond to the flavour indices of the virtual particles.

Comments

In the calculations we have presented so far, we have neither mentioned the ghosts WFRC, nor the corrections to the gluon-ghost-ghost vertex. This omission is due to the fact that, in practice, we have used the FEYNARTS/FORMCALC framework to perform all the one-loop calculations detailed above. More specifically, if in FEYNARTS/FORMCALC internal gluons are chosen to be in the Feynman gauge (which requires the presence of ghosts to cancel unphysical polarization modes of the gluons), external gluons are on the other hand treated in the axial gauge. In FEYNARTS/FORMCALC, ghosts can therefore appear inside loops, but can never be on external legs, which is why they do not need to be renormalized.

In addition, note that in the present section, we have also voluntarily omitted the corrections to the gluon-gluon-squark-antisquark vertex, because those are conventionally included into the box diagram contributions in FEYNARTS/FORMCALC which are discussed just below.

5.6 Box contributions

The last remaining one-loop diagrams that we need to include into our calculations are the four-point diagrams, also referred to as box diagrams. There are 42 of them in total, out of which 10 contribute to the quark-antiquark channel (see Fig. 5.17), and 32 contribute to the gluon channel (see Figs. 5.18 and 5.19). The calculation of the box contributions involves rather large expressions, which is why they are not detailed in the present manuscript. A few qualitative remarks can however be made concerning those box diagrams. First of all, box diagrams contain infrared divergences, just like the self-energies and the vertex corrections, and according to the KLN theorem, those divergences, but the simple collinear poles of the initial state, are expected to cancel against the IR divergences originating from the real contributions. Second, the ten box diagrams of the quark-antiquark channel are in principle UV-finite, because

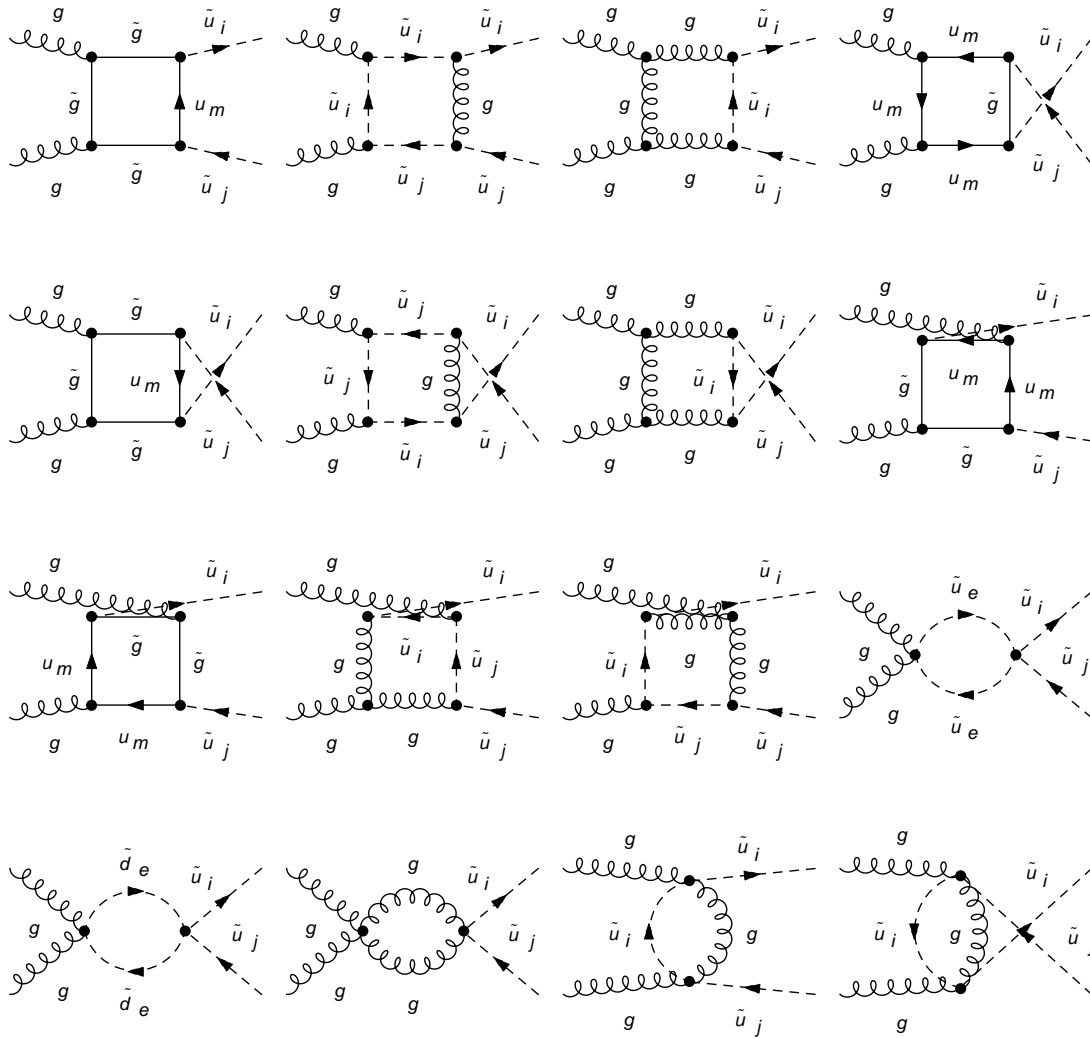


Figure 5.19: Second set of box diagrams contributing to the gluon-gluon channel. The flavour indices of the external squarks are denoted by i, j , while k, l correspond to the flavour indices of the virtual particles.

two independent FEYNARTS tree-level model files. The first one being the FVMSSM model file, directly provided by FEYNARTS, while the second was generated by means of FEYNRULES. The analytical results obtain with both model files perfectly agree.

After the implementation of a model file containing the vertices of the counter-term Lagrangian, and the definition of the renormalization constants, we have explicitly checked the UV-finiteness of the virtual contribution. At present, we are at the level of checking the infrared finiteness of the NLO corrections, and have implemented for the process of our interest the procedure of mass factorization, in a MATHEMATICA notebook, in order to subtract the remaining collinear poles of the initial state that can be absorbed into the redefinition of the parton distributions at next-to-leading order.

Chapter 6

Matching NLO predictions with parton showers

Fixed-order calculations, such as the one discussed in the previous chapter, involve, in most cases, due to the complexity of the calculations, only a limited number of particles in the final-state, in contrast to what we observe experimentally, and are only valid when partons are hard and well-separated. In order to account for a more realistic final-state, and to resum large logarithms arising from soft/collinear regions of the phase-space, one usually adopts the Parton Shower (PS) approach, which consists in using the collinear factorization approximation to decompose the amplitude of a process with $n + 1$ particles in the final-state, into a n partons final-state multiplied by the Altarelli-Parisi splitting kernels¹. In the PS approach, the successive emission of two partons is completely decorrelated, and can be interpreted as a Markovian process². More details on Parton Shower algorithms, and their implementation into Shower Monte-Carlo (SMC) programs can be found in [224], and references therein.

Fixed-order calculations, and parton showers are complementary approaches, and combining them is the purpose of the so-called matching procedure. At next-to-leading order, this matching procedure exhibits a double-counting problem³, which can fortunately be evaded by means of the MC@NLO [225], and POWHEG [226] methods. In this chapter, we choose to use the first method, implemented in the context of the MADGRAPH5_aMC@NLO framework, and present for the first time the full automation of collider predictions matched to parton showers at the next-to-leading accuracy in QCD within non-trivial extensions of the standard model. As an application, we explore scenarios beyond the standard model where new coloured scalar and Majorana particles are pair-produced. This work is not related to the previous chapter.

This chapter is organized as follows: in Section 6.1 we present our results for stop and sgluon pair production at next-to-leading order in SUSY-QCD, matched with parton shower. In Section 6.2 we present our results obtained for gluino pair-production at NLO in SUSY-QCD matched with PS, in a scenario where all the squarks, but the stops, are mass degenerate, and where the latter are decoupled so that no on-shell subtraction is required for the real contribution.

6.1 Coloured scalar pair production

Motivated by the conceptual issues accompanying the Standard Model, many new physics theories have been developed over the last decades. Most of them exhibit an extended coloured

¹Assuming that only two of the $n + 1$ partons are collinear one to another

²The probability of not emitting a parton between two given scales corresponds to the so-called Sudakov form factor.

³Parton showers include approximate real corrections in the soft/collinear limit.

sector, and related new phenomena are expected to be observable at high-energy hadron colliders such as the LHC. In particular, effects induced by hypothetical coloured scalar particles have received special attention from both the ATLAS and CMS collaborations. Many LHC analyses are indeed seeking for the scalar partners of the Standard Model quarks (the squarks) and gluons (the sgluons) that are predicted, for instance, in minimal [44, 116] and non-minimal [227, 228] supersymmetric or in vector-like confining theories [229].

In this context, it is clear that an approach to precision predictions that is fully general in any considered theory is highly desirable, and the MADGRAPH5_aMC@NLO framework [230] is in a prime position to provide it. Its structure for tackling leading-order (LO) computations has indeed already proved to be very efficient at satisfying the needs of both the theoretical and experimental high energy physics communities. Generalizing this flexibility to the next-to-leading order (NLO) case is however not straightforward, essentially because of the necessity of specifying model-dependent counter-terms, including those arising from the renormalization of the Lagrangian. Recent developments [231] in the FEYNRULES package [232] have allowed to overcome this main obstacle and paved the way to the full automation of NLO QCD predictions matched to parton showers for generic theories.

We describe the details of this implementation by working through two specific cases and revisit some LHC phenomenology associated with stops and sgluons in the context of simplified models of new physics [233, 234]. Employing state-of-the-art simulation techniques, we match NLO-QCD matrix elements to parton showers and present precision predictions for several kinematical observables after considering both the production and the decay of the new particles. In more detail, we make use of FEYNRULES to implement all possible couplings of the new fields to quarks and gluons and employ the NLOCT program [231] to generate a UFO module [235] containing, in addition to tree-level model information, the ultraviolet and R_2 counter-terms necessary whenever the loop integral numerators are computed in four dimensions, as in MADLOOP [236] that uses the Ossola-Papadopoulos-Pittau (OPP) reduction formalism [237]. This UFO library is then linked to the MADGRAPH5_aMC@NLO framework which is used, for the first time, for predictions in the context of new physics models featuring an extended coloured sector. We focus in this chapter on the pair production of those new heavy states at NLO in QCD. Their decay is then taken into account separately, at the leading order and with the spin information retained, by means of the MADSPIN [238] and MADWIDTH [239] programs.

In the rest of this section, we define the simplified models describing stop/sgluon dynamics, and detail the renormalization of the effective Lagrangians, and the validation of the UFO models generated by NLOCT. Our results follow, and consist of total rates and differential distributions illustrating some kinematical properties of the produced new states and their decay products.

Benchmark scenarios for stop hadroproduction

Following a simplified model approach, we extend the Standard Model by a complex scalar field σ_3 (a stop) of mass m_3 . This field lies in the fundamental representation of $SU(3)_c$, so that its strong interactions are standard and embedded into $SU(3)_c$ -covariant derivatives. We enable the stop to decay via a coupling to a single top quark and a gauge-singlet Majorana fermion χ of mass m_χ that can be identified with a bino in complete supersymmetric models. Finally, despite of being allowed by gauge invariance, the single stop couplings to down-type quarks, as predicted in R -parity violating supersymmetry, are ignored for simplicity. We model all considered interactions by the Lagrangian

$$\mathcal{L}_3 = D_\mu \sigma_3^\dagger D^\mu \sigma_3 - m_3^2 \sigma_3^\dagger \sigma_3 + \frac{i}{2} \bar{\chi} \not{\partial} \chi - \frac{1}{2} m_\chi \bar{\chi} \chi + \left[\sigma_3 \bar{t} (\tilde{g}_L P_L + \tilde{g}_R P_R) \chi + \text{h.c.} \right], \quad (6.1)$$

where we denote the strengths of the stop couplings to the fermion χ by \tilde{g} , and where $P_{L,R}$ are the usual left- and right-handed projectors.

Aiming to precision predictions at the NLO accuracy, a renormalization procedure is required in order to absorb all ultraviolet divergences yielded by virtual loop-diagrams. This is achieved through counter-terms that are derived from the tree-level Lagrangian by replacing all bare fields (generically denoted by Ψ) and parameters (generically denoted by A) by

$$\Psi \rightarrow Z_\Psi^{1/2} \Psi \approx \left[1 + \frac{1}{2} \delta Z_\Psi\right] \Psi \quad \text{and} \quad A \rightarrow A + \delta Z_A, \quad (6.2)$$

where the renormalization constants δZ are restricted in our case to QCD contributions at the first order in the strong coupling α_s . Like in usual supersymmetric setups, the \tilde{g} couplings are of a non-QCD nature so that our simplified model does not feature new strong interactions involving quarks. The wave-function renormalization constant of the latter is therefore unchanged with respect to the Standard Model, contrary to the one of the gluon that must appropriately compensate stop-induced contributions. Adopting the on-shell renormalization scheme, the gluon and stop wave-function (δZ_g and δZ_{σ_3}) and mass (δm_3^2) renormalization constants read

$$\delta Z_g = \delta Z_g^{(SM)} - \frac{g_s^2}{96\pi^2} \left[\frac{1}{\bar{\epsilon}} - \log \frac{m_3^2}{\mu_R^2} \right], \quad \delta Z_{\sigma_3} = 0, \quad (6.3)$$

$$\delta m_3^2 = -\frac{g_s^2 m_3^2}{12\pi^2} \left[\frac{3}{\bar{\epsilon}} + 7 - 3 \log \frac{m_3^2}{\mu_R^2} \right], \quad (6.4)$$

where $\delta Z_g^{(SM)}$ collects the Standard Model components of δZ_g . Moreover, we denote the renormalization scale by μ_R and following standard conventions, the ultraviolet divergent parts of the renormalization constants are written in terms of the quantity $1/\bar{\epsilon} = 1/\epsilon - \gamma_E + \log 4\pi$ where γ_E is the Euler-Mascheroni constant, and ϵ is the regulator of DREG

The renormalization of the strong coupling is achieved by subtracting, at zero-momentum transfer, all heavy particle contributions from the gluon self-energy. This ensures that the running of α_s solely originates from $n_f = 5$ flavors of light quarks and gluons, and any effect induced by the massive top and stop fields is decoupled and absorbed into the renormalization constant of α_s ,

$$\frac{\delta \alpha_s}{\alpha_s} = \frac{\alpha_s}{2\pi\bar{\epsilon}} \left[\frac{n_f}{3} - \frac{11}{2} \right] + \frac{\alpha_s}{6\pi} \left[\frac{1}{\bar{\epsilon}} - \log \frac{m_t^2}{\mu_R^2} \right] + \frac{\alpha_s}{24\pi} \left[\frac{1}{\bar{\epsilon}} - \log \frac{m_3^2}{\mu_R^2} \right]. \quad (6.5)$$

All loop-calculations achieved in this work rely on the OPP formalism. It is based on the decomposition of any loop amplitude in both cut-constructible and rational elements, the latter being related to the ϵ -pieces of the loop-integral denominators (R_1) and numerators (R_2). For any renormalizable theory, there is a finite number of R_2 terms, and they all involve interactions with at most four external legs that can be seen as counter-terms derived from the tree-level Lagrangian [240]. Considering corrections at the first order in QCD, the σ_3 -field induces three additional R_2 counter-terms with respect to the Standard Model case,

$$R_2^{\sigma_3^\dagger \sigma_3} = \frac{ig_s^2}{72\pi^2} \delta_{c_1 c_2} [3m_3^2 - p^2], \quad R_2^{g\sigma_3^\dagger \sigma_3} = \frac{53ig_s^3}{576\pi^2} T_{c_2 c_3}^{a_1} (p_2 - p_3)^{\mu_1}, \quad (6.6)$$

$$R_2^{gg\sigma_3^\dagger \sigma_3} = \frac{ig_s^4}{1152\pi^2} \eta^{\mu_1 \mu_2} [3\delta^{a_1 a_2} - 187\{T^{a_1}, T^{a_2}\}]_{c_3 c_4},$$

where c_i , μ_i , and p_i indicate the color index, Lorentz index, and the four-momentum of the i^{th} particle incoming to the $R_2^{i \dots}$ vertex, respectively. Moreover, the matrices T denote fundamental representation matrices of $SU(3)$.

m_3 [GeV]	8 TeV	
	σ^{LO} [pb]	σ^{NLO} [pb]
100	$389.3^{+34.2\%}_{-23.9\%}$	$554.8^{+14.9\%+1.6\%}_{-13.5\%-1.6\%}$
250	$4.118^{+40.4\%}_{-27.2\%}$	$5.503^{+13.1\%+3.7\%}_{-13.7\%-3.7\%}$
500	$(6.594 \times 10^{-2})^{+45.5\%}_{-29.1\%}$	$(7.764 \times 10^{-2})^{+12.1\%+6.7\%}_{-14.1\%-6.7\%}$
750	$(3.504 \times 10^{-3})^{+48.8\%}_{-30.5\%}$	$(3.699 \times 10^{-3})^{+12.3\%+10.2\%}_{-14.6\%-10.2\%}$
1000	$(2.875 \times 10^{-4})^{+51.5\%}_{-31.5\%}$	$(2.775 \times 10^{-4})^{+13.1\%+15.5\%}_{-15.2\%-15.5\%}$

Table 6.1: Total cross sections for stop pair production at the LHC, running at $\sqrt{s} = 8$ TeV. Results are presented together with the associated scale and PDF (not shown for the LO case) uncertainties. Monte Carlo errors are of about 0.2-0.3% and omitted.

m_3 [GeV]	13 TeV	
	σ^{LO} [pb]	σ^{NLO} [pb]
100	$1066^{+29.1\%}_{-21.4\%}$	$1497^{+14.1\%+1.2\%}_{-12.1\%-1.2\%}$
250	$15.53^{+35.2\%}_{-24.8\%}$	$21.56^{+12.1\%+2.4\%}_{-12.3\%-2.4\%}$
500	$0.3890^{+39.6\%}_{-26.4\%}$	$0.5062^{+11.2\%+4.4\%}_{-12.8\%-4.4\%}$
750	$(3.306 \times 10^{-2})^{+41.8\%}_{-27.5\%}$	$(4.001 \times 10^{-2})^{+10.8\%+6.1\%}_{-12.9\%-6.1\%}$
1000	$(4.614 \times 10^{-3})^{+43.6\%}_{-28.3\%}$	$(5.219 \times 10^{-3})^{+10.9\%+7.9\%}_{-13.2\%-7.9\%}$

Table 6.2: Same as Tab. 6.1 but for $\sqrt{s} = 13$ TeV.

Contrary to complete supersymmetric scenarios, the \tilde{g} operators present a non-trivial one-loop ultraviolet behaviour that is not compensated by effects of other fields such as gluinos. Since we focus on QCD NLO corrections to the strong production of a pair of σ_3 fields followed by their LO decays, the related counter-terms are therefore omitted from this document.

Our stop simplified model has been implemented in FEYNRULES, and we have employed the NLOCT package to automatically generate all QCD ultraviolet and R_2 counter-terms (including the Standard Model ones). The output has been validated against our analytical calculations, which constitutes a validation of the handling of new massive colored states by NLOCT. Finally, the analytical results have been exported to a UFO module that we have imported into MADGRAPH5_aMC@NLO. For our numerical analysis, we consider scenarios where m_3 and m_χ are kept free. The $\tilde{g}_{L,R}$ parameters are fixed to typical values for supersymmetric models featuring a bino-like neutralino and a maximally-mixing top squark,

$$\tilde{g}_L = 0.25 \quad \text{and} \quad \tilde{g}_R = 0.06 . \quad (6.7)$$

Benchmark scenarios for sgluon hadroproduction

We construct a simplified model describing sgluon dynamics by supplementing the Standard Model with a real scalar field σ_8 (a sgluon) of mass m_8 lying in the adjoint representation of the QCD gauge group. Its strong interactions are described by gauge-covariant kinetic terms and we enable single sgluon couplings to quarks and gluons, like in complete models where such interactions are loop-induced. The corresponding effective Lagrangian reads

$$\mathcal{L}_8 = \frac{1}{2} D_\mu \sigma_8 D^\mu \sigma_8 - \frac{1}{2} m_8^2 \sigma_8 \sigma_8 + \frac{\hat{g}}{\Lambda} \sigma_8 G_{\mu\nu} G^{\mu\nu} + \sum_{q=u,d} \left[\sigma_8 \bar{q} (\hat{g}_q^L P_L + \hat{g}_q^R P_R) q + \text{h.c.} \right] , \quad (6.8)$$

where $G^{\mu\nu}$ refers to the gluon field strength tensor and the single sgluon interaction strengths are denoted by \hat{g} . Although the \hat{g} operators induce single sgluon production, we ignore it in this

m_8 [GeV]	8 TeV	
	σ^{LO} [pb]	σ^{NLO} [pb]
100	$3854^{+34.4\%}_{-24.1\%}$	$5573^{+14.9\%+1.6\%}_{-13.6\%-1.6\%}$
250	$38.89^{+41.3\%}_{-27.7\%}$	$54.32^{+14.5\%+3.9\%}_{-14.6\%-3.9\%}$
500	$0.5878^{+47.6\%}_{-30.0\%}$	$0.7431^{+15.8\%+7.6\%}_{-16.2\%-7.6\%}$
750	$(2.977 \times 10^{-2})^{+52.0\%}_{-31.9\%}$	$(3.353 \times 10^{-2})^{+17.2\%+12.1\%}_{-17.3\%-12.1\%}$
1000	$(2.328 \times 10^{-3})^{+55.9\%}_{-33.4\%}$	$(2.398 \times 10^{-3})^{+19.0\%+19.1\%}_{-18.4\%-19.1\%}$

Table 6.3: Total cross sections for sgluon pair production at the LHC, running at $\sqrt{s} = 8$ TeV. Results are presented together with the associated scale and PDF (not shown for the LO case) uncertainties. Monte Carlo errors are of about 0.2-0.3% and omitted.

m_8 [GeV]	13 TeV	
	σ^{LO} [pb]	σ^{NLO} [pb]
100	$10560^{+29.2\%}_{-21.5\%}$	$14700^{+13.6\%+1.2\%}_{-11.9\%-1.2\%}$
250	$150.4^{+35.7\%}_{-25.1\%}$	$214.5^{+12.9\%+2.5\%}_{-12.9\%-2.5\%}$
500	$3.619^{+40.8\%}_{-27.0\%}$	$4.977^{+13.3\%+4.7\%}_{-14.1\%-4.7\%}$
750	$0.2951^{+43.6\%}_{-28.4\%}$	$0.3817^{+14.0\%+6.9\%}_{-14.8\%-6.9\%}$
1000	$(3.983 \times 10^{-2})^{+46.1\%}_{-29.5\%}$	$(4.822 \times 10^{-2})^{+15.1\%+9.3\%}_{-15.6\%-9.3\%}$

Table 6.4: Same as Tab. 6.3 but for $\sqrt{s} = 13$ TeV.

work since the presence of a *complete* basis of dimension-five operators at tree-level is required to guarantee the cancellation, after renormalization, of all loop-induced ultraviolet divergences. We postpone the associated study to a future work. The \hat{g} couplings being technically of higher-order in QCD (as in complete theories), the quark fields are renormalized like in the Standard Model. In contrast, the sgluon QCD interactions induce a modification of the on-shell gluon wave-function renormalization constant δZ_g and yield non-vanishing on-shell sgluon wave-function (δZ_{σ_8}) and mass (δm_8^2) renormalization constants,

$$\begin{aligned} \delta Z_g &= \delta Z_g^{(SM)} - \frac{g_s^2}{32\pi^2} \left[\frac{1}{\bar{\epsilon}} - \log \frac{m_8^2}{\mu_R^2} \right], & \delta Z_{\sigma_8} &= 0, \\ \delta m_8^2 &= -\frac{3g_s^2 m_8^2}{16\pi^2} \left[\frac{3}{\bar{\epsilon}} + 7 - 3 \log \frac{m_8^2}{\mu_R^2} \right]. \end{aligned} \quad (6.9)$$

Sgluon effects are also subtracted, at zero-momentum transfer, from the gluon self-energy and absorbed in the renormalization of the strong coupling,

$$\frac{\delta \alpha_s}{\alpha_s} = \frac{\alpha_s}{2\pi\bar{\epsilon}} \left[\frac{n_f}{3} - \frac{11}{2} \right] + \frac{\alpha_s}{6\pi} \left[\frac{1}{\bar{\epsilon}} - \log \frac{m_t^2}{\mu_R^2} \right] + \frac{\alpha_s}{8\pi} \left[\frac{1}{\bar{\epsilon}} - \log \frac{m_8^2}{\mu_R^2} \right]. \quad (6.10)$$

They finally induce new R_2 counter-terms,

$$R_2^{\sigma_8\sigma_8} = \frac{ig_s^2}{32\pi^2} \delta_{a_1 a_2} [3m_8^2 - p^2], \quad R_2^{g\sigma_8\sigma_8} = \frac{7g_s^3}{64\pi^2} f_{a_1 a_2 a_3} (p_2 - p_3)^{\mu_1}, \quad (6.11)$$

$$R_2^{gg\sigma_8\sigma_8} = \frac{ig_s^4}{384\pi^2} \eta^{\mu_1 \mu_2} \left[72(d_{a_1 a_4 e} d_{a_2 a_3 e} + d_{a_1 a_3 e} d_{a_2 a_4 e}) - 141d_{a_1 a_2 e} d_{a_3 a_4 e} \right. \quad (6.12)$$

$$\left. - 92\delta_{a_1 a_2} \delta_{a_3 a_4} + 50(\delta_{a_1 a_3} \delta_{a_2 a_4} + \delta_{a_1 a_4} \delta_{a_2 a_3}) \right], \quad (6.13)$$

in the same notations as in the previous section.

We have implemented the sgluon simplified model in FEYNRULES and generated a UFO model that we have linked to MADGRAPH5_aMC@NLO by means of the NLOCT package. The generated model has then been validated analytically against the above results. Our numerical study relies on benchmark scenarios inspired by an R -symmetric supersymmetric setup with non-minimal flavor violation in the squark sector [241], in which the only non-vanishing coupling parameters are fixed to

$$\begin{aligned} \frac{\hat{g}_g}{\Lambda} &= 1.5 \cdot 10^{-6} \text{ GeV}^{-1} , \\ (\hat{g}_u^{L,R})_{3i} &= (\hat{g}_u^{L,R})_{i3} = 3 \cdot 10^{-3} \quad \forall i = 1, 2, 3 . \end{aligned} \tag{6.14}$$

LHC phenomenology

In Tabs. 6.1, 6.2, 6.3, and 6.4, we provide stop and sgluon pair production cross sections for LHC collisions at center-of-mass energies of $\sqrt{s} = 8$ and 13 TeV and for different mass choices. The results are evaluated both at the LO and NLO accuracy, and presented together with the associated theoretical uncertainties. For the central values, we have fixed the renormalization and factorization scales to the stop/sgluon mass and used the NNPDF 2.3 parton distributions [136]. Scale uncertainties have been derived by varying both scales by a factor of two up and down, and the parton distribution uncertainties have been extracted from the cross section values spanned by the NNPDF density replica.

The results of Tabs. 6.1, 6.2, 6.3, and 6.4 have been confronted to predictions obtained with the public packages PROSPINO [188] (stop pair production) and MADGOLEM [242] (sgluon pair production). Stop-pair total production rates have been found to agree at the level of the numerical integration error, while virtual and real contributions to sgluon-pair production are agreeing separately at the amplitude level. We have additionally performed independent calculations of the loop contributions based on FEYNARTS [147], that we have found to agree with our predictions. Realistic descriptions of LHC collisions require to match hard scattering matrix elements to a modeling of QCD environment. To this aim, we make use of the MC@NLO method [243] as implemented in MADGRAPH5_aMC@NLO. We match in this way the hard scattering process to the PYTHIA 8 parton showering and hadronization [244], after employing the MADSPIN and MADWIDTH programs to handle stop and sgluon decays. Jet reconstruction is then performed by means of the anti- k_T algorithm with a radius parameter set to 0.4 [245], as included in the FASTJET program [246], and events are finally analyzed with the MADANALYSIS 5 package [247]. Normalizing the results to an integrated luminosity of 100 fb^{-1} , we present, in Fig. 6.1, the distribution of a key observable for stop searches, namely the missing transverse energy. We show LO and NLO predictions for 13 TeV collisions as calculated by MADGRAPH5_aMC@NLO in the context of three benchmark scenarios for which $(m_3, m_\chi) = (500, 50) \text{ GeV}$ (red), $(1000, 50) \text{ GeV}$ (green) and $(500, 200) \text{ GeV}$ (blue). Similarly, we describe the hadronic activity H_T associated with the production of a sgluon pair in Fig. 6.2 in the case of a sgluon mass of 500 GeV (red) and 1000 GeV (green)⁴.

Summary

In this section, we have demonstrated that a joint use of the FEYNRULES, NLOCT and MADGRAPH5_aMC@NLO programs enables the full automation of the Monte Carlo simulations of high-energy physics collisions at the next-to-leading order accuracy in QCD and for non-trivial

⁴With the current level of precision of the experimental searches, the current limits on the stop and sgluon masses, that are extracted on the basis of NLO total rates but LO simulations for the distributions, can be assumed to hold. Evaluating the NLO effects on the shapes and how this translates in terms of a modification of the limits goes beyond the scope of this work.

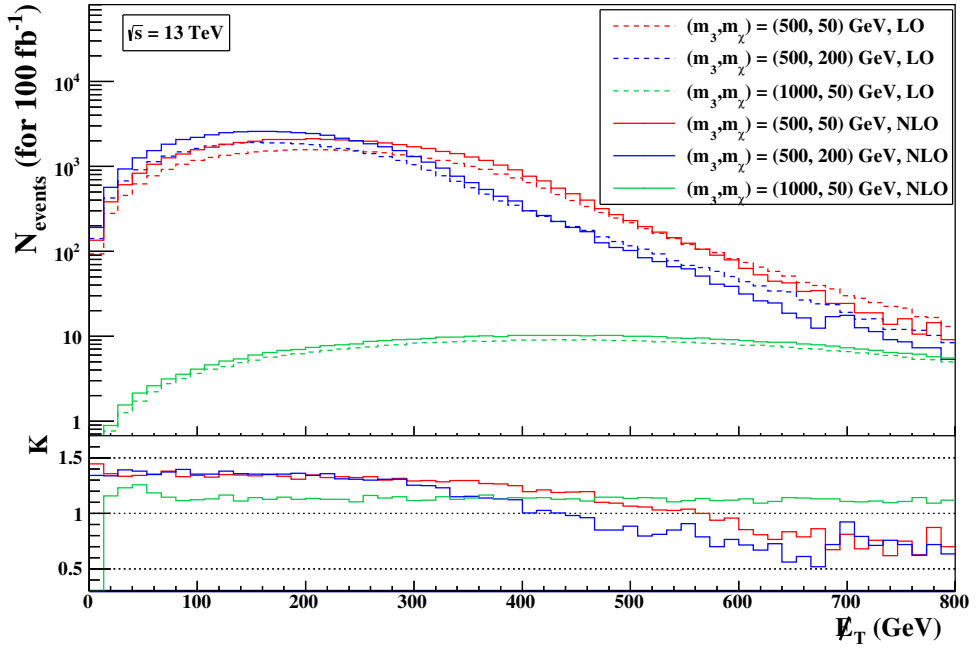


Figure 6.1: Missing transverse energy spectrum for a stop pair production and decay signal. We consider several mass setups and show results at the NLO and LO accuracy (upper panel), together with their bin-by-bin ratio (lower panel).

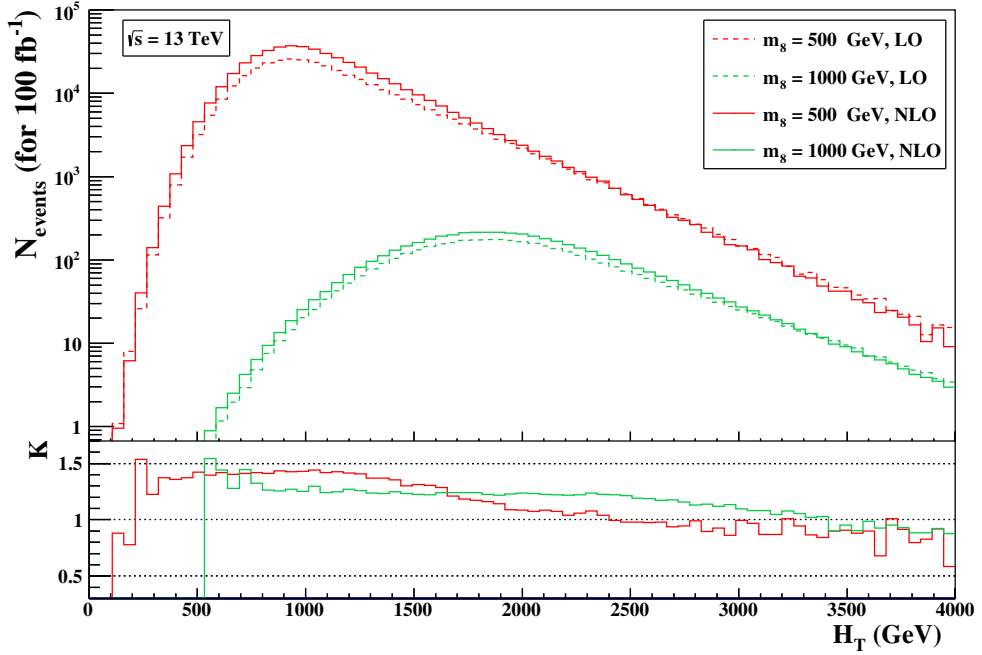


Figure 6.2: Same as Fig. 6.1 for the H_T spectrum of sgluon signals.

extensions of the Standard Model. This has been illustrated with simplified models such as those used for supersymmetry searches at the LHC. In this context, we have adopted setups that exhibit extra coloured particles and non-usual interaction structures and presented the analysis of two exemplary signals with the automated tool MADANALYSIS 5.

In the aim of an embedding within experimental software, we have designed a webpage

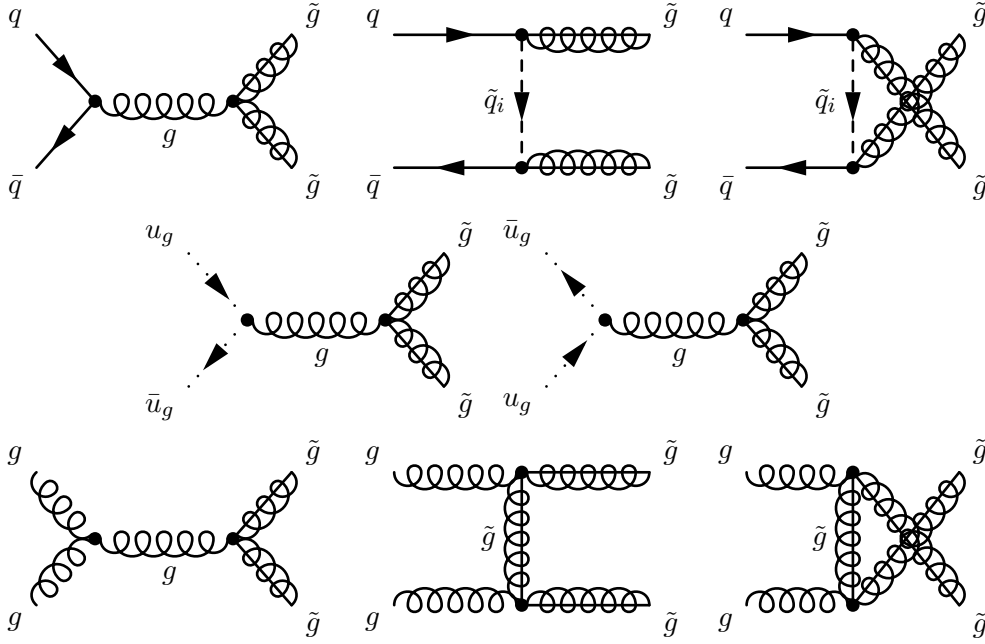


Figure 6.3: Tree-level Feynman diagrams for the production of a pair of gluinos in quark-antiquark (top) and gluon-gluon collisions (bottom). Ghost contributions, mandatory for calculations performed in Feynman gauge, are also shown (middle).

<http://feynrules.irmp.ucl.ac.be/wiki/NLOModels>, where hundreds of differential distributions are available for validation purposes, together with the associated FEYNRULES and UFO models.

6.2 Gluino pair production

In this last section, we match for the first time NLO QCD matrix-element-based predictions to parton showers for gluino pair-production. Virtual contributions are evaluated following the Ossola-Papadopoulos-Pittau (OPP) formalism as implemented in MADLOOP [236,237], and combined with real emission contributions by means of the FKS subtraction method as embedded in MADFKS [248,249]; these two modules being fully incorporated in MADGRAPH5_aMC@NLO. The matching to parton showers is then achieved by employing the MC@NLO method [243]. After accounting for (LO) gluino decays, we study the impact of both the NLO contributions and the parton showers in the context of LHC physics.

Theoretical framework

Our study of gluino pair-production and decay is based on an MSSM-inspired simplified model. We complement the Standard Model with three generations of non-mixing left-handed and right-handed squark fields $\tilde{q}_{L,R}$ of mass $m_{\tilde{q}_{L,R}}$ and with a Majorana fermionic gluino field \tilde{g} of mass $m_{\tilde{g}}$. The dynamics of the new fields is described by the following Lagrangian,

$$\begin{aligned} \mathcal{L}_{\text{SQCD}} = & D_\mu \tilde{q}_L^\dagger D^\mu \tilde{q}_L + D_\mu \tilde{q}_R^\dagger D^\mu \tilde{q}_R + \frac{i}{2} \tilde{g} \not{D} \tilde{g} - m_{\tilde{q}_L}^2 \tilde{q}_L^\dagger \tilde{q}_L - m_{\tilde{q}_R}^2 \tilde{q}_R^\dagger \tilde{q}_R - \frac{1}{2} m_{\tilde{g}} \tilde{g} \tilde{g} \\ & + \sqrt{2} g_s \left[-\tilde{q}_L^\dagger T(\tilde{g} P_L q) + (\tilde{q} P_L \tilde{g}) T \tilde{q}_R + \text{h.c.} \right] - \frac{g_s^2}{2} \left[\tilde{q}_R^\dagger T \tilde{q}_R - \tilde{q}_L^\dagger T \tilde{q}_L \right] \left[\tilde{q}_R^\dagger T \tilde{q}_R - \tilde{q}_L^\dagger T \tilde{q}_L \right], \end{aligned} \quad (6.15)$$

$m_{\tilde{g}}$ [GeV]	σ^{LO} [pb]	σ^{NLO} [pb]
200	2104 ^{+30.3%+14.0%} _{-21.9%-14.0%}	3183 ^{+10.8%+1.8%} _{-11.6%-1.8%}
500	15.46 ^{+34.7%+19.5%} _{-24.1%-19.5%}	24.90 ^{+12.5%+3.7%} _{-13.4%-3.7%}
750	1.206 ^{+35.9%+23.5%} _{-24.6%-23.5%}	2.009 ^{+13.5%+5.5%} _{-14.1%-5.5%}
1000	1.608 · 10 ^{-1+36.3%+26.4%} _{-24.8%-26.4%}	2.743 · 10 ^{-1+14.4%+7.3%} _{-14.8%-7.3%}
1500	6.264 · 10 ^{-3+36.2%+29.4%} _{-24.7%-29.4%}	1.056 · 10 ^{-2+16.1%+11.3%} _{-15.8%-11.3%}
2000	4.217 · 10 ^{-4+35.6%+29.8%} _{-24.5%-29.8%}	6.327 · 10 ^{-4+17.7%+17.8%} _{-16.6%-17.8%}

Table 6.5: LO and NLO QCD inclusive cross sections for gluino pair-production at the LHC, running at a center-of-mass energy of $\sqrt{s} = 13$ TeV. The results are shown together with the associated scale and PDF relative uncertainties.

that contains all interactions allowed by QCD gauge invariance and supersymmetry, as well as squark and gluino kinetic and mass terms. In our notation, T stands for the fundamental representation matrices of $SU(3)$, P_L (P_R) for the left-handed (right-handed) chirality projector and g_s is the strong coupling constant. Flavour and colour indices are left understood for brevity.

In addition, we enable the (possibly three-body) decays of the coloured superpartners by including (s)quark couplings to a gauge-singlet Majorana fermion χ of mass m_χ that is identified with a bino,

$$\mathcal{L}_{\text{decay}} = \frac{i}{2}\bar{\chi}\not{\partial}\chi - \frac{1}{2}m_\chi\bar{\chi}\chi + \sqrt{2}g' \left[-\tilde{q}_L^\dagger Y_q (\bar{\chi} P_L q) + (\bar{q} P_L \chi) Y_q \tilde{q}_R + \text{h.c.} \right]. \quad (6.16)$$

In this Lagrangian, Y_q denotes the hypercharge quantum number of the (s)quarks and g' the hypercharge coupling.

At NLO in QCD, gluino pair-production receives contributions from real emission diagrams as well as from the interferences of tree-level diagrams with virtual one-loop diagrams that exhibit ultraviolet divergences. These must be absorbed through a suitable renormalization of the parameters and of the fields appearing in $\mathcal{L}_{\text{SQCD}}$. To this aim, we replace all (non-)fermionic bare fields Ψ (Φ) and bare parameters y by the corresponding renormalized quantities,

$$\begin{aligned} \Phi &\rightarrow \left[1 + \frac{1}{2}\delta Z_\Phi \right] \Phi, \quad \Psi \rightarrow \left[1 + \frac{1}{2}\delta Z_\Psi^L P_L + \frac{1}{2}\delta Z_\Psi^R P_R \right] \Psi, \\ y &\rightarrow y + \delta y, \end{aligned} \quad (6.17)$$

where the renormalization constants δZ and δy are truncated at the first order in the strong coupling α_s . The wave-function renormalization constants of the massless quarks ($\delta Z_q^{L,R}$), of the top quark ($\delta Z_t^{L,R}$), of the gluon (δZ_g) and the top mass renormalization constant (δm_t) are given, when adopting the on-shell renormalization scheme, by

$$\begin{aligned} \delta Z_g &= -\frac{g_s^2}{24\pi^2} \left[-\frac{1}{3} + B_0(0, m_t^2, m_t^2) + 2m_t^2 B_0'(0, m_t^2, m_t^2) - \frac{n_c}{3} + n_c B_0(0, m_{\tilde{g}}^2, m_{\tilde{g}}^2) \right. \\ &\quad \left. + 2n_c m_{\tilde{g}}^2 B_0'(0, m_{\tilde{g}}^2, m_{\tilde{g}}^2) + \sum_{\tilde{q}} \left[\frac{1}{6} + \frac{1}{4} B_0(0, m_{\tilde{q}}^2, m_{\tilde{q}}^2) - m_{\tilde{q}}^2 B_0'(0, m_{\tilde{q}}^2, m_{\tilde{q}}^2) \right] \right], \end{aligned} \quad (6.18)$$

$$\delta Z_q^{L,R} = \frac{g_s^2 C_F}{8\pi^2} B_1(0, m_{\tilde{g}}^2, m_{\tilde{q}_{L,R}}^2),$$

$$\begin{aligned} \delta Z_t^{L,R} &= \frac{g_s^2 C_F}{16\pi^2} \left[1 + 2B_1(m_t^2, m_{\tilde{g}}^2, m_{\tilde{t}_{L,R}}^2) + 2B_1(m_t^2, m_t^2, 0) + 8m_t^2 B'_0(m_t^2, m_t^2, 0) \right. \\ &\quad \left. + 4m_t^2 B'_1(m_t^2, m_t^2, 0) + 2m_t^2 \sum_{i=L,R} B'_1(m_t^2, m_{\tilde{g}}^2, m_{\tilde{t}_i}^2) \right], \end{aligned} \quad (6.19)$$

$$\delta m_t = -\frac{g_s^2 C_F m_t}{16\pi^2} \left[-1 + 4B_0(m_t^2, m_t^2, 0) + 2B_1(m_t^2, m_t^2, 0) + \sum_{i=L,R} B_1(m_t^2, m_{\tilde{g}}^2, m_{\tilde{t}_i}^2) \right],$$

where the $B_{0,1}$ (and A_0 , for further references) functions and their derivatives stand for the standard two-point (one-point) Passarino-Veltman loop-integrals [175]. Moreover, $n_c = 3$ and $C_F = (n_c^2 - 1)/(2n_c)$ denote respectively the number of colors and the quadratic Casimir invariant associated with the fundamental representation of $SU(3)$. The gluino wave-function and mass renormalization constants $\delta Z_{\tilde{g}}^{L,R}$ and $\delta m_{\tilde{g}}$ are given by

$$\begin{aligned} \delta Z_{\tilde{g}} &= \frac{g_s^2}{16\pi^2} \left[n_c + 2n_c B_1(m_{\tilde{g}}^2, m_{\tilde{g}}^2, 0) + 8n_c m_{\tilde{g}}^2 B'_0(m_{\tilde{g}}^2, m_{\tilde{g}}^2, 0) + 4n_c m_{\tilde{g}}^2 B'_1(m_{\tilde{g}}^2, m_{\tilde{g}}^2, 0) \right. \\ &\quad \left. + \sum_{\tilde{q}=\tilde{q}_L, \tilde{q}_R} \left\{ B_1(m_{\tilde{g}}^2, m_{\tilde{q}}^2, m_{\tilde{q}}^2) + 2m_{\tilde{g}}^2 B'_1(m_{\tilde{g}}^2, m_{\tilde{q}}^2, m_{\tilde{q}}^2) \right\} \right], \end{aligned} \quad (6.20)$$

$$\delta m_{\tilde{g}} = \frac{g_s^2 m_{\tilde{g}}}{16\pi^2} \left[n_c - 4n_c B_0(m_{\tilde{g}}^2, m_{\tilde{g}}^2, 0) - 2n_c B_1(m_{\tilde{g}}^2, m_{\tilde{g}}^2, 0) - \sum_{\tilde{q}=\tilde{q}_L, \tilde{q}_R} B_1(m_{\tilde{g}}^2, m_{\tilde{q}}^2, m_{\tilde{q}}^2) \right],$$

while the squark wave-function ($\delta Z_{\tilde{q}}$) and mass ($\delta m_{\tilde{q}}^2$) renormalization constants read,

$$\begin{aligned} \delta Z_{\tilde{q}} &= \frac{g_s^2 C_F}{8\pi^2} \left[-B_0(m_{\tilde{q}}^2, m_{\tilde{g}}^2, m_{\tilde{q}}^2) + B_0(m_{\tilde{q}}^2, m_{\tilde{q}}^2, 0) + (m_{\tilde{g}}^2 - m_{\tilde{q}}^2 + m_{\tilde{q}}^2) B'_0(m_{\tilde{q}}^2, m_{\tilde{g}}^2, m_{\tilde{q}}^2) \right. \\ &\quad \left. + 2m_{\tilde{q}}^2 B'_0(m_{\tilde{q}}^2, m_{\tilde{q}}^2, 0) \right], \end{aligned} \quad (6.21)$$

$$\begin{aligned} \delta m_{\tilde{q}}^2 &= \frac{g_s^2 C_F}{8\pi^2} \left[A_0(m_{\tilde{q}}^2) - A_0(m_{\tilde{g}}^2) - 2m_{\tilde{q}}^2 B_0(m_{\tilde{q}}^2, m_{\tilde{q}}^2, 0) + (m_{\tilde{q}}^2 - m_{\tilde{g}}^2 \right. \\ &\quad \left. - m_{\tilde{q}}^2) B_0(m_{\tilde{q}}^2, m_{\tilde{g}}^2, m_{\tilde{q}}^2) - A_0(m_{\tilde{q}}^2) \right], \end{aligned}$$

with $(-)^L \equiv 1$ and $(-)^R \equiv -1$, and with $m_q \neq 0$ for top squarks only. As a result of the structure of the gluino-squark-quark interactions, squark mixing effects proportional to the corresponding quark masses are generated at the one-loop level and must be accounted for in the renormalization procedure. In our simplified setup, we consider $n_f = 5$ flavors of massless quarks so that these effects are only relevant for the sector of the top squarks. In this case, matrix renormalization is in order,

$$\begin{pmatrix} \tilde{t}_L \\ \tilde{t}_R \end{pmatrix} \rightarrow \begin{pmatrix} \tilde{t}_L \\ \tilde{t}_R \end{pmatrix} + \frac{1}{2} \begin{pmatrix} \delta Z_{\tilde{t}_L} & \delta Z_{\tilde{t}_L, \text{LR}} \\ \delta Z_{\tilde{t}_L, \text{RL}} & \delta Z_{\tilde{t}_R} \end{pmatrix} \begin{pmatrix} \tilde{t}_L \\ \tilde{t}_R \end{pmatrix}, \quad (6.22)$$

and we impose that the stop sector is renormalized so that left-handed and right-handed stops are still defined as non-mixed states at the one-loop level. In the MSSM, this is made possible by stop couplings to the Higgs sector that generate an off-diagonal mass counter-term,

$$\delta \mathcal{L}_{\text{off}} = -\delta m_{\tilde{t}_L, \text{LR}}^2 (\tilde{t}_L^\dagger \tilde{t}_R + \tilde{t}_R^\dagger \tilde{t}_L). \quad (6.23)$$

These Higgs couplings being absent in our simplified model, we therefore introduce $\delta \mathcal{L}_{\text{off}}$ explicitly. The off-diagonal stop wave-function ($\delta Z_{\tilde{t}_L, \text{LR}} = \delta Z_{\tilde{t}_R, \text{LR}}$) and mass ($\delta m_{\tilde{t}_L, \text{LR}}^2$) renormalization

constants are then found to be

$$\begin{aligned}\delta Z_{\tilde{t},\text{LR}} &= \frac{g_s^2 C_F m_{\tilde{g}} m_t}{4\pi^2 (m_{\tilde{t}_R}^2 - m_{\tilde{t}_L}^2)} \sum_{i=L,R} (-)^i B_0(m_{\tilde{t}_i}^2, m_t^2, m_{\tilde{g}}^2), \\ \delta m_{\tilde{t},\text{LR}}^2 &= \frac{g_s^2 C_F m_{\tilde{g}} m_t}{8\pi^2} \sum_{i=L,R} B_0(m_{\tilde{t}_i}^2, m_t^2, m_{\tilde{g}}^2),\end{aligned}\tag{6.24}$$

where $\delta Z_{\tilde{t},\text{LR}}$ has been symmetrized. In this way, it incorporates the renormalization of the stop mixing angle (taken vanishing in our model) which does not need to be explicitly introduced [250].

In order to ensure that the running of α_s solely originates from gluons and n_f active flavors of light quarks, we renormalize the strong coupling by subtracting at zero-momentum transfer, in the gluon self-energy, all massive particle contributions. This gives

$$\begin{aligned}\frac{\delta\alpha_s}{\alpha_s} &= \frac{\alpha_s}{2\pi\bar{\varepsilon}} \left[\frac{n_f}{3} - \frac{11n_c}{6} \right] + \frac{\alpha_s}{6\pi} \left[\frac{1}{\bar{\varepsilon}} - \log \frac{m_t^2}{\mu_R^2} \right] \\ &+ \frac{\alpha_s n_c}{6\pi} \left[\frac{1}{\bar{\varepsilon}} - \log \frac{m_{\tilde{g}}^2}{\mu_R^2} \right] + \frac{\alpha_s}{24\pi} \sum_{\tilde{q}} \left[\frac{1}{\bar{\varepsilon}} - \log \frac{m_{\tilde{q}}^2}{\mu_R^2} \right].\end{aligned}\tag{6.25}$$

The ultraviolet-divergent parts of $\delta\alpha_s/\alpha_s$ are written in terms of the quantity $\frac{1}{\bar{\varepsilon}} = \frac{1}{\varepsilon} - \gamma_E + \log 4\pi$ where γ_E is the Euler-Mascheroni constant and ε is connected to the number of space-time dimensions $D = 4 - 2\varepsilon$.

Finally, the artificial breaking of supersymmetry by the mismatch of the two gluino and the $(D - 2)$ transverse gluon degrees of freedom must be compensated by finite counter-terms. Imposing that the definition of the strong coupling g_s is identical to the Standard Model one, only quark-squark-gluino vertices and four-scalar interactions have to be shifted [166],

$$\begin{aligned}\mathcal{L}_{\text{SCT}} &= \sqrt{2} g_s \frac{\alpha_s}{3\pi} \left[-\tilde{q}_L^\dagger T_a (\tilde{g}^a P_L q) + (\bar{q} P_L \tilde{g}^a) T_a \tilde{q}_R + \text{h.c.} \right] \\ &+ \frac{g_s^2}{2} \frac{\alpha_s}{4\pi} \left[\tilde{q}_R^\dagger \{T_a, T_b\} \tilde{q}_R + \tilde{q}_L^\dagger \{T_a, T_b\} \tilde{q}_L \right] \\ &\quad \times \left[\tilde{q}_R^\dagger \{T^a, T^b\} \tilde{q}_R + \tilde{q}_L^\dagger \{T^a, T^b\} \tilde{q}_L \right] \\ &- \frac{g_s^2}{2} \frac{\alpha_s}{4\pi} \left[\tilde{q}_R^\dagger T_a \tilde{q}_R - \tilde{q}_L^\dagger T_a \tilde{q}_L \right] \left[\tilde{q}_R^\dagger T^a \tilde{q}_R - \tilde{q}_L^\dagger T^a \tilde{q}_L \right],\end{aligned}\tag{6.26}$$

where we have introduced adjoint color indices for clarity.

In our phenomenological study, loop-calculations are performed numerically in four dimensions by means of the MADLOOP package and therefore require the extraction of rational parts that are related to the ε -pieces of the loop-integral denominators (R_1 , which are automatically reconstructed within the OPP reduction procedure) and numerators (R_2). For any renormalizable theory, the number of R_2 terms is finite and they can be seen as counter-terms derived from the bare Lagrangian [240]. In the context of the $\mathcal{L}_{\text{SQCD}}$ Lagrangian, all necessary R_2 counter-terms can be found in Ref. [251].

The setup described above has been implemented in the FEYNRULES package and we have made use of the NLOCT program to automatically calculate all the ultraviolet and R_2 counter-terms of the model. The specificity of the renormalization of the stop sector has been implemented via a new option of NLOCT, `SupersymmetryScheme->"OS"`, that allows to treat all scalar fields that mix at the loop-level as described above. We have validated the output against our analytical calculations, and these results represent the first validation of NLOCT in the context of computations involving massive Majorana colored particles. We have finally generated a UFO version of the model that can be loaded into MADGRAPH5_aMC@NLO and which

we have made publicly available on <http://feynrules.irmp.ucl.ac.be/wiki/NLOmodels>. We have further validated the model, together with the numerical treatment of the loop-diagrams by MADLOOP, by comparing MADGRAPH5_aMC@NLO predictions to those of the code PROSPINO [188], using a fully degenerate mass spectrum due to the limitations of the latter.

LHC phenomenology

In Table 6.5, we compute gluino pair-production total cross sections for proton-proton collisions at a center-of-mass energy of $\sqrt{s} = 13$ TeV and for different gluino masses. Squarks are decoupled ($m_{\tilde{t}_L} = 16$ TeV, $m_{\tilde{t}_R} = 17$ TeV and $m_{\tilde{q}_L} = m_{\tilde{q}_R} = 15$ TeV) so that any resonant squark contribution appearing in the real-emission topologies is off-shell and therefore suppressed. The latter production modes can be seen as the associated production of a gluino and a squark that subsequently decays into a gluino and a quark. Including these contributions as parts of the NLO QCD corrections for gluino pair-production would hence result in a double-counting when considering together all superpartner production processes inclusively. Moreover, these resonant channels require a special treatment in the fully-automated MADGRAPH5_aMC@NLO framework, that is left to future work [252]. Our choice for the squark spectrum corresponds to the one made by ATLAS and CMS collaborations in their respective gluino searches [253–256].

Our results are evaluated both at the LO and NLO accuracy in QCD and presented together with scale and parton distribution (PDF) uncertainties. For the central values, we set the renormalization and factorization scales to half the sum of the transverse mass of all final state particles and use the NNPDF 3.0 set of parton distributions [128] accessed via the LHAPDF 6 library [257]. Scale uncertainties are derived by varying both scales independently by factors 1/2, 1 and 2, and the PDF uncertainties have been extracted from the cross section values spanned by all NNPDF distribution replicas following the NNPDF recommendations [258]. We observe a significant enhancement of the cross section of about 50% due to genuine NLO contributions, as well as a sizable reduction of the uncertainties. In particular, the apparent drastic reduction of the PDF uncertainties is related to the poor quality of the LO NNPDF fit when compared to the NLO fit [128].

In order to achieve realistic simulations of LHC collisions, we first handle gluino decays by using tree-level decay matrix-elements as calculated by the MADSPIN [238] and MADWIDTH [239] programs. Due to the three-body nature of the gluino decays, spin correlations are here omitted as MADSPIN can only handle them for two-body decays. We then interface the partonic events obtained in this way to a parton showering and hadronization description as provided by the PYTHIA 8 package [259], and use the anti- k_T jet reconstruction algorithm [245] with a radius parameter set to 0.4, as implemented in FASTJET [246], to reconstruct all final state parton-level and hadron-level jets for fixed-order and parton-shower-matched calculations respectively. Finally, the phenomenological analysis of the generated events is performed with MADANALYSIS 5 [247].

Key differential distributions particularly sensitive to both NLO and shower effects are presented in Fig. 6.4. We show the transverse-momentum (p_T) spectra of the first five leading jets (first five subfigures) for two benchmark scenarios featuring either a light ($m_{\tilde{g}} = 1$ TeV) or a heavy ($m_{\tilde{g}} = 2$ TeV) gluino, as well as a rather light bino ($m_{\tilde{\chi}} = 50$ GeV). We compare fixed-order predictions (dashed) to results matched to parton showers (solid) and consider both LO (blue) and NLO (red) accuracy in QCD. We observe that the differential K -factors (*i.e.*, the bin-by-bin ratios of the NLO result to the LO one) both with and without parton-shower matching strongly depend on the jet p_T . The NLO effects therefore not only increase the overall normalization of the distributions, but also distort their shapes. The K -factor is indeed greater at low p_T than at high p_T , so that the traditional procedure of using LO predictions scaled by inclusive K -factors cannot be used for an accurate gluino signal description.

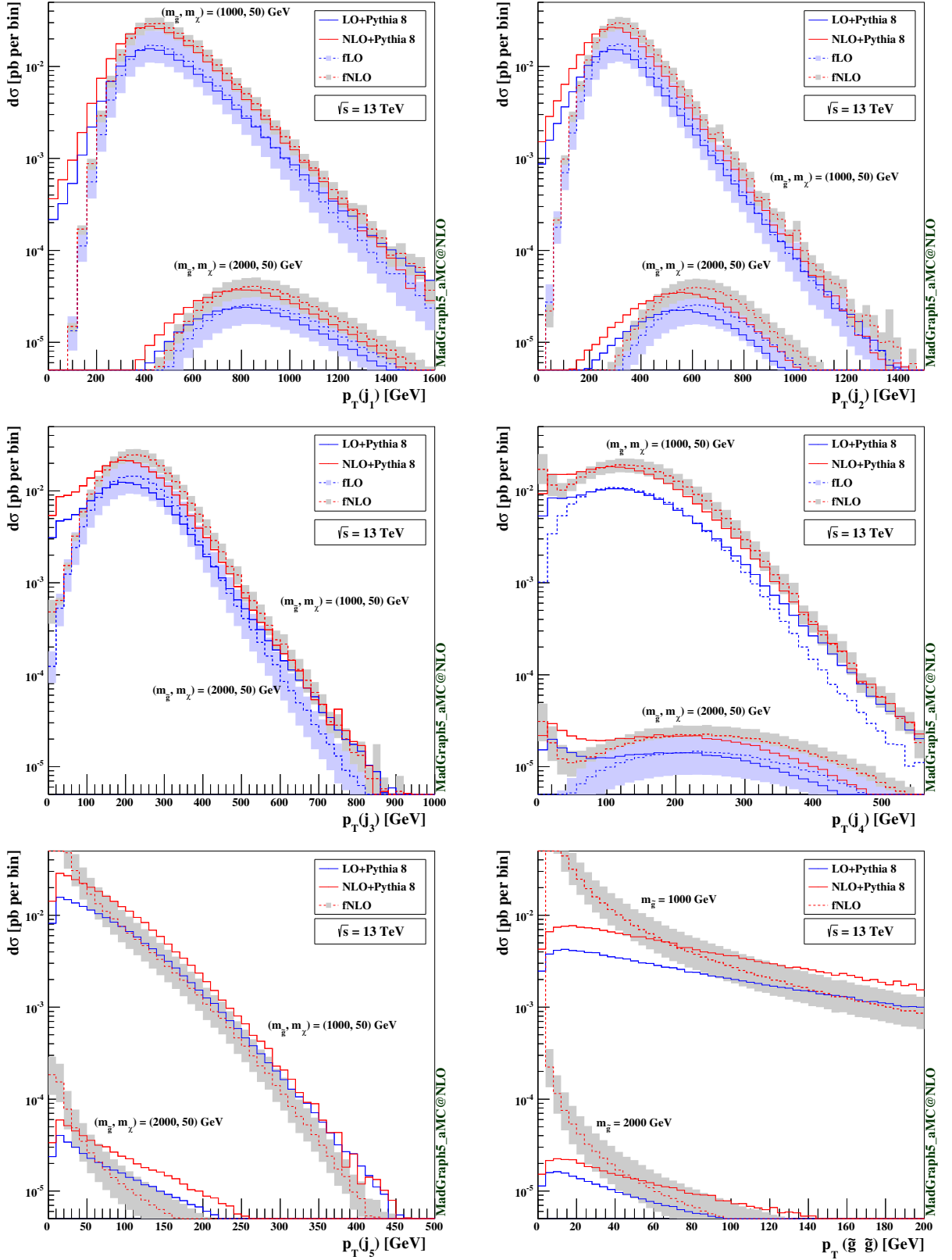


Figure 6.4: First five leading jet and gluino-pair transverse-momentum spectra for the production of a pair of gluinos decaying each into two jets and a neutralino. We consider two mass configurations and show results at the NLO (red) and LO (blue) accuracy in QCD, at the fixed-order (dashed, fLO and fNLO) and after matching to the PYTHIA 8 parton shower description (solid). Theoretical uncertainties related to the fixed order calculations are shown as blue (LO) and gray (NLO) bands.

Fig. 6.4 also underlines the effects of matching LO and NLO matrix elements to parton showers. Since most parton-level jets originate from the decay of very massive gluinos, the fixed-order p_T distributions peak at large p_T values. In addition, the low- p_T region of these spectra is depleted. As a result of the matching to parton showers, the fixed-order NLO distributions are distorted and softened. While the change is milder in the large- p_T tails whose shapes are controlled by the hard matrix element, the low- p_T regions are mostly sensitive to resummation and become populated. The parton shower emissions from hard partons are indeed often not reclustered back with the jet they are issued from, hence distorting the jet p_T spectra. For this reason, resummation effects become significant below the peak of the various p_T distributions. This effect is also illustrated on the last subfigure of Fig. 6.4, where we show the p_T spectrum of the gluino pair in the small p_T range. We have verified that the matched results agree with the fixed-order ones for very large p_T values of the order of the gluino mass.

Conclusions

We have performed the first calculation of NLO supersymmetric QCD corrections to gluino pair- production matched to parton showers and have studied the impact of both the NLO contributions and of the parton showers. We have shown that observable effects could be induced on the exclusion limits and that more accurate calculations are crucial for extracting model parameters in case of a discovery. Our calculation has been performed fully automatically and we have applied it to the case of a simplified model similar to one of those used by the ATLAS and CMS collaborations for their respective gluino searches. In addition, we have publicly released the UFO model associated with our computation, that is sufficiently general to be readily used to explore the phenomenology associated with any supersymmetric QCD process. Finally, our results also shows that all technical obstacles for automating the matching of fixed-order calculations for inclusive supersymmetric particle production at the NLO in QCD to parton showers have been cleared, up to the ambiguity issue of the double counting arising in real emission resonant contributions [252].

Chapter 7

Conclusions and outlook

Supersymmetry is one of the leading candidate for Beyond the Standard Model physics, and is extensively searched for at LHC. In this thesis we have focused on the phenomenology of $\mathcal{N} = 1$ supersymmetric theories, for which we have provided theoretical predictions at leading order (LO), and next-to-leading order (NLO) in perturbation theory, at polarized and unpolarized hadron colliders. In Chapter 1, we have reviewed the successes and limitations of the Standard Model of particle physics, and have motivated the necessity to study theories that go Beyond the Standard Model. Then, we have chosen to restrict to one particular type of extension of the SM, namely $\mathcal{N} = 1$ supersymmetry.

In Chapter 2, we have provided a short introduction to $\mathcal{N} = 1$ supersymmetry, where we have first recalled some basic facts about SUSY (history, motivations, superalgebra and properties of the supermultiplets), before introducing the superspace formalism, and detailing the various steps inherent to the construction of supersymmetric Lagrangians. In the second part of this chapter, we have then focused on one particular implementation of $\mathcal{N} = 1$ supersymmetry, namely the Minimal Supersymmetric Standard Model, for which we have described the mechanism of electroweak symmetry breaking, and detailed the various sectors of the theory at tree-level.

In Chapter 3, we have shown how the availability of polarized beams at high-energy hadron colliders can provide a unique handle on the discrimination between different beyond the Standard Model scenarios that lead to the same final-state signatures in unpolarized collisions. First of all, we have discussed in a model-independent way why single and double-spin asymmetries in polarized collisions allow us for the separation between different initial-state production mechanisms. Then we have considered different benchmark scenarios for monotop production and have shown how the measurement of spin asymmetries in polarized collisions could help to discriminate between different models. Therefore, while polarized beams are certainly not required for BSM discoveries, they can provide very useful information on the properties of the hypothetical BSM sector, in particular in the determination of its couplings to Standard Model particles.

In Chapter 4, we have provided a short introduction to one-loop calculation techniques. More specifically, we have first recalled the various challenges of NLO calculations, before giving a constructive (and mathematically consistent) definition of both Dimensional Regularization, and Dimensional Reduction. Then, in the second part of this chapter, we have detailed how to evaluate scalar integrals that are frequently encountered in the context of one-loop calculations, and have introduced the Passarino-Veltman reduction scheme designed to decompose each vector and tensor loop integral into a linear combination of simpler scalar integrals. Finally, the last part of this chapter has been dedicated to the procedure of multiplicative renormalization, which aims at absorbing UV divergences into the redefinition of all the bare fields and parameters of the original tree-level Lagrangian. In this last section, we have derived all the renormalization

constants that are necessary to ensure the UV-finiteness of the theory at one-loop (for generic scalar, fermions, and vector fields with mixing).

In Chapter 5, we have applied the concepts reviewed in the previous chapter for the first time to the case of squark-antisquark hadroproduction at next-to-leading order in SUSY-QCD with Non-Minimal Flavour Violation (NMFV). In the first part of this chapter, we have detailed the field content of the model, have given the analytical expression of the tree-level matrix element, and have defined the set-up employed to renormalize the theory at the one-loop level. In the second part of this chapter, we have then focused on the derivation of the self-energies and vertex corrections, and provided the analytical expression of all the Renormalization Constants (RCs) needed for the process of our interest. In the third part of chapter we have finally discussed the box contributions, and provided a short status report on this on-going calculation.

In Chapter 6, we have presented for the first time the full automation of collider predictions matched with parton showers at the next-to-leading accuracy in QCD within non-trivial extensions of the Standard Model. As an application, we have explored scenarios beyond the Standard Model where new coloured scalar (stops and sgluons), and Majorana particles (gluinos) can be pair produced in hadron collisions. Using simplified models to describe the new field interactions with the Standard Model, we have presented precision predictions for the LHC within the MADGRAPH5_aMC@NLO framework.

On the short term, our goals are to extend the work presented in this thesis in two directions. The first one concerns squark-antisquark hadroproduction at NLO in SUSY-QCD with NMFV, and consists in including all the real corrections in our code in order to finalize the calculation, produce numerical results, and ultimately publish them (in the coming months). The second one would be to generalize the results obtained for gluino pair production matched with parton shower at NLO in SUSY-QCD to the case where intermediate resonances are kinematically allowed to be on-shell, *i.e.* to automatically perform the on-shell subtraction in a gauge invariant way. A publication is there again expected in the coming months.

Appendix A

Conventions

In this appendix, we specify the conventions that are used in all the calculations performed in this thesis, and recall some basic facts about the tensor formalism, Dirac algebra and Weyl fermions. The Greek indices of the middle of the alphabet denote Lorentz indices and range from zero to three, while Latin indices correspond to space indices and range from one to three. For the Minkowski metric $\eta^{\mu\nu}$ and its inverse $\eta_{\mu\nu}$, we employ the particle physics conventions $\eta^{\mu\nu} = \text{diag}(1, -1, -1, -1)$ and $\eta_{\mu\nu} = \text{diag}(1, -1, -1, -1)$. The contravariant four-vector position and momentum are defined as

$$x^\mu = (t, \vec{x}), \quad p^\mu = (E, \vec{p}), \quad (\text{A.1})$$

and the space-time derivative is given by

$$\partial_\mu = (\partial/\partial t, \vec{\nabla}). \quad (\text{A.2})$$

The Lorentz indices can be raised or lowered by means of the metric tensor such that

$$x^\mu = \eta^{\mu\nu} x_\nu, \quad \text{and} \quad x_\mu = \eta_{\mu\nu} x^\nu. \quad (\text{A.3})$$

In this manuscript, we systematically use the natural units

$$\hbar = c = 1. \quad (\text{A.4})$$

The Dirac algebra in four-dimensions reads

$$\begin{aligned} \{\gamma^\mu, \gamma^\nu\} &= 2\eta^{\mu\nu} \mathbb{1}_4, & \gamma^5 &= i\gamma^0\gamma^1\gamma^2\gamma^3, & \{\gamma^\mu, \gamma^5\} &= 0, \\ (\gamma^\mu)^\dagger &= \gamma^0\gamma^\mu\gamma^0, & (\gamma^0)^2 &= \mathbb{1}_4, & (\gamma^5)^2 &= \mathbb{1}_4, & (\gamma^5)^\dagger &= \gamma^5, \end{aligned}$$

where the gamma matrices take the following form in the chiral representation

$$\gamma^5 = \begin{pmatrix} -1 & 0 \\ 0 & 1 \end{pmatrix}, \quad \gamma^0 = \begin{pmatrix} 0 & 1 \\ 1 & 0 \end{pmatrix}, \quad \gamma^\mu = \begin{pmatrix} 0 & \sigma^\mu \\ \bar{\sigma}^\mu & 0 \end{pmatrix}, \quad \gamma^{\mu\nu} = \begin{pmatrix} \sigma^{\mu\nu} & 0 \\ 0 & \bar{\sigma}^{\mu\nu} \end{pmatrix}, \quad (\text{A.5})$$

and where we have introduced in the previous equation the Pauli matrices

$$\sigma^\mu = (\mathbb{1}_2, \vec{\sigma}), \quad \bar{\sigma}^\mu = (\mathbb{1}_2, -\vec{\sigma}), \quad (\text{A.6})$$

defined such that

$$\begin{aligned} \sigma^0 &= \begin{pmatrix} 1 & 0 \\ 0 & 1 \end{pmatrix}, & \sigma^1 &= \begin{pmatrix} 0 & 1 \\ 1 & 0 \end{pmatrix}, & \sigma^2 &= \begin{pmatrix} 0 & -i \\ i & 0 \end{pmatrix}, & \sigma^3 &= \begin{pmatrix} 1 & 0 \\ 0 & -1 \end{pmatrix}, \\ \bar{\sigma}^0 &= \begin{pmatrix} 1 & 0 \\ 0 & 1 \end{pmatrix}, & \bar{\sigma}^1 &= \begin{pmatrix} 0 & -1 \\ -1 & 0 \end{pmatrix}, & \bar{\sigma}^2 &= \begin{pmatrix} 0 & i \\ -i & 0 \end{pmatrix}, & \bar{\sigma}^3 &= \begin{pmatrix} -1 & 0 \\ 0 & 1 \end{pmatrix}. \end{aligned}$$

We moreover recall that

$$\sigma^{\mu\nu} = \frac{1}{4}(\sigma^\mu \bar{\sigma}^\nu - \sigma^\nu \bar{\sigma}^\mu) , \quad (\text{A.7})$$

$$\bar{\sigma}^{\mu\nu} = \frac{1}{4}(\bar{\sigma}^\mu \sigma^\nu - \bar{\sigma}^\nu \sigma^\mu) , \quad (\text{A.8})$$

and that the chiral projectors are defined as

$$P_L = \frac{1 - \gamma^5}{2} , \quad P_R = \frac{1 + \gamma^5}{2} , \quad (\text{A.9})$$

and satisfy the following properties

$$P_L + P_R = \mathbb{1}_4 , \quad P_L P_R = P_R P_L = 0 , \quad P_L^2 = P_L , \quad P_R^2 = P_R . \quad (\text{A.10})$$

In supersymmetry, we prefer to employ Weyl spinors rather than Dirac or Majorana spinors. The latter can be decomposed in terms of two-component Weyl spinors such that

$$\psi_D = \begin{pmatrix} \lambda_\alpha \\ \bar{\chi}^{\dot{\alpha}} \end{pmatrix} , \quad \psi_M = \begin{pmatrix} \lambda_\alpha \\ \bar{\lambda}^{\dot{\alpha}} \end{pmatrix} , \quad (\text{A.11})$$

where λ_α , and $\bar{\lambda}^{\dot{\alpha}}$, $\bar{\chi}^{\dot{\alpha}}$ are respectively left-handed, and right-handed Weyl spinors, and where the indices α and $\dot{\alpha}$ range from 1 to 2. Undotted indices are used for left-handed spinors, while dotted indices are used for right-handed spinors. Note in addition that the hermitian conjugate of a left-handed Weyl spinor is a right-handed Weyl spinor and the other way around

$$\bar{\chi}^{\dot{\alpha}} = \chi_\alpha^\dagger , \quad (\bar{\chi}^{\dot{\alpha}})^\dagger = \chi_\alpha . \quad (\text{A.12})$$

For the contraction of repeated spinor indices, we follow the Van Der Waerden conventions defined such that

$$\lambda^\alpha \psi_\alpha = \lambda \cdot \psi , \quad \text{and} \quad \bar{\chi}^{\dot{\alpha}} \bar{\lambda}^{\dot{\alpha}} = \bar{\chi} \cdot \bar{\lambda} , \quad (\text{A.13})$$

where the antisymmetric Levi-Civita tensor is used to raise and lower spinor indices

$$\lambda^\alpha = \varepsilon^{\alpha\beta} \lambda_\beta , \quad \lambda_\alpha = \varepsilon_{\alpha\beta} \lambda^\beta , \quad \bar{\lambda}^{\dot{\alpha}} = \varepsilon^{\dot{\alpha}\dot{\beta}} \bar{\lambda}_{\dot{\beta}} , \quad \bar{\lambda}_{\dot{\alpha}} = \varepsilon_{\dot{\alpha}\dot{\beta}} \bar{\lambda}^{\dot{\beta}} ,$$

and where we recall that

$$\begin{aligned} i\sigma^2 &= \begin{pmatrix} 0 & 1 \\ -1 & 0 \end{pmatrix} , & \varepsilon_{\alpha\beta} &= \begin{pmatrix} 0 & 1 \\ -1 & 0 \end{pmatrix} , & \varepsilon^{\alpha\beta} &= \begin{pmatrix} 0 & -1 \\ 1 & 0 \end{pmatrix} , \\ -i\sigma^2 &= \begin{pmatrix} 0 & -1 \\ 1 & 0 \end{pmatrix} , & \varepsilon_{\dot{\alpha}\dot{\beta}} &= \begin{pmatrix} 0 & 1 \\ -1 & 0 \end{pmatrix} , & \varepsilon^{\dot{\alpha}\dot{\beta}} &= \begin{pmatrix} 0 & -1 \\ 1 & 0 \end{pmatrix} . \end{aligned}$$

In our conventions, we set

$$\varepsilon_{0123} = +1 , \quad \text{and} \quad \varepsilon^{0123} = -1 . \quad (\text{A.14})$$

Appendix B

Basic facts on $\mathfrak{su}(N)$

A Lie algebra consists of a vector space \mathfrak{g} and an antisymmetric bilinear map

$$[-, -] : \mathfrak{g} \times \mathfrak{g} \longrightarrow \mathfrak{g} , \quad (\text{B.1})$$

called a Lie bracket, which satisfies the Jacobi identity

$$[X, [Y, Z]] + [Y, [Z, X]] + [Z, [X, Y]] = 0 \quad \forall X, Y, Z \in \mathfrak{g} . \quad (\text{B.2})$$

Lie algebras considered in particle physics are real, in other words, \mathfrak{g} is a real vector space and its structure constants are thus real. This means, in particular, that in a unitary representation, they are realized as hermitian traceless matrices. Fixing a basis $\{T^a\}$ for a real \mathfrak{g} , the Lie bracket is specified by the structure constants $f_{abc} = -f_{bac}$ such that

$$[T^a, T^b] = if^{abc}T^c , \quad (\text{B.3})$$

allowing us to rewrite Jacobi identity as

$$[T^a, [T^b, T^c]] + [T^b, [T^c, T^a]] + [T^c, [T^a, T^b]] = 0 . \quad (\text{B.4})$$

In what follows, we focus exclusively on $\mathfrak{su}(N)$, since this algebra is the one we need for the calculation of the QCD color factors. $\mathfrak{su}(N)$ is the Lie Algebra associated to the special unitary group $SU(N)$ comprising all unitary $N \times N$ matrices of determinant 1.

Fundamental representation of $\mathfrak{su}(N)$

The $\{T^a\}$ are the generators of the fundamental representation of the $\mathfrak{su}(N)$ algebra. They correspond to a set of $N \times N$ hermitian traceless matrices with the following algebraic properties

$$\text{Tr}(T^a) = 0 , \quad \text{Tr}(T^a T^b) = \frac{1}{2} \delta^{ab} , \quad (\text{B.5})$$

$$\{T^a, T^b\} = \frac{1}{N} \delta^{ab} + d^{abc} T^c , \quad (\text{B.6})$$

where d^{abc} are the symmetric structure constants, and N is the dimension of the representation.

Adjoint representation of $\mathfrak{su}(N)$

The adjoint representation of $\mathfrak{su}(N)$ algebra is spanned by the antisymmetric structure constants f^{abc} , which define a basis of $(N^2 - 1) \times (N^2 - 1)$ matrices such that

$$(F^a)^{bc} = -if^{abc} , \quad (\text{B.7})$$

where the $(F^a)^{bc}$ are the generators of the adjoint representation of $\mathfrak{su}(N)$. In the adjoint representation, the Jacobi identity reads

$$f^{ade} f^{bcd} + f^{bde} f^{cad} + f^{cde} f^{abd} = 0 , \quad (\text{B.8})$$

or equivalently

$$[F^a, F^b] = i f^{abc} F^c . \quad (\text{B.9})$$

Projection Operator

The generators of the fundamental representation and the identity matrix constitute a basis on which it is possible to decompose any $N \times N$ hermitian matrix M such that $M = m_0 \mathbb{1}_N + m_a T^a$. Using the properties of (B.5) we obtain

$$\begin{aligned} \text{Tr}(M) &= m_0 N \implies m_0 = \frac{1}{N} \text{Tr}(M) , \\ \text{Tr}(T^a M) &= m_b \text{Tr}(T^a T^b) = \frac{1}{2} m_b \delta_{ab} = \frac{1}{2} m_a \implies m_a = 2 \text{Tr}(T^a M) , \end{aligned}$$

and thus

$$M = \frac{1}{N} \text{Tr}(M) \mathbb{1}_N + 2 \text{Tr}(T^a M) T^a . \quad (\text{B.10})$$

Let us now consider one entry of the hermitian matrix M , we have

$$\begin{aligned} M_{ij} &= \frac{1}{N} M_{kk} \delta_{ij} + 2 T_{kl}^a M_{lk} T_{ij}^a , \\ M_{lk} \delta_{il} \delta_{jk} &= \frac{1}{N} M_{lk} \delta_{ij} \delta_{kl} + 2 T_{kl}^a M_{lk} T_{ij}^a . \end{aligned}$$

After simplification of the M_{lk} , we obtain the following expression for the projection operator

$$T_{ij}^a T_{kl}^a = \frac{1}{2} \left(\delta_{il} \delta_{jk} - \frac{1}{N} \delta_{ij} \delta_{kl} \right) \quad (\text{B.11})$$

Casimir Operator

$T^a T^a$ is a Casimir operator of the fundamental representation whose entries are given by

$$(T^a T^a)_{ij} = T_{ik}^a T_{kj}^a = \frac{1}{2} \left(\delta_{ij} \delta_{kk} - \frac{1}{N} \delta_{ik} \delta_{jk} \right) = \frac{1}{2} \left(N \delta_{ij} - \frac{1}{N} \delta_{ij} \right) = \frac{N^2 - 1}{2N} \delta_{ij} ,$$

or equivalently in a more compact way

$$(T^a T^a)_{ij} = C_F \delta_{ij} \quad \text{with} \quad C_F = \frac{N^2 - 1}{2N} . \quad (\text{B.12})$$

The off-diagonal entries of the Casimir operator $T^a T^a$ are identically zero, and the diagonal ones are equal to C_F . This operator is therefore proportional to the unit matrix and thus must commute with all the generators of the fundamental representation. Analogously, The Casimir operator in the adjoint representation of $\mathfrak{su}(N)$ is defined as

$$(F^c F^c)^{ab} = (F^c)^{ad} (F^c)^{db} = -f^{cad} f^{cdb} = f^{acd} f^{bcd} = N \delta^{ab} \quad (\text{B.13})$$

or equivalently

$$(F^c F^c)^{ab} = C_A \delta^{ab} \quad \text{with} \quad C_A = N . \quad (\text{B.14})$$

$F^c F^c$ is proportional to $\mathbb{1}_{N^2-1}$ and thus must commute with all the generators of the adjoint.

Useful identities

Using (B.5), (B.6) and (B.11), we obtain the following expressions

$$f^{abc} = -2i\mathrm{Tr}(T^a[T^b, T^c]) \quad (\text{B.15})$$

$$d^{abc} = 2\mathrm{Tr}(T^a\{T^b, T^c\}) \quad (\text{B.16})$$

$$T^a T^b = \frac{1}{2} \left(\frac{1}{N} \delta^{ab} + (d^{abc} + if^{abc}) T^c \right) \quad (\text{B.17})$$

$$\mathrm{Tr}(T^a T^b T^c) = \frac{1}{4} (d^{abc} + if^{abc}) \quad (\text{B.18})$$

$$\mathrm{Tr}(T^a T^b T^a T^c) = -\frac{1}{4N} \delta^{bc} \quad (\text{B.19})$$

$$\mathrm{Tr}(T^a T^c T^c T^b) = \frac{N^2 - 1}{4N} \delta^{ab} \quad (\text{B.20})$$

Appendix C

Parton distributions C++ interface

Source file : header.h

```
#include <iostream>
#include <iomanip>
#include <fstream>
#include <cmath>
#include <string>
#include <sstream>
#include "LHAPDF/LHAPDF.h"
using namespace std;

// Define the scale you want to probe:
const double scale = 1e2;
const double Q = scale;
const double Q2 = Q * Q;

// Define the PDF set you want to use:
const string pdfset = "NNPDFpol11_100";

// Extrapolation flag
const bool EXTRAPOLATION_FLAG = true;

// Number of sampled points in the x-range
const int NxPoints = (const int) 1e4;

// Define the x-range you want to probe:
const double xmin = log(1e-3);
const double xmax = log(1.0);
const double delta = (xmax - xmin) / double(NxPoints);

// Function prototypes
double Compute_Std_Dev (int n, double *, double);
```

Source file : utils.cpp

```
#include "header.h"

double Compute_Std_Dev (int n, double *y, double Avg)
{
    double sum = 0.0;
    for (int k = 0; k < n; k++)
    {
        sum += (y[k] - Avg) * (y[k] - Avg);
    }
    sum /= double (n - 1);
    return sqrt(sum);
}
```

Source file : PDF.cpp

```
#include "header.h"

int main (void)
{
    string pdfext = ".LHgrid";
    string pdfname = (string) pdfset + pdfext;

    //Initialization of the PDF set
    LHAPDF::setVerbosity (0);
    LHAPDF::initPDFSet (pdfname);
    int Nbrep = LHAPDF::numberPDF();

    if (EXTRAPOLATION_FLAG == true)
    {
        LHAPDF::extrapolate(true);
    }

    // Creating directory for data files
    string sep = "-";
    string folder = "data";
    stringstream energy; energy << Q2;
    string units = "GeV2";
    string dir = pdfset + sep + folder + sep + energy.str() + sep + units;

    // Creating directory for data
    mkdir(dir.c_str(), S_IRWXU);

    // Enter directory recently created
    chdir(dir.c_str());

    // Initialization for result + error
    double avg = 0.0;
    double err = 0.0;
```

Source file : PDF.cpp

```
// String for data files extensions
string ext = ".dat";

// Declare output file stream
ofstream output;

// Loop over the various types of partons
for (int j = -5; j < 6; j++)
{
    // Creates data file for each parton distribution
    stringstream ss; ss << j + 5;
    string filename = dir + sep + ss.str() + ext;
    const char* string1 = filename.c_str();
    output.open (string1);

    // Creates a 1D array of fixed size for the probed x values
    double *x = new double[NxPoints];

    // Loop over various values of x
    for (int i = 0; i < NxPoints; i++)
    {
        // X values probed
        x[i]= exp (xmin + double(i) * delta);

        // Central value (average) for a PDF j at a scale Q and at x[i]
        LHAPDF::initPDF (0);
        avg = LHAPDF::xfx(x[i], Q, j);

        double *pdf = new double[Nbrep];

        // Loop over the number of replicas for a given x
        for(int nrep = 1; nrep <= Nbrep; nrep++)
        {
            LHAPDF::initPDF (nrep);
            pdf[nrep-1] = LHAPDF::xfx(x[i], Q, j);
        }

        // 1-sigma error band for one pdf at a given x
        err = Compute_Std_Dev (Nbrep, pdf, avg);

        // Writing results in data files + 1-sigma error band
        output << setprecision (6) << scientific;
        output << x[i] << " " << avg << " " << err << " " << err << endl;
        output << x[i] << " " << avg + err << " " << err << " " << avg - err << endl;

        delete[] pdf;
    }
    delete[] x;
    output.close ();
}
return 0;
}
```

Source file : Makefile

```
CXX = g++
CXXFlags = -Wall -Wextra -pedantic -O2 -g -Weffc++ -Wcast-qual
-Wcast-align -Wconversion -Wdouble-promotion -Wunused
-Wunsafe-loop-optimizations -Wuninitialized
LIB= -L$(shell lhapdf-config libdir) -lLHAPDF
INC= -I$(shell lhapdf-config incdir)
EXEC= PDF_interface
SRC= $(wildcard *.cpp)
OBJ= $(SRC: .cpp=.o)
HEAD = header.h

$(EXEC):$(OBJ)
    $(CXX) $^ -o $@ $(INC) $(LIB)

%.o: %.cpp $(HEAD)
    $(CXX) $(CXXFlags) -o $@ -c $^

.PHONY: clean

clean:
    rm $(EXEC)
```

Appendix D

Euler-Gamma and Beta functions

The Euler-Gamma function

The Euler-Gamma function $\Gamma(z)$ with $z \in \mathbb{C}$ appears frequently in loop calculations when using dimensional regularization, and corresponds to an extension of the factorial function

$$\Gamma(n) = (n-1)! \quad \text{with } n \in \mathbb{N}^*, \text{ such that } \Gamma(n+1) = n \Gamma(n), \quad (\text{D.1})$$

to complex and real arguments. The Euler-Gamma function is defined for all complex and real numbers, except for negative integers where the function exhibits simple poles. $\forall z \in \mathbb{C}$ with $\Re(z) > 0$, $\Gamma(z)$ is defined via the following convergent improper integral

$$\Gamma(z) = \int_0^{+\infty} t^{z-1} e^{-t} dt. \quad (\text{D.2})$$

Exploiting the property of (D.1), the previous definition of $\Gamma(z)$ can be extended by means of analytic continuation to regions in the complex plane where $\Re(z) \leq 0$ such that

$$\Gamma(z+1) = z \Gamma(z) \quad \text{with } z \in \mathbb{C}. \quad (\text{D.3})$$

The Euler-Gamma function has the following basic properties

$$\Gamma(1) = 1, \quad \Gamma(2) = 1, \quad \Gamma(1/2) = \sqrt{\pi}, \quad \Gamma'(1) = -\gamma_E, \quad (\text{D.4})$$

where γ_E is the Euler-Mascheroni constant defined such that

$$\gamma_E = 0.577216. \quad (\text{D.5})$$

Another useful relation is the so-called Legendre duplication formula, which is given by

$$\Gamma(z) \Gamma\left(z + \frac{1}{2}\right) = 2^{1-2z} \sqrt{\pi} \Gamma(2z) \quad (\text{D.6})$$

The Beta function

The Beta function $B(\alpha, \beta)$ with $\alpha, \beta \in \mathbb{C}$ is defined in this thesis such that

$$B(\alpha, \beta) = \int_0^1 t^{\alpha-1} (1-t)^{\beta-1} dt, \quad \Re(\alpha) > 0, \Re(\beta) > 0, \quad (\text{D.7})$$

where $B(\alpha, \beta)$ is symmetric under permutation of α , and β . The beta function can be related to the Euler-Gamma function by means of the following equation

$$B(\alpha, \beta) = \frac{\Gamma(\alpha) \Gamma(\beta)}{\Gamma(\alpha + \beta)} \quad (\text{D.8})$$

Proof:

According to (D.2), the product of two Euler Γ functions can be written as

$$\Gamma(\alpha) \Gamma(\beta) = \int_0^{+\infty} x^{\alpha-1} e^{-x} dx \int_0^{+\infty} y^{\beta-1} e^{-y} dy .$$

Performing the change of variables $x = v^2$, $dx = 2v dv$, and $y = u^2$, $dy = 2u du$, gives

$$\Gamma(\alpha) \Gamma(\beta) = 4 \int_0^{+\infty} v^{2\alpha-1} e^{-v^2} dv \int_0^{+\infty} u^{2\beta-1} e^{-u^2} du .$$

The previous expression can be further simplified by means of the following change of variables $v = \rho \cos \theta$ and $u = \rho \sin \theta$, such that

$$\begin{aligned} \Gamma(\alpha) \Gamma(\beta) &= 4 \int_0^{+\infty} (\rho^2)^{\alpha+\beta-1} e^{-\rho^2} d\rho^2 \int_0^{+\pi/2} (\cos \theta)^{2\alpha-1} (\sin \theta)^{2\beta-1} d\theta \\ &\stackrel{(D.2)}{=} 2 \Gamma(\alpha + \beta) \int_0^{+\pi/2} (\cos \theta)^{2\alpha-1} (\sin \theta)^{2\beta-1} d\theta \\ &= \Gamma(\alpha + \beta) \int_0^1 (\cos^2 \theta)^{\alpha-1} (1 - \cos^2 \theta)^{\beta-1} d \cos^2 \theta . \end{aligned}$$

Setting $t = \cos^2 \theta$ and dividing each member of the equation by $\Gamma(\alpha + \beta)$ then gives back (D.8)

$$B(\alpha, \beta) = \int_0^1 t^{\alpha-1} (1-t)^{\beta-1} dt = \frac{\Gamma(\alpha) \Gamma(\beta)}{\Gamma(\alpha + \beta)} .$$

Angular part of loop integrals

As detailed in Section 4.3, it is always possible to decompose the integrand of a scalar loop integral into a radial and an angular part (after having performed a Wick rotation and having introduced the spherical coordinates). The goal of this section is to provide an analytical expression for the angular part Ω_D of the D -dimensional scalar integrals. As we are going to see now, Ω_D can be explicitly written in terms of Euler-Gamma functions. The starting point of the proof is the definition of the Gaussian integral

$$\sqrt{\pi} = \int_{-\infty}^{+\infty} dx e^{-x^2} , \quad (D.9)$$

such that we *de facto* have

$$(\sqrt{\pi})^D = \int_{-\infty}^{+\infty} d^D x e^{-\sum x_i^2} = \int_{-\infty}^{+\infty} d^D x e^{-x^2} = \int d\Omega_D \int_0^{+\infty} x^{D-1} e^{-x^2} dx ,$$

where we have used in the last step the spherical coordinates to split the radial and the angular part of the integrand. The integral can then be rewritten as

$$(\sqrt{\pi})^D = \frac{1}{2} \int d\Omega_D \int_0^{+\infty} (x^2)^{D/2-1} e^{-x^2} dx^2 = \frac{1}{2} \int d\Omega_D \int_0^{+\infty} t^{D/2-1} e^{-t} dt . \quad (D.10)$$

Using the definition of the Euler-Gamma function (D.2), the previous equation simplifies to

$$\Omega_D = \int d\Omega_D = 2 \frac{(\sqrt{\pi})^D}{\Gamma(D/2)} , \quad (D.11)$$

which is, according to (D.4), equivalent to

$$\Omega_D = \int d\Omega_D = 2 \frac{\Gamma(1/2)^D}{\Gamma(D/2)} . \quad (D.12)$$

Appendix E

γ^5 in D -dimensions

Dimensional regularization has been applied with great success to gauge theories like QCD or QED¹. In contrast, gauge theories involving chiral fermions like the electroweak Standard Model, or calculations sensitive to polarization effects have been notoriously known to exhibit mathematical inconsistencies related to the analytic continuation of γ^5 in $D \neq 4$ dimensions [260]. In this appendix, we first point out that a naive extension of the definition of γ^5 from 4 to D dimensions is the source of the aforementioned inconsistencies. Then we review the virtues and drawbacks of the various prescriptions that have been designed to handle γ^5 in DREG, with a special emphasis put on the 't Hooft-Veltman-Breitenlohner-Maison (HVBM) scheme, and on the Naive Dimensional Regularization (NDR) scheme. In four-dimensions γ^5 is defined as

$$\gamma^5 = \frac{i}{4!} \varepsilon_{\mu\nu\rho\sigma} \gamma^\mu \gamma^\nu \gamma^\rho \gamma^\sigma . \quad (\text{E.1})$$

This definition implies that

$$\begin{aligned} (\gamma^5)^2 &= \mathbb{1}, & \{\gamma^\mu, \gamma^5\} &= 0, \\ \text{Tr}(\gamma^5) &= 0, & \text{Tr}(\gamma^\mu \gamma^5) &= 0, & \text{Tr}(\gamma^\mu \gamma^\nu \gamma^5) &= 0, & \text{Tr}(\gamma^\mu \gamma^\nu \gamma^\rho \gamma^5) &= 0, \\ & & \text{Tr}(\gamma^\mu \gamma^\nu \gamma^\rho \gamma^\sigma \gamma^5) &= 4i \varepsilon^{\mu\nu\rho\sigma} . \end{aligned} \quad (\text{E.2})$$

Naively, we would expect the properties of (E.2) to hold for any value of D , this is however not true. If we assume, cyclicity of the trace and an anticommuting γ^5 such that

$$\{\gamma^\mu, \gamma^5\} = 0 \quad \forall \mu = 0, \dots, D-1 \quad (\gamma^5)^2 = \mathbb{1} , \quad (\text{E.3})$$

we obtain the following properties of γ^5 in D dimensions

$$\begin{aligned} 2D \text{Tr}(\gamma^5) &= 0 \\ \text{Tr}(\gamma^\mu \gamma^5) &= 0, & 2(2-D) \text{Tr}(\gamma^\mu \gamma^\nu \gamma^5) &= 0, & \text{Tr}(\gamma^\mu \gamma^\nu \gamma^\rho \gamma^5) &= 0 \\ 2(D-4) \text{Tr}(\gamma^\mu \gamma^\nu \gamma^\rho \gamma^\sigma \gamma^5) &= 0 . \end{aligned} \quad (\text{E.4})$$

It is clear from the last line of (E.4) that only the particular case $D = 4$ allows us to recover the usual non-zero trace of γ^5 given in (E.2). The analytic continuation into D dimensions requires by definition the trace operation to be meromorphic, *i.e.* there should exist a smooth transition when taking the limit $D \rightarrow 4$. The problem is that the trace of γ^5 and four Dirac matrices given in (E.4) has to be zero for $D \neq 4$. The meromorphicity of the trace operation thus enforces a vanishing trace of Dirac matrices in (E.4) for any value of D , even for $D = 4$.

¹For calculations of unpolarized quantities only.

Consequently, we cannot recover the original four-dimensional result of (E.2), and that is why the naive anticommuting scheme is said to be mathematically inconsistent. More intuitively, the mathematical inconsistency of the NDR scheme can be understood as resulting from the fact that γ^5 is an ill-defined object for $D \neq 4$, and hence that all its usual algebraic properties in four dimensions cannot be simultaneously maintained in D dimensions.

Several schemes have been proposed to solve this issue. The most commonly accepted is the so-called 't Hooft-Veltman-Breitenlohner-Maison scheme, which was originally proposed by 't Hooft and Veltman in [152], and Akyeampong and Delbourgo [261], before being generalized by Breitenlohner and Maison [262], Thompson and Yu [263], and Collins [157]. The HVBM scheme consists in defining γ^5 as a generic four-dimensional object given by (E.1), which anticommutes with the four-dimensional part of the other γ -matrices, and commutes with remaining part

$$\{\gamma^\mu, \gamma^5\} = 0 \quad \text{if } \mu = 0, 1, 2, 3, \quad (\text{E.5})$$

$$[\gamma^\mu, \gamma^5] = 0 \quad \text{otherwise.} \quad (\text{E.6})$$

An alternative way to formulate the HVBM scheme can be summarized as follows. Knowing that in DREG we can decompose the D -dimensional vector space Q_D into a direct sum of the usual four-dimensional space Q_4 and a residual infinite dimensional space Q_{D-4} such that

$$Q_D = Q_4 \oplus Q_{D-4}, \quad (\text{E.7})$$

and that γ^5 is ill-defined in D dimensions, it is safer to assume that γ^5 lives only in Q_4 (which is orthogonal to Q_{D-4}). Objects living in orthogonal vector spaces commutes by definition, therefore the anticommutation relation is preserved for the four-dimensional component of γ^μ , and γ^5 commutes with γ^μ otherwise. Introducing the four-dimensional component $\tilde{\gamma}^\mu$ of γ^μ and its $D - 4$ counterpart $\tilde{\tilde{\gamma}}^\mu$ it is possible to rewrite (E.5) and (E.6) in a more compact way as

$$\{\gamma^\mu, \gamma^5\} = \{\tilde{\gamma}^\mu, \gamma^5\} + \{\tilde{\tilde{\gamma}}^\mu, \gamma^5\} \stackrel{(\text{E.5})}{=} \{\tilde{\tilde{\gamma}}^\mu, \gamma^5\} \stackrel{(\text{E.6})}{=} 2\gamma^5 \tilde{\tilde{\gamma}}^\mu. \quad (\text{E.8})$$

In a very general manner, the HVBM scheme allows for a systematic and mathematically consistent treatment of γ^5 at all orders in perturbation theory, and gives the correct result for the (physical) axial anomalies in the limit where $D = 4$, which is not possible with a chirally-symmetric scheme like the NDR [264]. This procedure however leads to more involved calculations, first because of (E.8), and second because of the fact that a non-anticommuting γ^5 generates spurious anomalies that violates chiral symmetry, and thus gauge invariance.

These spurious anomalies are artefacts originating from the choice of the γ^5 prescription, and have to be removed through an appropriate choice of counterterms in the Lagrangian². The real complication of the HVBM scheme hence resides in the fact that in order to get a rid of the anomalies that would spoil renormalizability of the theory³, Ward-Takahashi (WT) as well as Slavnov-Taylor (ST) identities have to be restored by hand, order by order in perturbation theory, through (finite) renormalization. This procedure of finite renormalization inherent to the use of the HVBM scheme adds another layer of complexity to the renormalization procedure, and seeing that Naive Dimensional Regularization and the HVBM scheme are expected to give the same results (at the exception of some pathological cases like the AVV triangles with a fermion-loop) we can understand why, despite being formally inconsistent, the NDR scheme is still used in a significant number of modern calculations.

²Note however that those counterterms are not chirally-symmetric.

³Renormalizability of abelian as well as non-abelian gauge theories heavily relies on the assumption that there exists a gauge invariant regularization.

Appendix F

NMFV SUSY-QCD Feynman rules

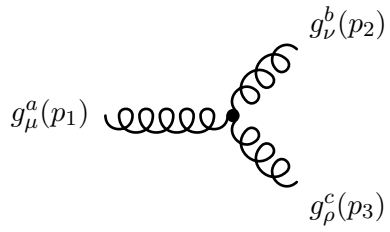
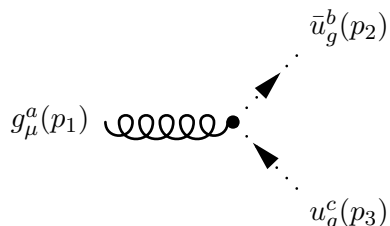
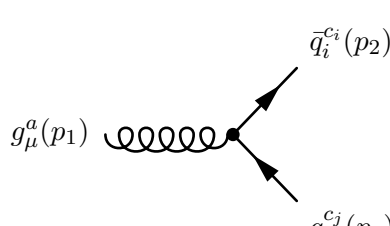
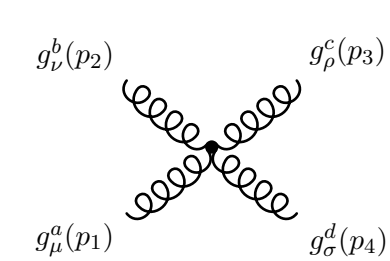
	$g_s f_{abc} \left[(p_1^\rho - p_2^\rho) \eta^{\mu\nu} + (p_3^\nu - p_1^\nu) \eta^{\rho\mu} + (p_2^\mu - p_3^\mu) \eta^{\nu\rho} \right],$
	$-g_s f_{abc} p_3^\mu,$
	$i g_s \gamma^\mu T_{c_i c_j}^a \delta_{ij},$
	$i g_s^2 \left[\eta^{\mu\sigma} \eta^{\nu\rho} [f^{ace} f^{bde} + f^{abe} f^{cde}] + \eta^{\mu\rho} \eta^{\nu\sigma} [f^{ade} f^{bce} - f^{abe} f^{cde}] + \eta^{\mu\nu} \eta^{\rho\sigma} [-f^{ade} f^{bce} - f^{ace} f^{bde}] \right].$

Table F.1: Feynman rules for the QCD sector. The four-momenta p_1, p_2, p_3 and p_4 , are all taken incoming to the vertices. The generators of the $\mathfrak{su}(3)_C$ algebra in the fundamental (resp. adjoint) representation are noted $T_{c_i c_j}^a$ (resp. f^{abc}). The indices c_i, c_j and a, b, c, d are respectively the colour indices of the fundamental and the adjoint representation. The indices μ, ν, ρ, σ are Lorentz indices, and i, j are flavour indices with $i, j = 1, 2, 3$.

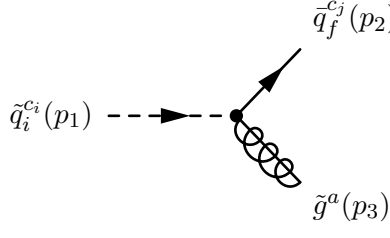
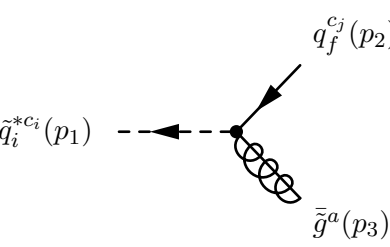
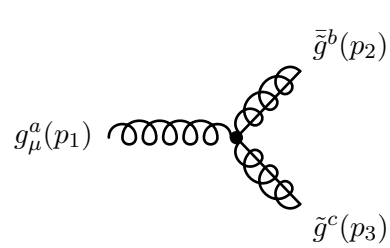
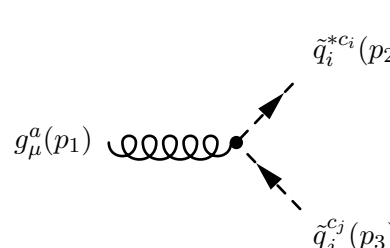
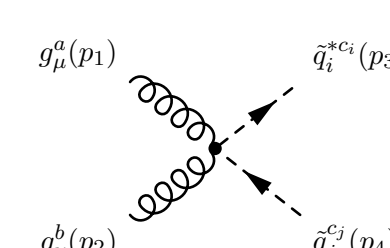
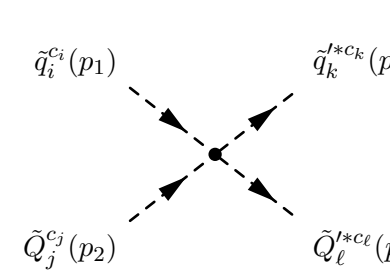
	$-i\sqrt{2}g_s \left[(R^{\bar{q}})_{if}^* e^{i\varphi_{\bar{g}}/2} P_R - (R^{\bar{q}})_{i(f+3)} e^{-i\varphi_{\bar{g}}/2} P_L \right] T_{c_j c_i}^a ,$
	$-i\sqrt{2}g_s \left[(R^{\bar{q}})_{if} e^{-i\varphi_{\bar{g}}/2} P_L - (R^{\bar{q}})_{i(f+3)} e^{i\varphi_{\bar{g}}/2} P_R \right] T_{c_i c_j}^a ,$
	$g_s f_{abc} \gamma^\mu ,$
	$i g_s (p_3^\mu - p_2^\mu) T_{c_i c_j}^a \delta_{ij} ,$
	$i g_s^2 (T^a T^b + T^b T^a)_{c_i c_j} \delta_{ij} \eta^{\mu\nu} ,$
	$-i g_s^2 \left[R(\tilde{q}_i^{c_i}, \tilde{q}_k^{*c_k}) R(\tilde{Q}_j^{c_j}, \tilde{Q}_\ell^{*c_\ell}) + R(\tilde{q}_i^{c_i}, \tilde{Q}_\ell^{*c_\ell}) R(\tilde{Q}_j^{c_j}, \tilde{q}_k^{*c_k}) \right] .$

Table F.2: Feynman rules for the SUSY-QCD sector. The four-momenta p_1, p_2, p_3 and p_4 , are all taken incoming to the vertices. The indices c_i, c_j, c_k, c_ℓ and a, b, c are all colour indices, μ and ν are Lorentz indices, and i, j, k, ℓ are flavour indices with $i, j, k, \ell = 1, 2, 3$. The notation \bar{g} allows one to uniquely define the fermion flow associated with vertices involving (Majorana) gluino fields. Note in addition that $R(\tilde{q}_i^{c_i}, \tilde{Q}_j^{c_j}) = \delta_{\tilde{q}\tilde{Q}} T_{c_j c_i}^a [(R^{\bar{q}})_{il}^* (R^{\bar{q}})_{jl} - (R^{\bar{q}})_{i(l+3)}^* (R^{\bar{q}})_{j(l+3)}]$ where the flavour index l is implicitly summed-over in the previous expression.

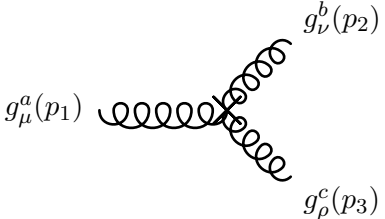
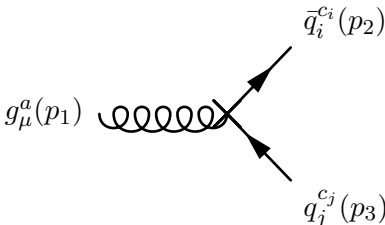
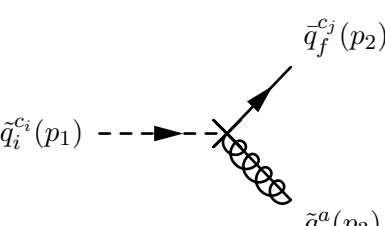
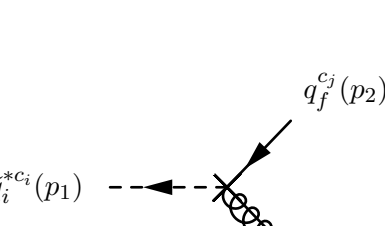
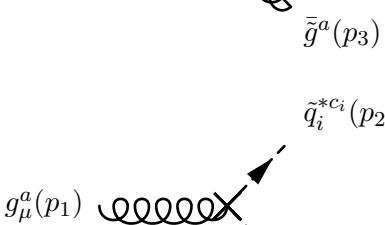
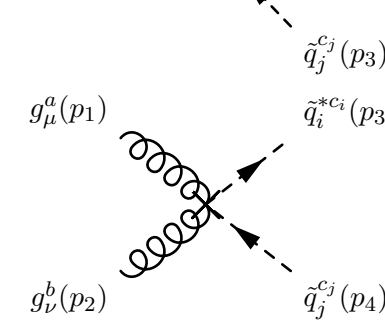
	$f_{abc} \left[(p_1 - p_2)^\rho \eta^{\mu\nu} + (p_3 - p_1)^\nu \eta^{\rho\mu} + (p_2 - p_3)^\mu \eta^{\nu\rho} \right] \left[\delta g_s + \frac{3}{2} g_s \delta Z_g \right],$
	$i\gamma^\mu \left[\delta g_s \delta_{ij} + \frac{g_s}{2} \left([(\delta Z_q^L)_{ij} + (\delta Z_q^{L\dagger})_{ij}] P_L + [(\delta Z_q^R)_{ij} + (\delta Z_q^{R\dagger})_{ij}] P_R + \delta Z_g \delta_{ij} \right) \right] T_{c_i c_j}^a,$
	$-i\sqrt{2} g_s T_{c_j c_i}^a \left[\left(\frac{\delta g_s}{g_s} (R_{\tilde{q}})_{if}^* + (\delta R_{\tilde{q}})_{if}^* + \frac{1}{2} (\delta Z_{\tilde{g}}^R (R_{\tilde{q}})_{if}^* + (R_{\tilde{q}})_{if'}^* (\delta Z_q^L)_{f'f}^* + (R_{\tilde{q}})_{jf}^* (\delta Z_{\tilde{q}})_{ji}) \right) e^{i\varphi_{\tilde{g}}/2} P_R - \left(\frac{\delta g_s}{g_s} (R_{\tilde{q}})_{i(f+3)}^* + (\delta R_{\tilde{q}})_{i(f+3)}^* + \frac{1}{2} (\delta Z_{\tilde{g}}^L (R_{\tilde{q}})_{i(f+3)}^* + (R_{\tilde{q}})_{i(f'+3)}^* (\delta Z_q^R)_{f'f}^* + (R_{\tilde{q}})_{j(f+3)}^* (\delta Z_{\tilde{q}})_{ji}) \right) e^{-i\varphi_{\tilde{g}}/2} P_L \right],$
	$-i\sqrt{2} g_s T_{c_i c_j}^a \left[\left(\frac{\delta g_s}{g_s} (R_{\tilde{q}})_{if} + (\delta R_{\tilde{q}})_{if} + \frac{1}{2} (\delta Z_{\tilde{g}}^{R*} (R_{\tilde{q}})_{if} + (R_{\tilde{q}})_{if'} (\delta Z_q^L)_{f'f} + (R_{\tilde{q}})_{jf} (\delta Z_{\tilde{q}})_{ji}^*) \right) e^{-i\varphi_{\tilde{g}}/2} P_L - \left(\frac{\delta g_s}{g_s} (R_{\tilde{q}})_{i(f+3)} + (\delta R_{\tilde{q}})_{i(f+3)} + \frac{1}{2} (\delta Z_{\tilde{g}}^{L*} (R_{\tilde{q}})_{i(f+3)} + (R_{\tilde{q}})_{i(f'+3)} (\delta Z_q^R)_{f'f} + (R_{\tilde{q}})_{j(f+3)} (\delta Z_{\tilde{q}})_{ji}^*) \right) e^{i\varphi_{\tilde{g}}/2} P_R \right],$
	$i(p_3^\mu - p_2^\mu) \left[\delta g_s \delta_{ij} + \frac{1}{2} g_s ((\delta Z_{\tilde{q}} + \delta Z_{\tilde{q}}^\dagger)_{ij} + \delta Z_g \delta_{ij}) \right] T_{c_i c_j}^a,$
	$i(T^a T^b + T^b T^a)_{c_i c_j} \eta^{\mu\nu} \left[2g_s \delta g_s \delta_{ij} + \frac{1}{2} g_s^2 ((\delta Z_{\tilde{q}} + \delta Z_{\tilde{q}}^\dagger)_{ij} + 2\delta Z_g \delta_{ij}) \right],$

Table F.3: Feynman rules for the counter-terms of the QCD, and SUSY-QCD sectors that are needed for squark-antisquark pair production at NLO with NMFV. The four-momenta p_1 , p_2 , p_3 and p_4 , are all taken incoming to the vertices. The indices c_i , c_j , c_k , c_l and a , b , c are all colour indices, μ and ν are Lorentz indices, and i , j , k , l are flavour indices with $i, j, k, l = 1, 2, 3$. The notation \tilde{g} allows one to uniquely define the fermion flow associated with vertices involving (Majorana) gluino fields.

Bibliography

- [1] **Particle Data Group** Collaboration, K. Olive *et. al.*, *Review of Particle Physics*, *Chin.Phys.* **C38** (2014) 090001.
- [2] Y. Ne'eman, *Derivation of strong interactions from a gauge invariance*, *Nucl.Phys.* **26** (1961) 222–229.
- [3] M. Gell-Mann, *Symmetries of baryons and mesons*, *Phys.Rev.* **125** (1962) 1067–1084.
- [4] M. Gell-Mann, *A Schematic Model of Baryons and Mesons*, *Phys.Lett.* **8** (1964) 214–215.
- [5] G. Zweig, *An $SU(3)$ model for strong interaction symmetry and its breaking. Version 1*, .
- [6] G. Zweig, *An $SU(3)$ model for strong interaction symmetry and its breaking. Version 2*, .
- [7] J. Bjorken, *Asymptotic Sum Rules at Infinite Momentum*, *Phys.Rev.* **179** (1969) 1547–1553.
- [8] R. P. Feynman, *Very high-energy collisions of hadrons*, *Phys.Rev.Lett.* **23** (1969) 1415–1417.
- [9] D. J. Gross and F. Wilczek, *Ultraviolet Behavior of Nonabelian Gauge Theories*, *Phys.Rev.Lett.* **30** (1973) 1343–1346.
- [10] H. D. Politzer, *Reliable Perturbative Results for Strong Interactions?*, *Phys.Rev.Lett.* **30** (1973) 1346–1349.
- [11] D. Gross and F. Wilczek, *Asymptotically Free Gauge Theories. 1*, *Phys.Rev.* **D8** (1973) 3633–3652.
- [12] H. Fritzsch, M. Gell-Mann, and H. Leutwyler, *Advantages of the Color Octet Gluon Picture*, *Phys.Lett.* **B47** (1973) 365–368.
- [13] D. Gross and F. Wilczek, *ASYMPTOTICALLY FREE GAUGE THEORIES. 2.*, *Phys.Rev.* **D9** (1974) 980–993.
- [14] H. D. Politzer, *Asymptotic Freedom: An Approach to Strong Interactions*, *Phys.Rept.* **14** (1974) 129–180.
- [15] G. 't Hooft, *THE BIRTH OF ASYMPTOTIC FREEDOM*, *Nucl.Phys.* **B254** (1985) 11–18.
- [16] S. Glashow, *Partial Symmetries of Weak Interactions*, *Nucl.Phys.* **22** (1961) 579–588.
- [17] S. Weinberg, *A Model of Leptons*, *Phys.Rev.Lett.* **19** (1967) 1264–1266.
- [18] A. Salam, *Weak and Electromagnetic Interactions*, *Conf.Proc.* **C680519** (1968) 367–377.

- [19] S. Glashow, J. Iliopoulos, and L. Maiani, *Weak Interactions with Lepton-Hadron Symmetry*, *Phys.Rev.* **D2** (1970) 1285–1292.
- [20] B. Pietrzyk, *LEP asymmetries and fits of the standard model*, hep-ex/9406001.
- [21] **CDF Collaboration** Collaboration, F. Abe *et. al.*, *Observation of top quark production in $\bar{p}p$ collisions*, *Phys.Rev.Lett.* **74** (1995) 2626–2631, [hep-ex/9503002].
- [22] **D0 Collaboration** Collaboration, S. Abachi *et. al.*, *Observation of the top quark*, *Phys.Rev.Lett.* **74** (1995) 2632–2637, [hep-ex/9503003].
- [23] F. Englert and R. Brout, *Broken Symmetry and the Mass of Gauge Vector Mesons*, *Phys.Rev.Lett.* **13** (1964) 321–323.
- [24] P. W. Higgs, *Broken symmetries, massless particles and gauge fields*, *Phys.Lett.* **12** (1964) 132–133.
- [25] P. W. Higgs, *Broken Symmetries and the Masses of Gauge Bosons*, *Phys.Rev.Lett.* **13** (1964) 508–509.
- [26] G. Guralnik, C. Hagen, and T. Kibble, *Global Conservation Laws and Massless Particles*, *Phys.Rev.Lett.* **13** (1964) 585–587.
- [27] P. W. Higgs, *Spontaneous Symmetry Breakdown without Massless Bosons*, *Phys.Rev.* **145** (1966) 1156–1163.
- [28] T. Kibble, *Symmetry breaking in nonAbelian gauge theories*, *Phys.Rev.* **155** (1967) 1554–1561.
- [29] **ATLAS Collaboration** Collaboration, G. Aad *et. al.*, *Observation of a new particle in the search for the Standard Model Higgs boson with the ATLAS detector at the LHC*, *Phys.Lett.* **B716** (2012) 1–29, [1207.7214].
- [30] **CMS Collaboration** Collaboration, S. Chatrchyan *et. al.*, *Observation of a new boson at a mass of 125 GeV with the CMS experiment at the LHC*, *Phys.Lett.* **B716** (2012) 30–61, [1207.7235].
- [31] **ATLAS, CMS Collaboration**, G. Aad *et. al.*, *Combined Measurement of the Higgs Boson Mass in pp Collisions at $\sqrt{s} = 7$ and 8 TeV with the ATLAS and CMS Experiments*, *Phys. Rev. Lett.* **114** (2015) 191803, [1503.07589].
- [32] <https://twiki.cern.ch/twiki/bin/view/AtlasPublic/HiggsPublicResults>.
- [33] <https://twiki.cern.ch/twiki/bin/view/CMSPublic/PhysicsResultsHIG>.
- [34] B. Pontecorvo, *Mesonium and anti-mesonium*, *Sov.Phys.JETP* **6** (1957) 429.
- [35] Z. Maki, M. Nakagawa, and S. Sakata, *Remarks on the unified model of elementary particles*, *Prog.Theor.Phys.* **28** (1962) 870–880.
- [36] N. Arkani-Hamed, S. Dimopoulos, and G. Dvali, *The Hierarchy problem and new dimensions at a millimeter*, *Phys.Lett.* **B429** (1998) 263–272, [hep-ph/9803315].
- [37] T. van Ritbergen and R. G. Stuart, *Complete two loop quantum electrodynamic contributions to the muon lifetime in the Fermi model*, *Phys.Rev.Lett.* **82** (1999) 488–491, [hep-ph/9808283].

- [38] T. van Ritbergen and R. G. Stuart, *On the precise determination of the Fermi coupling constant from the muon lifetime*, *Nucl.Phys.* **B564** (2000) 343–390, [hep-ph/9904240].
- [39] M. Steinhauser and T. Seidensticker, *Second order corrections to the muon lifetime and the semileptonic B decay*, *Phys.Lett.* **B467** (1999) 271–278, [hep-ph/9909436].
- [40] K. G. Wilson, *The Renormalization Group and Strong Interactions*, *Phys.Rev.* **D3** (1971) 1818.
- [41] L. Susskind, *Dynamics of Spontaneous Symmetry Breaking in the Weinberg-Salam Theory*, *Phys.Rev.* **D20** (1979) 2619–2625.
- [42] G. 't Hooft, *Naturalness, chiral symmetry, and spontaneous chiral symmetry breaking*, *NATO Sci.Ser.B* **59** (1980) 135.
- [43] M. Veltman, *The Infrared - Ultraviolet Connection*, *Acta Phys.Polon.* **B12** (1981) 437.
- [44] H. P. Nilles, *Supersymmetry, Supergravity and Particle Physics*, *Phys.Rept.* **110** (1984) 1–162.
- [45] W. A. Bardeen, *On naturalness in the standard model*, .
- [46] I. Masina and M. Quiros, *On the Veltman Condition, the Hierarchy Problem and High-Scale Supersymmetry*, *Phys.Rev.* **D88** (2013) 093003, [1308.1242].
- [47] C. F. Kolda and H. Murayama, *The Higgs mass and new physics scales in the minimal standard model*, *JHEP* **0007** (2000) 035, [hep-ph/0003170].
- [48] G. F. Giudice, *Naturally Speaking: The Naturalness Criterion and Physics at the LHC*, **0801.2562**.
- [49] J. R. Ellis, K. Enqvist, D. V. Nanopoulos, and F. Zwirner, *Observables in Low-Energy Superstring Models*, *Mod.Phys.Lett.* **A1** (1986) 57.
- [50] R. Barbieri and G. Giudice, *Upper Bounds on Supersymmetric Particle Masses*, *Nucl.Phys.* **B306** (1988) 63.
- [51] M. Einhorn and D. Jones, *The Effective potential and quadratic divergences*, *Phys.Rev.* **D46** (1992) 5206–5208.
- [52] L. Reina, *TASI 2011: lectures on Higgs-Boson Physics*, **1208.5504**.
- [53] P. W. Graham, D. E. Kaplan, and S. Rajendran, *Cosmological Relaxation of the Electroweak Scale*, **1504.07551**.
- [54] S. Weinberg, *Gauge Hierarchies*, *Phys.Lett.* **B82** (1979) 387.
- [55] G. 't Hooft, C. Itzykson, A. Jaffe, H. Lehmann, P. Mitter, *et. al.*, *Recent Developments in Gauge Theories. Proceedings, Nato Advanced Study Institute, Cargese, France, August 26 - September 8, 1979*, *NATO Sci.Ser.B* **59** (1980) pp.1–438.
- [56] F. Lyonnet, I. Schienbein, F. Staub, and A. Wingerter, *PyR@TE: Renormalization Group Equations for General Gauge Theories*, *Comput.Phys.Commun.* **185** (2014) 1130–1152, [1309.7030].
- [57] J. C. Pati and A. Salam, *Unified Lepton-Hadron Symmetry and a Gauge Theory of the Basic Interactions*, *Phys.Rev.* **D8** (1973) 1240–1251.

- [58] J. C. Pati and A. Salam, *Lepton Number as the Fourth Color*, *Phys.Rev.* **D10** (1974) 275–289.
- [59] H. Georgi and S. Glashow, *Unity of All Elementary Particle Forces*, *Phys.Rev.Lett.* **32** (1974) 438–441.
- [60] H. Georgi, H. R. Quinn, and S. Weinberg, *Hierarchy of Interactions in Unified Gauge Theories*, *Phys.Rev.Lett.* **33** (1974) 451–454.
- [61] P. Langacker, *The standard model and beyond*, .
- [62] N. Cabibbo, *Unitary Symmetry and Leptonic Decays*, *Phys.Rev.Lett.* **10** (1963) 531–533.
- [63] M. Kobayashi and T. Maskawa, *CP Violation in the Renormalizable Theory of Weak Interaction*, *Prog.Theor.Phys.* **49** (1973) 652–657.
- [64] **Planck** Collaboration, P. Ade *et. al.*, *Planck 2013 results. XVI. Cosmological parameters*, *Astron.Astrophys.* **571** (2014) A16, [1303.5076].
- [65] **Planck Collaboration** Collaboration, P. Ade *et. al.*, *Planck 2015 results. XIII. Cosmological parameters*, 1502.01589.
- [66] **WMAP** Collaboration, G. Hinshaw *et. al.*, *Nine-Year Wilkinson Microwave Anisotropy Probe (WMAP) Observations: Cosmological Parameter Results*, *Astrophys.J.Suppl.* **208** (2013) 19, [1212.5226].
- [67] J. Rosa, “Introduction to cosmology - lecture 7 - thermal history of the universe II.”
- [68] J. M. Cline, *Baryogenesis*, hep-ph/0609145.
- [69] D. E. Morrissey and M. J. Ramsey-Musolf, *Electroweak baryogenesis*, *New J.Phys.* **14** (2012) 125003, [1206.2942].
- [70] A. Sakharov, *Violation of CP Invariance, c Asymmetry, and Baryon Asymmetry of the Universe*, *Pisma Zh.Eksp.Teor.Fiz.* **5** (1967) 32–35.
- [71] G. 't Hooft, *Symmetry Breaking Through Bell-Jackiw Anomalies*, *Phys.Rev.Lett.* **37** (1976) 8–11.
- [72] N. Manton, *Topology in the Weinberg-Salam Theory*, *Phys.Rev.* **D28** (1983) 2019.
- [73] F. R. Klinkhamer and N. Manton, *A Saddle Point Solution in the Weinberg-Salam Theory*, *Phys.Rev.* **D30** (1984) 2212.
- [74] C. Grojean, G. Servant, and J. D. Wells, *First-order electroweak phase transition in the standard model with a low cutoff*, *Phys.Rev.* **D71** (2005) 036001, [hep-ph/0407019].
- [75] V. Kuzmin, V. Rubakov, and M. Shaposhnikov, *On the Anomalous Electroweak Baryon Number Nonconservation in the Early Universe*, *Phys.Lett.* **B155** (1985) 36.
- [76] D. S. Gorbunov and V. A. Rubakov, *Introduction to the theory of the early universe: Hot big bang theory*, .
- [77] V. Rubakov and M. Shaposhnikov, *Electroweak baryon number nonconservation in the early universe and in high-energy collisions*, *Usp.Fiz.Nauk* **166** (1996) 493–537, [hep-ph/9603208].

- [78] C. Jarlskog, *Commutator of the Quark Mass Matrices in the Standard Electroweak Model and a Measure of Maximal CP Violation*, *Phys.Rev.Lett.* **55** (1985) 1039.
- [79] K. Kajantie, M. Laine, K. Rummukainen, and M. E. Shaposhnikov, *Is there a hot electroweak phase transition at $m(H)$ larger or equal to $m(W)$?*, *Phys.Rev.Lett.* **77** (1996) 2887–2890, [hep-ph/9605288].
- [80] K. Rummukainen, M. Tsypin, K. Kajantie, M. Laine, and M. E. Shaposhnikov, *The Universality class of the electroweak theory*, *Nucl.Phys.* **B532** (1998) 283–314, [hep-lat/9805013].
- [81] F. Csikor, Z. Fodor, and J. Heitger, *Endpoint of the hot electroweak phase transition*, *Phys.Rev.Lett.* **82** (1999) 21–24, [hep-ph/9809291].
- [82] T. van Albada, J. N. Bahcall, K. Begeman, and R. Sancisi, *The Distribution of Dark Matter in the Spiral Galaxy NGC-3198*, *Astrophys.J.* **295** (1985) 305–313.
- [83] F. Zwicky, *Die Rotverschiebung von extragalaktischen Nebeln*, *Helv.Phys.Acta* **6** (1933) 110–127.
- [84] V. Rubin, N. Thonnard, and J. Ford, W.K., *Rotational properties of 21 SC galaxies with a large range of luminosities and radii, from NGC 4605 / $R = 4kpc$ / to UGC 2885 / $R = 122 kpc$ /*, *Astrophys.J.* **238** (1980) 471.
- [85] R. D. Peccei, *QCD, strong CP and axions*, *J. Korean Phys. Soc.* **29** (1996) S199–S208, [hep-ph/9606475].
- [86] B. Fuks, J. Proudom, J. Rojo, and I. Schienbein, *Characterizing New Physics with Polarized Beams at High-Energy Hadron Colliders*, *JHEP* **05** (2014) 045, [1403.2383].
- [87] H. Eberl, B. Fuks, E. Ginina, B. Herrmann, W. Porod, and J. Proudom, (to appear), .
- [88] C. Degrande, B. Fuks, V. Hirschi, J. Proudom, and H.-S. Shao, *Automated next-to-leading order predictions for new physics at the LHC: the case of colored scalar pair production*, *Phys. Rev.* **D91** (2015), no. 9 094005, [1412.5589].
- [89] C. Degrande, B. Fuks, V. Hirschi, J. Proudom, and H.-S. Shao, *Gluino pair-production matched to parton showers at the next-to-leading order*, 1510.00391.
- [90] J.-L. Gervais and B. Sakita, *Field Theory Interpretation of Supergauges in Dual Models*, *Nucl.Phys.* **B34** (1971) 632–639.
- [91] Y. Golfand and E. Likhtman, *Extension of the Algebra of Poincare Group Generators and Violation of p Invariance*, *JETP Lett.* **13** (1971) 323–326.
- [92] P. Ramond, *Dual Theory for Free Fermions*, *Phys.Rev.* **D3** (1971) 2415–2418.
- [93] A. Neveu and J. Schwarz, *Quark Model of Dual Pions*, *Phys.Rev.* **D4** (1971) 1109–1111.
- [94] D. Volkov and V. Akulov, *Is the Neutrino a Goldstone Particle?*, *Phys.Lett.* **B46** (1973) 109–110.
- [95] J. Wess and B. Zumino, *Supergauge Transformations in Four-Dimensions*, *Nucl.Phys.* **B70** (1974) 39–50.

- [96] R. Haag, J. T. Lopuszanski, and M. Sohnius, *All Possible Generators of Supersymmetries of the s Matrix*, *Nucl.Phys.* **B88** (1975) 257.
- [97] <https://twiki.cern.ch/twiki/bin/view/AtlasPublic/SupersymmetryPublicResults>.
- [98] <https://twiki.cern.ch/twiki/bin/view/CMSPublic/PhysicsResultsSUS>.
- [99] S. R. Coleman and J. Mandula, *All Possible Symmetries of the S Matrix*, *Phys.Rev.* **159** (1967) 1251–1256.
- [100] H. Murayama, *Supersymmetry phenomenology*, in *Particle physics. Proceedings, Summer School, Trieste, Italy, June 21-July 9, 1999*, pp. 296–335, 2000. hep-ph/0002232.
- [101] B. C. Allanach *et. al.*, *SUSY Les Houches Accord 2*, *Comput. Phys. Commun.* **180** (2009) 8–25, [0801.0045].
- [102] L. Girardello and M. T. Grisaru, *Soft Breaking of Supersymmetry*, *Nucl. Phys.* **B194** (1982) 65.
- [103] B. Fuks, *Supersymmetry - When Theory Inspires Experimental Searches*. PhD thesis, U. Strasbourg, 2014. 1401.6277.
- [104] **OPAL, DELPHI, LEP Working Group for Higgs boson searches, ALEPH, L3** Collaboration, R. Barate *et. al.*, *Search for the standard model Higgs boson at LEP*, *Phys. Lett.* **B565** (2003) 61–75, [hep-ex/0306033].
- [105] **DELPHI, OPAL, ALEPH, LEP Working Group for Higgs Boson Searches, L3** Collaboration, S. Schael *et. al.*, *Search for neutral MSSM Higgs bosons at LEP*, *Eur. Phys. J.* **C47** (2006) 547–587, [hep-ex/0602042].
- [106] J. Andrea, B. Fuks, and F. Maltoni, *Monotops at the LHC*, *Phys.Rev.* **D84** (2011) 074025, [1106.6199].
- [107] J.-L. Agram, J. Andrea, M. Buttignol, E. Conte, and B. Fuks, *Monotop phenomenology at the Large Hadron Collider*, *Phys.Rev.* **D89** (2014) 014028, [1311.6478].
- [108] E. L. Berger, B. Harris, and Z. Sullivan, *Single top squark production via R -parity violating supersymmetric couplings in hadron collisions*, *Phys.Rev.Lett.* **83** (1999) 4472–4475, [hep-ph/9903549].
- [109] E. L. Berger, B. Harris, and Z. Sullivan, *Direct probes of R -parity violating supersymmetric couplings via single top squark production*, *Phys.Rev.* **D63** (2001) 115001, [hep-ph/0012184].
- [110] N. Desai and B. Mukhopadhyaya, *R -parity violating resonant stop production at the Large Hadron Collider*, *JHEP* **1010** (2010) 060, [1002.2339].
- [111] B. Fuks, *Beyond the Minimal Supersymmetric Standard Model: from theory to phenomenology*, *Int.J.Mod.Phys.* **A27** (2012) 1230007, [1202.4769].
- [112] H. Davoudiasl, D. E. Morrissey, K. Sigurdson, and S. Tulin, *Hylogenesis: A Unified Origin for Baryonic Visible Matter and Antibaryonic Dark Matter*, *Phys.Rev.Lett.* **105** (2010) 211304, [1008.2399].
- [113] H. Davoudiasl, D. E. Morrissey, K. Sigurdson, and S. Tulin, *Baryon Destruction by Asymmetric Dark Matter*, *Phys.Rev.* **D84** (2011) 096008, [1106.4320].

- [114] J. F. Kamenik and J. Zupan, *Discovering Dark Matter Through Flavor Violation at the LHC*, *Phys.Rev.* **D84** (2011) 111502, [1107.0623].
- [115] E. Alvarez, E. C. Leskow, J. Drobnak, and J. F. Kamenik, *Leptonic Monotops at LHC*, *Phys.Rev.* **D89** (2014) 014016, [1310.7600].
- [116] H. E. Haber and G. L. Kane, *The Search for Supersymmetry: Probing Physics Beyond the Standard Model*, *Phys.Rept.* **117** (1985) 75–263.
- [117] T. Appelquist, H.-C. Cheng, and B. A. Dobrescu, *Bounds on universal extra dimensions*, *Phys.Rev.* **D64** (2001) 035002, [hep-ph/0012100].
- [118] N. Craigie, K. Hidaka, and P. Ratcliffe, *The Role Helicity Asymmetries Could Play in the Search for Supersymmetric Interactions*, *Phys.Lett.* **B129** (1983) 310.
- [119] P. Taxil and J. Virey, *Discovery limits for a new contact interaction at future hadronic colliders with polarized beams*, *Phys.Rev.* **D55** (1997) 4480–4483, [hep-ph/9607390].
- [120] J. Virey, *Hunting for contact interactions at HERA with polarized lepton and proton beams*, *Eur.Phys.J.* **C8** (1999) 283–299, [hep-ph/9809439].
- [121] P. Taxil, E. Tugcu, and J. Virey, *Constraints on leptophobic gauge bosons with polarized neutrons and protons at RHIC*, *Eur.Phys.J.* **C24** (2002) 149–157, [hep-ph/0111242].
- [122] T. Gehrmann, D. Maitre, and D. Wyler, *Spin asymmetries in squark and gluino production at polarized hadron colliders*, *Nucl.Phys.* **B703** (2004) 147–176, [hep-ph/0406222].
- [123] G. Bozzi, B. Fuks, and M. Klasen, *Slepton production in polarized hadron collisions*, *Phys.Lett.* **B609** (2005) 339–350, [hep-ph/0411318].
- [124] J. Debove, B. Fuks, and M. Klasen, *Model-independent analysis of gaugino-pair production in polarized and unpolarized hadron collisions*, *Phys.Rev.* **D78** (2008) 074020, [0804.0423].
- [125] M. Wiest, D. R. Stump, D. O. Carlson, and C. Yuan, *Studying anomalous $W W$ gamma and $W W Z$ couplings with polarized p anti- p collisions*, *Phys.Rev.* **D52** (1995) 2724–2736, [hep-ph/9506327].
- [126] **SPIN Collaboration** Collaboration, R. Baiod, P. Martin, and A. Russell, *Polarized protons in the Tevatron Collider, Contribution to the 10th Topical Workshop on Proton-Antiproton Collider Physics, Batavia, Illinois* (1995) 206–216.
- [127] A. De Roeck, D. Barber, and G. Radcliff, *Polarized protons at high-energies, Proceedings of the DESY workshop on Polarized Protons at High Energies, Hamburg, Germany* (1999).
- [128] **NNPDF** Collaboration, R. D. Ball *et. al.*, *Parton distributions for the LHC Run II*, *JHEP* **04** (2015) 040, [1410.8849].
- [129] **The NNPDF Collaboration** Collaboration, R. D. Ball *et. al.*, *Unbiased determination of polarized parton distributions and their uncertainties*, *Nucl.Phys.* **B874** (2013) 36–84, [1303.7236].
- [130] E. R. Nocera, *Unbiased spin-dependent Parton Distribution Functions*, 1403.0440.

- [131] M. Whalley, D. Bourilkov, and R. Group, *The Les Houches accord PDFs (LHAPDF) and LHAGLUE*, hep-ph/0508110.
- [132] G. Altarelli, S. Forte, and G. Ridolfi, *On positivity of parton distributions*, *Nucl.Phys.* **B534** (1998) 277–296, [hep-ph/9806345].
- [133] R. D. Ball, S. Forte, and G. Ridolfi, *Scale dependence and small x behavior of polarized parton distributions*, *Nucl.Phys.* **B444** (1995) 287–309, [hep-ph/9502340].
- [134] J. M. Campbell, J. Huston, and W. Stirling, *Hard Interactions of Quarks and Gluons: A Primer for LHC Physics*, *Rept.Prog.Phys.* **70** (2007) 89, [hep-ph/0611148].
- [135] D. de Florian, R. Sassot, M. Stratmann, and W. Vogelsang, *Extraction of Spin-Dependent Parton Densities and Their Uncertainties*, *Phys.Rev.* **D80** (2009) 034030, [0904.3821].
- [136] R. D. Ball, V. Bertone, S. Carrazza, C. S. Deans, L. Del Debbio, *et. al.*, *Parton distributions with LHC data*, *Nucl.Phys.* **B867** (2013) 244–289, [1207.1303].
- [137] A. D. Martin, R. Roberts, W. Stirling, and R. Thorne, *MRST2001: Partons and α_s from precise deep inelastic scattering and Tevatron jet data*, *Eur.Phys.J.* **C23** (2002) 73–87, [hep-ph/0110215].
- [138] **The NNPDF Collaboration** Collaboration, R. D. Ball *et. al.*, *Theoretical issues in PDF determination and associated uncertainties*, *Phys.Lett.* **B723** (2013) 330–339, [1303.1189].
- [139] D. Boer, M. Diehl, R. Milner, R. Venugopalan, W. Vogelsang, *et. al.*, *Gluons and the quark sea at high energies: Distributions, polarization, tomography*, 1108.1713.
- [140] **NNPDF Collaboration**, R. D. Ball *et. al.*, *Polarized Parton Distributions at an Electron-Ion Collider*, *Phys.Lett.* **B728** (2014) 524–531, [1310.0461].
- [141] E. C. Aschenauer, T. Burton, T. Martini, H. Spiesberger, and M. Stratmann, *Prospects for Charged Current Deep-Inelastic Scattering off Polarized Nucleons at a Future Electron-Ion Collider*, *Phys.Rev.* **D88** (2013) 114025, [1309.5327].
- [142] E. C. Aschenauer, R. Sassot, and M. Stratmann, *Helicity Parton Distributions at a Future Electron-Ion Collider: A Quantitative Appraisal*, *Phys.Rev.* **D86** (2012) 054020, [1206.6014].
- [143] R. Barbier, C. Berat, M. Besancon, M. Chemtob, A. Deandrea, *et. al.*, *R-parity violating supersymmetry*, *Phys.Rept.* **420** (2005) 1–202, [hep-ph/0406039].
- [144] **R parity Working Group Collaboration** Collaboration, B. Allanach *et. al.*, *Searching for R parity violation at Run II of the Tevatron*, hep-ph/9906224.
- [145] D. Berdine, N. Kauer, and D. Rainwater, *Breakdown of the Narrow Width Approximation for New Physics*, *Phys.Rev.Lett.* **99** (2007) 111601, [hep-ph/0703058].
- [146] I.-W. Kim and K. M. Zurek, *Flavor and Collider Signatures of Asymmetric Dark Matter*, *Phys.Rev.* **D89** (2014) 035008, [1310.2617].
- [147] T. Hahn, *Generating Feynman diagrams and amplitudes with FeynArts 3*, *Comput.Phys.Commun.* **140** (2001) 418–431.

- [148] P. Nogueira, *Automatic Feynman graph generation*, *J. Comput. Phys.* **105** (1993) 279–289.
- [149] T. Kinoshita, *Mass singularities of Feynman amplitudes*, *J. Math. Phys.* **3** (1962) 650–677.
- [150] T. D. Lee and M. Nauenberg, *Degenerate Systems and Mass Singularities*, *Phys. Rev.* **133** (1964) B1549–B1562.
- [151] W. Beenakker, H. Kuijf, W. L. van Neerven, and J. Smith, *QCD Corrections to Heavy Quark Production in p anti- p Collisions*, *Phys. Rev.* **D40** (1989) 54–82.
- [152] G. 't Hooft and M. Veltman, *Regularization and Renormalization of Gauge Fields*, *Nucl.Phys.* **B44** (1972) 189–213.
- [153] C. Bollini and J. Giambiagi, *Dimensional Renormalization: The Number of Dimensions as a Regularizing Parameter*, *Nuovo Cim.* **12** (1972), no. 1 20–26.
- [154] G. Cicuta and E. Montaldi, *Analytic renormalization via continuous space dimension*, *Lett.Nuovo Cim.* **4** (1972) 329–332.
- [155] J. Ashmore, *A Method of Gauge Invariant Regularization*, *Lett.Nuovo Cim.* **4** (1972) 289–290.
- [156] K. G. Wilson, *Quantum field theory models in less than four-dimensions*, *Phys.Rev.* **D7** (1973) 2911–2926.
- [157] J. C. Collins, *RENORMALIZATION. AN INTRODUCTION TO RENORMALIZATION, THE RENORMALIZATION GROUP, AND THE OPERATOR PRODUCT EXPANSION*, .
- [158] S. Weinzierl, *The Art of computing loop integrals*, hep-ph/0604068.
- [159] J. Zinn-Justin, *Chiral anomalies and topology*, *Lect.Notes Phys.* **659** (2005) 167–236, [hep-th/0201220].
- [160] W. Siegel, *Supersymmetric Dimensional Regularization via Dimensional Reduction*, *Phys.Lett.* **B84** (1979) 193.
- [161] Z. Bern and D. A. Kosower, *The Computation of loop amplitudes in gauge theories*, *Nucl. Phys.* **B379** (1992) 451–561.
- [162] Z. Bern, A. De Freitas, L. J. Dixon, and H. L. Wong, *Supersymmetric regularization, two loop QCD amplitudes and coupling shifts*, *Phys. Rev.* **D66** (2002) 085002, [hep-ph/0202271].
- [163] W. B. Kilgore, *Regularization Schemes and Higher Order Corrections*, *Phys.Rev.* **D83** (2011) 114005, [1102.5353].
- [164] R. Boughezal, K. Melnikov, and F. Petriello, *The four-dimensional helicity scheme and dimensional reconstruction*, *Phys.Rev.* **D84** (2011) 034044, [1106.5520].
- [165] W. Hollik and D. Stockinger, *Regularization and supersymmetry restoring counterterms in supersymmetric QCD*, *Eur. Phys. J.* **C20** (2001) 105–119, [hep-ph/0103009].

- [166] S. P. Martin and M. T. Vaughn, *Regularization dependence of running couplings in softly broken supersymmetry*, *Phys. Lett.* **B318** (1993) 331–337, [hep-ph/9308222].
- [167] L. Brink, J. H. Schwarz, and J. Scherk, *Supersymmetric Yang-Mills Theories*, *Nucl.Phys.* **B121** (1977) 77.
- [168] W. Siegel, *Inconsistency of Supersymmetric Dimensional Regularization*, *Phys.Lett.* **B94** (1980) 37.
- [169] L. Avdeev and A. Vladimirov, *Dimensional Regularization and Supersymmetry*, *Nucl.Phys.* **B219** (1983) 262.
- [170] L. V. Avdeev, G. A. Chochia, and A. A. Vladimirov, *On the Scope of Supersymmetric Dimensional Regularization*, *Phys. Lett.* **B105** (1981) 272.
- [171] D. Stockinger, *Regularization by dimensional reduction: consistency, quantum action principle, and supersymmetry*, *JHEP* **0503** (2005) 076, [hep-ph/0503129].
- [172] G. 't Hooft and M. Veltman, *Scalar One Loop Integrals*, *Nucl.Phys.* **B153** (1979) 365–401.
- [173] A. Denner, U. Nierste, and R. Scharf, *A Compact expression for the scalar one loop four point function*, *Nucl. Phys.* **B367** (1991) 637–656.
- [174] A. Denner, *Techniques for calculation of electroweak radiative corrections at the one loop level and results for W physics at LEP-200*, *Fortsch. Phys.* **41** (1993) 307–420, [0709.1075].
- [175] G. Passarino and M. J. G. Veltman, *One Loop Corrections for $e^+ e^-$ Annihilation Into $\mu^+ \mu^-$ in the Weinberg Model*, *Nucl. Phys.* **B160** (1979) 151.
- [176] H. Eberl, A. Bartl, and W. Majerotto, *SUSY QCD corrections to scalar quark pair production in $e^+ e^-$ annihilation*, *Nucl. Phys.* **B472** (1996) 481–494, [hep-ph/9603206].
- [177] Y. Yamada, *Radiative corrections to sfermion mass splittings*, *Phys. Rev.* **D54** (1996) 1150–1154, [hep-ph/9602279].
- [178] A. Bartl, H. Eberl, K. Hidaka, T. Kon, W. Majerotto, and Y. Yamada, *QCD corrections to Higgs boson decays into squarks in the minimal supersymmetric standard model*, *Phys. Lett.* **B402** (1997) 303–313, [hep-ph/9701398].
- [179] S. Kraml, *Stop and sbottom phenomenology in the MSSM*. PhD thesis, Vienna, OAW, 1999. hep-ph/9903257.
- [180] G. L. Kane, A. A. Petrov, J. Shao, and L.-T. Wang, *Initial determination of the spins of the gluino and squarks at LHC*, *J. Phys.* **G37** (2010) 045004, [0805.1397].
- [181] J. Hubisz, J. Lykken, M. Pierini, and M. Spiropulu, *Missing energy look-alikes with 100 pb^{-1} at the LHC*, *Phys. Rev.* **D78** (2008) 075008, [0805.2398].
- [182] H. K. Dreiner, M. Kramer, J. M. Lindert, and B. O’Leary, *SUSY parameter determination at the LHC using cross sections and kinematic edges*, *JHEP* **04** (2010) 109, [1003.2648].
- [183] P. R. Harrison and C. H. Llewellyn Smith, *Hadroproduction of Supersymmetric Particles*, *Nucl. Phys.* **B213** (1983) 223. [Erratum: Nucl. Phys.B223,542(1983)].

- [184] E. Reya and D. P. Roy, *SUPERSYMMETRIC PARTICLE PRODUCTION AT p anti- p COLLIDER ENERGIES*, *Phys. Rev.* **D32** (1985) 645.
- [185] S. Dawson, E. Eichten, and C. Quigg, *Search for Supersymmetric Particles in Hadron - Hadron Collisions*, *Phys. Rev.* **D31** (1985) 1581.
- [186] W. Beenakker, R. Hopker, M. Spira, and P. Zerwas, *Squark production at the Tevatron*, *Phys. Rev. Lett.* **74** (1995) 2905–2908, [hep-ph/9412272].
- [187] W. Beenakker, R. Hopker, M. Spira, and P. Zerwas, *Squark and gluino production at hadron colliders*, *Nucl. Phys.* **B492** (1997) 51–103, [hep-ph/9610490].
- [188] W. Beenakker, M. Kramer, T. Plehn, M. Spira, and P. Zerwas, *Stop production at hadron colliders*, *Nucl. Phys.* **B515** (1998) 3–14.
- [189] W. Beenakker, R. Hopker, and M. Spira, *PROSPINO: A Program for the production of supersymmetric particles in next-to-leading order QCD*, hep-ph/9611232.
- [190] G. F. Sterman, *Summation of Large Corrections to Short Distance Hadronic Cross-Sections*, *Nucl. Phys.* **B281** (1987) 310.
- [191] S. Catani and L. Trentadue, *Resummation of the QCD Perturbative Series for Hard Processes*, *Nucl. Phys.* **B327** (1989) 323.
- [192] A. Kulesza and L. Motyka, *Threshold resummation for squark-antisquark and gluino-pair production at the LHC*, *Phys. Rev. Lett.* **102** (2009) 111802, [0807.2405].
- [193] A. Kulesza and L. Motyka, *Soft gluon resummation for the production of gluino-gluino and squark-antisquark pairs at the LHC*, *Phys. Rev.* **D80** (2009) 095004, [0905.4749].
- [194] M. Beneke, P. Falgari, and C. Schwinn, *Soft radiation in heavy-particle pair production: All-order colour structure and two-loop anomalous dimension*, *Nucl. Phys.* **B828** (2010) 69–101, [0907.1443].
- [195] W. Beenakker, S. Brensing, M. Kramer, A. Kulesza, E. Laenen, and I. Niessen, *Supersymmetric top and bottom squark production at hadron colliders*, *JHEP* **08** (2010) 098, [1006.4771].
- [196] M. A. Beneke, P. Falgari, and C. Schwinn, *Soft and Coulomb Gluon Resummation in Squark-Antisquark Production at the LHC*, *PoS RADCOR2009* (2010) 012, [1001.4627].
- [197] P. Falgari, C. Schwinn, and C. Wever, *NLL soft and Coulomb resummation for squark and gluino production at the LHC*, *JHEP* **06** (2012) 052, [1202.2260].
- [198] C. Borschensky, M. Krämer, A. Kulesza, M. Mangano, S. Padhi, T. Plehn, and X. Portell, *Squark and gluino production cross sections in pp collisions at $\sqrt{s} = 13, 14, 33$ and 100 TeV*, *Eur. Phys. J.* **C74** (2014), no. 12 3174, [1407.5066].
- [199] W. Beenakker, C. Borschensky, M. Krämer, A. Kulesza, E. Laenen, S. Marzani, and J. Rojo, *NLO+NLL squark and gluino production cross-sections with threshold-improved parton distributions*, 1510.00375.
- [200] U. Langenfeld and S.-O. Moch, *Higher-order soft corrections to squark hadro-production*, *Phys. Lett.* **B675** (2009) 210–221, [0901.0802].

- [201] U. Langenfeld, *Threshold Improved QCD Corrections for Stop-Antistop production at Hadron colliders*, *JHEP* **07** (2011) 052, [1011.3341].
- [202] W. Beenakker, S. Brensing, M. Kramer, A. Kulesza, E. Laenen, and I. Niessen, *NNLL resummation for squark-antisquark pair production at the LHC*, *JHEP* **01** (2012) 076, [1110.2446].
- [203] W. Beenakker, T. Janssen, S. Lepoeter, M. Krämer, A. Kulesza, E. Laenen, I. Niessen, S. Thewes, and T. Van Daal, *Towards NNLL resummation: hard matching coefficients for squark and gluino hadroproduction*, *JHEP* **10** (2013) 120, [1304.6354].
- [204] S. Bornhauser, M. Drees, H. K. Dreiner, and J. S. Kim, *Electroweak contributions to squark pair production at the LHC*, *Phys. Rev.* **D76** (2007) 095020, [0709.2544].
- [205] A. Arhrib, R. Benbrik, K. Cheung, and T.-C. Yuan, *Higgs boson enhancement effects on squark-pair production at the LHC*, *JHEP* **02** (2010) 048, [0911.1820].
- [206] W. Hollik, M. Kollar, and M. K. Trenkel, *Hadronic production of top-squark pairs with electroweak NLO contributions*, *JHEP* **02** (2008) 018, [0712.0287].
- [207] M. Beccaria, G. Macorini, L. Panizzi, F. M. Renard, and C. Verzegnassi, *Stop-antistop and sbottom-antisbottom production at LHC: A One-loop search for model parameters dependence*, *Int. J. Mod. Phys.* **A23** (2008) 4779–4810, [0804.1252].
- [208] W. Hollik and E. Mirabella, *Squark anti-squark pair production at the LHC: The Electroweak contribution*, *JHEP* **12** (2008) 087, [0806.1433].
- [209] J. Germer, W. Hollik, and E. Mirabella, *Hadronic production of bottom-squark pairs with electroweak contributions*, *JHEP* **05** (2011) 068, [1103.1258].
- [210] R. Gavin, C. Hangst, M. Krämer, M. Mühlleitner, M. Pellen, E. Popenza, and M. Spira, *Squark Production and Decay matched with Parton Showers at NLO*, *Eur. Phys. J.* **C75** (2015), no. 1 29, [1407.7971].
- [211] C. Hangst, *Matching Squark Production and Decay at Next-to-Leading Order Accuracy with Parton Showers*. PhD thesis, Karlsruhe Institute of Technology, 2014.
- [212] D. Gonçalves-Netto, D. López-Val, K. Mawatari, T. Plehn, and I. Wigmore, *Automated Squark and Gluino Production to Next-to-Leading Order*, *Phys. Rev.* **D87** (2013), no. 1 014002, [1211.0286].
- [213] D. Goncalves, D. Lopez-Val, K. Mawatari, and T. Plehn, *Automated third generation squark production to next-to-leading order*, *Phys. Rev.* **D90** (2014), no. 7 075007, [1407.4302].
- [214] G. Bozzi, B. Fuks, B. Herrmann, and M. Klasen, *Squark and gaugino hadroproduction and decays in non-minimal flavour violating supersymmetry*, *Nucl. Phys.* **B787** (2007) 1–54, [0704.1826].
- [215] B. Fuks, B. Herrmann, and M. Klasen, *Flavour Violation in Gauge-Mediated Supersymmetry Breaking Models: Experimental Constraints and Phenomenology at the LHC*, *Nucl. Phys.* **B810** (2009) 266–299, [0808.1104].
- [216] B. Fuks, B. Herrmann, and M. Klasen, *Phenomenology of anomaly-mediated supersymmetry breaking scenarios with non-minimal flavour violation*, *Phys. Rev.* **D86** (2012) 015002, [1112.4838].

- [217] T. Hahn and M. Perez-Victoria, *Automatized one loop calculations in four-dimensions and D-dimensions*, *Comput. Phys. Commun.* **118** (1999) 153–165, [hep-ph/9807565].
- [218] B. Chokoufe Nejad, T. Hahn, J. N. Lang, and E. Mirabella, *FormCalc 8: Better Algebra and Vectorization*, *J. Phys. Conf. Ser.* **523** (2014) 012050, [1310.0274].
- [219] T. Appelquist and J. Carazzone, *Infrared Singularities and Massive Fields*, *Phys. Rev.* **D11** (1975) 2856.
- [220] J. C. Collins, F. Wilczek, and A. Zee, *Low-Energy Manifestations of Heavy Particles: Application to the Neutral Current*, *Phys. Rev.* **D18** (1978) 242.
- [221] W. J. Marciano, *Flavor Thresholds and Lambda in the Modified Minimal Subtraction Prescription*, *Phys. Rev.* **D29** (1984) 580.
- [222] P. Nason, S. Dawson, and R. K. Ellis, *The Total Cross-Section for the Production of Heavy Quarks in Hadronic Collisions*, *Nucl. Phys.* **B303** (1988) 607.
- [223] P. Nason, S. Dawson, and R. K. Ellis, *The One Particle Inclusive Differential Cross-Section for Heavy Quark Production in Hadronic Collisions*, *Nucl. Phys.* **B327** (1989) 49–92. [Erratum: *Nucl. Phys.*B335,260(1990)].
- [224] S. Höche, *Introduction to parton-shower event generators*, in *Theoretical Advanced Study Institute in Elementary Particle Physics: Journeys Through the Precision Frontier: Amplitudes for Colliders (TASI 2014) Boulder, Colorado, June 2-27, 2014*, 2014. 1411.4085.
- [225] S. Frixione and B. R. Webber, *The MC@NLO event generator*, hep-ph/0207182.
- [226] S. Frixione, P. Nason, and C. Oleari, *Matching NLO QCD computations with Parton Shower simulations: the POWHEG method*, *JHEP* **11** (2007) 070, [0709.2092].
- [227] A. Salam and J. Strathdee, *Supersymmetry and Fermion Number Conservation*, *Nucl.Phys.* **B87** (1975) 85.
- [228] P. Fayet, *Fermi-Bose Hypersymmetry*, *Nucl.Phys.* **B113** (1976) 135.
- [229] C. Kilic, T. Okui, and R. Sundrum, *Vectorlike Confinement at the LHC*, *JHEP* **1002** (2010) 018.
- [230] J. Alwall, R. Frederix, S. Frixione, V. Hirschi, F. Maltoni, *et. al.*, *The automated computation of tree-level and next-to-leading order differential cross sections, and their matching to parton shower simulations*, *JHEP* **1407** (2014) 079.
- [231] C. Degrande, *Automatic evaluation of UV and R2 terms for beyond the Standard Model Lagrangians: a proof-of-principle*, 1406.3030.
- [232] A. Alloul, N. D. Christensen, C. Degrande, C. Duhr, and B. Fuks, *FeynRules 2.0 - A complete toolbox for tree-level phenomenology*, *Comput.Phys.Commun.* **185** (2014) 2250–2300.
- [233] J. Alwall, P. Schuster, and N. Toro, *Simplified Models for a First Characterization of New Physics at the LHC*, *Phys.Rev.* **D79** (2009) 075020.
- [234] **LHC New Physics Working Group** Collaboration, D. Alves *et. al.*, *Simplified Models for LHC New Physics Searches*, *J.Phys.* **G39** (2012) 105005.

- [235] C. Degrande, C. Duhr, B. Fuks, D. Grellscheid, O. Mattelaer, *et. al.*, *UFO - The Universal FeynRules Output*, *Comput.Phys.Commun.* **183** (2012) 1201–1214.
- [236] V. Hirschi, R. Frederix, S. Frixione, M. V. Garzelli, F. Maltoni, *et. al.*, *Automation of one-loop QCD corrections*, *JHEP* **1105** (2011) 044.
- [237] G. Ossola, C. G. Papadopoulos, and R. Pittau, *Reducing full one-loop amplitudes to scalar integrals at the integrand level*, *Nucl.Phys.* **B763** (2007) 147–169.
- [238] P. Artoisenet, R. Frederix, O. Mattelaer, and R. Rietkerk, *Automatic spin-entangled decays of heavy resonances in Monte Carlo simulations*, *JHEP* **1303** (2013) 015.
- [239] J. Alwall, C. Duhr, B. Fuks, O. Mattelaer, D. G. Ozturk, *et. al.*, *Computing decay rates for new physics theories with FeynRules and MadGraph5/aMC@NLO*, 1402.1178.
- [240] G. Ossola, C. G. Papadopoulos, and R. Pittau, *On the Rational Terms of the one-loop amplitudes*, *JHEP* **0805** (2008) 004.
- [241] S. Calvet, B. Fuks, P. Gris, and L. Valery, *Searching for sgluons in multitop events at a center-of-mass energy of 8 TeV*, *JHEP* **1304** (2013) 043.
- [242] D. Goncalves-Netto, D. Lopez-Val, K. Mawatari, T. Plehn, and I. Wigmore, *Sgluon Pair Production to Next-to-Leading Order*, *Phys.Rev.* **D85** (2012) 114024.
- [243] S. Frixione and B. R. Webber, *Matching NLO QCD computations and parton shower simulations*, *JHEP* **0206** (2002) 029.
- [244] T. Sjostrand, S. Mrenna, and P. Z. Skands, *A Brief Introduction to PYTHIA 8.1*, *Comput.Phys.Commun.* **178** (2008) 852–867.
- [245] M. Cacciari, G. P. Salam, and G. Soyez, *The Anti- $k(t)$ Jet Clustering Algorithm*, *JHEP* **0804** (2008) 063.
- [246] M. Cacciari, G. P. Salam, and G. Soyez, *FastJet User Manual*, *Eur.Phys.J.* **C72** (2012) 1896.
- [247] E. Conte, B. Fuks, and G. Serret, *MadAnalysis 5, A User-Friendly Framework for Collider Phenomenology*, *Comput.Phys.Commun.* **184** (2013) 222–256.
- [248] S. Frixione, Z. Kunszt, and A. Signer, *Three jet cross-sections to next-to-leading order*, *Nucl. Phys.* **B467** (1996) 399–442, [hep-ph/9512328].
- [249] R. Frederix, S. Frixione, F. Maltoni, and T. Stelzer, *Automation of next-to-leading order computations in QCD: The FKS subtraction*, *JHEP* **10** (2009) 003, [0908.4272].
- [250] H. Eberl, M. Kincel, W. Majerotto, and Y. Yamada, *One loop corrections to the chargino and neutralino mass matrices in the on-shell scheme*, *Phys. Rev.* **D64** (2001) 115013, [hep-ph/0104109].
- [251] H.-S. Shao and Y.-J. Zhang, *Feynman Rules for the Rational Part of One-loop QCD Corrections in the MSSM*, *JHEP* **06** (2012) 112, [1205.1273].
- [252] C. Degrande, B. Fuks, D. Goncalves-Netto, V. Hirschi, D. Lopez-Val, K. Mawatari, D. Pagani, J. Proudome, H. Shao, and M. Zaro, (to appear), .

- [253] **ATLAS** Collaboration, G. Aad *et. al.*, *Search for squarks and gluinos with the ATLAS detector in final states with jets and missing transverse momentum using $\sqrt{s} = 8$ TeV proton–proton collision data*, *JHEP* **09** (2014) 176, [1405.7875].
- [254] **ATLAS** Collaboration, G. Aad *et. al.*, *Summary of the searches for squarks and gluinos using $\sqrt{s} = 8$ TeV pp collisions with the ATLAS experiment at the LHC*, 1507.05525.
- [255] **CMS** Collaboration, S. Chatrchyan *et. al.*, *Search for new physics in the multijet and missing transverse momentum final state in proton–proton collisions at $\sqrt{s} = 8$ TeV*, *JHEP* **06** (2014) 055, [1402.4770].
- [256] **CMS** Collaboration, V. Khachatryan *et. al.*, *Searches for Supersymmetry using the M_{T2} Variable in Hadronic Events Produced in pp Collisions at 8 TeV*, *JHEP* **05** (2015) 078, [1502.04358].
- [257] A. Buckley, J. Ferrando, S. Lloyd, K. Nordström, B. Page, M. Rüfenacht, M. Schönherr, and G. Watt, *LHAPDF6: parton density access in the LHC precision era*, *Eur. Phys. J. C* **75** (2015), no. 3 132, [1412.7420].
- [258] F. Demartin, S. Forte, E. Mariani, J. Rojo, and A. Vicini, *The impact of PDF and alphas uncertainties on Higgs Production in gluon fusion at hadron colliders*, *Phys. Rev.* **D82** (2010) 014002, [1004.0962].
- [259] T. Sjöstrand, S. Ask, J. R. Christiansen, R. Corke, N. Desai, P. Ilten, S. Mrenna, S. Prestel, C. O. Rasmussen, and P. Z. Skands, *An Introduction to PYTHIA 8.2*, *Comput. Phys. Commun.* **191** (2015) 159–177, [1410.3012].
- [260] M. Bohm, A. Denner, and H. Joos, *Gauge theories of the strong and electroweak interaction*, .
- [261] D. Akyeampong and R. Delbourgo, *Dimensional regularization, abnormal amplitudes and anomalies*, *Nuovo Cim.* **A17** (1973) 578–586.
- [262] P. Breitenlohner and D. Maison, *Dimensional Renormalization and the Action Principle*, *Commun.Math.Phys.* **52** (1977) 11–38.
- [263] G. Thompson and H. Yu, *GAMMA(5) IN DIMENSIONAL REGULARIZATION*, *Phys.Lett.* **B151** (1985) 119–122.
- [264] T. Trueman, *Spurious anomalies in dimensional renormalization*, *Z.Phys.* **C69** (1996) 525–536, [hep-ph/9504315].